Reaction Mechanisms for Catalytic Partial Oxidation Systems -Application to Ethylene Epoxidation

by

Bharthwaj Anantharaman

B.Tech Chemical Engineering
Indian Institute of Technology, Madras, 2000

M.S. Chemical Engineering Practice
Massachusetts Institute of Technology, 2002

SUBMITTED TO THE DEPARTMENT OF CHEMICAL ENGINEERING IN PARTIAL FULFILLMENT OF THE REQUIREMENTS FOR THE DEGREE OF

DOCTOR OF PHILOSOPHY IN CHEMICAL ENGINEERING
AT THE
MASSACHUSETTS INSTITUTE OF TECHNOLOGY

JUNE 2005

Author.....
Bharthwaj Anantharaman
Department of Chemical Engineering
April 2005

Certified by.....
Gregory J. McRae
Hoyt C. Hottel Professor of Chemical Engineering
Thesis Supervisor

Certified by.....
William H. Green, Jr.
Texaco-Mangelsdorf Associate Professor of Chemical Engineering
Thesis Supervisor

Accepted by.....
Daniel Blankschtein
Professor of Chemical Engineering
Chairman, Committee for Graduate Students

Reaction Mechanisms for Catalytic Partial Oxidation Systems -Application to Ethylene Epoxidation

by

Bharthwaj Anantharaman

Submitted to the Department of Chemical Engineering
on April 20, 2005 in Partial Fulfillment of the
Requirements for the Degree of Doctor of Philosophy in
Chemical Engineering

ABSTRACT

With the rapid advances in kinetic modeling, building elementary surface mechanisms have become vital to understand the complex chemistry for catalytic partial oxidation systems. Given that there is selected experimental knowledge on surface species and a large number of unknown thermochemical, rate parameters, the challenge is to integrate the knowledge to identify all the important species and accurately estimate the parameters to build a detailed surface mechanism. This thesis presents computational methodology for quickly calculating thermodynamically consistent temperature/coverage-dependent heats of formation, heat capacities and entropies, correction approach for improving accuracy in heats of formation predicted by composite G3-based quantum chemistry methods, and detailed surface mechanism for explaining selectivity in ethylene epoxidation. Basis of the computational methodology is the Unity Bond Index-Quadratic Exponential Potential (UBI-QEP) approach, which applies quadratic exponential potential to model interaction energies between atoms and additive pairwise energies to compute total energy of an adsorbed molecule. By minimizing the total energy subject to bond order constraint, formulas for chemisorption enthalpies have been derived for surface species bound to on-top, hollow and bridge coordination sites with symmetric, asymmetric and chelating coordination structures on transition metal catalysts. The UBI-QEP theory for diatomics has been extended for polyatomic adsorbates with empirical modifications to the theory. Formulas for activation energies have been derived for generic reaction types, including simple adsorption, dissociation-recombination, and disproportionation reactions. Basis of the correction approach is the Bond Additivity Correction (BAC) procedures, which apply atomic, molecular and bond-wise modifications to enthalpies of molecules predicted by G3B3 and G3MP2B3 composite quantum chemistry methods available in Gaussian® suite of programs. The new procedures have improved the accuracy of thermochemical properties for open and closed shell molecules containing various chemical moieties, multireference configurations, isomers and degrees of saturation involving elements from first 3 rows of the periodic table. The detailed mechanism explains the selectivity to ethylene oxide based on the parallel branching reactions of surface oxametallacycle to epoxide and acetaldehyde. Using Decomposition Tree Approach, surface reactions and species have been generated to develop a comprehensive mechanism for epoxidation. As a result of these developments in the thesis, chemisorption enthalpies can now

be estimated within 3 kcal/mol of experimental values for transition metal catalysts and enthalpies predicted by G3B3 and G3MP2B3 Gaussian methods can be corrected within 0.5 kcal/mol. Examples of heterogeneous reaction systems involving silver-catalyzed ethylene epoxidation demonstrate the effectiveness of the methodologies developed in this work.

Thesis Supervisor: Gregory J. McRae, Hoyt C. Hottel Professor of Chemical Engineering
Thesis Supervisor: William H. Green, Jr., Texaco-Mangelsdorf Associate Professor of Chemical Engineering

DEDICATION

This thesis is dedicated to my parents, Geetha and Anantharaman, and the family they have built for Bhargavi and me. Their love and affection have constantly motivated me throughout this thesis. Upon their deep-rooted and careful foundation lies the small piece of my work.

ACKNOWLEDGEMENTS

I would like to extend my sincere thanks to my thesis advisors Prof. Gregory McRae and Prof. William Green for giving me ample support, invaluable guidance and broad vision to shape this thesis. Their constant motivation and technical guidance have seen me through various enjoyable phases of graduate school. Members of my thesis committee, Prof. Klavs Jensen and Prof. Paul Barton deserve my sincere appreciation for their suggestions to thesis research. I would like to thank the research scientist, Dr. Carl Melius who offered me all the resources for an enjoyable professional and personal experience during my summer fellowship at Lawrence Livermore National Laboratory. I would like to thank my office mates: Sara Passone, Nina Chen, Manish Bajaj, Jeremy Jhonson and Patrick deMan for sharing their thoughts and many a lighter moments in the past years. I would like to thank my friends in Green group for fruitful discussions. Special mention goes to Rob Ashcraft and Sandeep Sharma for managing the computational resources.

Contents

List of Figures

List of Tables

Chapter 1: Introduction

1.1 Thesis Statement

Oxidation processes that are driven by heterogeneous catalysts can be divided into 2 groups, namely partial oxidation where the desired product is not thermodynamically the most stable and total oxidation reactions where the desired reaction products (carbon dioxide and water) are the most stable. The former type of reaction is generally applied for the production of bulk organic chemicals while the latter is practiced for energy conversion or pollution abatement. Oil is the principal source of organics with natural gas as a source of synthesis gas (CO and H_2) becoming increasingly important. Heterogeneous partial oxidations are industrially important processes with the outputs used as feedstock for polymer and plastics production. Research in catalytic partial oxidation has been primarily targeted towards increasing the yield and selectivity of the reactions. This is pursued to not only improve economic profitability of the process but also mitigate pollution and global warming due to carbon dioxide production. To increase selectivity and yield of catalytic partial oxidation processes, we need to understand the surface mechanism and develop elementary surface reactions. In achieving this objective outlined above, several contributions of the thesis are identified:

- Development of a computational methodology for estimating thermochemical and rate parameters for catalytic reactions on transition metals.
- Corrections to composite quantum chemistry methods for improved accuracy and predictive capability of thermochemical properties of gas phase species which are involved in gas as well as surface chemistry.

- Systematic generation of surface mechanism with elementary kinetics for ethylene epoxidation.
- Evaluation of the role of surface chemistry and the reverse reaction of epoxide in influencing the selectivity of ethylene epoxidation.
- Uncertainty and sensitivity analyses identifying the important parameters affecting ethylene oxide concentrations in epoxidation.

1.2 Motivations

Ethylene oxide, an important raw material for several commodity chemicals, is commercially produced by the partial oxidation of ethylene on silver catalyst. The worldwide production capacity of ethylene oxide exceeds 22 billion pounds per annum. Current process for ethylene oxide is based on 50-year old technology and there is constant motivation to improve the process. Improving yield and selectivity will not only increase profits through ethylene oxide production but also address climatic problems by reducing carbon dioxide emission. Current research in epoxide is to understand the surface mechanism of epoxidation on silver. However, there are key challenges for developing a surface mechanism based on elementary kinetics:

- *Identification of Surface Species and Reactions*

  The first decision, also the most important decision, encountered in developing surface mechanism is the identification of species and reactions involved. Information on the reactants, observed products and intermediates from surface science experiments need to be used while developing surface mechanisms.

- *Estimation of Thermochemical Properties for Kinetic Models*

A key challenge in the development of detailed reaction mechanisms for heterogeneous catalysis is the availability of thermophysical data needed for estimating rate constants. Current literature models for catalysis contain irreversible steps and are thermodynamically inconsistent since no convenient software for this purpose is available. The methods for estimating thermochemical and rate parameters of surface reactions need to be integrated into an automated program.

- *Interplay of Gas Transport and Surface Chemistry*

  Boundary layers around the catalyst offer diffusional resistance to transport of gaseous reactants and products from the gas phase to surface and vice-versa. The relative importance of transport and surface chemistry needs to be understood with the goal of improving the selectivity of epoxide.

- *Propagation of Uncertainty*

  One of the common characteristics of the rate and thermodynamic parameters of a catalyst simulation is the uncertainty involved in the theoretical estimations and experimental measurements. Therefore, we need to study the propagation of uncertainty in the form of probability distribution in addition to sensitivity analysis for small perturbations in parameters around nominal values.

1.3 Objectives

The goal of the thesis is to develop mechanisms for heterogeneous catalytic partial oxidation systems with specific application to ethylene epoxidation. Several important elements are identified to overcome the list of challenges mentioned in the previous section:

- Application of systematic mechanism generation techniques based on Decomposition Tree Approach for hypothesizing mechanism based on limited set of known reactive species.
- Development and implementation of a computer program that integrates the existing methodologies for estimating thermodynamically consistent thermochemical properties of a catalyst simulation.
- Explanation of selectivity-conversion trends from the reversible equilibrium of ethylene oxide-surface oxametallacycles.
- Application of Deterministic Equivalent Modeling Method (DEMM) to estimate the uncertainties propagated by the kinetic and thermodynamic parameters in the form of probability distribution functions.

1.4 Thesis Outline

Different components of the thesis are outlined in Figure 1.1.

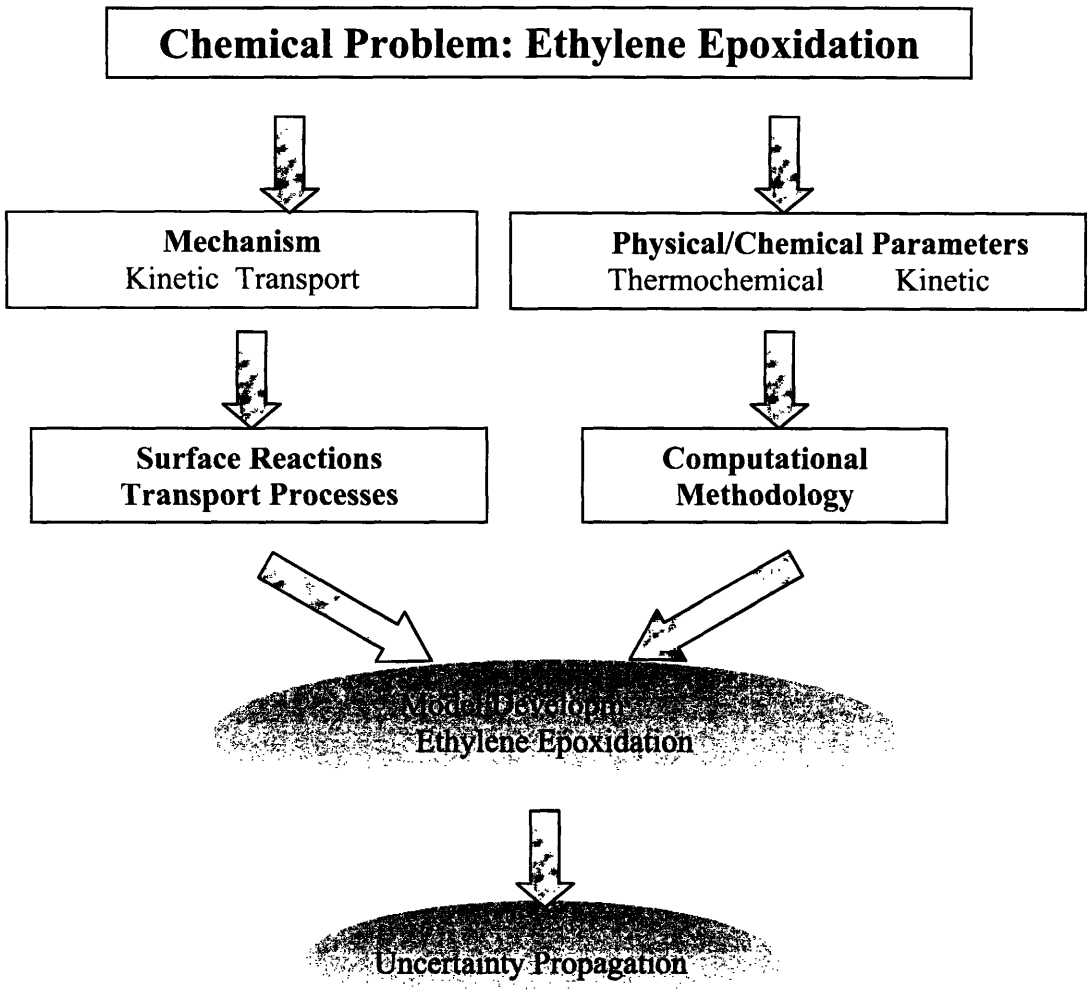

Figure 1.1 Different Components of the Thesis

As shown in Figure 1.1, ethylene epoxidation is the partial oxidation system studied. The first step is to understand kinetic mechanism and estimate the different thermodynamic and kinetic parameters. The estimated parameters are used to develop kinetic models for ethylene epoxidation. Systematic uncertainty propagation is required to identify the uncertain parameters

that affect the predicted ethylene oxide concentrations and selectivities. The parameters are used to identify the uncertainties propagated in the ethylene oxide concentrations.

Key contributions of the thesis are presented in Chapters 3, 4 and 6 to 8. Chapter 3 formulates the kinetics of surface reactions and specifies the software requirements to modify the coverage-dependent functionality of surface CHEMKIN. Chapter 4 presents the development of a computational methodology for the estimation of thermochemical parameters and thermodynamically consistent rate parameters of a general surface mechanism on transition metal catalysts. Chapter 6 develops Bond Additivity Correction (BAC) procedures for the G3B3 and G3MP2B3 based quantum chemistry methods, with the assessment of overall as well as specific accuracy of correction procedures for various functional groups involving atoms from the first 3 rows of periodic table. Chapter 7 explains the important factors affecting the branching ratio and selectivity of epoxide based on a surface mechanism that includes the key reactions of surface oxametallacycle. Chapter 8 applies Decomposition Tree Approach to generate an extensive surface mechanism for ethylene epoxidation based on the knowledge of species observed in lab-scale experimental reactors and plant-scale industrial reactors.

Chapter 2: Issues in Developing Surface Mechanisms

This chapter presents the main issues involved in developing surface mechanisms for catalytic partial oxidation systems. The chapter is organized in the following order. Section 2.1 discusses the various methodologies involved in estimating thermochemical and rate parameters of a catalyst simulation with the goal of quick and accurate computation of parameters. Section 2.2 discusses the current literature for generation of mechanisms for different reaction systems. Issues pertinent to the formulation of surface kinetics are discussed with attention focused on thermodynamically consistent coverage-dependent surface mechanisms. Section 2.3 presents the literature on heterogeneous catalytic partial oxidation of ethylene with progress in the area of surface science experiments and kinetic models towards understanding the important surface intermediates and reactions in the mechanism.

2.1 Estimation of Thermochemical and Rate Parameters

Currently, there are methodologies available for estimating thermochemical and rate parameters for surface reactions. Unity Bond Index-Quadratic Exponential Potential (UBI-QEP) approach also known as Bond Order Conservation (BOC) theory has been used to compute molecular chemisorption enthalpies of surface species and activation energies for surface reactions [1-8]. BOC approach which is based on the quasi-spherical nature of the interaction potential and the bond index conservation of chemical bonds on transition metal surfaces was reported to derive a quantum mechanical basis [8]. The geometries of different close packed structures of catalysts were approximated as packing of spheres and the electronic interactions of the valence shell were considered quasi-spherical. In order to conserve the formation and destruction of bonds along

the minimum-energy path and quantify the conservation of bond characteristics during such process, bond order was introduced on the basis of quantum mechanics. Then a phenomenological bond order, based on physically observable bond distance was developed and this forms a basis of the BOC theory. A phenomenological approach based on the physically observable parameters including bond lengths was easier to use for different catalytic systems of interest. This approach was used to derive quantitative analytical expressions for the calculation of activation energies using the experimental heats of chemisorptions, gas phase dissociation energies and coverage-dependent parameters of energies. These were the bulk thermodynamic quantities describing the interaction of surface species with the catalyst surfaces.

BOC approach was extensively used in literature for different catalyst systems. Parades-Olivera et al. used the approach to calculate energetics of elementary reactions involved in the direct synthesis of methanol from methane over noble metal catalysts: Ni, Pd, Pt and Au [9]. The calculated energies were used to guide conditions under which complete oxidation of methane could be avoided. Tao et al. estimated the energetics of adsorption and step-wise decomposition reactions of PH_3, PCI_3 and $P(CH_3)_3$ estimated using the bond order conservation Morse potential (BOC-MP) method [10]. The energetics calculated using BOC approach were compared against experimental data and results were found to agree qualitatively with the data. Gobal and Azizian investigated the adsorption and decomposition of NO_2 on transition metals [11]. BOC approach was used to study the product distributions and the surface species involved in the catalytic decomposition of NO_2 on different transition metal catalysts. Hu and Ruckenstein used BOC approach to suggest a mechanism for the catalytic reaction of NO over Cu supported on MCMB [12]. Au and Wang investigated the surface mechanism for the partial oxidation of methane over supported Rh catalysts [13]. Nature of the active sites on the catalyst

was also studied based on the energetics of surface reactions calculated using BOC approach. Gobal and Azizian analyzed the thermodyanamics of surface species in the reactions of NO and C on Pt catalyst [14]. Hei at al., after studying the carbon dioxide reforming of methane on several transition metal catalysts, identified the rate determining steps and activity sequence of different catalysts [15]. Jirsak et al. performed a thermochemical analysis to study the interaction of sulfur dioxide on Ru (001) [16]. From calculations, they predicted the presence of SO_3 and SO_4 on the catalyst surface, which was confirmed experimentally under large exposures of sulfur dioxide. Wang et al. used BOC approach to calculate the activation energies for surface reactions in the synthesis of methanol over clean and oxygen-modified Cu (100) surface [17]. Besides identifying the volcano relationship between surface oxygen coverage and reaction activity, they found that the ratio between copper ions and copper oxide controls activity of the catalyst. Yang et al. (2000) estimated the rate parameters for the steam reforming of methane into synthesis gas [18].

Azizian and Gobal confirmed experimental studies for the decomposition of methyl iodide on Ni(111) surface either alone or in the presence of hydrogen [19]. There was good agreement between results obtained using BOC approach and experiments not only for the Ni(111) surface, but also for the Ni(100) and Ni(110) surface. Azizian and Gobal studied the catalytic decomposition of methyl iodide on Cu(111) surface and concluded that the TPD peak for methyl radical was due to the desorption of a part of the reactive methyl surface species [20]. Zeigarnik et al. calculated the binding energies of atomic carbon on nickel, palladium, platinum, rhodium, ruthenium, iridium, iron, copper and gold [21]. The binding strengths and surface activities towards carbon-carbon scission were used to arrange different catalysts in a series. This arrangement was relevant for ethane hydrogenolysis since carbon-carbon bond scission is

the rate-determining step. Azizian and Gobal (2001) proposed a reaction mechanism based on the thermodynamics of underlying surface reactions [22]. They used BOC approach to estimate the thermodynamic parameters of surface reactions. Wang et al. coupled DFT calculations with BOC approach to compare the surface-structural sensitivity of reverse water-gas shift reaction over different copper surfaces [23]. Hu combined entire range BOC approach with hydrid Density Functional Theory to accurately predict the bulk bond lengths of crystals [24]. They also correlated the bulk properties of crystals with the properties of small clusters and corresponding molecules. Khanra et al. compared the predicted results against experimental data for the hydrogenation of unsaturated aldehydes on Pt(111) and Ag(111) surface [25]. The total activity and selectivity for allyl alcohol was found to increase with the surface coverage of acrolein. The predicted selectivity was higher for Ag(111) surface than that for Pt(111) surface. Table 2.1 summarizes the different literature works reviewed and the corresponding catalyst systems for which BOC approach has been applied.

Table 2.1 Different Catalyst Systems for which BOC Approach is Used

Literature Work	Catalyst Systems
[9]	Ni, Pd, Pt, Au
[12]	Cu
[13]	Rh
[14]	Pt
[16]	Ru
[17]	Cu
[19]	Ni
[20]	Cu
[21]	Ni, Pd, Pt, Rh, Ru, Ir, Fe, Cu & Au
[23]	Cu
[25]	Pt, Ag
[26]	Hg

Collision and transition state theory were used to initially estimate preexponential factors either for calculating yield bounds or optimizing kinetic parameters for catalysts [27-30]. The preexponential factor given by collision theory for unimolecular association and simple desorption reactions is 10^{13} s^{-1}, while the one for Langmuir-Hinshelwood type bimolecular reactions is 10^{11} s^{-1}. Translational, rotational, vibrational partition functions for the reactants, transition states and products were also used to estimate the preexponential factors. These estimates typically served as initial guess for some optimization algorithms which then refine the preexponential factors. This approach was used in kinetic modeling of hydrogen oxidation on Platinum.

2.2 Systematics of Generating Surface Mechanism

We present a brief literature review of the different mechanism generation methods available for gas phase systems. Gasteiger et al. developed a program EROS for predicting reaction mechanism and automatic generation of reaction rate rules from reaction databases [31]. Blurock et al. developed a software system to manage, manipulate and generate reaction data and used them to automatically develop a detailed mechanism from a set of reaction families Iterative application of the reaction patterns on sets of molecules was described [32]. Glaude et al. developed a computer-aided design mechanism for the oxidation of n-octane and n-decane in the gas phase [33]. The agreement between model predictions and experimental values was satisfactory both for conversions and the distribution of the products formed. This modeling required improvement in the generation of the secondary reactions of alkenes, which were the main primary products obtained during the oxidation of these two alkanes in the range of temperature studied. Woo et al. established a quantitative link between measurable experimental

changes and kinetics analysis to explain the behavior of styrene-based polymers alone and in binary mixtures during pyrolysis [34]. Experiments with low molecular weight polystyrene and poly(α-methylstyrene) were carried out which showed that a higher selectivity to monomer was obtained for poly(α-methylstyrene) than for polystyrene. The experimental results were interpreted using a detailed mechanistic model which described the reactions of α-methylstyrene and styrene trimers and was generated using software for automated model construction to describe 901 species using over 4000 reactions.

Different algorithms developed for generating mechanisms were based on graph theory [32, 35-49]. Molecular species were naturally represented by graphs, which were identified by their vertices and edges where vertices were atom types and edges were bonds. The mechanism was generated using a set of reaction patterns (sub-graphs). These subgraphs were the internal representations for a given class of reaction thus allowing for the possibility of eliminating unimportant product species a priori. Furthermore, each molecule was canonically represented by a set of topological indices including connectivity index, balaban index, schulz TI index, WID index, and thus eliminated the probability for regenerating the same species twice. Warth et al. developed advanced software for the automatic generation of mechanisms to model the gas-phase oxidation of some components of gasoline, alkanes and ethers. Programming of this system was mainly based on a referenced canonical treelike description of molecules and can handle both acyclic and cyclic compounds [50]. Klinke et al. extended the tools of mechanism generation to handle heterogeneous Fischer-Tropsch synthesis on Ni(111) and Co(0001) surfaces [51]. Linear free energy relationships using heat of reaction as the reactivity index were used to estimate activation energies and preexponential factors. Unknown heats of adsorption for many adsorbates estimated using a phenomenological approach were integrated in an automatically

constructed reaction mechanism describing Fischer-Tropsch synthesis via carbene polymerization. Bendtsen et al. integrated scaled sensitivity analysis, automated reaction pathway generation and explorative analysis of accumulated rate of progress matrices for analyzing NO_x enhanced oxidation of methane at 700–1200K [52]. Bounaceur applied a computer-aided design of comprehensive primary and simplified secondary mechanisms in the case of alkanes pyrolysis by writing systematically all the generic reactions: initiations, isomerizations, decompositions by ß-scission, metatheses, additions and terminations. The system generated a primary mechanism in which only the initial organic molecule or the organic molecules contained in the initial mixture were considered as reactants. A secondary mechanism, including reactions whose reactants were the molecular products formed by the primary mechanism, could be created following diverse rules [53]. Battin-Leclerc used EXGAS, a system for automatic generation of detailed mechanism in modeling ignition delays of butynes and oxidation of alkenes [54]. Matheu et al. presented a fast method for computing pressure dependence of rate constants on-the-fly during automated mechanism generation for a series of pressure-dependent reactions through cycloalkyl radical intermediates, including systems with over 90 isomers and 200 accessible product channels [55]. Grenda et al. constructed automated computational mechanism-generation technique for methane pyrolysis following a detailed set of elementary reactions, estimated required reaction, and constructed a kinetic model which agreed well with experimental data for several species [56]. Ratkiewicz applied the chemical graph theory approach for generating elementary reactions of complex systems [57]. Matheu et al. predicted the observed autocatalysis and concentration profiles by employing pressure-dependent reactions generally and systematically during computerized mechanism construction with rate constants computed for chemically or thermally activated pressure-dependent reactions [58].

Hsi-Wu Wong et al. used molecule canonicalization and encoding algorithm based automatic mechanism generation to understand the fundamental kinetics of complex reaction systems such as silicon hydride clustering chemistry [59]. In this algorithm, the molecules were expressed explicitly as trees, and all linearly independent cycles of every size in the molecule were found. The cycles sorted according to their size and functionality, were used to include ring corrections. John Ross discussed new methods to determine the casual connectivity of chemical species, the reaction pathway, and the reaction mechanisms of complex reaction systems from prescribed measurements and theories [60]. By detecting and not guessing reaction mechanisms, casual connectivities of the chemical species could be obtained from specially designed experiments and necessary theories for their interpretation. Pulse methods were used to determine the casual connectivities of reaction networks. Stoichiometric coefficients of the intermediate reactions could be derived by observing the changes in concentrations of intermediate species.

The above methods presented in literature generate surface mechanisms by predicting the rates of elementary surface reactions and screening unimportant reactions, species based on rates and sensitivity analysis. However, Decomposition Tree Approach developed by Achilles [61] was based on algorithm for hypothesizing mechanisms given an incomplete list of reactive species. The algorithm provided alternative explanations of the observations of species, and served as a basis for hypothesizing species that may be missing from the original list. Using the observations as guideline for developing systematic algorithm, procedures for representing and ordering molecular structrures were presented to enable the automatic generation of missing species and possible reactions. Natural constraints on allowable combinations of possible reactions were translated into an integer programming formulation. By following the algorithm for solving integer program, all mechanistic hypotheses consistent with the constraints could be

identified in the order of their complexity based on the implementation and physical nature of the process.

A general and flexible formalism with mass-action kinetics was developed for surface mechanisms [62, 63]. The foundation of microkinetic analysis has drastically changed the way rates of surface-catalyzed reactions are parametrized. In the initial stages of development, some parameters arose from experimental data whereas others were fitted to data. However, even in best cases, some tuning is typically necessary for quantitative model predictions. During this process, parameters of reaction mechanisms may violate thermodynamics. Hence, mathematical expressions pertaining to thermodynamic constraints were reviewed [64]. Examples of ethylene hydrogenation, ammonia synthesis, and hydrogen oxidation were presented to assess the thermodynamic validity of literature mechanisms. Due to increased interactions among surface species, coverage dependence was incorporated in the activation energies [65].

2.3 Heterogeneous Catalytic Partial Oxidation of Ethylene

Many surface science experiments in ethylene epoxidation focused on the form of surface oxygen involved in the active reaction process. Backx et al. (1981) observed molecular oxygen to desorb or dissociate from the surface of silver above 170K [66]. Low chemisorption enthalpy of 10.0 kcal/mol for molecular oxygen was reported [67,68]. Campbell and Paffett found molecular oxygen on Ag(110) to dissociate at 130K for a dosage of 1100 L O_2 [69]. Campbell and Backx et al. found atomic oxygen to desorb at high temperatures (550 and 600K on Ag(111) and Ag(110), respectively) [66,70]. Engelhardt and Menzel investigated the adsorption of oxygen on Ag(110), (111), and (100) surfaces by LEED and AES, and by the measurement of work function changes and of kinetics, at and above room temperature and at oxygen pressures

up to 10^{-5} Torr [71]. Backx et al. observed different desorption peaks for oxygen when they ran several cycles of oxygen adsorption at room temperatures followed by TPD analysis [66]. For six cycles, the desorption peak continued to increase with the final cycle observed at around 880K. A desorption peak at 900K was observed by Bowker et al. [72]. These temperatures are much higher than the typical temperatures at which surface atomic oxygen was observed to desorb, thereby indicating the presence of subsurface oxygen. Backx et al. used TPD study with isotopes to show that adsorbed atomic oxygen on Ag(110) diffuses into the subsurface region above 423K and does not desorb or diffuse into the bulk until above 723K [66]. However, the saturation subsurface oxygen was limited to a few (~ 2) monolayers, as observed from experiments by Campbell [70]. He dosed 1400 Torr oxygen on Ag(111) at 443K for 640 seconds; only two monolayers desorbed during a subsequent TPD experiment. Subsurface oxygen was characterized in several other studies using XPS and TPD [67,69,73].

Calculated heats of chemisorption of oxygen atom with 0.25 monolayer oxygen on silver were 81.15 and 78.62 kcal/mol. for fcc and hcp hollow sites [74]. Li et al. conducted extensive DFT calculations to identify atomic oxygen adsorbed on catalyst as the most stable active oxygen species for epoxidation conditions corresponding to industrial reactors [75]. The obtained phase diagram revealed that atomic oxygen actuated silver as the partial oxidation catalyst. Ethylene known to adsorb weakly on silver [76-78], was reported to desorb at low temperatures: 130 and 155K [69,79]. Campbell and Paffett used TDS to report an activation energy of desorption of 8.9 kcal/mol on clean Ag(110) surface for an exposure of 10^{-6} mbar sec. of ethylene. The desorption temperatures for ethylene on clean and oxygen doped silver surface (oxygen coverage = 0.5) were 130K and 170K, respectively [67,79]. Barteau and Madix

reported an increase in the heat of chemisorption of ethylene from 8.9 kcal/mol. for a clean silver surface to 10.7 kcal/mol. for an oxygen doped surface [67].

Surface oxametallacycle having an O-C-C backbone with O and C atoms attached to silver surface was spectroscopically identified and characterized in epoxidation reactions [80,81]. By dosing Ag(111) surface with ethylene oxide at 250K, Linic and Barteau observed the formation of a stable surface intermediate through HREELS studies. Good agreement between the vibrational frequencies of the HREELS and IR spectra implied that the surface intermediate was oxametallacycle. Linic and Barteau used DFT to calculate the rate constants for parallel branching of oxametallacycle to epoxide and acetaldehyde [82]. Sault and Madix observed acetate intermediates when acetaldehyde was fed over Ag(110) dosed with oxygen at 5×10^{-7} torr for 200 seconds, corresponding to surface oxygen coverage between 0.2 and 0.4 ML [83].

Silver acetate decomposed to form acetic anhydride under highly anhydrous conditions [84]. Cordi and Falconer reported the quantitative CO_2 production rate to vary from 0-4 μmol/sec/g of catalyst in the temperature range 300-700K [85]. They observed CO_2 from the TPO of acetaldehyde on Ag (alumina-supported silver). Quantitative rate of production of CO_2 measured by Borman and Westerterp varied from 10^{-6} to 10^{-3} mol/sec/kg of catalyst (or equivalently 10^{-3} to 1 μmol/sec/g of catalyst) [86].

Stuve and Madix studied the adsorption and reaction of water on clean and oxygen covered Ag(110) surfaces using high resolution electron energy loss (EELS), temperature programmed desorption (TPD), and X-ray photoelectron (XPS) spectroscopy [87]. The reaction of adsorbed H_2O with pre-adsorbed oxygen to produce adsorbed hydroxyl groups was observed by EELS in the temperature range 205 to 255K. The adsorbed hydroxyl groups recombined at 320K to yield both a TPD water peak at 320K and adsorbed atomic oxygen.

Campbell and Paffett observed that the surface coverage of oxygen dropped when chlorine (corresponding to a coverage, $\theta_{Cl} = 0.3$) was added to the Ag(110) [69]. The saturation coverage of atomic oxygen was observed to be suppressed almost linearly with chlorine coverage of 0.5 [88]. Alves et al. calculated the binding energy of chlorine on silver using self-consistent-field molecular orbital theory with unrestricted Hartree-Fock calculations using the effective core potential approximation and double-zeta basis sets [89]. The calculated binding energy of chlorine in Ag_3 cluster is 3.36 eV corresponding to a heat of chemisorption, 77.46 kcal/mol.

2.4 Summary

In this chapter, we have reviewed the key issues pertaining to parameter estimation, mechanism generation, thermodynamic consistency and coverage dependence for general surface mechanisms. BOC approach is widely used for estimating chemisorption enthalpies and activation energies for surface reactions on transition metals. This approach is tested out for various reactions on transition metal catalysts, and the predicted chemisorption enthalpies compare well with experimental data for different adsorbates. Since kinetic modeling is shifting focus from lumped kinetics to elementary surface reactions, it becomes important to enforce thermodynamic consistency for the surface mechanism. Mathematical formulations relevant to thermodynamic consistency have been reviewed in literature. In ethylene epoxidation, experimental and theoretical works have progressed to identify important surface intermediates and reactions in the underlying surface mechanism. Different forms of oxygen have been studied on silver catalyst, surface oxametallacycle isolated during low pressure experiments, and the promoter effect of chlorine observed for industrial reactors.

References

1. H. Sellers (1993). On analytic potential functions for reactions on metal surfaces: The case of H *--->2H on the liquid mercury surface. *Journal of Chemical Physics*, *98*, 627-633.
2. H. Sellers and E. Shustorovich (1996). Coordination modes and bonding of sulfur oxides on transition metal surfaces: combined ab initio and BOC-MP results. *Surface Science*, 346, 322-336.
3. H. Sellers and E. Shustorovich (2002). Intrinsic activation barriers and coadsorption effects for reactions on metal surfaces: Unified formalism within the UBI-QEP approach. *Surface Science Reports*, 504, 167-182.
4. E. Shustorovich (1986). Chemisorption phenomena: analytic modeling based on perturbation theory and bond-order conservation. *Surface Science Reports*, 6, 1-63.
5. E. Shustorovich (1990). The Bond-Order conservation approach to chemisorption and heterogeneous catalysis: Applications and implications. *Advances in Catalysis*, 37, 101-163.
6. E. Shustorovich and A. T. Bell (1991). Synthesis and decomposition of ammonia on transition metal surfaces: bond-order-conservation-Morse-potential analysis. *Surface Science*, 259, L791-L796.
7. E. Shustorovich and A. T. Bell (1993). Decomposition and reduction of NO on transition metal surfaces: bond order conservation Morse potential analysis. *Surface Science*, 298, 127-138.
8. E. Shustorovich and H. Sellers (1998). The UBI-QEP method: A practical theoretical approach to understanding chemistry on transition metal surfaces. *Surface Science Reports*, 31, 1-119.
9. P. P. Olivera and H. Sellers (1995). Direct synthesis of methanol over metallic catalyst. *Surface Science*, 327, 330-357.
10. H. S. Tao (1997). Decomposition of $P(CH_3)_3$ on Ru(0001): comparison with PH_3 and PCl_3. *Surface Science*, 375, 257-267.
11. F. Gobal and S. Azizian (1997). On the investigation of the adsorption and decomposition of NO_2 on transition metals by Bond Order Conservations Morse Potential analysis. *Langmuir*, 13, 5999-6000.
12. Y. H. Hu and E. Ruckenstein (1997). The catalytic reaction of NO over Cu supported on meso-carbon microbeads of ultrahigh surface area. *Journal of Catalysis*, 172, 110-117.
13. C. T. Au and H.Y. Wang (1997). Mechanistic studies of methane partial oxidation to syngas over SiO_2-supported Rhodium catalysts. *Journal of Catalysis*, 167, 337-345.
14. F. Gobal and S. Azizian (1998). A study of the thermodynamics of surface intermediates formations in the reactions between adsorbed atom and molecules on Pt (111) by the method of BOC-MP. *Journal of Molecular Catalysis A: Chemical*, 136, 169-174.
15. M. J. Hei, H. B. Chen, J. Yib, Y. J. Lin, Y. Z. Lin, G. Weia and D. W. Liao (1998). CO_2 - reforming of methane on transition metal surfaces. *Surface Science*, 417, 82-96.
16. T. Jirsak, J. A. Rodriguez, S. Chaturvedi, and J. Hrbek (1998). Chemistry of SO_2 on Ru(001): formation of SO_3 and SO_4. *Surface Science*, 418, 8-21.
17. G. Wang, Y. Zhao, Z. Cai, Y. Pan, X. Zhao, Y. Li, Y. Sun, and B. Zhong (2000). Investigation of the active sites of CO_2 hydrogenation to methanol over a Cu-based catalyst by the UBI-QEP approach. *Surface Science*, 465, 51-58.

18. W. S. Yang, H. W. Xiang, Y. W. Li, and Y. H. Sun (2000). Micro-kinetic analysis and Monte Carlo simulation in methane partial oxidation into synthesis gas. *Catalysis Today*, 61, 237-242.
19. S. Azizian and F. Gobal (2000). Investigation of the energetics of the decomposition of methyl iodide on Ni 111 surface by the method of BOC-MP. *Journal of Molecular Catalysis A: Chemical*, 153, 191-197.
20. S. Azizian and F. Gobal (2000). Mechanism of catalytic decomposition of CH_3I on the Cu(111) surface: A UBI-QEP approach. *Langmuir*, 16, 8095-8099.
21. A. V. Zeigarnik, R.E. Valde's-Pe'rez and O.N. Myatkovskaya (2000). C-C Bond Scission in Ethane Hydrogenolysis. *Journal of Physical Chemistry B*, 104, 10578-10587.
22. S. Azizian and F. Gobal (2001). A study of the mechanism of methyl iodide decomposition on Cu(110) surface: A UBI-QEP-Based approach. *Langmuir,* 17, 583-587.
23. G. C. Wang, L. Jiang, X. Y. Pang, Z. S. Cai, Y. M. Pan, X. Z. Zhao, Y. Morikawa and J. Nakamura (2003). A theoretical study of surface-structural sensitivity of the reverse water-gas shift reaction over Cu(hkl)surfaces. *Surface Science*, 543, 118 -130.
24. Y. H. Hu (2003). ER-BOC calculations of crystal bulk properties from smallest cluster models. *Journal of American Chemical Society*, 125, 4388-4390.
25. B. C. Khanra, Y. Jugnet and J.C. Bertolini (2004). Energetics of acrolein hydrogenation on Pt(111) and Ag(111) surfaces: a BOC-MP model study. *Journal of Molecular Catalysis A: Chemical*, 208, 167-174.
26. H. Sellers (1993). On analytic potential functions for reactions on metal surfaces: The case of H *--+2H on the liquid mercury surface. *Journal of Chemical Physics*, 98, 627-633.
27. P. Aghalayam, Y. K. Park and D. G. Vlachos (2000). Construction and optimization of complex surface reaction mechanisms. *AIChE Journal*, 46, 2017-2029.
28. J. A. Dumesic, D. F. Rudd, L. M. Aparicio and J. E. Rekoske (1993). The microkinetics of heterogeneous catalysis. Washington, DC: American Chemical society.
29. Y. K. Park, P. Aghalayam, and D. G. Vlachos (1999). A generalized approach for predicting coverage-dependent reaction parameters of complex surface reactions: Application of H2 oxidation over platinum. *Journal of Physical Chemistry A*, 8101-8107.
30. Y. S. Su, J. Y. Ying, and W. H. Green (2003). Upper bound on the yield for oxidative coupling of methane. *Journal of Catalysis*, 218, 321-333.
31. J. Gasteiger, M. Marsili, M. G. Hutchings, H. Saller, P. Rose and K. Rafeiner (1990). Models for the representation of knowledge about chemical reactions. *Journal of Chemical Informatics and Computer Science,* 30, 467-476.
32. E. S. Blurock (1995). Reaction system for modeling chemical reaction. *Journal of Chemical Informatics and Computer Science*, 35, 607-616.
33. P. A. Glaude, V. Warth, R. Fournet, F. Battin-Leclerc, G. Scacchi, G. M. Come (1998). Modelling of the oxidation of N-Octane and N-Decane using automatic generation of mechanisms. *Internationl Journal of Chemical Kinetics*, 30, 949-959.
34. O. Sang Woo, L. J. Broadbelt (1998). Recovery of high-valued products from styrene-based polymers through coprocessing: experiments and mechanistic modeling. *Cataysis Today*, 40, 121-140.
35. D. M. Matheu, W. H. Green, Jr. and J. M. Grenda (2003). Computational application of automated pressure-dependent mechanism generation: Reaction through cycloalkyl intermediates. *International Journal of Chemical Kinetics*, 35, 95-119.

36. L. J. Broadbelt, S. M. Stark and M. T. Klein (1994). Computer generated pyrolysis modeling: On-the-fly generation of species, reactions, and rates. *Industrial Engineering and Chemistry Research,* 33, 790-799.
37. L. J. Broadbelt, S. M. Stark and M. T. Klein (1995). Termination of computer-generated reaction mechanisms: Species rank-based convergence criterion. *Industrial Engineering and Chemistry Research*, 34, 2566-2573.
38. C. Chevalier, W. J. Pitz, J. Warnatz, C. K. Westbrook and H. Melenk (1992). Hydrocarbon ignition: Automatic generation of reaction mechanisms and applications to modeling of engine shock. *Proceedings of the Combustion of Institute*, 24, 93-101.
39. S. J. Chinnick, D. L. Baulch and P. B. Ayscough (1988). An expert system for hydrocarbon pyrolysis reactions. *Chemometrics and Intelligent Laboratory Systems,* 5, 39-52.
40. A. M. Dean (1990). Detailed kinetic modeling of autocatalysis in methane pyrolysis. *Jounral of Physical Chemistry*, 94, 1432-1439.
41. M. Dente, S. Pierucci, S. E. Ranzi and G. Bussani (1992). New improvements in modeling kinetic schemes for hydrocarbon pyrolysis reactors. *Chemical Engineering Science*, 47, 2629-2634.
42. F. P. DiMaio, P. G. Lignola (1992). KING. Kinetic Network Generator. *Chemical Engineering Science*, 51, 2713-2718.
43. W. H. Green, P. I. Barton, B. Bhattacharjee, D. M. Matheu, D. A. Schwer, J. Song, R. Sumathi, H. H. Carstensen, A. M. Dean and J. M. Grenda (2001). Computer construction of detailed chemical kinetic models for gas-phase reactors. *Industrial Engineering and Chemistry Research*, 40, 5362-5370.
44. J. M. Grenda, I. P. Androulakis and J. W. Bozzelli (2001). Combined use of automated kinetic mechanism generation and reduction in the development of chemical reaction models. *2nd Joint Meeting of the U.S. Sections of the Combustion Institute; The Combustion Institute.* Pittsburgh, PA.
45. J. M. Grenda, J. W. Bozzelli and A. M. Dean. Automated methods of treating chemically activated reactions in kinetic mechanism generation. *Eighth International Conference on Numerical Combustion.* Amelia Island, FL.
46. J. M. Grenda, A. M. Dean, W. H. Green, Jr. and P. K. Peczak (1998). Recent advances in automated kinetic mechanism generation. Presented at the work-in-progress poster (Wipp) session. *27th International Symposium on Combustion.* Boulder, CO.
47. D. M. Matheu, T. A. Lada, W. H. Green, Jr., A. M. Dean and J. M. Grenda (2001). Rate-based screening of pressure-dependent reaction networks. *Computer Physics and Communications,* 138, 237-249.
48. S. E. Prickett and M. L. Mavrovouniotis (1997). Construction of complex reaction systems III. An example: Alkylation of olefins. *Computers in Chemical Engineering*, 21, 1325-1337.
49. A. S. Tomlin, T. Turanyi and M. J. Pilling (1997). Chapter 4: Mathematical tools for the construction, investigation and reduction of combustion mechanisms. In low-temperature combustion and autoignition. In: M. J. Pilling, ed. *Comprehensive Chemical Kinetics Series.* Vol. 35: Elsevier: Amsterdam.
50. V. Warth, F. Battin-Leclerc, R. Fournet, P. A. Glaude, G. M. Co'me and G. Scacchi (2000). Computer based generation of reaction mechanisms for gas-phase oxidation. *Computers & Chemistry*, 24, 541–560.

51. D. J. Klinke and L. J. Broadbelt (1999). Construction of a mechanistic model of Fischer-Tropsch synthesis on Ni(111) and Co(0001) surfaces. *Chemical Engineering Science*, 54, 3379-3389.
52. A. B. Bendtsen, P. Glarborg and K. Dam-Johansen (2001). Visualization methods in analysis of detailed chemical kinetics modelling. *Compuers & Chemistry (Oxford)*, 25, 161-170.
53. R. Bounaceur, V. Warth, P. Marquaire, G. Scacchi, F. Domine', D. Dessort, B. Pradier and O. Brevart (2002). Modeling of hydrocarbons pyrolysis at low temperature. Automatic generation of free radicals mechanisms. *Journal of Analytical and Applied Pyrolysis*, 64, 103-122.
54. F. Battin-Leclerc (2002). Development of kinetic models for the formation and degradation of unsaturated hydrocarbons at high temperature. *Physical Chemistry and Chemical Physics*, 4, 2072-2078.
55. D. M. Matheu, P. Aghalayam, W. H. Green, Jr. and J. M. Grenda (2002). Capturing pressure-dependence in automated mechanism generation for pyrolysis and combustion. *17th International Symposium on Gas Kinetics; IPTC.* Universita¨t Essen: Essen, Germany.
56. J. M. Grenda, I. P. Androulakis,.A. M. Dean and W. H. Green, Jr. (2003). Application of computational kinetic mechanism generation to model the autocatalytic pyrolysis of methane. *Industrial & Engineering Chemistry Research*, 42, 1000-1010.
57. A. Ratkiewicz and T. N. Truong (2003). Application of chemical graph theory for automated mechanism generation. *Journal of Chemical Informatics and Computational Science*, 43, 36-44.
58. D. M. Matheu, A. M. Dean, J. M. Grenda and W. H. Green, Jr. (2003). Mechanism generation with integrated pressure dependence: A new model for methane pyrolysis. *Journal of Physical Chemistry A*, 107, 8552-8565.
59. H. Wong, L. Xuegeng, M. T. Swihart and L. J. Broadbelt (2004). Detailed kinetic modeling of silicon nanoparticle formation chemistry via automated mechanism generation. *Journal of Physical Chemistry A*, 108, 10122-10132.
60. J. Ross (2003). New approaches to the deduction of complex reaction mechanisms. *Accounts of Chemistry Research*, 36, 839-847.
61. G. C. Achilles (1992). A systematic approach to mechanistic model building: developing and testing complex reaction mechanisms. Ph. D. Thesis, Carnegie Mellon University, Department of Chemical Engineering.
62. M. E. Coltrin, R. J. Kee and F. M. Rupley (1991). Surface Chemkin: A generalized formalism and interface for analyzing heterogeneous chemical kinetics at a gas-surface interface. *International Journal of Chemical Kinetics*, 23, 1111-1128.
63. R. J. Kee, M. E. Coltrin and P. Glarborg (2003). *Chemically Reacting Flow: Theory & Practice.* New Jersey: Wiley-Interscience Publications.
64. A. B. Mhadeshwar, H. Wang and D. G. Vlachos (2003). Thermodynamic consistency in microkinetic development of surface reaction mechanisms. *Journal of Physical Chemistry B*, 107, 12721-12733.
65. Y. K. Park, P. Aghalayam and D. G. Vlachos (1999). A generalized approach for predicting coverage-dependent reaction parameters of complex surface reactions: Application of H_2 oxidation over platinum. *Journal of Physical Chemistry A*, 8101-8107.

66. C. Backx, C. P. M. de Groot and P. Biloen (1981). Adsorption of oxygen on Ag(110) studied by high resolution ELS and TPD. *Surface Science,* 104, 300-317.
67. M. A. Barteau and R. J. Madix (1980). The adsorption of molecular oxygen species on Ag(110). 97, 101-110.
68. C. T. Campbell (1985). Atomic and molecular oxygen adsorption on Ag(111). *Surface Science,* 157 (1), 43-60.
69. C. T. Campbell and M .T. Paffett (1984). The interactions of O_2, CO, and CO_2 with Ag(110). *Surface Science*, 143, 517-535.
70. C. T. Campbell (1985). The selective epoxidation of ethylene catalyzed by Ag(111): A comparison with Ag(110). *Journal of Catalysis*, 94, 436-444.
71. H. A. Engelhardt and D. Menzel (1976). Adsorption of oxygen on silver single crystal surfaces. *Surface Science*, 57, 591-618.
72. M. Bowker, P. Pudney and G. Roberts (1989). Oxyen adsorption on silver powder. *Journal of Chemical Society and Faraday Transactions*, 85, 2635-2640.
73. R. W. Joyner and M. W. Roberts (1979). A study of the adsorption of oxygen on silver at high pressure by electron spectroscopy. *Chemical Physical Letters*, 60, 459-462.
74. W. Li, C. Stampfl and M. Scheffler (2002). Oxygen Adsorption on Ag(111): A Density-Functional Theory Investigation, *Physical Review B*, 65 (075407), 1-19.
75. W. Li, C. Stampfl and M. Scheffler (2003). Why is a noble metal catalytically active? The role of the O-Ag interaction in the function of silver as an oxidation catalyst. Los Alamos National Laboratory, Preprint Archive, Condensed Matter, 1-4, arXiv:cond-mat/0305297.
76. T. E. Felter, W. H. Weinberg, P. A. Zhdan, and G. K. Boresknov (1980). An XPS and UPS investigation of the adsorption of ethylene on the (111) surface of silver., *Surface Science*, 97, L313-L319.
77. A. E. Marcinowsky and J. M. Berty (1973). Ethylene adsorption on oxygenated silver: evidence for two types of chemisorbed oxygen, *Journal of Catalysis*, 29, 494-499.
78. J. Mikami, S. Satoh and H. Kobayashi (1970). Studies of the catalytic oxidation of ethylene by means of the pulse technique, *Journal of Catalysis,* 18, 265-270.
79. B. Kruger and C. Benndorf (1986). Ethylene and ethylene oxide adsorption on Ag(110), *Surface Science*, 178, 704-715.
80. G. S. Jones, M. Mavrikakis, M. A. Barteau and J. M. Vohs (1998). First synthesis, experimental and theoretical vibrational Spectra of an oxametallacycle on a metal surface. *Journal of American Chemical Society*, 120, 3196-3204.
81. S. Linic and M. A. Barteau (2002). Formation of a stable surface oxametallacycle that produces ethylene oxide, *Journal of American Chemical Society*, 124 (2), 310-315.
82. S. Linic and M. A. Barteau (2003). Control of ethylene epoxidation selectivity by surface oxametallacycles. *Journal of American Chemical Society*, 125, 4034-4035.
83. A. G. Sault and R. J. Madix (1986a). The mechanism of acetate oxidation on Ag(110). *Surface Science*, 172, 598-614.
84. A. D. Kirshenbaum, A. G. Streng and M. Hauptschein (1953). Studies of thermal decomposition of silver salts of perfluorocarboxylic acids. *Journal of American Chemical Society*, 75, 3141-3145.
85. E. M. Cordi and J. L. Falconer (1997). Oxidation of volatile organic compounds on a Ag/Al_2O_3 catalyst. *Applied Catalysis A: General*, 151, 179-191.

86. P. C. Borman and K. R. Westerterp (1995). An experimental study of the kinetics of the selective oxidation of ethene over a silver on alpha-alumina catalyst. 34, 49-58.
87. E. J. Stuve and R. J. Madix (1981). The adsorption and reaction of H_2O on clean and oxygen covered Ag(110), *Surface Science*, 111, 11-25.
88. G. Rovida, F. Pratesi and E. Ferroni (1976). Interaction of dichloroethane and oxygen with the silver (110) surface, *Journal of Catalysis*, 41, 140-147.
89. J. L. A. Alves, H. W. Leite Alves, and C. M. C. de Castilho (1996). Hydrogen, oxygen and chlorine adsorption on Ag(110) surface: a cluster calculation. *Materials Science and Engineering*, B37, 139-141.

Chapter 3: Formulation of Surface Kinetics

This chapter formulates the surface kinetics for a general mechanism. The chapter is organized in following order. In Section 3.1, we present the traditional approaches to modeling kinetics of surface reactions. The key thermodynamic considerations required to model the surface kinetics are presented in Section 3.2. Thermochemical properties of surface species that determine the kinetics and spontaneity of surface reactions are described. Section 3.3 introduces the Software Requirements Specification (SRS) to modify the coverage-dependent functionality in SURFACE CHEMKIN. Purpose and scope of the SRS are explained in detail. Variables that are used to formulate surface kinetics are defined. The product perspectives, product functions, user characteristics, constraints as well as assumptions and dependencies for the proposed coverage-dependent modification are explained in Section 3.4. Specific requirements for the modifications including external interfaces and underlying equations are described in Section 3.5. The underlying equations describing thermodynamically consistent coverage-dependent surface mechanism are formulated in detail.

3.1 Traditional Approaches in Modeling Surface Kinetics

Traditionally, kinetic models for surface reactions are developed in literature based on overall reaction and lumped kinetics with a rate expression for the surface mechanism. It is a common practice to express the overall reaction rate as function of the concentration of reactants and products, with lumped kinetics based on Langmuir-Hinshelwood or Eley-Rideal mechanism. The kinetic parameters used in these expressions are fit from laboratory and plant data. The

empirical rate expression is often limited by the range of operating conditions from which the data have been collected and the ability to extend the rate expression for other operating conditions is subject to question.

Modeling approach for surface reactions is shifting focus from overall kinetics to elementary reactions, with the investigation of individual reaction steps and determination of kinetic parameters to explain qualitatively and quantitatively the chemical events. Due to the advancement of computational techniques, predictive kinetics is used to compute the parameters which are validated against experimental data based on a gamut of surface science experiments. The elementary reaction steps are easily represented as a set of differential equations which are then numerically solved using the latest solvers available for Ordinary Differential Equations (ODE), Partial Differential Equations (PDE) and Differential Algebraic Equation (DAE) systems [1-15]. When shifting focus from lumped to elementary kinetics, key issues need to be considered in formulating the surface kinetics and maintaining thermodynamic consistency of surface reactions.

Unlike homogeneous gas phase reactions where there is a consistent formulation to describe the mass action kinetics and rate of elementary reactions, there is considerably less standardization in describing heterogeneous reaction rates involving gas-phase, surface, and bulk species. The surface CHEMKIN® formalism is developed to provide a framework for describing complex reactions between gas-phase, surface, and bulk phase species [16]. New terminologies and concepts emerge in modeling surface kinetics, as research in surface science progresses over time. Part of a problem in describing the surface reaction rates arise from the lack of consistency in defining terminologies used to model the surface chemistry. Rates are often described in terms of adsorption isotherms, sticking coefficients or elementary rate

constants. Surface coverage is used for either fraction of total coverage or the number of sites that species occupy on the surface. Surface site is used to denote physical location on a surface, such as a threefold or an edge site, or it sometimes refers to a chemical species on the surface or just an empty site or vacancy. Vacancy is sometimes considered chemically same as the catalyst with the respective thermochemical and physical properties or just an empty moiety without any mass or property. From a modeler's perspective, it becomes important to provide a general, flexible and compact formulation that takes into account self-consistent definitions of different terms. This chapter focuses on derivation of governing equations for surface chemistry with a compact, thermodynamically consistent formulation of surface kinetics.

3.2 Thermodynamic Considerations

3.2.1 Thermochemical Properties of Surface Species

The important thermochemical properties describing surface species and elementary surface reactions are the entropies, heat capacities, molecular chemisorption enthalpies and heats of formation. Entropy change for simple adsorption has been estimated around -20 cal/mol/K [17]. Enthalpy of adsorption is the negative of heat of chemisorption, which is the heat released when a molecule adsorbs on catalyst surface. Magnitude of the enthalpy depends on the nature of adsorption and binding of adsorbate to catalyst. Chemisorbed species which are more strongly bound than physisorbed species have more negative heat of adsorption.

Negative entropy and enthalpy of reaction have important thermodynamic implications on the spontaneity and equilibrium of reaction. Free energy change has to be negative for a reaction to be spontaneous.

$$\Delta H < T\Delta S \tag{3.1}$$

Thus, the surface reaction has to be exothermic enough to overcome the entropy loss to favor the equilibrium in the forward direction of the reaction. It is important to note that equilibrium of reaction has implication on the favorable direction and not on the rate of the reaction. How fast the reaction proceeds is determined by kinetics and the activation barrier of the reaction.

3.2.2 Thermodynamic Consistency

In literature, several independent studies are conducted to estimate preexponential factors and activation energies of different elementary reactions in a surface mechanism. Grouping rate parameters from independent studies might violate thermodynamic consistency and the first law of thermodynamics. An example of thermodynamic inconsistency is the difference in bond energies of a surface species; these bond energies calculated from activation energies of different surface reactions involving the same species. This problem arises because there are many more surface reactions than the number of surface species in a typical mechanism; and the number of linearly independent reactions is equal to the number of surface species. Thermodynamic inconsistency might occur even if we set the heat of an elementary reaction as the difference between activation energies of forward and reverse steps. Thermodynamic consistency is important for surface reactions and reactor models since unphysical rates, coverages and steady states would result from inconsistent models. The concentrations of species will not be physical if the individual equilibrium constants are inconsistent with the overall thermodynamics of the reaction. The overall energy release predicted by a catalytic reaction system is strongly affected by accuracy and consistency in rate parameters used in the models. This is particularly evident

when performing non-isothermal heat transfer calculations, when the heat of overall reaction is used to study the net heat transfer in reaction system.

Thermodynamic consistency with respect to enthalpy and entropy of elementary reactions impose constraints on the activation energies, preexponential factors of forward and reverse reactions. Overall reaction can be formed with respect to different catalytic cycles in the surface mechanism, and each cycle corresponds to the reaction between complete reactants to form complete products. Thermodynamic consistency with respect to overall reaction implies that the enthalpy of overall is same as the linear combination of the enthalpies of elementary reactions leading to overall.

3.3 Software Requirements Specification

A Software Requirements Specification (SRS) is prepared to modify coverage-dependent functionality in SURFACE CHEMKIN. The document explains current problem in the coverage dependencies in SURFACE CHEMKIN, reasons for modifying the coverage-dependent functionalities, key input parameters and data required to implement the modifications.

3.3.1 Purpose of the SRS

Thermochemical and rate parameters of surface reactions are dependent on the surface coverages of different species taking part in the reactions. Coverage dependence, which arises from physical and chemical interactions among different adsorbates on the surface, is reported from various surface science experiments in literature. Since late 1960's, coverage dependence in the chemisorption enthalpies of different surface species has been experimentally measured for

many catalyst systems.[18]. However, theoretical modeling has emerged relatively recently for specific reaction systems. Heats of chemisorption and activation energies of surface reactions are mathematically expressed as functions of coverages of different surface species, which are then integrated as part of detailed chemical kinetic models for surface reactions.

SURFACE CHEMKIN has been developed as a general kinetic formalism for surface reactions [19]. The formalism, implemented as FORTRAN package in the widely used CHEMKIN® software, is used to model surface kinetics of different reactions. Coverage dependence in the rate parameters of surface reactions is included in SURFACE CHEMKIN-III, which provides the option of specifying coverage parameters for surface species and reactions. This is used in conjunction with CHEMKIN pre-processors for the gas phase and surface chemistry reaction mechanisms and transport properties.

However in the current formulation of SURFACE CHEMKIN, the coverage-dependent coefficients are specified in the reaction file of the surface mechanism. This enables the use of dependence in only the activation energies of surface reactions and not chemisorption enthalpies (or heats of formation) of surface species. To account for dependence in chemisorption enthalpies and non-linear dependence in activation energies, it is essential to explicitly include coverage dependencies in the thermo file of surface mechanism. The proposition is particularly useful when using Bond Order Conservation (BOC) approach (also known as Unity Bond Index-Quadratic Exponential Potential approach) for predicting activation energies of surface reactions [20-27].

By including coverage dependencies in the surface thermo file, it would be easy to model the change in heats of formation of surface species and activation energies of surface reactions as the coverages evolve with time or distance along the reactor. Small changes in surface coverages

might have a significant impact on the predicted heats of formation and activation energies. For example, a decrease in oxygen coverage from 0.25 ML to 0.11 ML increases the heat of formation of oxygen by 5 kcal/mol, corresponding to several orders of magnitude changes in rates of oxidation reactions [28]. Hence, it is necessary to modify the coverage-dependent functionality in SURFACE CHEMKIN.

3.3.2 Scope of the SRS

This SRS is intended for chemical kineticists or software engineers who are interested in designing, implementing and testing proposed modifications in SURFACE CHEMKIN. The SRS proposes to modify the thermo part of SURFACE CHEMKIN file, by including coverage dependencies in the heats of formation of surface species. This is different from the current version of CHEMKIN which includes the dependence only in the reaction part of CHEMKIN file. The software product to be produced due to SRS is a modified version of SURFACE CHEMKIN.

The product will compute the following coverage-dependent energies during the fly of reactor simulation:

a. Heat of formation of surface species using zero-coverage heats of formation and coverage-dependent coefficients of heats of formation.
b. Activation energy of forward reactions using zero-coverage activation energies and coverage-dependent coefficients of activation energy.
c. Activation energy of reverse reactions using those of forward reactions and thermodynamic consistency of overall reactions.

d. Coverage-dependent activation energy of both forward and reverse reactions using BOC (UBI-QEP) method; the underlying analytical formulas based on these methods need to be supplied as part of the CHEMKIN code.

The software product will enforce thermodynamic consistency in the coverage-dependent coefficients for heats of formation of surface species. The partial derivative of heat of formation of j^{th} species with respect to coverage of m^{th} species should be same as the partial derivative of heat of formation of m^{th} species with respect to coverage of j^{th} species. The user has to ensure the above thermodynamic consistency, when manually typing the coverage-dependent coefficients in the surface thermo file. It may be optional for SURFACE CHEMKIN to fill in one coefficient based on the other, or give a warning if the two coefficients are not equal to within some tolerance.

Modified version of SURFACE CHEMKIN can be applied for catalytic reactor simulations, where the coverages of surface species change during the course of simulations. It enables to calculate thermodynamically consistent coverage-dependent heats of formation and activation energies which evolve as a function of time or reactor distance during the course of simulation. The modified version of SURFACE CHEMKIN needs the same system requirements as the current version.

3.3.3 Overview

In the SRS, we first present the overall description of current problem and proposed modifications to address the problem. Next, we present the specific requirements and inputs needed from the user to implement the modified software. We use worked out examples and supporting information to illustrate the effectiveness of modifications in SURFACE CHEMKIN.

3.4 Overall Description

This subsection describes the general factors that affect modified SURFACE CHEMKIN and main requirements of the software. We present the key perspectives and functions of the modified software, characteristics and requirements needed from part of the user, the important constraints in the use of software, the main assumptions involved in solving the underlying equations and dependencies and compatibilities of the software.

Modified SURFACE CHEMKIN, which is intended to replace current version of SURFACE CHEMKIN, is a component of the larger system comprising the entire CHEMKIN® package that handles chemical kinetics, thermodynamic and transport properties in the gas phase and surface. Using the SURFACE CHEMKIN is analogous to using the CHEMKIN package, and this can be used only after the CHEMKIN interpreter has been executed. The CHEMKIN interpreter introduces the chemical elements that are used in either the gas-phase reaction mechanism or surface reaction mechanism. SURFACE CHEMKIN is composed of 2 blocks of FORTRAN code, 1. Surface interpreter and 2. Surface Subroutine Library

To apply SURFACE CHEMKIN to a problem, the user must execute an application problem that describes the particular set of governing equations. The application can call CHEMKIN and SURFACE CHEMKIN subroutines that define terms in the equations relating to equation of state, chemical production rates, and thermodynamics. Subroutines in the Library can be called from FORTRAN or C. Following the CHEMKIN interpreter, the user runs the SURFACE CHEMKIN interpreter, which first reads the symbolic description of surface reaction mechanism and then extracts appropriate thermodynamic information for chemical species from a thermodynamic database. CHEMKIN and SURFACE CHEMKIN can share a common

database, which essentially has the same format used by NASA complex chemical equilibrium code of Gordon and McBride. The output of SURFACE CHEMKIN interpreter is the Surface Linking File, which contains all the pertinent information on the elements, species and reactions in the surface reaction mechanism. Information of gas-phase species comes from the CHEMKIN Linking file, and this is duplicated in the two linking files.

The Surface Linking file is read by an initialization routine in the Surface Subroutine Library that is called from the user's code. The Surface Subroutine Library returns information on elements, species, reactions, thermodynamic properties, and chemical production rates. Generally, input to these routines is the state variables of gas and surface phases, pressure, temperature, and species composition. The species composition is specified in terms of gas phase mole fractions, surface site fractions, and bulk phase activities. Surface site densities are also input to complete the specification of the state of the surface.

In addition to all the functions that current version is capable of, modified version of SURFACE CHEMKIN will compute the following coverage-dependent energies during the fly of reactor simulation:

a. Heat of formation of surface species using zero-coverage heats of formation and coverage-dependent coefficients.
b. Activation energy of forward reactions using zero-coverage activation energies and coverage-dependent coefficients.
c. Activation energy of reverse reactions using activation energy of forward reactions and thermodynamic consistency of overall reactions.

d. Coverage-dependent activation energy of both forward and reverse reactions using BOC (UBI-QEP) method; the underlying analytical formulas should be supplied as part of CHEMKIN code.

3.4.1 User Characteristics

Modified version of the software is intended for users running CHEMKIN applications that involve SURFACE CHEMKIN modules. Typically, these are the different applications used to perform catalytic reactor simulations that combine kinetics and transport of gas phase and surface species. Specifically, the modified SURFACE CHEMKIN will require the user to know the following:

a. Coverage-dependent heats of formation of surface species. Experimental data on the heats of formation at different coverages is preferable, but theoretical calculations could be used to address the lack of experimental data.
b. Coverage-dependent coefficients in heats of formation. This information can be extracted from (a).
c. Coverage-dependent activation energy of one side of the reaction (either forward or reverse).

3.4.2 Constraints

Since the software product is a modification of the current version of SURFACE CHEMKIN, the constraints that will limit software developer's options for the modified version are same as those for the current version.

3.4.3 Assumptions and Dependencies

Following are the main assumptions involved in proposed modifications:

a. Linear coverage dependence in the heats of formation of surface species.

b. Thermodynamic consistency in the coverage-dependent coefficients for heats of formation; the partial derivative of heat of formation of j^{th} species with respect to coverage of m^{th} species is assumed to be same as the partial derivative of heat of formation of m^{th} species with respect to coverage of j^{th} species.

3.5 Specific Requirements

This section contains the software requirements, describing the inputs to and outputs from software system.

3.5.1 External Interfaces

SURFACE CHEMKIN file consists of 2 parts: the thermo and reaction files. The thermo file corresponds to thermodynamic data of all surface species including NASA polynomial coefficients, while the reaction file corresponds to rate parameters of all the surface reactions. These parts serve as the key input sources to provide various thermodynamic and kinetic parameters. Different inputs are:

1. Coverage-dependent coefficients in the heat of formation of surface species.
2. Heat of formation of surface species at zero coverage.

3. Activation energy of surface reaction at zero coverage.
4. Coverage coefficients for the activation energy.

Different outputs are:

1. Heat of formation computed at a given coverage.
2. Activation energy computed at a given coverage.

Details of each input follow:

a. **Name of item**: Coverage-dependent coefficients in the heats of formation of surface species.

b. **Description of purpose**: Model the coverage dependence in the heats of formation of surface species on the surface coverage of all the species present in the surface mechanism.

c. **Source of input**: Thermo file. The recommendation is to specify the coverage-dependent coefficients starting the fifth line for each surface species. Currently, 4 lines allotted for each surface species are used to input the NASA polynomial coefficients that describe the polynomial expansion for the enthalpy, heat capacity and entropy of the species as functions of temperature.

d. **Valid range, accuracy, and/or tolerance**: Positive or negative real values between $-\infty$ and $+\infty$. The accuracy and tolerance in the coverage-dependent coefficients rely on the experimental or theoretical data used for the calculation of these coefficients.

e. **Units of measure**: Typically, the units are either kcal/mol or kJ/mol.

a. **Name of item**: Heat of formation of surface species at zero coverage.

b. **Description of purpose**: Specify the hypothetical heat of formation of surface species on a clean catalyst surface, when surface coverages of all the species are set to zero.

c. **Source of input**: Thermo file. The recommendation is to specify the heat of formation at zero coverage as a function of the NASA polynomial coefficients.

d. **Valid range, accuracy, and/or tolerance**: Positive or negative real values between $-\infty$ and $+\infty$. The accuracy and tolerance in the heat of formation are dependent on the experimental or theoretical data.

e. **Units of measure**: Typically, the units are either kcal/mol or kJ/mol.

a. **Name of item**: Activation energy of surface reaction at zero coverage.

b. **Description of purpose**: Specify the activation energy of surface reaction, when the surface coverages of all species are set to zero.

c. **Source of input**: Reaction file.

d. **Valid range, accuracy, and/or tolerance**: Positive real values between 0 and $+\infty$. The accuracy and tolerance in the activation energy are based on the experimental or theoretical data used.

e. **Units of measure**: Typically, the units are either kcal/mol or kJ/mol.

a. **Name of item**: Coverage-dependent coefficients in the activation energies of surface reactions.

b. **Description of purpose**: Model the coverage dependence in the activation energies of surface reactions.

c. **Source of input**: Reaction file.

d. **Valid range, accuracy, and/or tolerance**: Positive or negative real values between -∞ and +∞. The accuracy and tolerance in the coverage-dependent coefficients rely on the experimental or theoretical data used for the calculation of these coefficients.

e. **Units of measure**: Typically, the units are either kcal/mol or kJ/mol.

Different outputs are described in detail:

a. **Name of item**: Coverage-dependent heat of formation computed at a given coverage.

b. **Description of purpose**: Calculate the coverage-dependent heats of formation of surface species during the fly of reactor simulation.

c. **Source of output**: SURFACE CHEMKIN output file.

d. **Valid range, accuracy, and/or tolerance**: Positive or negative real values between -∞ and +∞. The accuracy relies on the accuracy of the coverage-dependent coefficients and heat of formation at zero coverage input in the SURFACE CHEMKIN input file.

e. **Units of measure**: Typically, the units are either kcal/mol or kJ/mol.

a. **Name of item**: Coverage-dependent activation energy computed at a given coverage.

b. **Description of purpose**: Calculate the coverage-dependent activation energy of surface reaction during the fly of reactor simulation.

c. **Source of Output**: SURFACE CHEMKIN output file.

d. **Valid range, accuracy, and/or tolerance**: Positive real values between 0 and +∞. The accuracy relies on the accuracy of coverage-dependent coefficients and activation energy at zero coverage.

e. **Units of measure**: Typically, the units are either kcal/mol or kJ/mol.

3.5.2 Underlying Equations for Thermodynamically Consistent Coverage-dependent Surface Kinetics

Below we formulate the kinetics for a general surface mechanism with N_r reversible reactions and N_s species:

$$\nu_r S \Leftrightarrow \nu_p S \,.$$

Different mathematical terms used are explained in the Glossary (Appendix C). Subscript "i", "j" and "m" indicate i^{th} reaction, j^{th} species and m^{th} species, respectively.

Molar production rate (mol/cm^2/s) for either gas or surface species

$$\dot{S} = (\nu_p{}^T - \nu_r{}^T)q \,. \tag{3.2}$$

Rate of progress (mol/cm^2) of i^{th} reaction

$$q_i = k_{f,i}\prod_{k=1}^{K}[s_k]^{\nu_{rik}} - k_{r,i}\prod_{k=1}^{K}[s_k]^{\nu_{pik}} \tag{3.3}$$

Molar concentration (mol/cm^3) of gas species

$$[s_k] = \frac{Y_k \rho}{W_k} \,. \tag{3.4}$$

Molar concentration (mol/cm^2) of surface species

$$[s_k] = \theta_k \Gamma \,. \tag{3.5}$$

Equilibrium relationship between forward and reverse rate constants

$$k_{r,i} = k_{f,i} / K_{eq,conc,i} \,. \tag{3.6}$$

Forward rate constant (appropriate mol-cm-s units) of i^{th} reaction

$$k_{f,i} = A_{f,i} T^{\beta_{f,i}} e^{(-\frac{E_{f,i}}{RT})} \quad (3.7)$$

Equilibrium constant

$$K_{eq,conc,i} = \exp(-\frac{\Delta G_i}{RT}) \times (\frac{RT}{1bar})^{\Delta n_{g,i}} . \quad (3.8)$$

Free energy change of a reaction

$$\Delta G_i = \Delta H_i - T\Delta S_i . \quad (3.9)$$

Coverage-dependent enthalpy (kcal/mol) of j^{th} species

$$H_j = H_j(\underline{\theta} = 0) + \sum_l c_{j,l}\theta_l \quad (3.10)$$

Thermodynamic consistency

$$\frac{\partial H_j}{\partial \theta_m} = \frac{\partial H_m}{\partial \theta_j}, \quad (3.11)$$

or

$$c_{j,m} = c_{m,j} . \quad (3.12)$$

Eq. 3.8, which relates equilibrium constant to change in Gibbs free energy of the reaction, accounts for the changes in number of moles of gas species during the course of reaction. The number of moles of surface species do not change during the course of reaction, since the surface sites are conserved. For example, adsorption of a methyl radical on one vacant site is written as:

$$CH_3 + {}^* \Leftrightarrow CH_3{}^*.$$

Eq. 3.10 which includes a linear coverage-dependence for the enthalpy of reaction is just a convenient assumption in the absence of detailed experimental knowledge of surface coverages. If many data points are available for the experimental surface coverages, higher order terms can be used to model the interactions among different coverages.

3.5.3 Thermodynamic Consistency in Surface Mechanism

Eqs. 3.11 and 3.12 ensure thermodynamic consistency in the coverage-dependent coefficients for enthalpies in that the partial derivative of intensive enthalpy of j^{th} species with respect to coverage of m^{th} species is same as the partial derivative of intensive enthalpy of m^{th} species with respect to coverage of j^{th} species.

In literature, several independent surface experiments and quantum calculations are performed to estimate rate parameters of elementary reactions in a mechanism. Grouping these parameters might violate thermodynamic consistency and the first law of thermodynamics. This problem arises since there are typically more surface reactions than species, but the number of linearly independent reactions is equal to species. Equilibrium constants for each reaction inconsistent with the thermodynamics of overall reaction lead to unphysical rates, equilibria, surface coverages, and steady state concentrations. Thermodynamic constraints of reaction networks have been reviewed and various methods to ensure consistency have been discussed in the literature [29].

3.5.4 Coverage Dependence in Thermodynamic and Rate Parameters

To illustrate the importance of coverage dependence in the heat of formation and activation energy of surface reactions, ethylene epoxidation on Ag(111) is used. Table 3.1 lists the key epoxidation reactions with coverage-dependent activation energies of forward and reverse reactions. The activation energies and heats of formation are functions of the surface coverages of oxygen and ethylene.

Table 3.1 Coverage-dependent Surface Mechanism for Epoxidation on Silver

		Activation Energies (kcal/mol)		**Heat of Reaction (kcal/mol)**
Step #	Reaction	E_f	E_r	ΔH
S1	$O_2 + 2\ AG(S) \Leftrightarrow 2\ O(S)$	0.0	$49.0 + 7.2\theta_{C2H4} - 71.4\theta_O$	$-49.0 - 7.2\theta_{C2H4} + 71.4\theta_O$
S2	$C_2H_4 + AG(S) \Leftrightarrow C_2H_4(S)$	0.0	$8.9 + 3.6\theta_O$	$-8.9 - 3.6\theta_O$
S3	$C_2H_4(S) + O(S) \Leftrightarrow H_2COCH_2(S) + AG(S)$	$14.9 - 32.1\theta_O + 3.6\theta_{C2H4}$	12.5	$2.4 - 32.1\theta_O + 3.6\theta_{C2H4}$
S4	$H_2COCH_2(S) \Leftrightarrow C_2H_4O + AG(S)$	16.0	11.0	5.0
S5	$H_2COCH_2(S) \Leftrightarrow CH_3CHO + AG(S)$	15.7	41.1	-25.4

The coverage-dependent coefficients in the heats of chemisorption are based on the experimental data [30-32]:

$$Q_O(\theta_{C2H4}) = 84.0 + 3.6\ \theta_{C2H4} - 35.7\ \theta_O, \tag{3.13}$$

$$Q_{C2H4}(\theta_O) = 8.9 + 3.6\ \theta_O. \tag{3.14}$$

Self coverage-dependence in the heat of chemisorption of oxygen is particularly important since atomic oxygen is found to be 5 kcal/mol less stable on 0.25 ML than on 0.11 ML oxygen covered silver.

Rates of the elementary reactions are expressed below:

$$r_1 = k_{f,1}[O_2]\theta_v^2 C_t^2 - k_{r,1}\theta_o^2 C_t^2, \tag{3.15}$$

$$r_2 = k_{f,2}[C_2H_4]\theta_v C_t - k_{r,2}\theta_{C2H4} C_t, \tag{3.16}$$

$$r_3 = k_{f,3}\theta_{C_2H_4}\theta_O C_t^2 - k_{r,3}\theta_{OMME}\theta_v C_t^2, \tag{3.17}$$

$$r_4 = k_{f,4}\theta_{OMME} C_t - k_{r,4}[C_2H_4O]\theta_v C_t, \tag{3.18}$$

and

$$r_5 = k_{f,5}\theta_{OMME}C_t - k_{r,5}[CH_3CHO]\theta_v C_t, \tag{3.19}$$

where

k_f, k_r are the rate constants of forward and reverse reactions, θ the coverage of surface species and C_t the surface site density. The concentrations of gas phase species are expressed in mol/cm^3, while site density is expressed in mol/cm^2. Set of ODEs for the rates-of-production of gas and surface species is given below:

$$\frac{d[O_2]}{dt} = -r_1, \tag{3.20}$$

$$\frac{d[C_2H_4]}{dt} = -r_2, \tag{3.21}$$

$$\frac{d[C_2H_4O]}{dt} = r_4, \tag{3.22}$$

$$\frac{d[CH_3CHO]}{dt} = r_5, \tag{3.23}$$

$$\frac{d\theta_O}{dt} = (2r_1 - r_3)/C_t, \tag{3.24}$$

$$\frac{d\theta_{C_2H_4}}{dt} = (r_2 - r_3)/C_t, \tag{3.25}$$

$$\frac{d\theta_{OMME}}{dt} = (r_3 - r_4 - r_5)/C_t, \tag{3.26}$$

and

$$\frac{d\theta_v}{dt} = (-2r_1 - r_2 + r_3 + r_4 + r_5)/C_t. \tag{3.27}$$

The ODEs are solved for experimental conditions observed in literature.

Kestenbaum et al. have measured the selectivities to ethylene oxide in microreactors for different operating temperatures, pressures and molar flow rates of reactants [33]. Series of experiments were conducted for varying temperatures on a Laser-LIGA catalyst at 5 bar, 5 L/h gas flow, 3% C_2H_4, 16.5% O_2 and N_2 as inerts in the feed to reactor. We use the microreactor

conditions to predict the concentration of ethylene oxide under coverage-dependent and independent thermodynamic and rate parameters. Five cases are investigated:

1. coverage-dependent thermodynamic parameters and activation energies, coverage-independent parameters evaluated at oxygen coverage of
2. 0.15
3. 0.10
4. 0.05
5. 0.00

It needs to be mentioned that the surface species are considered for the 5 cases and their coverages are solved for using kinetic model based on 5-step mechanism. Coverage-independent parameters simply mean that the activation energies and heats of reactions are fixed as constants. They dont vary as function of coverages during the course of simulation. Figure 3.1 compares the ethylene oxide concentration predicted by the 5-step kinetic model with and without coverage dependence.

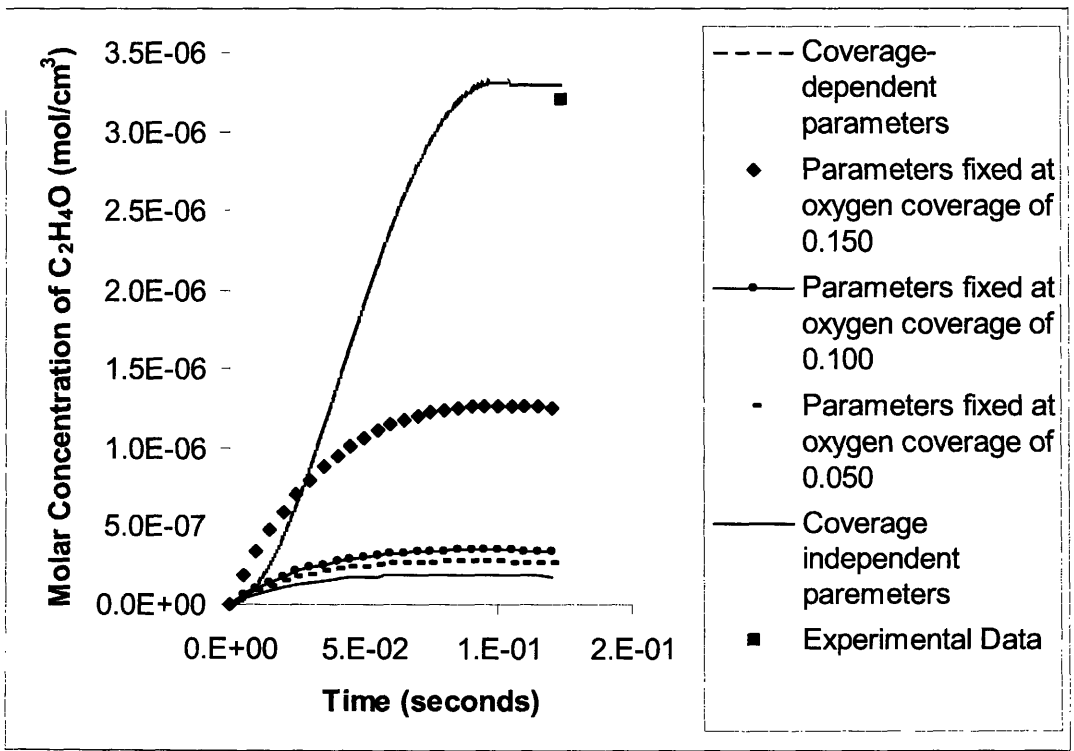

Figure 3.1 Variation of EO Concentration with Time

From Figure 3.1, we observe that the concentration of EO predicted by considering coverage dependence is much higher than that by ignoring it. Ethylene oxide concentration predicted by the coverage-dependent set of parameters is 3.3E-6 mol/cm^3, while the experimentally observed concentration based on the selectivity observed is 3.1E-6 mol/cm^3 for a residence time of 0.124 seconds in the microreactor. Figure 3.2 compares the predicted selectivity against experimental values for various operating conditions under which the microreactor was run. The mole fraction of C_2H_4 is varied from 6.4% to 15.4%, temperature from 275-290C, pressure from 4-5 atm, and residence time from 0.124-0.469 seconds.

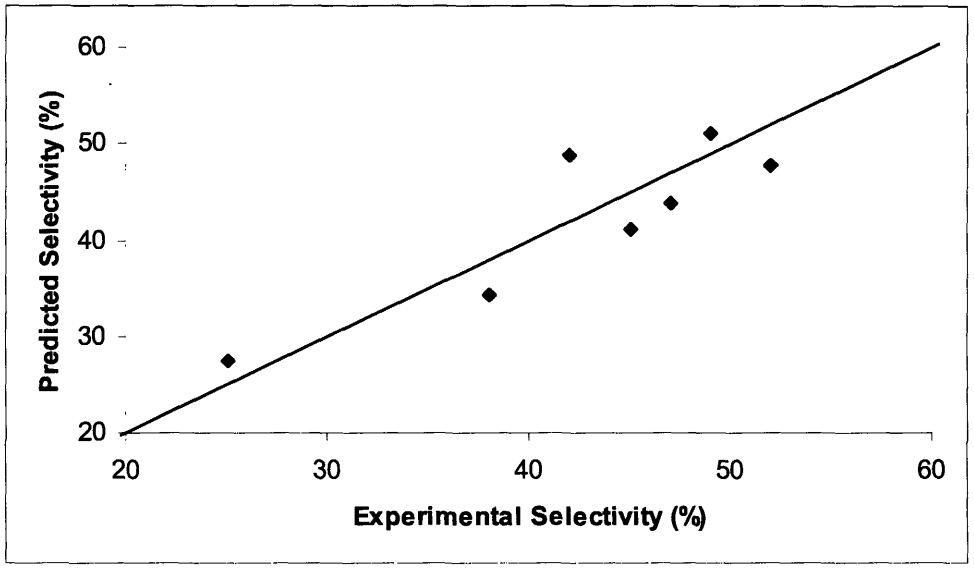

Figure 3.2 Predicted Selectivity Compared against Experimental Selectivity for Various Microreactor Operating Conditions

Figure 3.3 shows the variation of oxygen coverage with the reaction time in the microreactor.

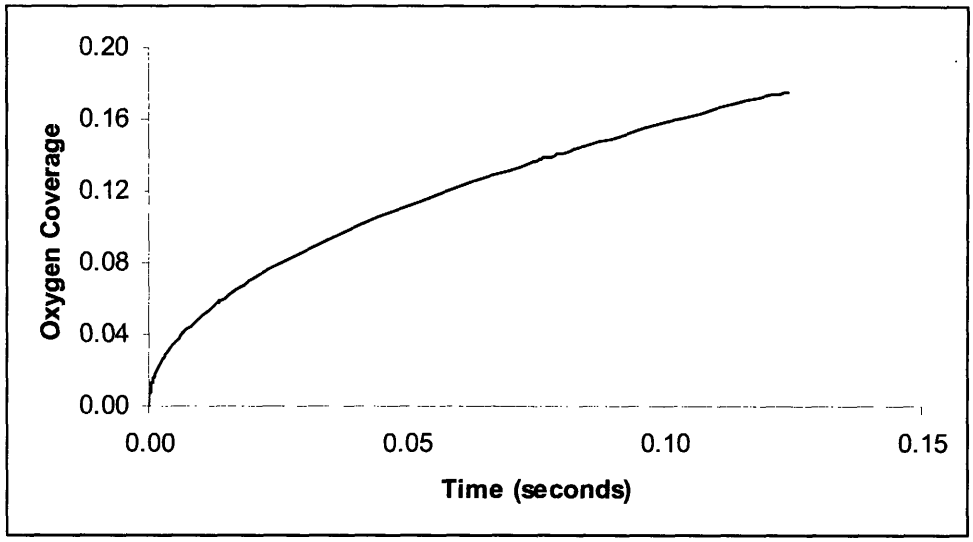

Figure 3.3 Variation of Oxygen Coverage with Time

From Figure 3.3, we observe that the range of oxygen coverage is between 0.00 and 0.16. Oxygen coverage between this range is used to fix the thermodynamic and rate parameters, as shown in Figure 3.1. Figure 3.4 shows the difference between coverage-dependent and independent thermodynamic and rate parameters. For illustration, heat of chemisorption of oxygen and activation energy for dissociative adsorption of oxygen (reverse of Step 1) are plotted as function of reaction time.

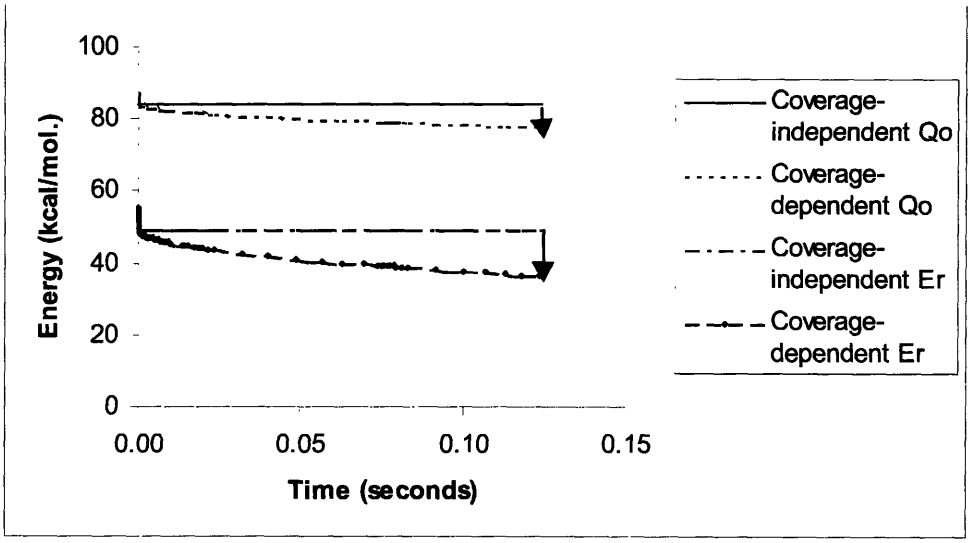

Figure 3.4 Coverage-independent and Dependent Chemisorption Enthalpy and Activation Energy of Dissociative Oxygen Adsorption

From Figure 3.4, we observe that the coverage-dependent parameters, which vary as a function of time, are quite different from the coverage-independent ones evaluated at zero-coverage limits. Changes in activation energy result in significant change in concentrations of epoxide, since the Arrhenius rate constant is exponentially dependent on the activation energy of reaction (See Figure 3.1).

3.6 Summary

In this chapter, we have presented the important underlying equations to describe the elementary kinetics for a general surface mechanism. Due to the coverage dependence of thermochemical and rate parameters, a Software Requirements Specification (SRS) has been presented to modify the coverage-dependent functionality in SURFACE CHEMKIN. Purpose of the modification is to include dependencies in both thermochemical and rate parameters which evolve during the course of reactor simulation as the surface coverages change. We recommend that the key inputs

including coverage-dependent coefficients in the heats of formation of surface species, zero-coverage heat of formation of surface species are specified in the thermo file, while zero-coverage activation energy of surface reaction and coverage coefficients of activation energy are specified in the reaction file. The suggested modifications in SRS are intended to serve CHEMKIN users performing reactor simulations that involve surface chemistry. Underlying equations explain the thermodynamically consistent coverage-dependent surface mechanism.

References

1. L. F. Shampine (1981). Type-insensitive ODE codes based on implicit A-stable formulas. *Mathematics of Computation,* 36, 499-510.
2. L. F. Shampine (1982). Type-insenstitive codes based on implicit A(α)-stable formulas. *Mathematics of Computation.* 39, 109-123.
3. L. F. Shampine (1982). Solving ODEs quasi-steady state. *Numerical Integration of Differential Equations and Large Linear Systems* (J.Hinze ed.) 234-245. Springer-Verlag.
4. A. C. Hindmarsh (1983). ODEPACK, a systematized collection of ODE solvers. In "Scientific Computing" (R. S. Stepleman et al., eds.) Vol. 1, pp. 55-64. IMACS.
5. L. R. Petzold (1982). A description of DASSL: A differential-algebraic system solver. Sandia National Laboratory Reports SAND 82-8637. Sandia Lab. Albuquerque, New Mexico.
6. L. R. Petzold (1983). Automatic selection of methods for solving stiff and nonstiff systems of ODES. *SIAM Journal of Scientific and Statistical Computing*, 4, 136-148.
7. K. Miller and R. Miller (1981). Moving finite elements. *SIAM Journal of Numerical Analysis*, 18, 1019-1032.
8. R. J. Gelinas, S. K. Doss and K. Miller (1981). The moving finite element method: Application to general partial differential equations with multiple large gradient. *Journal of Computational Physics.* 40, 202-249.
9. S. F. Davis and J. E. Flaherty (1982). An adaptive finite element method for initial boundary-value problems for partial differential equations. *SIAM Journal of Scientific and Statistical Computing*, 3, 6-27.
10. A. B.White (1983). On the numerical solution of initial initial/boundary-value problems in one space dimension. *SIAM Journal of Numerical Analysis*, 19, 683-697.
11. H. A. Dwyer, R. J. Kee and B. R.Sanders (1980). Adaptive grid methods for problems in fluid mechanics and heat transfer. *AIAA Journal,* 18, 1205-1212.
12. H. A. Dwyer, M. D. Smooke and R. J. Kee (1982). Adaptive gridding for finite difference solutions to heat and mass transfer problems. *Numerical Grid Generation* (J. F.Thompson, ed.) pp.339-356. North-Holland, Publ. Amsterdam.
13. J. H. Bolstad (1982). An adaptive finite difference method for hyperbolic systems in one space dimension. Ph.D. Thesis, Stanford University, Stanford, California.
14. M. Berger and J. Oliger (1983). Adaptive mesh refinement for hyperbolic partial differential equations. *Rep. NA-83-02.* Computer Science Department, Stanford Univeristy, Stanford, California.
15. M. D. Smooke and M. L. Koszykowski (1983). Fully adaptive one-dimensional mixed initial boundary-value problems with applications to unstable problems in combustion. *SIAM Journal of Numerical Analysis.*
16. M. E. Coltrin, R. J. Kee and F. M. Rupley. Surface CHEMKIN: A Generalized formalism and interface for analyzing heterogeneous chemical kinetics at a gas-surface interface (1991). *International Journal of Chemical Kinetics*, 23, 1111-1128.
17. H. Sellers (2003). Entropies of desorption from temperature programmed desorption data: Trends and applications to rate constant determinations. *Journal of Physical Chemistry B,* 107, A-C.
18. V. E. Vasserberg, A. A. Balandin, F. E. Englina and T. V. Georgievskaya (1966). Number of active sites on aluminum oxide catalysts and the occurrence of surface chains in catalytic dehydration. *Doklady Akademii Nauk SSSR*, 169, 861-864.

19. M. E. Coltrin, R. J. Kee and F. M. Rupley (1991). Surface Chemkin: a general formalism and software for analyzing heterogeneous chemical kinetics at a gas-surface interface. *International Journal of Chemical Kinetics*, 23, 1111-1128.
20. E. Shustorovich (1990). The Bond-Order conservation approach to chemisorption and heterogeneous catalysis: Applications and implications. *Advances in Catalysis*. 37, 101-163.
21. E. Shustorovich and H. Sellers (1998). The UBI-QEP method: A practical theoretical approach to understanding chemistry on transition metal surfaces. *Surface Science Reports*, 31, 1-119.
22. E. Shustorovich and A. T. Bell (1993). Decomposition and reduction of NO on transition metal surfaces: bond order conservation Morse potential analysis. *Surface Science*, 298, 127-138.
23. H. Sellers (1993). On analytic potential functions for reactions on metal surfaces: The case of H*--->2H on the liquid mercury surface. *Journal of Chemical Physics*, 98, 627-633.
24. P. Paredes-Olivera, E. M. Patrito and H. Sellers (1995). Direct synthesis of methanol over metallic catalyst. *Surface Science*, 327, 330-357.
25. H. Sellers and E. Shustorovich (1996). Coordination modes and bonding of sulfur oxides on transition metal surfaces: combined ab initio and BOC-MP results. *Surface Science*, 346, 322-336.
26. E. M. Patrito, P. Olivera, and H. Sellers (1997). On the nature of the SO^{2-}_4/Ag(111) and SO^{2-}_4/Au(111) surface bonding. *Surface Science*, 380, 264-282.
27. H. Sellers and E. Shustorovich (2002). Intrinsic activation barriers and coadsorption effects for reactions on metal surfaces: Unified formalism within the UBI-QEP approach. *Surface Science Reports*, 504, 167-182.
28. W. Li, C. Stampfl and M. Scheffler (2002). Oxygen adsorption on Ag(111): A density-functional theory investigation. *Physical Review B*, 65, 1-19.
29. A. B. Mhadeshwar, H. Wang and D. G. Vlachos (2003). Thermodynamic consistency in microkinetic development of surface reaction mechanisms. *Journal of Physical Chemistry B*, 107, 12721-12733.
30. W. Li, C. Stampfl and M. Scheffler (2002). Oxygen adsorption on Ag(111): A density-functional theory investigation. *Physical Review B*, 65, 1-19.
31. M. A. Barteau and R. J. Madix (1980). The adsorption of molecular oxygen species on Ag(110). 97, 101-110.
32. B. Kruger and C. Benndorf (1986). Ethylene and ethylene oxide adsorption on Ag(110), *Surface Science*, 178, 704-715.
33. H. Kestenbaum, A. Lange de Oliviera, W. Schmidt and F. Schuth (2002). Silver catalyzed oxidation of ethylene to ethylene oxide in a microreaction system. Industrial Engineering and Chemistry Research, 41, 710-719.

Chapter 4: Computational Methodology for Thermochemical and Thermodynamically Consistent Rate Parameters

This chapter presents the development and implementation of a computational methodology for estimating thermochemical and rate parameters of surface reactions. Section 4.2 describes the procedures to calculate thermochemical and rate parameters of surface reactions. The formulas for chemisorption enthalpies, activation energies, entropies, heat capacities, and preexponential factors are derived. The computational procedures are presented as flowsheets. Section 4.3 includes example problems for the calculation of thermochemical and rate parameters. Section 4.4 compares the predicted parameters against literature values for various catalysts.

4.1 Introduction

Detailed consistent surface kinetic models are invaluable to accurately predict the physics and chemistry of surface reactions. The predictions make reasonable extrapolations for a broad range of reactor conditions, not limited to data available in literature. Constructing kinetic models requires a large number of generally unknown thermochemical and rate parameters, which need to be rapidly estimated. Unity Bond Index-Quadratic Exponential Potential (UBI-QEP) approach based on Bond Order Conservation (BOC) theory has been used to compute the chemisorption enthalpies and activation energies for reactions involving atoms and diatomics [1-8]. Here we extend the UBI-QEP method to estimate thermochemical and kinetic parameters

for polyatomics. Collision and transition state theory have been used in the literature to initially estimate preexponential factors either for calculating yield bounds or optimizing kinetic parameters for catalysts [9-12]. A general and flexible formalism with mass-action kinetics for surface reactions has been presented and incorporated into the CHEMKIN program suite by Kee, Rupley, and coworkers [13-14]. Mathematical expressions pertaining to thermodynamic constraints have been reviewed [15]. In the literature, coverage dependence has been incorporated in the activation energies [11].

It is difficult to construct and solve a thermodynamically-consistent detailed catalyst model for the case where the thermodynamic and rate parameters depend on coverages using existing publicly-available software. It also requires computational efforts to estimate all the required activation energies consistent with the thermodynamics at all possible coverages. Currently, literature models for catalysis contain irreversible steps and are thermodynamically inconsistent since no convenient software for this purpose is available. The present work is to integrate the methods for estimating thermochemical and rate parameters of surface reactions into an automated program. Specifically, the goal is to develop a computational methodology for thermodynamically consistent parameters of a catalyst simulation. A computer program based on Unity Bond Index-Quadratic Exponential Potential (UBI-QEP) model, developed by Sellers, calculates the chemisorption enthalpies and activation energies for diatomics adsorbed on transition metals. Our methodology extends the UBI-QEP approach to polyatomic adsorbates with empirical modifications to the underlying theory. Similar to diatomic adsorabtes, separate formulas for chemisorption enthalpies are derived for closed-shell and free-radical polyatomic adsorbates.

The current work makes the following contributions to surface kinetics on transition metals:

- Temperature/coverage-dependent heats of formation, heat capacities, and entropies of surface species.
- Tight physical bounds of preexponential factors for generic reaction types.
- Analytical expressions of activation energies.
- Thermodynamically consistent Chemkin® formatted output.

4.2 Procedures

In this section, we present the procedures to calculate thermochemical and rate parameters of surface reactions. In Subsection 4.2.1, we explain the Unity Bond Index-Quadratic Exponential Potential (UBI-QEP) theory used to calculate molecular chemisorption enthalpies and activation energies. In Subsection 4.2.2, we present formulas and procedures to estimate the enthalpies. Corresponding formulas and procedures for activation energies are provided in Subsection 4.2.3. Methodology for calculating temperature-dependent enthalpies, heat capacities and entropies of surface species are explained in Subsection 4.2.4. In Subsection 4.2.5, collision theory, transition state theory and surface diffusion are used to estimate preexponential factors of forward reactions. Thermodynamic consistency is used to estimate the rates of all the reverse reactions.

4.2.1 UBI-QEP Approach and the Variational Procedure for Chemisorption Enthalpies of Atoms, Diatomic Molecules

To impart thermodynamic consistency in surface mechanisms and to avoid the great effort involved in accurate first-principle quantum calculations, UBI-QEP approach also known as Bond Order Conservation theory (BOC) is increasingly tried for estimating chemisorption enthalpies and activation energies of diatomics on different transition metal catalysts [1-8]. Energy of interaction between the 2 bonded atoms in surface species is described as a Morse potential, which is quadratic exponential function of the inter-atomic radius. This potential is expressed as a function of bond index (x) and bond energy (BE) of chemical bond between the 2 atoms:

$$E = BE(x^2 - 2x). \tag{4.1}$$

Bond index, a normalized bond order as defined by Shustorovich & Sellers (1998), is an exponential function of inter-atomic radius or bond distance r. The bond index characterizes the atomic wavefunctions with exponential radial expressions of atomic distances:

$$x = e^{(\frac{r-r_0}{b})}, \tag{4.2}$$

where r_0 is the inter-atomic radius at equilibrium and b is the normalization constant. Note that the bond index is not the normal bond order (defined as the number of electron pairs involved in a bond between 2 atoms). Bond orders for single and double bonds are 1 and 2. When r is the inter-atomic radius r_0 for a double bond, bond index (x) is 1 and the bond order is 2. For chemisorbed species in the UBI-QEP model, most of the bond indices $x<1$, even though some of them might have conventional bond orders greater than 1.

In Eq. 4.1, the bond energy (BE) between a contact atom in the adsorbate and the surface atom is taken to be the hypothetical mono-coordinated heat of chemisorption of that atom (Q_0). The bond energy between 2 neighboring atoms in the adsorbate part is considered to be the gas phase dissociation energy (D) of the bond. UBI-QEP energy of a surface species is the sum of interaction energies of all bonds between each contact atom and neighboring atoms; the neighboring atoms could be either metal atom or other atoms in the adsorbate. The UBI constraint states that the total valence of a diatomic is conserved to unity, and each fractional valence contributes to bond or coordination that an atom is involved with its neighbors in the molecule. Energy E is binding energy to surface and minimization of the energy with respect to constraint results in molecular chemisorption enthalpy.

Figure 4.1 shows a diatomic molecule AB attached via bridge coordination of A and B with the contact atoms in an on-top site with A and B bound to each other.

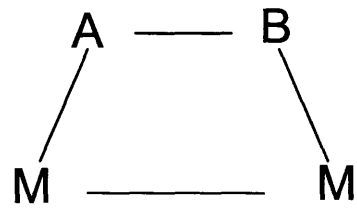

Figure 4.1 Bridge Coordination of Diatomic Molecule AB with Contact Atoms in an On-Top Site

We explain the variational procedure used to derive chemisorption enthalpy of diatomic molecules in the UBI-QEP model. We minimize the energy of surface species,

$$\min E(x_{AB}, x_A, x_B), \tag{4.3}$$

subject to

$$\sum_i x_i = 1, \tag{4.4}$$

where

$$E = D_{AB}(x_{AB}^2 - 2x_{AB}) + Q_{0A}(x_A^2 - 2x_A) + Q_{0B}(x_B^2 - 2x_B) \quad (4.5)$$

Using the method of Lagrange multipliers,

$$\frac{d}{dx_i}\left\{E(x_{AB}, x_A, x_B) + \lambda(\sum_i x_i - 1)\right\} = 0 \quad (4.6)$$

Evaluating the derivative and rearranging:

$$x_A = 1 - \frac{\lambda}{2Q_{0A}}, \quad (4.7)$$

$$x_B = 1 - \frac{\lambda}{2Q_{0B}}, \quad (4.8)$$

$$x_{AB} = 1 - \frac{\lambda}{2D_{AB}}, \quad (4.9)$$

where

$$\lambda = \frac{4}{\frac{1}{D_{AB}} + \frac{1}{Q_{0A}} + \frac{1}{Q_{0B}}} \quad (4.10)$$

At this optimal choice of all the x's, we find the minimum, E_{min}:

$$E_{\min} = Q_{0A}\left(\frac{\lambda^2}{4Q_{0A}^2} - 1\right) + Q_{0B}\left(\frac{\lambda^2}{4Q_{0B}^2} - 1\right) + D_{AB}\left(\frac{\lambda^2}{4D_{AB}^2} - 1\right). \quad (4.11)$$

Chemisorption energy is the difference between energy E_{gas} of the gas phase bond ($-D_{AB}$) and energy of the surface species (E_{min}):

$$Q_{chemisorption} = Q_{0A} + Q_{0B} - \frac{4}{\frac{1}{Q_{0A}} + \frac{1}{Q_{0B}} + \frac{1}{D_{AB}}}. \quad (4.12)$$

Heats of chemisorption used in the above expressions are the mono-coordinated heats of chemisorption. When an adsorbate atom is bonded to several surface atoms (eg: in a hollow site), the mono-coordinated heat of chemisorption (Q_{0A}) is the bond energy with each contact atom. Q_{0A} is typically backed out from the experimental chemisorption heat (Q_A) and the coordination number (n) based on the UBI-QEP approach:

$$Q_{0A} = \frac{Q_A}{2 - \frac{1}{n}}. \tag{4.13}$$

Here, n might be 3, 4 or 5 depending on whether the experimental heat of adsorption, $Q_A(n)$ corresponds to a three-fold fcc(111) or hcp(001) hollow, four-fold fcc(100) hollow or a five-fold bcc(100) hollow adsorption. The variational procedure to derive chemisorption enthalpy of an atom A bound to n metal atoms in a hollow site is:

$$\min E(x_{A1},...,x_{An}) \tag{4.14}$$

subject to

$$\sum_i x_i = 1, \tag{4.15}$$

where

$$E = Q_{0A}\sum_{i=1}^{n}(x_{Ai}^2 - 2x_{Ai}). \tag{4.16}$$

Using Lagrange multipliers and evaluating the derivatives:

$$x_{Ai} = 1 - \frac{\lambda}{2Q_{0A}}, \qquad \text{for i=1,...,n} \tag{4.17}$$

where

$$\lambda = 2Q_{0A}(1 - \frac{1}{n}) \tag{4.18}$$

For the optimal choices of x, E_{min}:

$$E_{\min} = Q_{0A}\sum_{i=1}^{n}(\frac{\lambda^2}{4Q_{0A}^2}-1). \tag{4.19}$$

Chemisorption energy of the atom is simply the negative of the energy of the surface species (E_{min}):

$$Q_{chemisorption} = Q_{0A}(2-\frac{1}{n}) \tag{4.20}$$

Eq. 4.13, which relates mono-coordinated chemisorption enthalpy to the physically observable and experimental atomic chemisorption enthalpy, is simply an algebraic manipulation of Eq. 4.20.

Figure 4.2 shows diatomic molecule AB attached via on-top coordination with A end down and attached to n metal atoms.

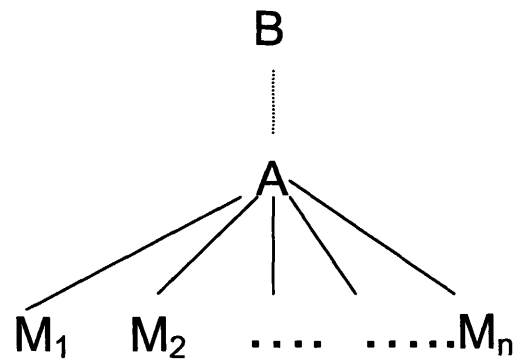

Figure 4.2 On-top Coordination of Diatomic Molecule AB with A end Down

The variational procedure is described below.

$$\min E(x_{AB}, x_{A1}, ..., x_{An}) \tag{4.21}$$

subject to

$$\sum_i x_i = 1, \tag{4.22}$$

where

$$E = D_{AB}(x_{AB}^2 - 2x_{AB}) + Q_{0A}\sum_{i=1}^{n}(x_{Ai}^2 - 2x_{Ai}) \quad (4.23)$$

Using Lagrange multipliers and evaluating the derivatives:

$$x_{Ai} = 1 - \frac{\lambda}{2Q_{0A}}, \qquad \text{for i=1,...,n} \quad (4.24)$$

$$x_{AB} = 1 - \frac{\lambda}{2D_{AB}}, \quad (4.25)$$

where

$$\lambda = \frac{2n}{\frac{1}{D_{AB}} + \frac{n}{Q_{0A}}} \quad (4.26)$$

For the optimal choices of x, E_{min}:

$$E_{\min} = D_{AB}(\frac{\lambda^2}{4D_{AB}^2} - 1) + Q_{0A}\sum_{i=1}^{n}(\frac{\lambda^2}{4Q_{0A}^2} - 1). \quad (4.27)$$

Chemisorption energy of the diatomic molecule is the difference between energy of the gas phase bond ($-D_{AB}$) and energy of the surface species:

$$Q_{chemisorption} = \frac{Q_{0A}^2}{\frac{Q_{0A}}{n} + D_{AB}}. \quad (4.28)$$

It has been found that Eq. 4.28 gives fairly accurate estimates for diatomics that weakly chemisorb (~10 – 35 kcal/mole binding); this set includes closed shell diatomics like CO and N_2, and radicals with delocalized unpaired electrons like NO and O_2. However, this formula does not work well for radicals with localized unpaired electrons such as NH and OH. In these cases, Sellers suggests using the full atomic chemisorption energy Q_A rather than Q_{0A}/n.

We setup the variational procedure for diatomic AB with strong binding and coordinated via atom A.

$$\min E(x_{AB}, x_A), \quad (4.29)$$

subject to

$$\sum_i x_i = 1, \tag{4.30}$$

where

$$E = D_{AB}(x_{AB}^2 - 2x_{AB}) + Q_A(x_A^2 - 2x_A). \tag{4.31}$$

Evaluating the derivatives:

$$x_A = 1 - \frac{\lambda}{2Q_A}, \tag{4.32}$$

$$x_{AB} = 1 - \frac{\lambda}{2D_{AB}}, \tag{4.33}$$

where

$$\lambda = \frac{2}{\frac{1}{D_{AB}} + \frac{1}{Q_A}}. \tag{4.34}$$

Chemisorption energy is:

$$Q_{chemisorption} = \frac{Q_A^2}{Q_A + D_{AB}}. \tag{4.35}$$

Monovalent radicals having tetravalent central atoms such as CH_3 are expected to have intermediate binding, with chemisorption enthaly in the range 36-45 kcal/mol. Molecular chemisorption enthalpies of intermediate binding are assumed as the arithmetic average of the enthalpies of weak and strong binding:

$$Q_{chemisorption} = 0.5\left(\frac{Q_{0A}^2}{\frac{Q_{0A}}{n} + D_{AB}} + \frac{Q_A^2}{Q_A + D_{AB}}\right). \tag{4.36}$$

4.2.2 Chemisorption Enthalpies of Polyatomic Molecules

Sellers and Shustorovich have given formulas for estimating the chemisorption enthalpies of atoms and diatoms [8]. Here we extend the concept to estimate the chemisorption enthalpies of polyatomic molecules. Figure 4.3 shows a polyatomic molecule attached via asymmetric bridge coordination with the contact atoms A and B in an on-top site, and the 2 atoms bound to each other.

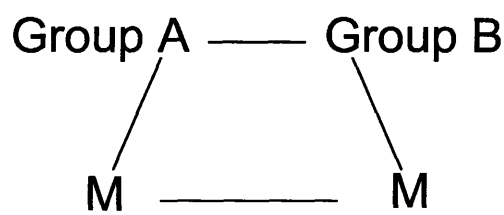

Figure 4.3 Asymmetric Bridge Coordination of Polyatomic with Contact Atoms A and B in an On-top Site

We setup the variational procedure to estimate the molecular chemisorption enthalpy:

$$\min E\left(x_{AB}, x_{GroupA}, x_{GroupB}\right), \tag{4.37}$$

subject to

$$\sum_i x_i = 1, \tag{4.38}$$

where

$$E = D_{AB}(x_{AB}^2 - 2x_{AB}) + Q_{0GroupA}(x_{GroupA}^2 - 2x_{GroupA}) + Q_{0GroupB}(x_{GroupB}^2 - 2x_{GroupB}) \tag{4.39}$$

Using Lagrange multipliers and evaluating the derivatives,

$$x_{GroupA} = 1 - \frac{\lambda}{2Q_{0GroupA}}, \tag{4.40}$$

$$x_{GroupB} = 1 - \frac{\lambda}{2Q_{0GroupB}}, \tag{4.41}$$

$$x_{AB} = 1 - \frac{\lambda}{2D_{AB}}, \tag{4.42}$$

where

$$\lambda = \frac{4}{\frac{1}{D_{AB}} + \frac{1}{Q_{0GroupA}} + \frac{1}{Q_{0GroupB}}}. \tag{4.43}$$

E_{min} at the optimal choice of x's is:

$$E_{\min} = Q_{0GroupA}\left(\frac{\lambda^2}{4Q_{0GroupA}^2} - 1\right) + Q_{0GroupB}\left(\frac{\lambda^2}{4Q_{0GroupB}^2} - 1\right) + D_{AB}\left(\frac{\lambda^2}{4D_{AB}^2} - 1\right). \tag{4.44}$$

Chemisorption energy is the difference between energy E_{gas} of the gas phase bond ($-D_{AB}$) and energy of the surface species (E_{min}):

$$E_{chemisorption} = Q_{0GroupA} + Q_{0GroupB} - \frac{4}{\frac{1}{Q_{0GroupA}} + \frac{1}{Q_{0GroupB}} + \frac{1}{D_{AB}}}. \tag{4.45}$$

Since Group A is attached via on-top coordination with the A end down and connected to n metal atoms, Eq. 4.28 is used to derive the chemisorption enthalpy of the group:

$$Q_{0GroupA} = \frac{Q_{0A}^2}{\frac{Q_{0A}}{n} + D_{reduced\_GroupA}}. \tag{4.46}$$

where $D_{reduced\_GroupA}$ is a function of the dissociation energies of all the bonds attached to A. Similarly, the chemisorption enthalpy of Group B attached via on-top coordination with the B end down and connected to n metal atoms is:

$$Q_{0GroupB} = \frac{Q_{0B}^2}{\frac{Q_{0B}}{n} + D_{reduced\_GroupB}}. \tag{4.47}$$

Now, we derive the expression for $D_{reduced\_GroupA}$ and hence, the chemisorption enthalpy for GroupA. Assume that there are m atoms, C_1, C_2, ..., C_m in Group A and n metal atoms, M_1, M_2, ..., M_n that are attached to A. The variational procedure for the chemisorption enthalpy of Group A is:

$$\min E(x_{AC1},...,x_{ACm},x_{A1},...,x_{An}) \tag{4.48}$$

subject to

$$\sum_{i=1}^{m} x_{ACi} + \sum_{j=1}^{n} x_{Ai} = m \tag{4.49}$$

,

where

$$E = \sum_{i=1}^{m} D_{ACi}(x_{ACi}^2 - 2x_{ACi}) + Q_{0A}\sum_{j=1}^{n}(x_{Ai}^2 - 2x_{Ai}) \tag{4.50}$$

.

Using Lagrange multipliers and evaluating the derivatives,

$$x_{ACi} = 1 - \frac{\lambda}{2D_{ACi}}, \quad \text{for i =1,...,m} \tag{4.51}$$

$$x_{Aj} = 1 - \frac{\lambda}{2Q_{0A}}, \qquad \text{for j =1,...,n} \tag{4.52}$$

where

$$\lambda = \frac{2n}{\dfrac{n}{Q_{0A}} + \dfrac{1}{D_{reduced\_GroupA}}} \tag{4.53}$$

.

and

$$D_{reduced\_GroupA} = \frac{1}{\sum_{i=1}^{m} \dfrac{1}{D_{ACi}}} . \tag{4.54}$$

E_{min} at the optimal choice of x's is:

$$E_{\min} = \frac{\lambda^2}{4}\left(\frac{n}{Q_{0A}} + \frac{1}{D_{reduced}}\right) - nQ_{0A} - \sum_{i=1}^{m} D_{ACi} \,. \tag{4.55}$$

Chemisorption energy is the difference between energy E_{gas} of the gas phase bonds and energy of the surface species (E_{min}).

Here,

$$E_{gas} = -\sum_{i=1}^{m} D_{ACi} \,. \tag{4.56}$$

$$E_{chemisorption} = nQ_{0A} - \frac{\lambda^2}{4}\left(\frac{n}{Q_{0A}} + \frac{1}{D_{reduced\_GroupA}}\right). \tag{4.57}$$

The chemisorption enthalpy of Group A simplifies to:

$$Q_{0GroupA} = \frac{Q_{0A}^2}{\frac{Q_{0A}}{n} + D_{reduced\_GroupA}}. \tag{4.58}$$

Hence, $D_{reduced\_GroupA}$ is the reciprocal of sum of the reciprocals of dissociation energies of all the bonds attached to atom A in Group A. Similarly, $D_{reduced\_GroupB}$ is the reciprocal of sum of the reciprocals of dissociation energies of all the bonds attached to atom B in Group B.

Symmetric dicoordination is a special case of asymmetric dicoordination where the 2 contact atoms are same, designated as A and Group A is same as Group B, designated as "Group" in common. Substiuting $Q_{0GroupA} = Q_{0GroupB} = Q_{0Group}$ and $D_{AB} = D_{AA}$ in Eq. 4.45 results in:

$$Q_{chemisorption} = \frac{2Q_{0Group}^2}{Q_{0Group} + 2D_{AA}}. \tag{4.59}$$

where

$$Q_{0Group} = \frac{Q_{0A}^2}{\frac{Q_{0A}}{n} + D_{reduced\_Group}}. \tag{4.60}$$

Figure 4.4 shows the chelating coordination of the molecule A-X-B with atoms A and B bound to the surface. In the binding of chelates, X is considered far from the catalyst surface so

that there is no significant X-surface bonding. An example of chelating coordination is the adsorption of HCOOH.

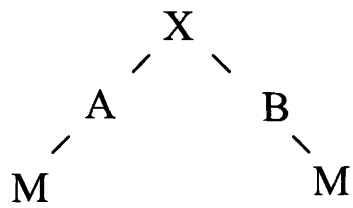

Figure 4.4 Chelating Coordination

Chelating coordination is a special case of asymmetric dicoordination, where A and B are not bonded to each other, but connected through a common atom or group of atoms X. Substituting $D_{AB} = 0$ in Eqs. 4.43 and 4.45 results in:

$$Q_{chemisorption} = Q_{0AX} + Q_{0BX} \tag{4.61}$$

For the general case when atoms A and B are attached to n metal atoms, the chemisorption enthalpies for Groups AX and BX are:

$$Q_{0AX} = \frac{Q_{0A}^2}{\frac{Q_{0A}}{n} + D_{reduced\_GroupAX}}, \tag{4.62}$$

and

$$Q_{0BX} = \frac{Q_{0B}^2}{\frac{Q_{0B}}{n} + D_{reduced\_GroupBX}}. \tag{4.63}$$

Carboxylates A=O, X=CH and B=O belong to the "chelating" category, with essentially only one strong bond to the surface. Stable heterocycle such as surface oxametallacyle has more than one strong bond on the surface. For example, oxametallacycle observed during surface studies in ethylene epoxidation contain A=O, X=CH_2, B=CH_2, hence there are two strong bonds to the surface. Difference between the bonding nature of carboxylates and oxametallacycles is due to the electronic configuration of the middle group X. If X is CH or N, there is the possibility of forming an AX or XB double bond. It is energetically favorable to pull one of the end groups up

off the surface and dissociate the surface-adsorbate bond. When X is CH_2, the middle atom (in this case carbon) is already saturated and hence cannot form any double bond. Thus, there is no stable intermediate formed if either Atom A or B is pulled off the surface. In the chelating ligands, there is only one strong bond because the most likely resonance form has one of the atoms (A or B) not chemically bonded to the surface. For example, for O-CH-O on a surface, the most likely resonance form is M-O-CH=O, with only a single bond to the surface. Hence, the formulas for chelating ligands give weaker binding than ordinary double-bonded ligands like $O\text{-}CH_2\text{-}O$ which do not have any significant resonance form other than $M\text{-}O\text{-}CH_2\text{-}O\text{-}M$ with two bonds to the surface. Similarly for allyl, the main resonance form is $M\text{-}CH_2\text{-}CH{=}CH_2$ with only one M-C bond. But, if cyclopropane is adsorbed on the catalyst surface and the ring opened up, $M\text{-}CH_2\text{-}CH_2\text{-}CH_2\text{-}M$ with two M-C bonds is formed. In the procedure for estimating molecular chemisorption enthalpies, we have included a rule to decide which intermediates have chelating interactions as opposed to forming stable heterocycles on the surface. If the adsorbate is of the form A-X-B and atoms A and B are bound to the surface, the rule identifies it to be polyatomic. Chelating coordination is the case where the Lewis structure only has one bond to the surface, distinct from multiple independent bonds to the surface in the heterocyclic case. If the coordination is chelating, the estimation rule uses the formula for chelating coordination. If the molecule forms a stable heterocycle on the surface, the formula for polyatomic asymmetric coordination is used.

In this subsection, UBI-QEP theory is simply extended to derive the chemisorption enthalpies of polyatomic molecules. Each polyatom is treated as a pseudo diatom which is a combination of 2 groups of atoms. Chemisorption enthalpy of each group is derived as a function of mono-coordinated enthalpy of contact atom and the reduced sum of bond

dissociation energies. However, the chemisorption enthalpies predicted by the extended UBI-QEP theory do not match the experimental data for polyatomics (See Table 4.11). It is a significant conclusion of our work that the direct extension of the UBI-QEP theory does not predict accurate chemisorption enthalpies. Since the equations do not work, we decide to empirically modify the UBI-QEP theory to predict accurate chemisorption enthalpies for polyatomics.

In this modification, the reduced sum of dissociation energies of bonds attached to contact atom (atom A) in a group of atoms (Group A) in a polyatomic molecule is replaced by the regular sum of the bond dissociation energies:

$$D_{GroupA} = \sum_{i=1}^{m} D_{ACi}\,, \tag{4.64}$$

where there are m atoms, C_1, C_2, …, C_m in Group A that are attached to A. With this proposition, the new set of formulae for chemisorption enthalpies of group of atoms is:

$$Q_{0GroupA} = \frac{Q_{0A}^2}{\frac{Q_{0A}}{n} + D_{GroupA}}, \tag{4.65}$$

$$Q_{0GroupB} = \frac{Q_{0B}^2}{\frac{Q_{0B}}{n} + D_{GroupB}}, \tag{4.66}$$

$$Q_{0Group} = \frac{Q_{0A}^2}{\frac{Q_{0A}}{n} + D_{Group}}, \tag{4.67}$$

$$Q_{0AX} = \frac{Q_{0A}^2}{\frac{Q_{0A}}{n} + D_{GroupAX}}, \tag{4.68}$$

and

$$Q_{0BX} = \frac{Q_{0B}^2}{\frac{Q_{0B}}{n} + D_{GroupBX}}. \tag{4.69}$$

Instead of taking the view that the electrons from the bonds in the adsorbate are moving to form bonds to the surface, as UBI-QEP theory suggests, one does better to consider how electrons

from the metal can fit into the valence-shell vacancies and antibonding orbitals on the adsorbate. A modified version of UBI-QEP theory that counts these vacancies instead of the number of bonds gives qualitatively correct results, but we have not found any theory as accurate as the empirical formulas we recommend for polyatomics, Eqs. 4.64-4.69 and Table 4.2.

As explained in Section 4.2.1, separate UBI-QEP treatments are applied for the molecular chemisorption enthalpies of radicals and complete species. UBI-QEP formulas for strong binding are used for NH_2 radical, intermediate binding are used for CH_3 and C_2H_5 radicals, and weak binding for all the complete species. Table 4.1 compares the chemisorption enthalpies predicted for NH, NH_2 and OH radicals based on the formulas for weak, intermediate and strong binding.

Table 4.1 Chemisorption Enthalpies for Radicals having Localized Unpaired Electrons

			Chemisorption enthalpy (kcal/mol)			
Species	**Coordination Mode**	**Catalyst**	**Predicted**			**Literature**
			Weak	**Intermediate**	**Strong**	
NH	Mono N	Pt(111)	49.3	59.9	70.5	71-74 ± 2
NH_2	Mono N	Pt(111)	25.2	36.2	47.2	44 ± 2
OH	Mono O	Pt(111)	21.9	30.3	38.6	34.2 ± 3

Predicted enthalpies vary significantly for the 3 binding strengths. By comparing the predicted enthalpies against literature values, we conclude that strong binding is required to describe chemisorption enthalpies of molecular radicals with localized unpaired electrons.

4.2.3 Formulas for Molecular Chemisorption Enthalpies

Table 4.2 lists the formulas for molecular chemisorption enthalpies of mono-, di-and polyatomic adsorbates with mono- and multi-coordination. Formulas corresponding to mono- (Expressions 4.70 and 4.71) and diatomics (Expressions 4.72 through 4.76) are reported from the literature work of Shustorovich and Sellers [8], while for polyatomics we recommend the extended empirically modified equations (Expressions 4.77 through 4.88). Typical range in chemisorption enthalpies of weak, intermediate and strong binding are 10-35, 36-45 and 46-120 kcal/mol, respectively, for diatomics and polyatomics. For all the adsorbates attached through one contact atom via on-top coordination, coordination number 1 is used to calculate the chemisorption enthalpy. For adsorbates attached through one contact atom via bridge coordination, coordination number 2 is used. For hollow coordination on fcc(111) or hcp(001), coordination number 3 is used. These rules for coordination numbers are used in Table 4.10, when predicting the chemisorption enthalpies for diatomics and polyatomics attached through one contact atom for different types of coordination. Note that Q_A used in Table 4.2 for the strong binding formula is the full heat of chemisorption which is related to Q_{0A}, the monocoordinated heat of chemisorption by Eq. 4.13.

Table 4.2 Formula for Chemisorption Enthalpies of Mono-, Di- and Polyatomic Adsorbates on Transition Metals

Catalyst System	Chemisorption Enthalpy	
Monoatomic		
Mono-coordinated	Q_{OA}	(4.70)
Multi-coordinated	$Q_{OA}(2-\frac{1}{n})$	(4.71)
Diatomic		
	Weak binding	

On-top coordination with A and B with the A end down and attached to 1 metal atom	$\frac{Q_{OA}^2}{Q_{OA}+D_{AB}}$	(4.72)
On-top coordination of A and B with the A end down and attached to n metal atoms	$\frac{Q_{OA}^2}{\frac{Q_{OA}}{n}+D_{AB}}$	(4.73)
Bridge coordination of A and B with the contact atoms in an on-top site	$Q_{0A}+Q_{0B}-\frac{4}{\frac{1}{Q_{0A}}+\frac{1}{Q_{0B}}+\frac{1}{D_{AB}}}$	(4.74)
Intermediate binding		
	$0.5(\frac{Q_{0A}^2}{\frac{Q_{0A}}{n}+D_{AB}}+\frac{Q_A^2}{Q_A+D_{AB}})$	(4.75)
Strong binding		
	$\frac{Q_A^2}{Q_A+D_{AB}}$	(4.76)
Polyatomic		
Weak binding		
Binding atoms = 1		
Coordination number = 1	$\frac{Q_{0A}^2}{Q_{0A}+D_{reduced\_Group}}$	(4.77)
Coordination number > 1	$\frac{Q_{0A}^2}{\frac{Q_{0A}}{n}+D_{reduced\_Group}}$	(4.78)
Binding atoms > 1		
Coordination number = 2		
Symmetric dicoordination	$\frac{2Q_{0Group}^2}{Q_{0Group}+2D_{AA}}$	(4.79)
	$Q_{0Group}=\frac{Q_{0A}^2}{\frac{Q_{0A}}{n}+D_{Group}}$	(4.80)
Asymmetric dicoordination	$Q_{0GroupA}+Q_{0GroupB}-\frac{4}{\frac{1}{Q_{0GroupA}}+\frac{1}{Q_{0GroupB}}+\frac{1}{D_{AB}}}$	(4.81)
	$Q_{0GroupA}=\frac{Q_{0A}^2}{\frac{Q_{0A}}{n}+D_{GroupA}}$	(4.82)

$$Q_{0GroupB} = \frac{Q_{0B}^2}{\frac{Q_{0B}}{n} + D_{GroupB}} \quad (4.83)$$

Chelating dicoordination

$$Q_{chemisorption} = Q_{0AX} + Q_{0BX} \quad (4.84)$$

$$Q_{0AX} = \frac{Q_{0A}^2}{\frac{Q_{0A}}{n} + D_{GroupAX}} \quad (4.85)$$

$$Q_{0BX} = \frac{Q_{0B}^2}{\frac{Q_{0B}}{n} + D_{GroupBX}} \quad (4.86)$$

Intermediate binding

$$0.5\left(\frac{Q_{0A}^2}{\frac{Q_{0A}}{n} + D_{GroupA}} + \frac{Q_A^2}{Q_A + D_{GroupA}}\right) \quad (4.87)$$

Strong binding

$$\frac{Q_A^2}{Q_A + D_{GroupA}} \quad (4.88)$$

In Table 4.2, all the required D's are computed using typical values for homolytic bond dissociation energies. The bond dissociation energies can be obtained from standard handbooks such as CRC handbook or NIST kinetics webbook. Table 4.3 lists the dissociation energies used in this study.

Table 4.3 Bond Dissociation Energies for Diatomic and Polyatomic Gas Phase Molecules

Molecule	Bond	Dissociation Energy (kcal/mol)
H_2	H-H	103
O_2	O-O	119
N_2	N-N	226
CO	C-O	256
NO	N-O	151
SO	S-O	125
OH	O-H	102
CH	C-H	81
NH	N-H	75
SH	S-H	82

CO_2	OC-O	127
NO_2	ON-O	73
SO_2	OS-O	132
SO_3	O_2S-O	83
CH_2	C-H_2	182
CH_3	C-H_3	293
CH_4	C-H_4	398
C_2H_5	C-C	99
	C-H	36
H_2O	HO-H	119
H_2O_2	HOO-H	88
	HO-OH	51
NH_2	N-H_2	169
NH_3	N-H_3	279
CH_3OH	CH_3O-H	104
	CH_3-OH	92
CH_3SH	CH_3S-H	87
	CH_3-SH	74
C_2H_4	H_2C-CH_2	175
C_2H_2	HC-CH	231
HCOOH	HCOO-H	106

The monocoordinated heats of chemisorption (Q_{0A}) on common transition metal catalysts are given in Table 4.4 and the corresponding references for experimental atomic binding energies are given in Table 4.5. The tables and the corresponding references are available in Shustorovich [8], the table is provided in this paper for ready reference to look up numbers as inputs for calculations. "est" in Table 4.5 refers to estimated quantities.

Table 4.4 Monocoordinated Atomic Heats of Chemisorption (kcal/mol)

Catalyst / Atoms	Cu	Ag	Au	Ni	Pd	Pt
H	33.6	31.2	27.6	37.8	37.2	36.6
O	61.8	48.0	45.0	69.0	52.3	51.0
N	69.0	60.0	58.2	81.0	78.0	69.6
C	72.0	87.0	84.0	102.6	96.0	90.0
S	52.6	46.8	48.0	67.2	57.0	55.2

Table 4.5 References for Atomic Heats of Chemisorption

Catalyst / Atoms	Cu	Ag	Au	Ni	Pd	Pt
H	[16,17]	[18]	est, [19]	[16,17]	[16]	[20]
O	[21]	[16,19]	[19]	[22,23]	[16]	[24]
N	est	est	est	[16]	[16]	[24]
C	est	est	est	[26]	[17]	[17]
S	[25]	[25]	est	[25]	est	[25]

Presented below are topological cases, which use different equations for calculating molecular chemisorption enthalpies.

Case 1:

a. HCN bonded to the catalyst surface through the N atom.

Q_{0A} refers to Q_{0N}, which is the hypothetical mono-coordinated chemisorption enthalpy. D_{Group} refers to the dissociation energy of the triple bond between C and N in HCN.

b. HCHO bonded to the surface through the O atom.

Q_{0A} refers to Q_{0O} and D_{Group} refers to the dissociation energy of the double bond between C and O.

Weak binding formula is used for Cases 1a and 1b.

Case 2:

CH_3 bonded to the surface through the C atom.

Q_{0A} refers to Q_{0C} and D_{Group} refers to sum of the dissociation energies of single bonds between C and each of the 3 H atoms.

Case 3:

CH_3CH_2 bonded to catalyst surface through C bonded to 2 H's.

Q_{0A} is Q_{0C} and D_{Group} is the sum of dissociation energies of bonds between C and the 2 H atoms, and the adjacent C atom.

Intermediate binding formula is used for Cases 2 and 3, since they are monovalent radicals with tetravalent central atoms.

Case 4:

CH_2 bonded to the surface through C.

Q_{0A} refers to Q_{0C} and D_{Group} refers to sum of the dissociation energies of single bonds between C and each of the 2 H atoms. Strong binding formula is used.

Case 5:

C_5H_9 (cyclopentyl radical) bonded to the surface through C with only one H.

Q_{0A} is Q_{0C} and D_{Group} is the sum of dissociation energies of single bond between C and the H atom, and the single bond between C atom and each of the 2 adjacent C atoms.

Case 6:

C_3H_5 (cyclopropyl radical) bonded to the surface through C with only one H.

Q_{0A} is Q_{0C} and D_{Group} is the sum of dissociation energies of the single bond between C and the H atom, and the single bond between C atom and each of the 2 adjacent C atoms.

Strong binding is used for Cases 5 and 6, since they are cylic compounds with localized unpaired electrons.

Case 7:

C_2H_4O (ethylene oxide or oxirane) bonded through O atom in ring form.

Q_{0A} is Q_{0O} and D_{Group} is the sum of dissociation energies of the single bond between O and the 2 C atoms.

Case 8:

C_2H_4 bonded to the catalyst surface through both C atoms.

Q_{0Group} IS Q_{0CH2}. D_{AA} is the dissociation energy of the double bond between 2 C atoms. Q_{C2H4} is calculated using the formula for symmetric dicoordination.

Case 9:

CH_3CHCH_2 where the CH_3 group is not bound to the surface but the other two C's are bound to the catalyst.

$Q_{0GroupA}$ is Q_{CH3CH} and $Q_{0GroupB}$ is Q_{CH2}. They are computed using Eqs. 4.82 and 4.83, respectively. Q_{0A} and Q_{0B} refer to Q_{0C}. D_{GroupA} is the sum of dissociation energies of bonds between C atom and H and C atom in CH_3. D_{GroupB} is the sum of dissociation energies of bonds between C atom and the 2 H atoms in CH_2. D_{AB} is the dissociation energy between the CH_3CH and CH_2 groups. Eq. 4.81 is used to compute the molecular chemisorption enthalpy, $Q_{CH3CHCH2}$.

Case 10:

C_6H_{10} (cyclohexene) bonded to the surface through the 2 C's involved in the double bond. Q_{0Group} is the heat of chemisorption of the ring-opened $CHCH_2CH_2CH_2CH_2CH$ tetra-radical. D_{AA} is the dissociation energy of the double bond between the 2 C atoms. D_{GroupA} is the sum of dissociation energies of single bond between C and H and adjacent C atoms. Since cyclohexene is coordinated symmetrically, we use Eq. 4.79.

Figure 4.5 shows the procedure for calculating molecular chemisorption enthalpy. Note that the Q referred to, in the figure, is the full heat of chemisorption, and not the mono-coordinated heat of chemisorption. For an atom, the full heat of chemisorption is related to the mono-coordinated heat of chemisorption by Eq. 4.13, as shown earlier. If the molecule whose heat of chemisorption needs to be evaluated is either a closed shell molecule or a radical with delocalized unpaired electrons, then the binding is weak. If the molecule is a localized radical with tetrahedral center, then the binding is intermediate. If the molecule is a localized radical on non-tetrahedral center, then the binding is strong.

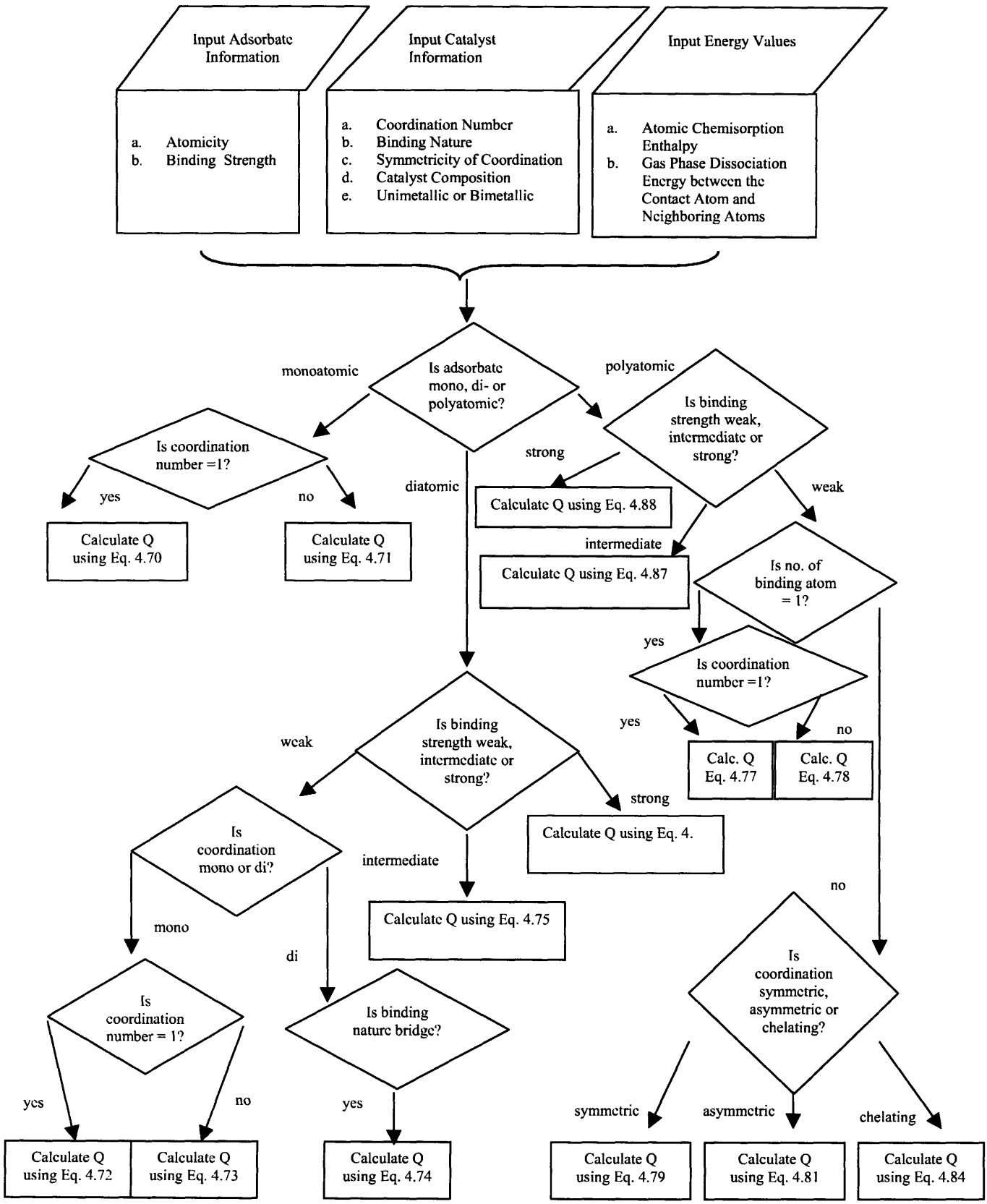
Input Adsorbate Information
a. Atomicity
b. Binding Strength
Input Catalyst Information
a. Coordination Number
b. Binding Nature
c. Symmetricity of Coordination
d. Catalyst Composition
e. Unimetallic or Bimetallic
Input Energy Values
a. Atomic Chemisorption Enthalpy
b. Gas Phase Dissociation Energy between the Contact Atom and Neighboring Atoms
Is adsorbate mono, di- or polyatomic?
monoatomic
diatomic
polyatomic
Is coordination number =1?
yes
no
Calculate Q using Eq. 4.70
Calculate Q using Eq. 4.71
Is binding strength weak, intermediate or strong?
strong
Calculate Q using Eq. 4.88
weak
intermediate
Calculate Q using Eq. 4.87
Is no. of binding atom = 1?
yes
Is coordination number =1?
yes
no
Calc. Q Eq. 4.77
Calc. Q Eq. 4.78
Is binding strength weak, intermediate or strong?
weak
strong
Calculate Q using Eq. 4.
Is coordination mono or di?
mono
di
intermediate
Calculate Q using Eq. 4.75
Is coordination number = 1?
yes
no
Calculate Q using Eq. 4.72
Calculate Q using Eq. 4.73
Is binding nature bridge?
yes
Calculate Q using Eq. 4.74
no
Is coordination symmetric, asymmetric or chelating?
symmetric
asymmetric
chelating
Calculate Q using Eq. 4.79
Calculate Q using Eq. 4.81
Calculate Q using Eq. 4.84

Figure 4.5 Computational Procedure for Chemisorption Enthalpies

As shown in Figure 4.5, parameters pertaining to adsorbate information, catalyst information and energy values are used to identify the atomicity of adsorbate (mono-, di- or polyatomic), coordination number (1, 2, 3...n), binding strength (weak, intermediate and strong), symmetricity of coordination (symmetric, asymmetric or chelating) and binding nature (on-top or bridge). Based on these inputs, appropriate formula is chosen to calculate molecular chemisorption enthalpy. These formulas are referenced by the equation numbers (Table 4.2).

4.2.4 Procedure for Calculating Activation Energies

Within UBI-QEP framework, total energy of a reaction system is the sum of UBI-QEP energies of each reactant and product (whether gas phase or surface) and the UBI constraint includes bond indices of all bonds broken and formed in the reaction. To illustrate total energy and UBI constraint, consider the dissociative adsorption reaction involving atom or groups of atoms, A and B:

$AB + 2^* \Leftrightarrow A^* + B^*$

Energy and UBI-constraint of reaction system are:

$$E = D_{AB}(x_{AB}{}^2 - 2x_{AB}) + Q_A(x_{AM}{}^2 - 2x_{AM}) + Q_B(x_{BM}{}^2 - 2x_{BM}) \qquad (4.89)$$

and

$$x_{AB} + x_{AM} + x_{BM} = 1, \qquad (4.90)$$

where x_{AB}, x_{AM}, and x_{BM} are bond orders for the A-B, A-M and B-M bonds.

Minimizing the energy subject to constraint and approximating an intermediate value of x_{AB} [5] lead to expression for activation energy:

$$E_f = 0.5(\frac{Q_A Q_B}{Q_A + Q_B} - Q_A - Q_B + D_{AB}) \quad . \quad (4.91)$$

If the calculated energy is negative, it is set to zero.

Q_{tot} and D_{tot} are defined for easy substitutions in the later formulas for activation energies:

$$Q_{tot} = \sum_{reactants} Q_{reactants} - \sum_{products} Q_{products} \quad (4.92)$$

and

$$D_{tot} = \Delta H - Q_{tot}, \quad (4.93)$$

where ΔH is the heat of reaction.

It needs to be noted that all heats of chemisorption (Q's) as well as gas phase dissociation energies (D's) are defined to be positive. Formulas for activation energies of different classes of reaction types are compiled in Table 4.6. The reactions are categorized into Types 1 through 7. Type 1 is simple adsorption, Types 2 through 5 are dissociation and recombination reactions, while Types 6 and 7 are disproportionation reactions.

Table 4.6 Formulas for Activation Energies of Generic Types of Surface Reactions

Reaction Type	Reaction	E_f
1	$AB + * \Leftrightarrow AB^*$	0
2	$AB + 2^* \Leftrightarrow A^* + B^*$	$\mathbf{max}(0, 0.5(D_{tot} + \frac{Q_A Q_B}{Q_A + Q_B} - Q_A - Q_B)$
3	$AB^* + * \Leftrightarrow A^* + B^*$	$\mathbf{max}(0, 0.5(D_{tot} + \frac{Q_A Q_B}{Q_A + Q_B} - Q_A - Q_B + Q_{AB})$
4	$AB + * \Leftrightarrow A + B^*$	$\mathbf{max}(0, 0.5(D_{tot} + \frac{Q_A Q_B}{Q_A + Q_B} - Q_A - Q_B))$
5	$AB^* \Leftrightarrow A + B^*$	$\mathbf{max}(0, 0.5(D_{tot} + \frac{Q_A Q_B}{Q_A + Q_B} - Q_A - Q_B + Q_{AB}))$

6	$A^* + BC^* \Leftrightarrow AB^* + C^*$	$\max(0, 0.5(D_{tot} + \frac{Q_{AB}Q_C}{Q_{AB}+Q_C} + Q_A + Q_{BC} - Q_{AB} - Q_C))$
7	$A + BC^* \Leftrightarrow AB + C^*$	$\max(0, 0.5(D_{tot} + \frac{Q_{AB}Q_C}{Q_{AB}+Q_C} - Q_A + Q_{BC} + Q_{AB} - Q_C))$

Figure 4.6 shows the procedure for calculating activation energies.

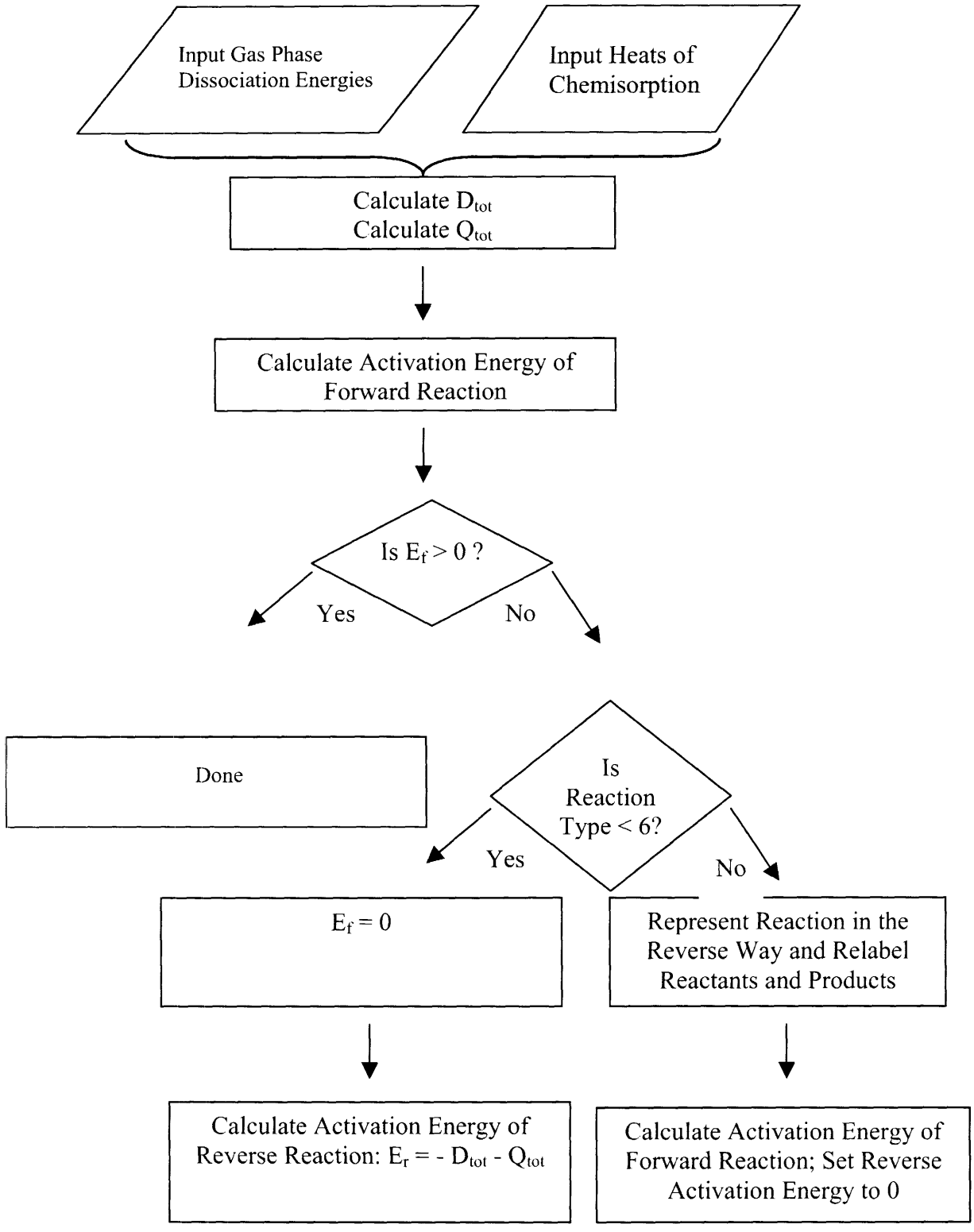
Input Gas Phase Dissociation Energies
Input Heats of Chemisorption
Calculate D_{tot}
Calculate Q_{tot}
Calculate Activation Energy of Forward Reaction
Is $E_f > 0$?
Yes
No
Done
Is Reaction Type < 6?
Yes
No
$E_f = 0$
Represent Reaction in the Reverse Way and Relabel Reactants and Products
Calculate Activation Energy of Reverse Reaction: $E_r = - D_{tot} - Q_{tot}$
Calculate Activation Energy of Forward Reaction; Set Reverse Activation Energy to 0

Figure 4.6 Computational Procedure for Activation Energies

First, input parameters pertaining to gas phase dissociation energies and heats of chemisorption are used to calculate D_{tot} and Q_{tot}. Based on the reaction type, appropriate formula (Table 4.6) is chosen to compute the activation energies of forward and reverse reactions.

4.2.5 Calculation of Heat Capacities, Heats of Formation and Entropies

Heat capacity of surface species is derived from that of gas species (or the adsorbate molecule). Every coordination between contact atom and surface is an additional bond to the gas phase molecule. Each adsorbate-surface bond increment results in 3 vibrational modes from stretching, bending (or deformation frequencies) and hindered internal rotations, which are at the cost of 3 modes of translational and rotation. At high temperature limits, the three new vibrational modes contribute 3R to heat capacity, which are at a cost of 3/2 R. Hence, heat capacity of the surface species is approximated as:

$$C_{P,T}(AB^*) = C_{P,T}(AB) + \frac{3}{2}R \qquad (4.94)$$

Trouton's rule is used for standard adsorption entropy (-20 cal/mol/K), unless accurate experimental data is available. Then, the standard heat of formation and entropy of surface species is related to enthalpy and entropy of gas species:

$$H(AB^*) = H(AB) - Q \qquad (4.95)$$

and

$$S(AB^*) = S(AB) - 20 \text{ cal/mol/K.} \qquad (4.96)$$

Entropy given by Trouton's rule is used, unless accurate experimental data is available for the entropy of adsorption. Enthalpies, entropies and heat capacities of the gas phase species and metals in their standard states are available in standard thermochemistry databases.

4.2.6 Initial Estimates of Preexponential Factors

Based on the phase of reactants, we classify the surface reactions into 3 broad types. In Type 1, a gas phase species directly collides with the adsorbed species or the vacant catalytic sites resulting in reactions, while surface species react with each other in Type 2. An adsorbed species dissociatively desorbs to form gas and surface species in Type 3.

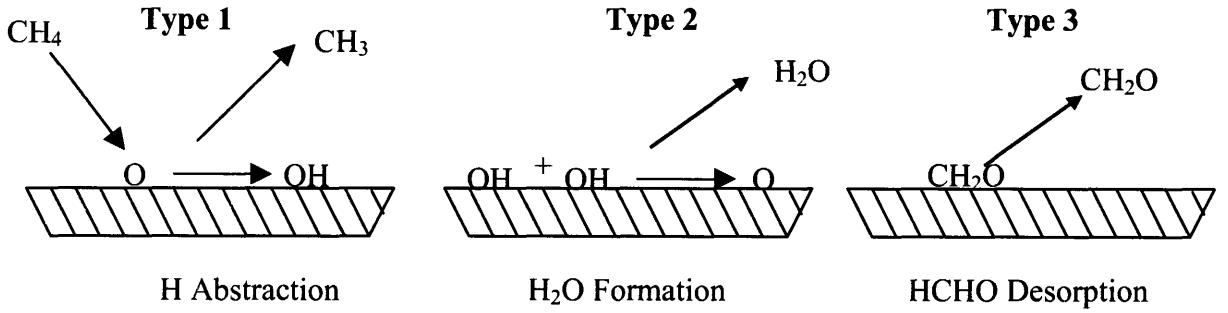

Figure 4.7 Types of Surface Reactions based on the Phase of Reactants

Figure 4.7 shows 3 surface reactions in the catalytic oxidative coupling of methane. H abstraction from CH_4 by adsorbed O, H_2O formation on catalytic surface by recombination of 2 adsorbed OH, and desorption of adsorbed HCHO are the 3 reactions.

We use collision theory to calculate the upper bound of Type 1 reaction:

$$A_{u,1} = \frac{1}{4s}\sqrt{\frac{8RT}{\pi m_A}}, \tag{4.97}$$

where s is the surface site density, R is the universal gas constant, T is the temperature, and m_A is the mass of gas species A colliding with the surface. Transition state theory is used for the lower bound:

$$A_{l,1} = \frac{RT}{h}\frac{\frac{Z_{TS}}{a}}{\frac{Z_A}{v}\frac{Z_{B^*}}{a}}, \tag{4.98}$$

where Z_{TS}, Z_A and Z_{B^*} are the partition functions of transition state, gas species A and surface species B^*, respectively. Translational partition function of Species A per unit volume is:

$$\frac{Z_{A_t}}{v} = \left(\sqrt{\frac{2\pi m_A k_B T}{h^2}}\right)^3, \tag{4.99}$$

where k_B is the Boltzmann constant and h is the Planck's constant. The rotational and vibrational partition functions are:

$$Z_{A_r} = \left(\frac{8\pi^2 I k_B T}{\sigma h^2}\right)^{\frac{3}{2}}, \tag{4.100}$$

and

$$Z_{A_v} = \prod_{i=1}^{s}\frac{1}{1-e^{(-\frac{h\nu_i}{k_B T})}}. \tag{4.101}$$

where I is the moment of inertia and σ is the symmetry number. Total partition function is a product of the translational, rotational and vibrational functions:

$$Z_A = Z_{A_t} Z_{A_r} Z_{A_v}. \tag{4.102}$$

Translational component of Species B per unit area of catalyst surface is:

$$\frac{Z_{B^*_t}}{a} = \left(\sqrt{\frac{2\pi m_{B^*} k_B T}{h^2}}\right)^2. \tag{4.103}$$

Rotational, vibrational and total partition functions are:

$$Z_{B^*_r} = \frac{8\pi^2 I k_B T}{\sigma h^2}, \tag{4.104}$$

$$Z_{B^*_v} = \prod_{i=1}^{s} \frac{1}{1 - e^{(-\frac{h\nu_i}{k_B T})}}, \tag{4.105}$$

and

$$Z_{B^*} = Z_{B^*_t} Z_{B^*_r} Z_{B^*_v}. \tag{4.106}$$

Since the transition state is a hypothetical species bound to the surface, the translational, rotational and vibrational partition functions of the transition state are calculated in the same way as those of surface species B. Mass of the transition state is sum of the masses of the reactants. The key information required is the vibrational frequencies of the transition state which are used to compute the vibrational partition function. To compute the lower bound, translational modes of the transition state are assumed to be frozen and translational partition function of the transition state is set to unity. The rotational and vibrational partition functions are set to unity as well.

Lower bound on the preexponential factor for Type 2 reactions is given by transition state theory:

$$A_{l,2} = \frac{RT}{h} \frac{Z_{TS}}{\frac{Z_{A^*}}{a} Z_{B^*}}. \tag{4.107}$$

Upper bound is given by the surface diffusion rate:

$$A_{u,2} = \frac{2\pi D}{\ln \sqrt{\frac{D}{k_{ads} P d^2}}}, \tag{4.108}$$

where D is the surface diffusivity, P is the pressure of the gas getting adsorbed, k_{ads} is the adsorption constant and d is the diffusion length scale. Surface diffusivity is given by:

$$D = D_0 e^{(\frac{E_{diff}}{RT})}, \tag{4.109}$$

where E_{diff} is the energy barrier for diffusion and D_0 is the diffusion coefficient when the energy barrier is 0. For Type 3 reactions, upper and lower bounds of preexponential factors are calculated by considering mobile transition state and reactant, respectively. To compute the upper bound, the translational part of the partition function for transition state ($Z_{TS,t}$) is allowed to move freely. The transition state is assumed to translate as freely as the surface reactant A. Hence, the translational partition function for the transition state is assumed to be:

$$Z_{TS,t} = Z_{B,t}(\frac{M_{TS}}{M_A}) \tag{4.110}$$

Since there is only one surface species undergoing simple desorption, the mass (and hence the moments of inertia) of the transition state would be similar to that of Reactant A. Hence, the translational and rotational partition functions for transition state and reactant A have similar orders-of-magnitude. If the vibrational frequencies are known for the transition state and the reactant, then the actual vibrational partition functions are computed. Otherwise, vibrational partition function of the transition state is assumed to be same as that of the reactant. Table 4.7 lists the orders-of-magnitudes (using base 10) of the bounds for different types of reactions.

Table 4.7 Orders-of-magnitude of Bounds on Preexponential Factors for General Surface Reactions[a]

Reaction Type	General Reaction	Orders-of-magnitude	
		Upper Bounds	Lower Bounds
1a	A + B* → Products	13	7
1b1	A + * → Products	13	12
1b2	A + 2 * → Products	22	20

2	$A^* + B^* \rightarrow$ Products	18	17
3	$A^* \rightarrow$ Products	13	13

[a]*Units*: $cm^3/mol.s$, Types 1a and 1b1; $cm^5/mol^2.s$, Type 1b2; $cm^2/mol.s$, Type 2; /s, Type 3.

The bounds have been validated against experimental data for catalytic systems. Initial estimates of preexponential factors for forward reactions are the geometric mean of upper and lower bounds. These estimates can be refined by additional calculations either by accounting for sticking coefficients or detailed partition functions computed using quantum chemistry. Initial estimates are important considering lack of experimental data, difficulties associated with kinetic measurements and uncertainties in limited data. The preexponential factor is computed as the product of sticking coefficient and collision rate (upper bound), if sticking coefficients are known experimentally for adsorption reactions (Types 1b1 and 1b2). Reported sticking coefficients are implicitly referenced to a computed collision rate, which is the probability that a molecule that collides with the surface sticks.

4.2.7 Implementation of Computational Methodology

Implemented as a collection of MATLAB codes, the computational methodology contains modules for estimating thermodynamic and rate parameters. Figure 4.8 schematically shows how the codes are integrated with Microsoft® Excel spreadsheet, which serves as the input module for calculating thermochemical and rate parameters.

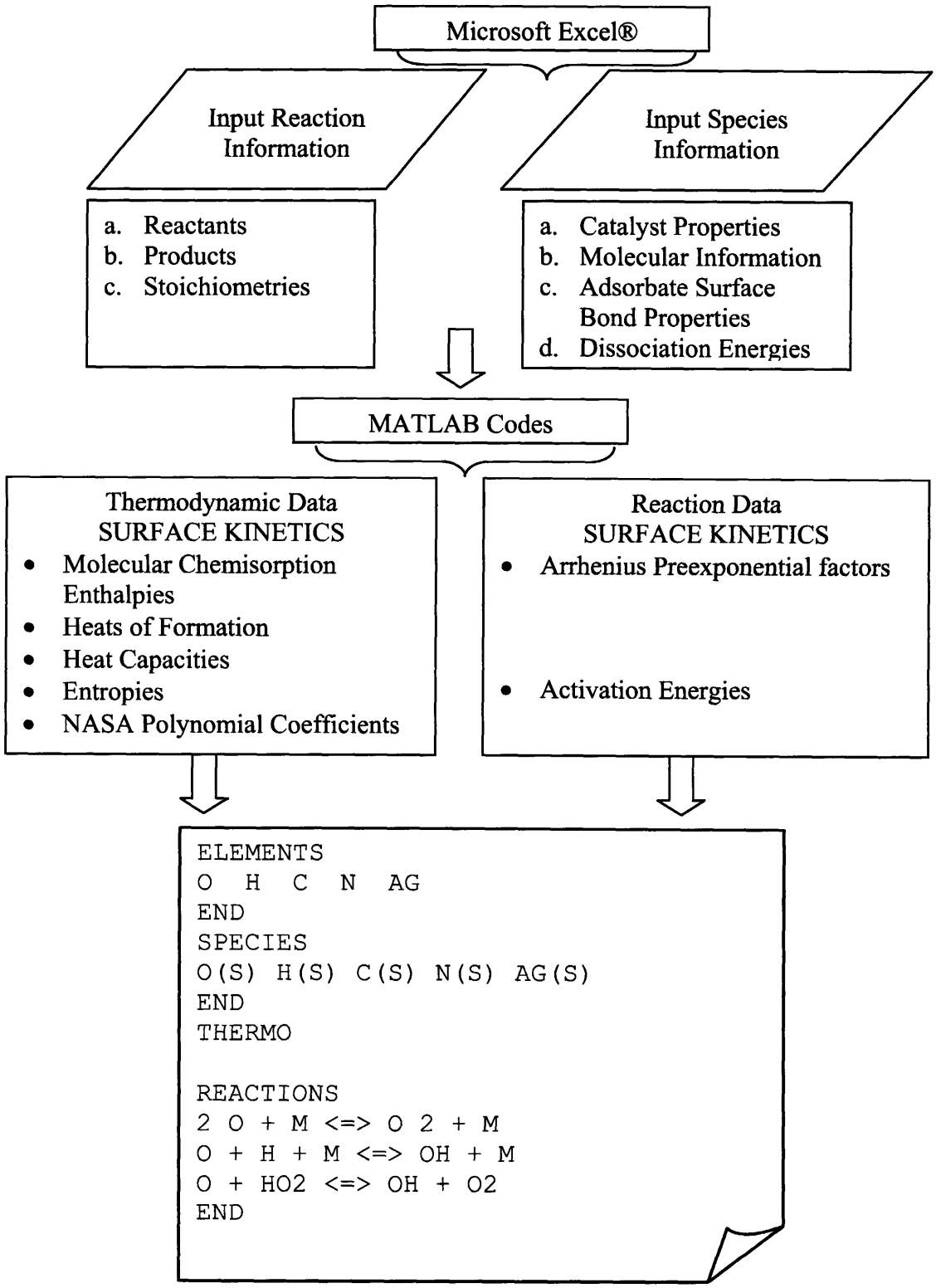
Microsoft Excel®
Input Reaction Information
Input Species Information
a. Reactants
b. Products
c. Stoichiometries
a. Catalyst Properties
b. Molecular Information
c. Adsorbate Surface Bond Properties
d. Dissociation Energies
MATLAB Codes
Thermodynamic Data SURFACE KINETICS
• Molecular Chemisorption Enthalpies
• Heats of Formation
• Heat Capacities
• Entropies
• NASA Polynomial Coefficients
Reaction Data SURFACE KINETICS
• Arrhenius Preexponential factors
• Activation Energies
ELEMENTS
O H C N AG
END
SPECIES
O(S) H(S) C(S) N(S) AG(S)
END
THERMO
REACTIONS
2 O + M <=> O 2 + M
O + H + M <=> OH + M
O + HO2 <=> OH + O2
END

Figure 4.8 Implementation of Computational Methodology

As shown in Figure 4.8, surface species and reaction information input in a spreadsheet, are read by MATLAB codes. Parameters predicted by the codes form thermodynamic and rate data for reaction system. They are output as a CHEMKIN formatted text, which can be used as a SURFACE CHEMKIN input file for higher-level reactor calculations. Software documentation and MATLAB codes are available in Appendices A and B.

4.3 Example Problem for Calculation of Thermochemical and Rate Parameters

4.3.1 Input Variables for Thermochemical Parameters

$C_2H_4(S)$ adsorbed on Ag is the catalyst system chosen to illustrate input variables for calculation of thermochemical parameters. The variables are categorized and defined in Table 4.8. In the example, C_2H_4 is attached to Ag catalyst via 2 C atoms with a coordination number of 2. The C atoms are weakly bound to catalyst and Π bonds in C_2H_4 are perpendicular to Ag surface with the coordination symmetric across double bond.

Table 4.8 Input Variables for the Calculation of Thermochemical Parameters of Surface Species

Variable	Definition	Variable type	Units	Example
Catalyst properties				
Catalyst material	Material name of the catalyst	String	N/A	SILVER

Metallicity	Unimetallic = 1 bimetallic = 2	Flag	N/A	1
Site density	Density of sites on catalyst	Floating point	moles/cm^2	1.05E-14
Standard state entropy of catalyst	Entropy of catalyst at 298K and 1 atm	Floating point	cal/mol/K	10.2
Adsorbate properties listed by each species				
Atomic information				
Species	Name of the adsorbate species	String	N/A	$C_2H_4(S)$
Atomicity	Monoatomic = 1 diatomic = 2 polyatomic = 3	Flag	N/A	1
Elements	Names of elements in the adsorbate species	String	N/A	C, H, AG
Adsorbate-Surface bond properties				
Number of atoms bound to surface	Number of atoms in adsorbate bound to the catalyst surface	Integer	N/A	2
Atoms bound to surface				
Atom1	Name of the first atom bound to surface	String	N/A	C
Atom 2	Name of the second atom bound to surface	String	N/A	C
Monocoordinated atomic chemisorption heats				
Atom 1	Chemisorption heat of Atom 1	Floating point	kcal/mol	87.0
Atom 2	Chemisorption heat of Atom 2	Floating point	kcal/mol	87.0
Coordination	Coordination	Flag	N/A	2

number	number of the adsorbate-surface bond			
Binding strength	Weak = 1 intermediate = 2 strong = 3	Flag	N/A	1
Coordination structure	Symmetric = 1 asymmetric = 2 chelating = 3	Flag	N/A	1
Gas phase properties				
Dissociation energy of bonds in gas molecule				
Bond 1	Dissociation energy of Bond 1	Floating point	kcal/mol	174.1
Bond 2	Dissociation energy of Bond 2	Floating point	kcal/mol	221.4
Bond 3	Dissociation energy of Bond 3	Floating point	kcal/mol	0.0
Standard state thermochemical properties of the gas molecule				
Enthalpy	Standard state enthalpy	Floating point	kcal/mol	12.5
Heat capacity	Standard state heat capacity	Floating point	cal/mol/K	10.3
Entropy	Standard state entropy	Floating point	cal/mol/K	52.4

4.3.2 Input Variables for Rate Parameters

Dissociative adsorption of O_2 on Ag is chosen to illustrate the input variables for calculating rate parameters: $O_2 + 2\ AG(S) \Leftrightarrow 2\ O(S)$. The variables are categorized and defined in Table 4.9.

Table 4.9 Input Variables for Calculation of Rate Parameters of Surface Species

Variable	Definition	Variable type	Units	Example
Reaction number	Serial number of the reaction in mechanism	Integer	N/A	1
Stoichiometry reactant 1	Stoichiometric coefficient of first reactant	Floating point	N/A	1
Reactant 1	Name of the first reactant	String	N/A	O_2
Stoichiometry reactant 2	Stoichiometric coefficient of second reactant (if it exists)	Floating point	N/A	2
Reactant 2	Name of the second reactant (if it exists)	String	N/A	AG(S)
Stoichiometry product 1	Stoichiometric coefficient of first product	Floating point	N/A	2
Product 1	Name of the first product	String	N/A	O(S)
Stoichiometry product 2	Stoichiometric coefficient of second product (if it exists)	Floating point	N/A	
Product 2	Name of the second product (if it exists)	String	N/A	
Dissociation energy of bonds in gas molecules				
Reactant	Dissociation energy of bond broken in the reactant	Floating point	kcal/mol	119.0
Product	Dissociation energy of bond formed in the product	Floating point	kcal/mol	0.0
Chemisorption enthalpy of adsorbate-surface bond				
Reactant 1	Enthalpy of bond broken in the reactant	Floating point	kcal/mol	0.0
Reactant 2	Enthalpy of bond broken	Floating point	kcal/mol	0.0

	in the reactant			
Product 1	Enthalpy of bond formed in the product	Floating point	kcal/mol	84.0
Product 2	Enthalpy of bond formed in the product	Floating point	kcal/mol	84.0

4.4 Results and Validation

4.4.1 Comparison of Chemisorption Enthalpies against Literature Data

In this section, we compare the molecular chemisorption enthalpies predicted by our methodology against literature values for complete species and radicals on various transition metals including Ag(100), Ag(110), Ag(111), Ni(100), Ni(110), Ni(111), Pt(111), Pd(110), Pd(111), Au(100) and Au(111). Table 4.10 compares the predicted against literature enthalpies for different catalysts, coordination sites and coordination modes. The reference sources and estimation methods for enthalpies reported in literature are given in Columns 7 and 8. Abbreviations for estimation methods are expanded in the Glossary (Appendix C). In the table, "bridge/l" and "bridge/s" indicate the long and short bridges of coordination. Words "mono" and "di" correspond to the number of contact atoms bound to catalyst. Except for SO_2, H_2, H, C_2H_5, CH_3, NH and NH_2 species, chemisorption enthalpies were experimentally measured in literature. The reported DFT-predicted chemisorption enthalpies of C_2H_5 and CH_3 on Pt(111) are 11.8 and 39 kcal/mol, respectively. It seems likely that atleast one of the 2 numbers is incorrect, since ethyl should be more strongly bound than methyl radical. This is because the dissociation energy of C-C bond in ethyl is less than that of C-H bond in methyl.

Table 4.10 Comparison of Predicted Chemisorption Enthalpies against Literature Data for Organic and Inorganic Adsorbates at On-top, Bridge and Hollow sites with Different Coordination Modes

				Molecular chemisorption enthalpy (kcal/mol)			
Species	**Catalyst**	**Coord. site**	**Coord. mode**	**Current work**	**Literature**	**Reference**	**Estimation method**
CH_3OH	Ag(111)	On-top	Mono O	9.4	10.5	[27]	UPS spectrum
CO	Ni(111)	On-top	Mono C	29.4	27, 31	[28,29]	EELS, Calorimetry
	Ni(100)	On-top	Mono C	29.4	29, 26	[29]	Calorimetry
	Ni(110)	On-top	Mono C	29.4	32	[29]	Calorimetry
H_2O	Pt(111)	On-top	Mono O	9.0	9.6	[27]	UPS spectrum
NO	Pd(111)	Bridge	Mono N	32.0	31	[16]	Work function changes
	Pt(111)	Bridge	Mono N	26.0	27, 26	[16]	Work function changes
N_2	Pt(111)	Bridge	Di N, N	11.4	9	[30]	Work function changes,
NH_3	Ni(111)	On-top	Mono N	18.2	20	[31]	UPS ESDIAD,

							LEED, TDS
	Pt(111)	On-top	Mono N	13.9	12	[7,17]	Overall order & Apparent activation energy
O_2	Pt(111)	Bridge	Di O, O	11.4	9	[32]	EELS, UPS, TDS
SO_2	Ag(111)	On-top	Mono S	7.1	8.5	[2]	RECP
		Bridge	Mono S	7.6	5.8		
		Hollow	Mono S	7.8	5.3		
		Bridge	Di O, O	19.2	20.2		
	Pd(111)	On-top	Mono S	10.1	11.5		
		Hollow	Mono S	11.5	10.7		
		Bridge	Di S, O	22.8	24.5		
	Ag(110)	On-top	Mono S	7.0	8.2		
		Bridge/s	Mono S	7.6	7		
		Hollow	Di O, O	26.7	26.3		
	Pd(110)	Bridge/l	Mono S	20.2	18.8		
		Bridge/l	Di O, O	22.3	19.5		
		Bridge/l	Di S, O	17.2	18.8		
	Ag(100)	On-top	Mono S	7.0	7		
		Hollow	Mono S	7.9	9		
	Au(100)	Hollow	Mono S	8.3	6.3		

		Bridge/ l	Di O, O	17.2	16.1		
		Hollow /l	Di O, O	23.8	25		
		Bridge/ l	Di S, O	14.9	13.7		
H_2	Pd(111)	Bridge	Di H, H	7.0	4.8		
		Hollow	Di H, H	3.1	4.8		
H	Pd(111)	Bridge	Mono H	55.8	58.5	[33]	DFT
		Hollow	Mono H	62.0	62.9		
	Au(111)	Bridge	Mono H	46.0	47.3		
C_2H_5	Pt(111)	Hollow	Mono C	30.4	11.8	[33]	DFT
CH_3	Pt(111)	On-top	Mono C	36.3	39	[34]	DFT
		Bridge		23.9	22.6, 23.3		
NH	Pt(111)	Hollow	Mono N	70.5	71-74	[7,35]	Overall order & Apparent activation energy
NH_2	Pt(111)	Hollow	Mono N	47.2	>42	[7,35]	Overall order & Apparent activation energy

Table 4.11 compares the enthalpies predicted by the extended UBI-QEP theory against the enthalpies predicted by empirical modification and the literature data for polyatomic adsorbates on different catalysts, coordination sites and coordination modes.

Table 4.11 Comparison of Chemisorption Enthalpies Predicted by the Polyatomic Extensions of UBI-QEP approach against Empirical Modfication and Literature Data for Polyatomic Organic and Inorganic Adsorbates

				Molecular chemisorption enthalpy (kcal/mol)			
Species	**Catalyst**	**Coord. site**	**Coord. mode**	**UBI-QEP extension**	**Empirical modification**	**Literature**	**Reference**
CH_3OH	Ag(111)	On-top	Mono O	23.8	9.4	10.5	[27]
H_2O	Pt(111)	On-top	Mono O	23.5	9.0	9.6	[27]
NH_3	Ni(111)	On-top	Mono N	37.7	18.2	20	[31]
	Pt(111)	On-top	Mono N	29.8	13.9	12	[7,17]
SO_2	Ag(111)	On-top	Mono S	19.4	7.1	8.5	[2]
		Bridge	Mono S	24.5	7.6	5.8	
		Hollow	Mono S	26.8	7.8	5.3	
		Bridge	Di O, O	22.2	19.2	20.2	
	Pd(111)	On-top	Mono S	26.4	10.1	11.5	
		Hollow	Mono S	38.2	11.5	10.7	
		Bridge	Di S, O	20.1	22.8	24.5	
	Ag(110)	On-top	Mono S	19.4	7.0	8.2	
		Bridge/ s	Mono S	24.5	7.6	7	
		Hollow	Di O, O	23.4	26.7	26.3	
	Pd(110)	Bridge/	Mono S	34.4	20.2	18.8	

		1					
		Bridge/ 1	Di O, O	25.9	22.3	19.5	
		Bridge/ 1	Di S, O	20.0	17.2	18.8	
	Ag(100)	On-top	Mono S	19.4	7.0	7	
		Hollow	Mono S	28.2	7.9	9	
	Au(100)	Hollow	Mono S	29.5	8.3	6.3	
		Bridge/ 1	Di O, O	19.7	17.2	16.1	
		Hollow /1	Di O, O	20.7	23.8	25	
		Bridge/ 1	Di S, O	20.7	14.9	13.7	
C_2H_5	Pt(111)	Hollow	Mono C	77.0	30.4	11.8	[33]
CH_3	Pt(111)	On-top	Mono C	43.2	36.3	39	[34]
		Bridge		53.3	23.9	22.6, 23.3	
NH_2	Pt(111)	Hollow	Mono N	43.3	47.2	>42	[7,35]

From Table 4.11, we observe that the direct extension of the UBI-QEP theory for polyatomics do not predict chemisorption enthalpies as well as the empirical modification in the bond dissociation energy of the group of atoms which form a part of the polyatomic molecule. The predicted and literature enthalpies from Table 4.10 are compared in Figure 4.9.

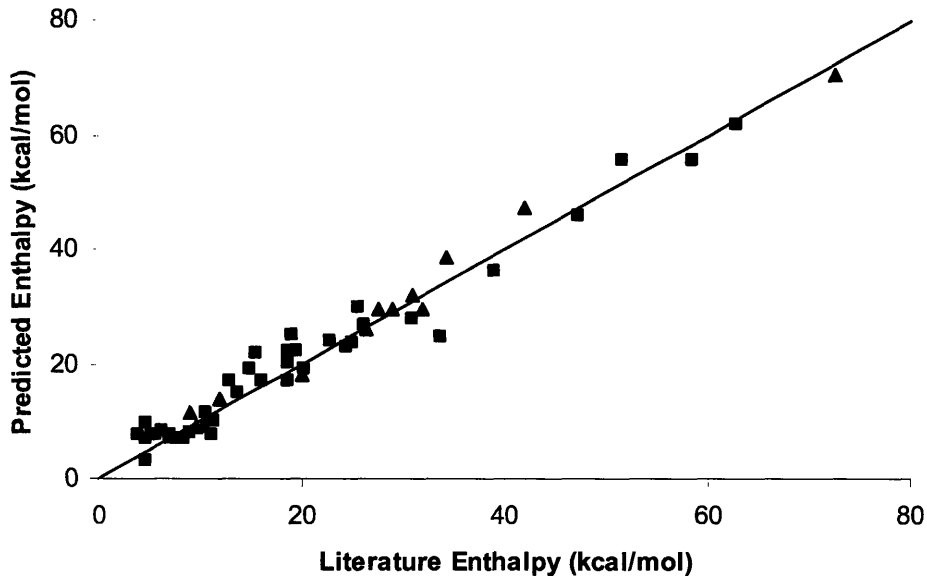

Figure 4.9 Predicted Chemisorption Enthalpies Compared against Literature Data

In Figure 4.9, the values based on experimental data are distinguished from those calculated using quantum chemistry by black triangles and squares, respectively. For the most part, we observe that predicted enthalpies are within 3 kcal/mol of literature values.

4.4.2 Validation of Bounds of Preexponential Factors

Based on the procedures outlined in Subsection 4.3, we calculate upper and lower bounds on preexponential factors of the different surface reactions in oxidative coupling of methane (at 800°C).

Table 4.12 Bounds on A-factors for OCM Surface Reactions at 800°C

Step #	Reactions	Forward reactions		Reverse reactions	
		Upper bounds	Lower bounds	Upper bounds	Lower bounds
1	$O_2 + 2\,{}^* \Leftrightarrow O^* + O^*$	1.6E22	7.9E20	2.5E18	4.8E17
2	$CH_4 + O^* \Leftrightarrow CH_3 + OH^*$	1.8E13	6.6E7	1.9E13	6.9E7

3	$2\,OH^* \Leftrightarrow H_2O + O^* + {}^*$	2.4E18	4.5E17	2.2E22	3.7E16
4	$C_2H_6 + O^* \Leftrightarrow C_2H_5 + OH^*$	1.4E13	3.7E7	1.4E13	3.7E7
5	$C_2H_4 + O^* \Leftrightarrow C_2H_3 + OH^*$	1.4E13	3.9E7	1.4E13	3.9E7
6	$CH_3OH + O^* \Leftrightarrow CH_3O + OH^*$	1.3E13	3.5E7	1.3E13	3.5E7
7	$CH_3 + O^* \Leftrightarrow CH_3O^*$	1.9E13	7.1E7	2.1E13	2.1E13
8	$CH_3O^* + O^* \Leftrightarrow OH^* + CH_2O^*$	2.1E18	3.6E17	2.1E18	3.5E17
9	$CH_2O^* \Leftrightarrow CH_2O + {}^*$	2.1E13	2.1E13	1.4E13	1.3E12
10	$CH_2O + O^* \Leftrightarrow CHO + OH^*$	1.4E13	3.7E7	1.4E13	3.7E7
11	$CO + O^* \Leftrightarrow CO_2 + {}^*$	1.4E13	3.9E7	1.1E13	1.1E12
12	$HOO + O^* \Leftrightarrow O_2 + OH^*$	1.3E13	3.4E7	1.3E13	3.4E7
13	$HOO + {}^* \Leftrightarrow HO + O^*$	1.3E13	1.3E12	1.8E13	6.2E7
14	$CH_3OO + 2\,{}^* \Leftrightarrow O^* + OCH_3{}^*$	1.3E22	6.6E20	2.1E18	3.6E17

Chemkin® units of preexponential factors
Units: cm^3/mol.s, forward and reverse reactions of Steps 2, 4, 5, 6, 10, 11, 12, and 13 and forward of Step 7 and reverse of Step 9; cm^5/mol.s, forward of Steps 1 and 14 and reverse of Step 3; cm^2/mol.s, forward of Steps 3 and 8 and reverse of Steps 1, 8, and 14; /s, forward of Step 9, and reverse of Step 7.

Table 4.13 compares the predicted bounds against experimental data for oxidative coupling of methane. Note that reactions in the table are shown in single direction since experimental values of preexponential factors are reported only for the forward direction of these reactions. "CR" stands for collision rates; collision rates were set as preexponential factors for some reactions. The remaining preexponential factors were reported through fitting of experimental data [36]. Preexponential factors were not available for some reactions as different ones were assumed in the mechanism [37].

Table 4.13 Predicted Bounds on A-factors versus Experimental Data for OCM

Reactions	Upper bounds	Lower bounds	Sn/Li/MgO [36]	Li/MgO [36]	CaO/CeO_2 [37]
$O_2 + 2^* \rightarrow O^* + O^*$	1.6E22	7.9E20	1.6E21	2.8E22	Not available
$CH_4 + O^* \rightarrow CH_3 + OH^*$	1.9E13	6.6E7	CR	CR	1.6E13
$2\ OH^* \rightarrow H_2O + O^* + ^*$	2.4E18	4.5E17	4.2E17	6.1E17	2.9E17
$C_2H_6 + O^* \rightarrow C_2H_5 + OH^*$	1.4E13	3.7E7	CR	CR	Not available
$C_2H_4 + O^* \rightarrow C_2H_3 + OH^*$	1.4E13	3.9E7	CR	CR	Not available
$CH_3 + O^* \rightarrow CH_3O^*$	1.9E13	7.1E7	3.5E10	8.1E9	4.8E9
$CO + O^* \rightarrow CO_2 + ^*$	1.4E13	3.9E7	CR	CR	Not available

From the table, we observe that experimental values lie within orders-of-magnitude of upper and lower bounds of preexponential factors for most of the surface reactions listed. For a few reactions, experimental values differ from the bounds by 1 or 2 orders. The calculated bounds of this work are also compared with reported preexponential factors for partial oxidation of methane to synthesis gas on Rh and oxidation of hydrogen on Pt (Table 4.14).

Table 4.14 Orders-of-magnitude Comparison of Predicted Bounds against Literature Values for Different Reaction Systems

Reaction type	Upper bound	Lower bound	[38]	[39]	[11]
$A + ^* \rightarrow$ Products	13	12	12	12	13
$A + 2^* \rightarrow$ Products	22	20	20	20	20
$A^* + B^* \rightarrow$ Products	18	17	18	18	18
$A^* \rightarrow$ Products	13	13	13	13	13

4.5 Summary

A key challenge in the development of detailed reaction mechanisms for heterogeneous catalysis is the availability of thermophysical data needed for estimating reaction rate constants. This chapter presents a new methodology for calculating temperature/coverage-dependent heats of formation, heat capacities, and entropies. Particular attention is given to the thermodynamic consistency of preexponential factors and activation energies. Unity Bond Index-Quadratic Exponential Potential (UBI-QEP) theory [1-8] is improved to compute molecular chemisorption enthalpies and activation energies for polyatomic molecules. The direct extension of UBI-QEP theory treats polyatoms as pseudo diatoms which is a combination of 2 groups of atoms. Based on the extended UBI-QEP theory, chemisorption enthalpy of each group is derived as a function of mono-coordinated chemisorption enthalpy and reduced sum of dissociation energies of atoms bound to the contact atom. However, the extended UBI-QEP equations don't predict chemisorption enthalpies that match with the experimental data. Hence, we empirically modify the equations and replace the reduced sum by the regular sum of bond dissociation energies to predict the chemisorption enthalpies of polyatomics. The predicted enthalpies agree within 3 kcal/mol of experimental values for mono-, di- and polyatomic adsorbates on Ag(111), Ni(111), Ni(100), Ni(110), Pt(111), Pd(111), Ag(110), Pd(110), Ag(100), Au(100) and Au(111). On-top, bridge and hollow coordination sites with symmetric, asymmetric and chelating coordination structures are studied. We predict tight physical upper and lower bounds for preexponential factors of generic reaction types. They have been validated against the literature values for oxidative coupling of methane on Sn/Li/MgO, Li/MgO and CaO/CeO_2, partial oxidation of CH_4 to synthesis gas on Rh, and oxidation of H_2 on Pt. The computational methodology is

implemented in a computer program that outputs the parameters as a Chemkin® formatted surface input file.

References

1. H. Sellers (1993). On analytic potential functions for reactions on metal surfaces: The case of H^{*}--->2H on the liquid mercury surface. *Journal of Chemical Physics*, 98, 627-633.
2. H. Sellers and E. Shustorovich (1996). Coordination modes and bonding of sulfur oxides on transition metal surfaces: combined ab initio and BOC-MP results. *Surface Science*, 346, 322-336.
3. H. Sellers and E. Shustorovich (2002). Intrinsic activation barriers and coadsorption effects for reactions on metal surfaces: Unified formalism within the UBI-QEP approach. *Surface Science Reports*, 504, 167-182.
4. E. Shustorovich (1986). Chemisorption phenomena: analytic modeling based on perturbation theory and bond-order conservation. *Surface Science Reports*, 6, 1-63.
5. E. Shustorovich (1990). The Bond-Order conservation approach to chemisorption and heterogeneous catalysis: Applications and implications. *Advances in Catalysis*, 37, 101-163.
6. E. Shustorovich and A. T. Bell (1991). Synthesis and decomposition of ammonia on transition metal surfaces: bond-order-conservation-Morse-potential analysis. *Surface Science*, 259(I3), L791-L796.
7. E. Shustorovich and A. T. Bell (1993). Decomposition and reduction of NO on transition metal surfaces: bond order conservation Morse potential analysis. *Surface Science*, 298, 127-138.
8. E. Shustorovich and H. Sellers (1998). The UBI-QEP method: A practical theoretical approach to understanding chemistry on transition metal surfaces. *Surface Science Reports*, 31, 1-119.
9. P. Aghalayam, Y. K. Park and D. G. Vlachos (2000). Construction and optimization of complex surface reaction mechanisms. *AIChE Journal*, 46, 2017-2029.
10. J. A. Dumesic, D. F. Rudd, L. M. Aparicio and J. E. Rekoske (1993). *The microkinetics of heterogeneous catalysis*. Washington, DC: American Chemical society.
11. Y. K. Park, P. Aghalayam and D. G. Vlachos (1999). A generalized approach for predicting coverage-dependent reaction parameters of complex surface reactions: Application of H2 oxidation over platinum. *Journal of Physical Chemistry A*, 8101-8107.
12. Y. S. Su, J. Y. Ying, and W. H. Green (2003). Upper bound on the yield for oxidative coupling of methane. *Journal of Catalysis*, 218, 321-333.
13. M. E. Coltrin, R. J. Kee, and F. M. Rupley (1991). Surface Chemkin: A Generalized Formalism and Interface for Analyzing Heterogeneous Chemical Kinetics at a Gas-Surface Interface. *International Journal of Chemical Kinetics*, 23, 1111-1128.
14. R. J. Kee, M. E. Coltrin and P. Glarborg (2003). *Chemically Reacting Flow: Theory & Practice*. New Jersey: Wiley-Interscience Publications.
15. A. B. Mhadeshwar, H. Wang and D. G. Vlachos (2003). Thermodynamic consistency in microkinetic development of surface reaction mechanisms. *Journal of Physical Chemistry B*, 107, 12721-12733.
16. G. Ertl (1979). The Nature of Surface Chemical Bond. In T. N. Rhodin & G. Ertl (Eds.), *The Nature of Surface Chemical Bond*. Amsterdam: North-Holland.
17. W. Tsai, J. J. Vajo and W. H. Weinberg (1985). Inhibition by hydrogen of the heterogeneous decomposition of ammonia on platinum. *Journal of Physical Chemistry*, 89, 4926-4932.
18. X. L. Zhou, J. M. White and B. E. Koel (1989). Chemisorption of atomic hydrogen on clean and chlorine-covered silver(111). *Surface Science*, 218, 201-210.

19. A. G. Sault, R. J. Madix and C. T. Campbell (1986). Adsorption of oxygen and hydrogen on gold(110)-(1*2). *Surface Science*, 169, 347-356.
20. G. E. Gdowski, J. A. Fair and R. J. Madix (1983). Reactive scattering of small molecules from platinum crystal surfaces: formaldehyde-d2, methanol, formic acid, and the nonanomalous kinetics of hydrogen atom recombination. *Surface Science*, 127, 541-554.
21. E. Giamello, B. Fubini, P. Lauro and A. Bossi (1984). A microcalorimetric method for the evaluation of copper surface area in copper-zinc oxide catalyst. *Journal of Catalysis*, 87, 443-451.
22. D. Brennan, D. O. Hayward and B. M. W. Trapnell (1960). Calorimetric determination of the heat of adsorption of oxygen on evaporated films of germanium and silicon. *Physics and Chemistry of Solids*, 14, 117-123.
23. W. F. Egelhoff, Jr. (1987). Core-level binding-energy shifts at surfaces and in solids. *Surface Science Reports, Volume Date 1986,* 6, 253-415.
24. H. L. Sellers (1994). In H. L. Sellers and J. T. Golab (Eds.). New York: Plenum Press.
25. C. H. Bartholomew, P. K. Agrawal and J. R. Katzer (1982). Sulfur poisoning of metals. *Advances in Catalysis*, 31, 135-242.
26. L. C. Isett and J. M. Blakely (1975). Binding energies of carbon to nickel (100) from equilibrium segregation studies. *Surface Science*, 47, 645-649.
27. B. A. Sexton and A. E. Hughes (1984). Methanol and formaldehyde molecular states on copper surfaces at 300 K. *Surface Science*, 146, L561-L565.
28. K. Christmann, O. Schober and G. Ertl (1974). Adsorption of CO on a Ni(111) surface. *The Journal of Chemical Physics*, 60, 4639-5140.
29. N. Al-Sarraf and D. A. King (1994). Calorimetric adsorption heats on low-index Nickel surfaces. *Surface Science*, 307-309, 1-7.
30. B. E. Nieuwenhuys (1981). Correlation between work function change and degree of electron back-donation in the adsorption of carbon monoxide and nitrogen on group VIII metals. *Surface Science*, 105, 505-516.
31. C. Klauber, M. D. Alvey and J. J. T. Yates (1985). NH_3 adsorption on Ni(110) and the production of the NH_2 species by electron irradiation. *Surface Science*, 154, 139-167.
32. J. L. Gland, B. A. Sexton and G. B. Fisher (1980). Oxygen interactions with the Pt(111) surface. *Surface Science*, 95, 587-602.
33. D. Mei, E. W. Hansen and M. Neurock (2003). Ethylene hydrogenation over bimetallic Pd/Au(111) surfaces: Application of quantum chemical results and dynamic Monte Carlo simulation. *Journal of Physical Chemistry B*, 107, 798-810.
34. G. Papoian, J. K. Nørskov and R. Hoffmann (2000). A comparative theoretical study of the hydrogen, methyl, and ethyl chemisorption on the Pt(111) surface. *Journal of American Chemical Society*, 122, 4129-4144.
35. J. J. Vajo, W. Tsai and W. H. Weinberg (1989). Mechanistic details of the heterogeneous decomposition of ammonia on platinum. *Journal of Physical Chemistry*, 89, 3243 - 3251.
36. P. M. Couwenberg, Q. Chen and G. B. Marin (1996). Kinetics of a gas-phase chain reaction catalyzed by a solid: Oxidative coupling of methane over Li/MgO-Based catalysts. *Industrial Engineering and Chemistry Research*, 35, 3999-4011.
37. D. Wolf, M. Slinko and E. K. Baerns (1998). Kinetic simulations of surface processes of the oxidative coupling of methane over a basic oxide catalyst. *Applied Catalysis A*, 166, 47-54.
38. D. Chatterjee, O. Deutschmann and J. Warnatz (2001). Detailed surface mechanism in a three-way catalyst. *Faraday Discussions*, 119, 371-384.

39. O. Deutschmann, R. Schwiedernoch, L. I. Maier and D. Chatterjee (2001). Natural gas conversion in monolithic catalysts: Interactions of chemical reactions and transport phenomena. In E. Iglesia, Spivey, J. J., Fleisch, T. H. (Ed.), *Natural gas conversion in monolithic catalysts: Interactions of chemical reactions and transport phenomena*: Elsevier.

Chapter 5: Quantum Chemistry Methods and Bond Additivity Corrections

This chapter presents the various levels of theory, basis sets used in quantum chemistry methods and the bond additivity corrections developed for some of the widely used composite methods. The chapter is organized in the following order. In Section 5.2, we describe the quantum chemistry methods and explain the different levels of theory involved. The wavefunction as well as the DFT-based quantum chemistry methods are described. In Section 5.3, we present the 2 commonly used types of basis sets: Pople's split-valence and Dunning's correlation-consistent basis sets. Notations describing the atomic orbitals as well as the valence and polarization functions used in these basis sets are explained. In Section 5.4, we present the composite G* methods (Gaussian methods) available in Gaussian® suite of programs for complex energy computations. The increasing levels of theory used for geometry optimizations as well as single point energy calculations are described in the context of higher level corrections to the electronic energy. G2 method is used as an example to illustrate improvements in single point electronic energies. In Section 5.5, we present the Bond Additivity Corrections (BAC) for composite quantum chemistry methods. First, the rationale behind bond additivity corrections is explained. Next, the atomic, molecular and bond corrections developed for MP4 as well as G2 methods are described.

5.1 Introduction

With the development of fast computers and computationally efficient optimization algorithms, computational quantum chemistry is increasingly used to estimate the thermochemical properties of several molecules. Often, trends in the estimates of these properties are helpful to gain a molecular understanding of different compounds and pose laboratory scale experiments to improve knowledge of the properties. Quick and reasonably accurate thermochemical properties can be used in the preliminary stages of process flowsheets to design products and processes.

5.2 Quantum Chemistry Methods

Quantum chemistry, which derives the quantum mechanical basis from electronic structure theory, is used to calculate the energies, equilibrium structures optimized with respect to energies and harmonic frequencies, reaction paths and activation energies of chemical reactions. The two broad methods to calculate electronic structures and total energies are based on ab-initio wavefunctions and Density Functional Theory (DFT).

5.2.1 Different Levels of Theory and Computational Time

Wavefunction-based Methods

Wavefunction-based methods, in the increasing level of theory, are Hartree Fock (HF), Moller-Plesset (MP2), Coupled Cluster with Double Substitutions (CCD), Coupled Clusters with Single

and Double substitutions (CCSD) and CCSD with Triple excitations CCSD(T)), Quadratic CI with Single and Double Substitutions (QCISD); and QCISD with Triple excitations QCISD(T). Correlation energy or the difference between calculated and experimental energies for these levels of theory are decreasing in the same order. Correlation energy for the HF method is about 1% of the total energy resulting in 1 eV per pair of electrons. Perturbative treatment of electron correlations in MP2 method accounts for 80% of the 1% correlation energy, self-consistent treatment of single and double substitutions in CCSD accounts for 95% and triple substitutions in CCSD(T) accounts for more than 99% of the 1% energy. The computational costs for HF, MP2, CCSD and CCSD(T) levels of theory scale up exponentially with the basis functions: A^3-A^4, A^5, A^6 and A^7.

The choice of orbitals occupied by the electrons in a molecule corresponds to configuration, and different linear combinations of Slater determinants for each configuration are used to account for spin and Pauli principles. The combinations are approximations of wave functions associated with molecular or atomic states. Even using the best orbitals, small gap remains between the calculated and experimental energy (the correlation energy). The gap, though 1% of the total electronic energy for HF method, can introduce significant error in the calculation of all non-stationary properties including atomization and isomerization energies, since the approximate wavefunction is far from the exact wavefunction in Hilbert space. Infinite set of products of orbitals or configurations form a basis for the exact wavefunction in Hilbert space. But, in practice the basis is truncated and only approximate wavefunctions can be reached. This approach is the Configuration Interaction (CI) method. Correlation errors may cancel for isogyric and isodesmic reactions. Wavefunction-based methods can be accurate if high level of configurational interactions is used. However, these methods are limited to 100

electrons and elegant ways of embedding an accurately described region into a less accurately described surrounding region should be used for larger systems to save computational time.

DFT Methods

DFT methods are less computationally demanding than wavefunction-based methods. DFT describes how the ground state electron density and total energy can be obtained by solving a set of one-electron Schrodinger equations (the Kohn-Sham equations) instead of the complicated many-electron Schrodinger equation. The former simplifies the computation. The two broad types of basis sets used in DFT are localized functions and plane waves. Usually, the core electrons are not treated explicitly, but instead are considered as frozen or accounted by a pseudopotential description of the ionic core. Choice of exchange correlation functional is a main approximation in the DFT calculations.

One of the popular methods for treating exchange correlation is the Becke's Hybrid description of the Exchange Correlation effects (B3LYP). In this method, a Hartree-Fock calculation is performed to derive the exact exchange energy, which is mixed with the DFT-based energy. B3LYP energy is usually 70-80% DFT energy and 20-30% HF energy. A lower contribution from DFT and a higher contribution from HF will improve the accuracy of B3LYP energies. HF is better than DFT for calculating energies of s and d orbitals, while DFT is better than HF for p orbitals. B3LYP hybrid method is computationally intensive. Less intensive methods are the ones that use generalized gradient approximations (GGA).

Each electron in orbital can be in either up (α) or down spin (β), and the spin multiplicities of molecules are based on the total number of spin states resulting from the different permutations, and raising and lowering of the base spin state. Each orbital is designated

by a wave function (Φ) and difference in the orbitals are taken into account while calculating the spin multiplicities. For example, $\alpha\beta + \beta\alpha$ is a singlet when $\Phi_1 = \Phi_2$ and triplet when $\Phi_1 \neq \Phi_2$, $\alpha\alpha$ is singlet when $\Phi_1 = \Phi_2$ and triplet when $\Phi_1 \neq \Phi_2$, $\alpha\beta$ is singlet when $\Phi_1 = \Phi_2$ and triplet when $\Phi_1 \neq \Phi_2$. Multiplicity of a molecule is determined by the number of unpaired electrons it contains. Most normal ground-state equilibrium structures consisting solely of electron pairs are singlet closed-shell molecules. Free radical open-shell molecules with one unpaired electron are doublets, and biradicals with two unpaired electrons are triplets. If S is half the number of unpaired electrons, spin multiplicity is given by $2S + 1$ and $\langle S^2 \rangle$ is $S(S + 1)$.

5.2.2 Different Basis Sets

Basis set refers to the set of nonorthogonal one-particle functions used to build molecular orbitals. Atomic orbital (AO) is one-electron function and Molecular Orbitals (MOs) built from AOs form the LCAO-MO approximation. The most convenient way to define a basis set for any nuclear configuration is to define a particular set of functions for each nucleus, depending only on the nuclear charge of that nucleus. There are two main types of basis functions in use:

1. Slater-Type Atomic Orbitals (STOs)
2. Gaussian-Type Atomic Orbitals (GTOs)

STOs and GTOs

STOs have exponential radial parts:

$$\Phi_c(r) = (x - A_x)^{c_x} (y - A_y)^{c_y} (z - A_z)^{c_z} e^{-\alpha |r - A|}, \qquad (5.1)$$

with a center A = (A_x, A_y, A_z), angular momentum a = (a_x, a_y, a_z) and nuclei-dependent exponent α. STOs, like exact wavefunctions, have cusps at the nuclei and decay exponentially. Unfortunately, integrals over STOs are expensive to compute. STOs are hydrogen-atom like for 1s orbitals, and accurate for short and long-range behavior. However, they lack radial nodes and are not purely spherical harmonics.

Basis functions constructed of GTOs would overcome the computational difficulties of STOs. GTO has the form:

$$\Phi_c(r) = (x - A_x)^{c_x} (y - A_y)^{c_y} (z - A_z)^{c_z} e^{-\alpha |r-A|^2} . \qquad (5.2)$$

GTOs decay very fast and have incorrect nuclear cusps, so many more GTOs than STOs are required to achieve the same accuracy. However, the speed with which integrals over GTOs can be calculated more than compensates for this. GTOs are no longer H-like, even for 1s. These are much easier to compute than STOs due to the application of Gaussian product theorem in former case.

To compromise between computational time and accuracy, linear combinations of GTOs are used to mimic STOs, giving rise to Contracted Gaussian-Type Orbitals (CGTOs). Linear combination of n GTOs gives rise to STO-nG basis. If STO properties are desired, they can be approximated by a sum of Gaussians, which leads to the STO-nG basis sets. These are an example of Contracted GTOs:

$$\Phi_c(r) = \sum_k^{K_A} D_{ck} (x - A_x)^{c_x} (y - A_y)^{c_y} (z - A_z)^{c_z} e^{-\alpha_k |r-A|^2} , \qquad (5.3)$$

where K_A is referred to as the degree of contraction and D_{ak} are the contraction coefficients. The contraction coefficients are not changed during a calculation, reducing the computational overhead.

Having different-sized basis functions allows the atomic orbital to get bigger or smaller when other atoms approach it. The minimal choice is one basis function (STO, GTO and CGTO) for each atomic orbital in the atom; double-zeta (DZ), triple-zeta (TZ), quadruple-zeta (QZ), 5Z, 6Z etc. are used to represent multiple basis functions for each atomic orbital. A split-valence basis uses only one basis function for core AO, and a different basis function for valence AO. For example, H and C atoms have 1 AO (1s) and 5 AOs (1s, 2s, $2p_x$, $2p_y$ and $2p_z$), respectively. Minimal basis with one basis function is used to describe the 1s orbital in H atom, while minimal basis with 5 basis functions are used to describe the 5 orbitals in C atom. DZ basis uses 10 basis functions, with 2 basis functions for each of the 5 orbitals. Split-valence DZ basis uses 9 basis functions, with 2 basis functions for each of the 4 valence orbitals and 1 basis function for the core orbital.

Different basis sets offer trade-offs between accuracy and speed of computations. Bigger the basis set, better would be the accuracy of the computation which comes at the cost of computational time. DFT is less dependent on basis set size than wavefunction-based methods. Convergence of ab initio results is slow with respect to basis set for non-DFT methods.

Pople's Basis Sets

Pople and coworkers developed basis set structure which is given for the whole molecule, rather than a particular atom. The notation emphasizes a split valence (SV) nature of these sets. Typicaly, n-ijG or n-ijkG are encoded for n, the number of primitives for the inner shells, and ij

or ijk, the number of primitives for contractions in the valence shell. The ij notations describe sets of valence double zeta quality and ijk sets of valence triple zeta quality. Generally, s and p contractions belonging to the same electron shell are folded into a sp-shell. In this case, number of s-type and p-type primitives is the same, and they have identical exponents. However, the coefficients for s- and p-type contractions are different.

4-31G basis set for hydrogen (1 valence electron) has a contraction scheme: (31) or (4s) →[2s]; for first row atoms, the scheme is: (8s,4p) →[3s,2p] or (431,31); and for second row atoms the contraction scheme is (12s,8p) →[4s,3p] or (4431,431). For water molecule, these contractions could be encoded as (431,31/31). The 6-311G set represents the following contractions for water (6311,311)/(311) or (11s,5p/5s) →[4s,3p/3s].

Pople's basis sets are also augmented with d-type polarization functions on heavy atoms (n-ijG* or n-ijkG*), and p-functions on hydrogens (n-ijG** or n-ijkG**). In methane, the 4-31G* encodes the split scheme of (431,31,1)/(31) or (8s,4p,1d/4s) →[3s,2p,1d/2s]. In HCN molecule, the 6-311G** would involve contractions, (6311,311,1)/(311,1) or (11s,5p,1d/5s,1p) →[4s,3p,1d/3s,1p]. 6-31G is Pople's split-valence double-zeta basis set which uses a CGTO made of 6 Gaussians to describe the core orbital and 1 CGTO made of 3 Gaussians, and one single Gaussian are used to describe the 2 valence orbitals. 6-31G* (or 6-31G(d)) is 6-31G with d polarization functions on non-hydrogen atoms; 6-31G** (or 6-31G(d,p)) is 6-31G* plus p polarization functions for hydrogen. 6-311G is a split-valence triple-zeta basis; it adds one GTO to 6-31G. 6-31+G is 6-31G plus diffuse s and p functions for non-hydrogen atoms; 6-31++G has diffuse functions for both hydrogen and non-hydrogen atoms. STO-3G and other Pople's basis sets use "SP" shells, which share exponents for s and p functions.

For atoms of the second row, nm-ijG notation is sometimes used. For example, 66-31G means that there is (a) 1 function containing 6 primitives on the innermost s-shell; (b) 1 set of functions belonging to the inner SP-shell (i.e. 2SP shell), each consisting of 6 gaussian primitives (i.e. 1 s-type function and p_x, p_y, p_z functions consisting of 6 primitives with the same exponents). Note though that coefficients in s and p type contractions are different; (c) 2 sets of SP functions for valence SP shell (one set consisting of contractions with 3 primitives and the other with 1 primitive). It is possible to write this as (16s,10p) →[4s,3p] or in more details as (6631,631) contraction scheme or alternatively as s(6/6/3/1), p(6/3/1).

Dunning's Basis Sets

Basis sets optimized at HF level might not be ideal for correlated computations. The correlation-consistent basis sets are optimized using correlated (CISD) wavefunctions. cc-pVXZ is a Dunning correlation-consistent, polarized valence, X-zeta basis with X=D,T,Q,5,6,7. Functions are added in shells. cc-pVDZ for C atom consists of 3s2p1d, cc-pVTZ would be 4s3p2d1f and cc-pVQZ would be 5s4p3d2f1g. Dunning basis sets are designed to converge smoothly toward the complete (infinite) basis set limit. A prefix "aug" means one set of diffuse functions is added for every angular momentum present in the basis; aug-cc-pVDZ for C atom has diffuse s,p,d. Functions describing core correlation are denoted by the letter "C" in the cc-pCVXZ or aug-cc-pCVXZ basis sets.

Dunning's basis sets are designed for high quality calculations using correlation methods. There are 4 basis sets:

- cc-pVDZ of valence double zeta quality.
- cc-pVTZ of valence triple zeta quality.

- cc-pVQZ of valence quadruple zeta quality.
- cc-pV5Z of valence quintuple zeta quality.

Each of these can be augmented by a single diffuse function of each type - s, p, f, g, h etc:

- AUG-cc-pVDZ of valence double zeta quality.
- AUG-cc-pVTZ of valence triple zeta quality.
- AUG-cc-pVQZ of valence quadruple zeta quality.
- AUG-cc-pV5Z of valence quintuple zeta quality.

Table 5.1 shows the number of valence and polarization functions for the different basis sets for various atoms. Note the augmented basis sets add a set of diffuse functions for each type of orbital.

Table 5.1 Valence and Polarization Functions for Correlation-consistent Basis Sets

Atoms	cc-pVDZ	cc-pVTZ	cc-pVQZ	cc-pV5Z
H	2s,1p	3s, 2p,1d	4s,3p, 2d, 1f	5s, 4p, 3d, 2f, 1g
He	2s, 1p	3s, 2p, 1d	4s, 3p, 2d, 1f	not available
B-Ne	3s, 2p, 1d	4s, 3p, 2d, 1f	5s, 4p, 3d, 2f, 1g	6s, 5p, 4d, 3f, 2g, 1h
Al-Ar	4s, 3p, 1d	5s, 4p, 1d, 1f	6s, 5p, 3d, 2f, 1g	7s, 6p, 4d, 3f, 2g, 1h

The largest basis set can only be used for very small molecules. The smallest however is comparable in size to 6-31G(d,p) - in fact smaller since it uses the 5d spherical harmonic d-functions rather than the 6d cartesian d-functions.

It is computationally hard to afford more than pDZ basis sets except for small molecules. Anions must have diffuse functions. cc-pVDZ is not necessarily better than 6-31G(d,p); however, cc-pVTZ is better than 6-311G(d,p) or similar. For example, minimal basis sets in H and C atoms are designated by 1s (1 function) and 2s1p (5 functions). Double-zeta basis and split-valence double-zeta basis in C atom are designated by 4s2p (10 functions) and 3s2p (9 functions).

Polarization functions are used to describe the shift in the AOs when many atoms approach the atom of interest. Basis function of angular momentum l is polarized, when mixed with basis function of angular momentum l+1 giving rise to pDZ, pTZ and pQZ basis sets. Thus, s orbital is polarized when mixed with p orbital and p orbital is polarized when mixed with d orbital. There are 5 and 6d polarization functions for d orbitals, 7and 10f polarization functions for f orbitals. Different basis sets were developed using different number of polarization functions, cc-pVXZ and newer Pople basis sets use 5d functions, while old Pople basis sets use 6d functions.

Diffuse functions are necessary for computations on anions, Rydberg states, electronegative atoms with significant electron density, and Van der Waals complexes for accurate polarizabilities and binding energies. The basis sets should be chosen to balance with correlation method; for example, cc-pVQZ is a suitable basis set for CCSD(T), but excess of what is adequate for HF. Basis set size is designated by the sets of functions it has for each angular momentum type.

5.3 Gaussian Methods Available in Gaussian Suite of Programs

Gaussian® 98 and Gaussian® 03 suite of programs are widely used for computational quantum chemistry for various levels of theory and choices of basis sets. G* methods are complex energy computations involving several pre-defined calculations for the geometry optimizations, frequencies, and single point energies at different levels of theory and basis sets. Final energies in G* methods are derived from a series of computations. These methods are readily available in Gaussian® suite of programs to improve both the accuracy and computational efficiency of the calculations. Over time, different G* methods with increasing levels of theory and basis sets were developed:

- G1: HF/MP2(Full)/6-31G(d)//QCISD(T,E4T)/6-311G(d,p)//MP4/6-311+G(d,p)// MP4/6-311G(2df,p) [1,2].
- G2: HF/MP2(Full)/6-31G(d)//QCISD(T,E4T)/6-311G(d,p)// MP4/6-311+G(d,p)// MP4/6-311G(2df,p)//MP2/6-311+G(3df,2p) [3].
- G2MP2: HF/MP2(Full)/6-31G(d)//QCISD(T)/6-311G(d,p)//MP2/6-311+G(3df,2p) [4].
- G3 – HF/MP2(Full)/QCISD(T,E4T)/6-31G(d)//MP4/6-31+G(d)//MP4/6-31G(2df,p)//MP2(Full)/GTLarge [5].
- G3MP2 – HF/MP2(Full)/QCISD(T)/6-31G(d)// MP2/GTMP2Large/ [6].
- G3B3 - B3LYP/ QCISD(T,E4T)/6-31G(d)//MP4/6-31+G(d)//MP4/6-31G(2df,p)//MP2=Full/GTLarge [7].
- G3MP2B3 – B3LYP/ QCISD(T)/6-31G(d)//MP2/GTMP2Large [7].

G2MP2 and G3MP2 are modified versions of G2 and G3 which use MP2 instead of MP4 for the basis set extension corrections, and are nearly as accurate as the full G2 and G3 methods,

respectively. G3B3 method uses B3LYP instead of HF for optimizing geometry and calculating frequencies, while G3MP2B3 uses MP2 instead of MP4 for basis set extension corrections. These methods are arranged in the increasing order of accuracy and computational efficiency.

G2 method, is chosen as an example, to illustrate the various levels of theory and basis sets used for frequency and single point energy calculations. G2 theory optimizes the geometry of molecules at MP2(FULL) level of theory with 6-31G(d) basis set.. Subsequently, single point energies are calculated for this geometry at increasing levels of theory and basis sets as shown in Table 5.2.

Table 5.2 Levels of Theory and Basis Sets for G2 Calculations

Theory	**Basis Sets**			
	6-311G(d,p)	**6-311+G(d,p)**	**6-311G(2df,p)**	**6-311+G(3df,2p)**
MP2	I	K	L	D
MP4	J	B	C	
QCISD(T)	A			X

Rows of the table give increasing better methods for calculating correlation effects, while the columns give a set of increasingly better basis sets. It is to be noted that 6-311+G(d,p) only adds a set of diffuse functions to the first basis set and 6-311G(2df,p) adds more diffuse basis functions. The last improves both the diffuse and polarization parts of the basis set.

Considering there are plausible methods and basis sets, calculating the energy at the basis set and method for the spot marked "X" is computationally the most demanding of all the basis

sets and methods. At the best method, the smallest basis set is used to get the energy (spot marked "A"). At each level of theory, energies at lower levels of theory are also calculated. Thus in getting the energy at "A", energies are also calculated at "I" and "J". Next, the energy at "B" is calculated and the effect of diffuse function as the difference in energy between "B" and "J" is computed. Then, the energy at "C" is computed and the effect of extending the polarization basis set as the energy difference between "C" and "J" is estimated. Finally, the energy at "D" is calculated, and the effect of even larger basis set as the energy difference between "D" and "I" is corrected by subtracting the energy difference "K" - "I" and "L" - "I".

We define:

$$\Delta E[+] = E["B"] - E["J"]. \tag{5.4}$$

$$\Delta E[2df] = E["C"] - E["J"]. \tag{5.5}$$

$$\Delta_{12} = (E["D"] - E["I"]) - (E["K"] - E["I"]) - (E["L"] - E["I"]). \tag{5.6}$$

$$= E["D"] + E["I"] - E["K"] - E["L"]. \tag{5.7}$$

Energy at "X" is estimated as:

$$E["X"] = E["A"] + \Delta E[+] + \Delta E[2df] + \Delta_{12}. \tag{5.8}$$

$$E["A"] = E["J"] + \Delta E[QC]. \tag{5.9}$$

where

$$\Delta E[QC] = E["A"] - E["J"]. \tag{5.10}$$

This difference is the effects of QCISD(T) on total energy. Thus, E["X"] is rewritten as:

$$E["X"] = E["J"] + \Delta E[QC] + \Delta E[+] + \Delta E[2df] + \Delta_{12}. \tag{5.11}$$

Different terms are added to correct the energy E["X"]:

1. A correction for the zero-point energy (ZPE) is estimated from the frequencies of the optimized geometries from HF/6-31G(d) calculation. This ZPE is then scaled by 0.893, as this improves the agreement with experiment for frequencies and ZPEs at this level of theory.

2. Spin-orbit correction is used for molecules containing 3rd row atoms where the ground state is degenerate such as ^{2}P or $^2\Pi$.

3. An empirical correction, the higher level correction E[HLC] determined as:

$E[HLC] = -An_\alpha - Bn_\beta$, where n_α and n_β are the number of α and β electrons. In the HLC, A is selected as 0.19 mHa to make the energy of the H atom exactly at -0.50 Ha. B is selected to minimize the average deviation between G2 estimated energy and experimental value for a test set of atomization energies, ionization energies, electron affinities and proton affinities.

Outputs for G* calculations, typically printed out by the Gaussian® suite of programs, conclude with the energies at 0K and specified temperature. The latter energy includes a full thermal rather than just the zero-point energy correction. G* theory predictions for enthalpy and Gibbs free energy, both computed using the thermal-corrected G* energies are reported. Note that the same quantities predicted at previous G* method are also printed out:

1. G* (0K)Energy

Zero-point-corrected electronic energy: $E_0 = E_{electric} + ZPE$

2. G* Energy

Thermal-corrected energy: $E = E_0 + E_{translational} + E_{rotational} + E_{vibrational}$

3. G* Enthalpy

Enthalpy computed using the G* predicted energy: $H = E + RT$

4. G* Free Energy

Gibbs free energy computed using the G* predicted energy: G = H – TS

5.4 Bond Additivity Corrections for Quantum Chemistry Methods

Errors in electronic energies obtained from ab initio quantum chemistry calculations could be due to the finite size of the basis sets used and the application of limited electron correlation in the calculations. These errors are therefore systematic and can be corrected to achieve much greater accuracy for predicted heats of formation by applying a variety of empirical corrections related to the elements and bonds in the molecule. These corrections are collectively termed Bond Additivity Corrections (BAC).

BAC suite of methods currently comprises several levels of theory. In the 1980s, BAC procedures were developed for quantum chemical calculations based on the MP4 method [8]. In this method, the molecular electronic energy is obtained from an ab initio electronic-structure calculation at the level of fourth-order Moller-Plesset perturbation theory. Methods using second-order Moller-Plesset perturbation theory (BAC-MP2) [9], G2 theory (BAC-G2) [10], and a hybrid method involving both density functional theory and MP2 have also been developed; these use a different approach for determining the empirical corrections to the ab initio electronic energy than the original BAC-MP4 method.

5.4.1 The BAC-MP4 Method

The BAC-MP4 method is shown schematically in Figure 5.1.

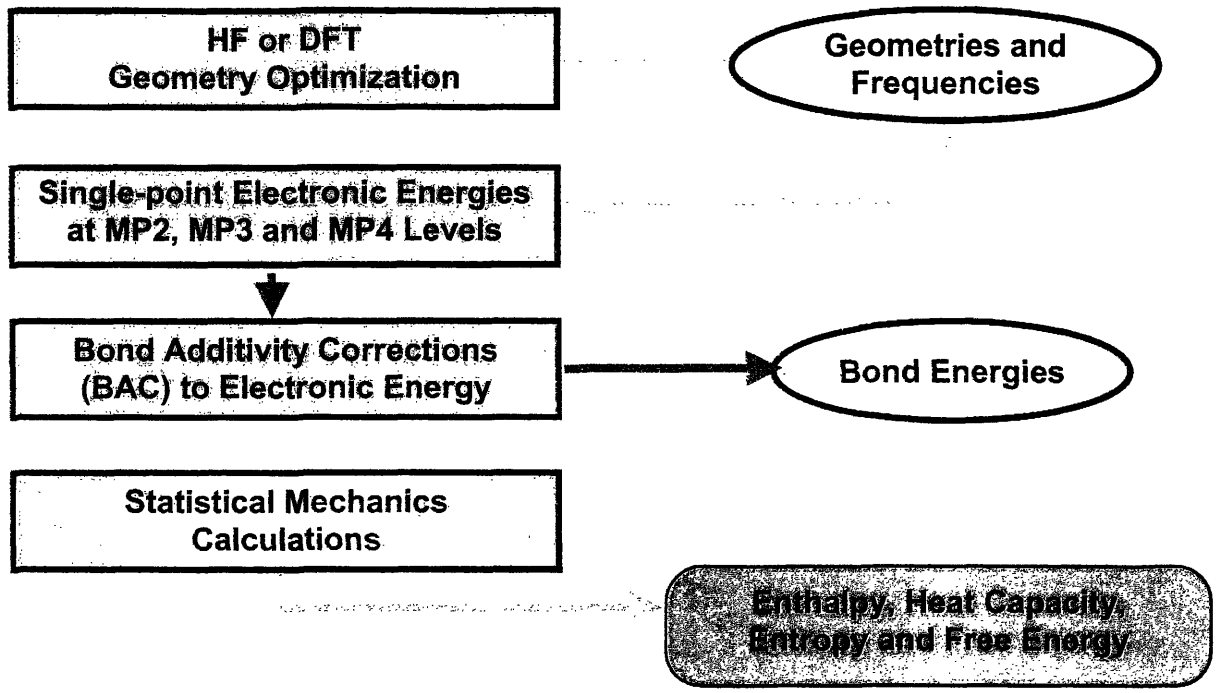

Figure 5.1 BAC-MP4 Procedure for Estimating Thermochemical Properties

All geometry optimizations and single point energy calculations are performed using the Gaussian® suite of quantum chemistry programs.

Molecular Geometries, Vibrational Frequencies and Moments of Inertia

The molecular equilibrium geometry is required input for the MP4 calculation used in the BAC-MP4 method. This geometry with frequencies and moments of inertia are also used in post-ab initio calculations to obtain thermodynamic data at temperatures above 0K. In the BAC-MP4 method, equilibrium geometries and harmonic vibrational frequencies are obtained from Hartree-Fock. Restricted Hartree-Fock (RHF) theory is used for closed shell molecules and unrestricted Hartree-Fock theory (UHF) is used for open-shell molecules. Vibrational frequencies calculated

at this level of theory are known to be systematically larger than experimental values; thus, each calculated frequency is adjusted by the scaling factor 1.12 [11].

Electronic Energies

To determine atomization enthalpies and thus heats of formation, the effects of electron correlation are included by performing single-point calculations, using Moller-Plesset perturbation theory (MP4 using the 6-31G(d,p) basis set with single, double, triple and quadruple substitutions) and the HF/6-31G(d) geometries.

Bond Additivity Corrections and Corrected Heats of Formation

The form of BAC parameters a_{ij}, A_{ij}, and B_k used to calculate the corrections for individual molecules is given below, using the example of a bond between atoms X_i and X_j in a molecule of the form $X_k - X_i - X_j$:

$$E_{BAC}(X_i - X_j) = f_{ij} g_{kij}, \tag{5.12}$$

where

$$f_{ij} = A_{ij} \exp(-\alpha_{ij} R_{ij}), \tag{5.13}$$

$$g_{kij} = (1. - h_{ik} h_{ij}), \tag{5.14}$$

$$h_{ik} = B_k \exp\{-\alpha_{ik}(R_{ik} - 1.4\,\text{Å})\}. \tag{5.15}$$

A_{ij} and a_{ij} are empirically derived parameters that depend on the X_i -X_j bond type and R_{ij} is the bond distance (Å). The factor B_k is used to derive a correction for the effects of neighboring atoms on the X_i -X_j bond and depends on the identity of atom k. A correction is also made in the case of open-shell molecules for spin contamination of the ground state by excited electronic

states. The error in electronic energy caused by this effect was estimated using the approach of Schlegel [12] and is given by:

$$E_{BAC}(S^2) = E(UMP3) - E(PUMP3), \qquad (5.16)$$

where E(UMP3) is the third-order MP energy using the UHF wavefunction and E(PUMP3) is the projected UMP3 energy.

The correction is generally small (~ 0.5 kcal/mol.) but may become large for molecules containing a high degree of unsaturation or low-lying electronic excited states. Closed-shell molecules that are UHF-unstable, such as SiH_2, also require an additional correction. The form of the correction is:

$$E_{BAC}(UHF-unstable) = K_{UHF-I}S(S+1), \qquad (5.17)$$

where K_{UHF-I} is 10.0 kcal/mol. (based on the heat of formation of O_3) and S is the spin obtained from the UHF/6-31G(d, p) calculation.

Atomization Energies and Heats of Formation at 0K

The sum of the BACs is combined with the MP4(SDTQ) electronic energy and unscaled zero point energy to obtain the heats of atomization and formation at 0K ($\sum D_o$ and ΔH_f^0 (0K), respectively). The calculated molecular electronic energy is added to the zero point energy (calculated from the unscaled vibrational frequencies). Next, the resulting energy is subtracted from the calculated electronic energies of the atoms to give an electronic heat of atomization:

$$E_{atomization} = E_i(atoms) - (E_{ab\_initio}(molecule) + E_{ZPE}). \qquad (5.18)$$

Referencing this energy against the experimental ΔH_f^0 (0K) of the atoms in gas phase yields the uncorrected molecular ΔH_f^0 (0K):

$$\Delta H^0_{f0,uncorrected} = \sum_{atoms} \Delta H^0_{f0,atoms} - E_{atomization} \cdot \qquad (5.19)$$

Subtracting the BAC corrections from this energy finally yields the corrected (BAC-MP4) ΔH_f^0 (0K):

$$\Delta H^0_{f0,BAC} = \Delta H^0_{f0,uncorrected} - E_{BAC-Correction} \cdot \qquad (5.20)$$

Thermodynamic Data as Function of Temperature

Entropies, heat capacities, enthalpies, and free energies as a function of temperature are calculated using the heats of formation at 0K, moments of inertia, and vibrational frequencies. Equations derived from statistical mechanics use standard expressions for an ideal gas in the canonical ensemble to compute the heat capacity, enthalpy, and entropy. For consistency with previous work, unscaled frequencies are used to determine ΔH_f^0 (0K), while the scaled frequencies are used to calculate thermochemistry at higher temperatures. Minor differences that would result from using the scaled frequencies to calculate ΔH_f^0 (0K) are incorporated into the BACs.

Treatment of Hindered Rotors

Contributions to heat capacity and entropy from rotating groups are accounted for by substituting a hindered rotor for the corresponding vibrational frequency determined by the HF calculation. Approximate analytical functions have been developed to estimate the hindered rotor energy E_{hr}, heat capacity C_{hr}, and entropy change ΔS_{hr}. The expressions are:

$$E_{hr} = RT(\frac{1}{2} + Y - g(Y))(\frac{x}{e^x - 1}), \qquad (5.21)$$

$$C_{hr} = R(\frac{1}{2} + Y^2 - g(Y) - g(Y)^2)(\frac{x^2}{(e^x - 1)^2}), \quad (5.22)$$

$$\Delta S_{hr} = R(\ln(SI_0) + Y - g(Y))(\frac{z^2 e^z}{(e^z - 1)^2}), \quad (5.23)$$

where

$$g(Y) = Y(\frac{SI_1}{SI_0}), \quad (5.24)$$

$$Y = \frac{V}{2RT}, \quad (5.25)$$

$$x = \frac{1.67}{I_r}\sqrt{\frac{V}{RT}}, \quad (5.26)$$

and

$$z = \frac{3.8}{I_r}. \quad (5.27)$$

where $SI_m(Y)$ is the scaled modified Bessel function of order m. The expressions in Eqs. 5.21-5.23 are exact for I r $\rightarrow$ ¥, as derived by Pitzer and Gwinn [13]. The largest error is in determining the barrier height V and the rotational "degeneracy" for non-symmetrical functional groups.

Error Estimates

Two major sources of uncertainty in the calculated heats of formation result from:

1) applicability of the theoretical methods to a given molecule and 2) lack of good reference compounds for the BACs. The magnitude of the first is estimated using an ad hoc method that uses the results from lower-level calculations:

$$Error(BAC-MP4) = \sqrt{1.0 + (\Delta H_{BAC-MP4} - \Delta H_{BAC-MP3})^2}$$
$$+(\Delta H_{BAC-MP4} - \Delta H_{BAC-MP4SDQ})^2 + 0.25(E_{BAC}(S^2) or E_{BAC}(UHF - I))^2 . \quad (5.28)$$

The second source of uncertainty of the order of a few kcal/mol. scales with number of bonds in the molecule. The use of different reference values would shift our calculated heats of formation as a group, with the consequence that calculated bond dissociation enthalpies and reaction enthalpies are less affected than the heats of formation. Overall, the uncertainties in BAC-MP4 heats of formation lie in the ± 2-7 kcal/mol. range.

5.4.2 The BAC-G2 Method

The BAC-G2 method applies BAC corrections to the standard G2 method, using the Gaussian quantum chemistry codes. The electronic structure calculations to determine the geometry, vibrational frequencies, and electronic energies are the same as those in the G2 method. Specifically, the geometry and vibrational frequencies in the BAC-G2 method are obtained from a Hartree-Fock (HF) calculation (restricted Hartree-Fock, RHF, for closed shell molecules and unrestricted Hartree-Fock, UHF, for open shell molecules) using the 6-31G(d) split-valence basis set with polarization functions on the heavy (non-hydrogen) atoms. At this level of theory, vibrational frequencies are systematically larger than experimental values. We therefore scale the HF harmonic frequencies down by 12%. The electronic energies at the QCI, MP4, and MP2 levels of theory, as well as the collective G1, G2MP2, and G2 electronic energies, are taken directly from the output of G2 method. The basis sets are same as those defined in the standard G2 method. The geometry used in single point calculations is obtained by reoptimizing the HF geometry at the MP2 level, again as defined in the G2 method.

BAC Corrections

Briefly, three types of corrections are used: atomic, molecular, and bondwise, indicated in Eqs. 5.29-5.31. The atomic correction depends on atom type:

$$E_{BAC-atom} = \sum_{k} E_{BAC-atom}(A_k), \tag{5.29}$$

where the sum runs over all atoms in the molecule. The value of $E_{BAC\text{-}atom}$ (A_k) depends on the atom type and A_k is an adjustable parameter.

$$E_{BAC-molecule} = E_{BAC-elec\_pair} = K_{elec\_pair}(Spin_{molecule} - \sum_{atoms} Spin_{atom}), \tag{5.30}$$

where K_{elec_pair} is an empirically adjusted parameter for a specific BAC method and spin refers to spin quantum number. The third type of BAC correction depends on the formation of chemical bonds. In this instance, we distinguish between bonds and pair-wise interactions. A bond is taken to mean the formation of an electron pair between the atoms. This correction addresses systematic errors arising from electron pairing not covered by molecular correction. The correction for each bond A-B in the molecule having neighbors C and D (e.g., C-A-B-D) is given by:

$$E_{BAC-bond}(AB) = A_{AB}e^{-\alpha R_{AB}} + \sum_{C} B_{CA} + \sum_{D} B_{DB}, \tag{5.31}$$

where the first term is the correction for the bond alone, while the corrections for its nearest neighbors are treated as a sum of corrections of each neighbor of the form:

$$B_{CA} = B_C + B_A. \tag{5.32}$$

The B_A's are constants that depend only on the type of atom. The bond distance dependence exists only in the first term for the bond itself. Furthermore, α no longer depends on the type of bond, as it did in the original BAC method. The parameters for each of the corrections are given in Table 5.3. The atomic corrections (Eq. 5.29) are straightforward. For the bond-wise

corrections (Eq. 5.31), the α exponent is taken to be 3.0 $Å^{-1}$, while the pre-exponential coefficient A_{AB} is taken to be the geometric mean of the individual atom types:

$$A_{AB} = -\sqrt{A_{AA}A_{BB}} \; . \qquad (5.33)$$

Eq. 5.31 also includes contributions from the nearest-neighbor B_{ij} terms (defined by Eq. 5.32). The accuracy of parameters comprising these terms (see Table 5.3) is difficult to assess because of their small size. This is due to the fact that to date we have only applied the BAC-G2 method to relatively small molecules (less than seven heavy, i.e., non-hydrogen, atoms), for which accurate experimental thermodynamic data exist. However, these terms become quite significant for larger molecules and halides. Unfortunately, given the limited accuracy of experimental data for larger non-hydrocarbon, unsaturated gas-phase species it will remain difficult to establish the accuracy of the B_{atom} terms.

Table 5.3 BAC-G2 Parameters

	K_{Elec_pair} = **0.860**		
Atom	A_{Atom}	B_{Atom}	A_{ii}
H	0.485	-0.146	1.462
C	1.081	0.051	0.0
N	1.498	-0.010	2.281
O	-0.501	-0.010	114.3
F	-1.942	0.215	373.1
Al	-1.500	0.000	300.0
Si	0.097	0.008	297.4
Cl	-0.776	0.087	1433.7

Heats of Formation

The corrected heat of formation at 0K can now be obtained from the calculated electronic energy. First, the electronic energy is added to the zero point energy, which is automatically included in the G2(0K) output of the Gaussian 94 and Gaussian 98 codes. Next, the resulting energy is subtracted from the electronic energies of the atoms to give an electronic heat of atomization:

$$E_{atomization} = \sum_{i}^{n} E_i(atoms) - (E_{ab\_initio}(molecule) + E_{ZPE}) . \qquad (5.34)$$

Referencing this energy against the BAC-G2 heat of formation at 0K of the atoms yields the uncorrected heat of formation at 0K:

$$\Delta H^0_{f0,uncorrected} = \sum_{atoms} \Delta H^0_{f0,atoms} - E_{atomization} . \qquad (5.35)$$

Subtracting the BAC corrections from this energy finally yields heat of formation at 0K:

$$\Delta H^0_{f0,BAC} = \Delta H^0_{f0,uncorrected} - E_{BAC-Correction} . \qquad (5.36)$$

Thermodynamic Data as Function of Temperature

Heats of formation, entropies and free energies at various temperatures are then obtained using equations derived from statistical mechanics (the same procedure as in the original BAC-MP4 method, which includes corrections for hindered rotors, such as methyl groups). Thus, for finite temperatures, the raw G2 energies (without BAC corrections) obtained from the BAC-G2 method do not correspond to those from the output of a Gaussian G2 calculation, since hindered rotors are included in the BAC procedure.

Error Estimates

Using an ad hoc expression similar to that formulated for the earlier BAC-MP4 method, error estimate (or confidence level) in the BAC-G2 method is obtained. In this case, we use the similarities between the G1 and G2-MP2 methods and the G2 method itself as an indication of the error:

$$Error(BAC-G2) = \sqrt{1+(\Delta H_{BAC-G2} - \Delta H_{BAC-G2MP2})^2 + (\Delta H_{BAC-G2} - \Delta H_{BAC-G1})^2}\,. \quad (5.37)$$

5.5 Summary

In this chapter, we have briefly described the DFT and wavefunction-based methods used in quantum chemistry calculations. HF, MP2, CCD, CCSD, CCSD(T)), QCISD and QCISD(T) are the wavefunction-based methods with increasing level of theory and their corresponding correlation energies decrease in the same order. The computational costs for HF, MP2, CCSD and CCSD(T) levels of theory scale up exponentially with the basis functions: A^3-A^4, A^5, A^6 and A^7. DFT methods which solve the one-electron Schrodinger equation is computationally less demanding than wavefunction-based methods. Localized and plane waves are the broad types of basis sets used in DFT with B3LYP the popular choice for treating exchange correlation by mixing the HF exact energy with DFT-based energy. STOs with H-atom like basis functions are accurate for short and long-range behavior, while contracted GTOs are linearly combined to mimic STOs for computational efficiency. Pople's basis sets given for the whole molecule rather than a particular atom employs a split valence nature of the sets with d-type polarizations and diffuse functions. Dunning's basis sets are correlation-consistent, polarized valence, with double, triple, quadruple and quintuple zeta qualities augmented by a single diffuse function each

of s, p, f, g and h types. G1, G2, G2MP2, G3, G3MP2, G3B3 and G3MP2B3 are the composite quantum chemistry methods with increasing levels of theory available in Gaussian® suite of programs. Since the errors in electronic energies obtained from ab initio methods could be systematic, they can be improved to achieve much greater accuracy for predicted heats of formation by applying a variety of empirical corrections related to elements and bonds in the molecule. Based on this concept, Bond Additivity Corrections (BAC) have been developed for MP4 and G2 methods in literature. Atomic, molecular and spin corrections are added to the electronic energy computed using the composite quantum chemistry methods.

References

1. J. A. Pople, M. Head-Gordon, D. J. Fox, K. Raghavachari and L. A. Curtiss (1989). Gaussian-1 theory: A general procedure for prediction of molecular energies. *Journal of Chemical Physics,* 90, 5622-.5629.
2. L. A. Curtiss, C. Jones, G. W. Trucks, K. Raghavachari and J. A. Pople (1990). Gaussian-1 theory of molecular energies for second-row compounds. *Journal of Chemical Physics,* 93, 2537-2545.
3. L. A. Curtiss, K. Raghavachari, G. W. Trucks, and J. A. Pople (1991). Gaussian-2 theory for molecular energies of first- and second-row compounds. *Journal of Chemical Physics,* 94, 7221-7230.
4. L. A. Curtiss, K. Raghavachari, and J. A. Pople (1993). Gaussian-2 theory using reduced Møller–Plesset orders. *Journal of Chemical Physics,* 98, 1293-1298.
5. L. A. Curtiss, K. Raghavachari, P. C. Redfern, V. Rassolov and J. A. Pople (1998). Gaussian-3 (G3) theory for molecules containing first and second-row atoms. *Journal of Chemical Physics,* 109, 7764-7776.
6. L. A. Curtiss, P. C. Redfern, K. Raghavachari, V. Rassolov, and J. A. Pople (1999). Gaussian-3 theory using reduced Møller-Plesset order. *Journal of Chemical Physics,* 110, 4703-4709.
7. A. G. Baboul, L. A. Curtiss, P. C. Redfern, and K. Raghavachari (1999). Gaussian-3 theory using density functional geometries and zero-point energies. *Journal of Chemical Physics,* 110, 7650-7657.
8. P. Ho and C. F. Melius (1990). Theoretical study of the thermochemistry of fluorosilanes (SiF_n and SiH_nF_m) compounds and hexafluorodisilane. *Journal of Physical Chemistry*, 94, 5120-5127.
9. M. R. Zachariah and C. F. Melius. Theoretical calculation of thermochemistry for molecules in the Si-P-H system. *Journal of Physical Chemistry*, 101, 913-918.
10. C. F. Melius and M. D. Allendorf (2000). Bond additivity corrections for quantum chemistry methods. *Journal of Physical Chemistry*, 104, 2168-2177.
11. P. C. Hariharan and J. A. Pople (1973). The influence of polarization functions on molecular orbital hydrogenation energies. *Theoretica Chimica Acta*, 28, 213-222.
12. H. B. Schlegel (1986). Potential energy curves using unrestricted Møller–Plesset perturbation theory with spin annihilation. *Journal of Chemical Physics,* 84, 4530-4534.
13. K. S. Pitzer and W. D. Gwinn (1942). Energy levels and thermodynamic functions for molecules with internal rotation I. Rigid frame with attached tops. *Journal of Chemical Physics,* 10, 428-440.

Chapter 6: Bond Additivity Corrections for G3B3 and G3MP2B3 Quantum Methods

This chapter presents the development, application and assessment of BAC procedures for the G3B3 and G3MP2B3 methods. The chapter is organized in the following order. In Section 6.2, we describe the BAC procedures and define the different forms of corrections to heats of formation of molecules. We present the approach to estimate thermochemical properties and discuss the reference set of molecules. In Section 6.3, we present the calculated BAC-G3B3 and BAC-G3MP2B3 parameters for atom, molecular and bond corrections. We compare the heats of formation predicted by BAC methods against experimental values and heats of formation predicted by uncorrected G3B3 and G3MP2B3 methods. We assess the overall as well as specific accuracy of BAC-G3B3 and BAC-G3MP2B3 methods in predicting the heats of formation of different compounds. We present a statistical analysis to compare the overall accuracy of various BAC procedures. For specific classes of compounds, we compare the heats of formation predicted by the BAC-G3B3 and BAC-G3MP2B3 methods against the values predicted by modified G3 methods: G3X, G3SX and G3X2 methods. These classes of compounds mainly involve third-row atoms, hypervalent species and Set A compounds [1], triatomic and larger nonhydrogen species used in the G3/99 reference set [2] and phosphorus oxides used to assess G3X2 theory [3,4]. Finally, we analyze the predictive capabilities of BAC-G3B3 and BAC-G3MP2B3 methods for ions and transition state structures.

6.1 Introduction

Efforts have been made since the 1950s to improve the accuracy of theoretical quantum chemistry methods for calculating thermochemical properties of different molecules [5-14]. Quantum chemistry methods have progressed and corrections added to these methods to improve the accuracy and predictive capability of estimated thermochemical properties. New hybrid methods that combine several low-level calculations have been employed to estimate the results of a high-level calculation with computational efficiency. Basis sets have evolved over time and they have been modified to improve the accuracy of calculations. For example, size-consistent Complete Basis Set (CBS) extrapolations have been developed to correct the truncation errors due to one-electron basis set and Quadratic CI (CBS-QCI) and coupled cluster methods (CCSD(T)) have been successfully applied to complete basis set approaches. A series of composite methods, referred to as Gaussian-n theories, have been progressively developed to optimize geometries, calculate frequencies and single point energies at increasing levels of theory and basis sets [15-21]. These pre-defined sets of computational methods are readily available in the Gaussian® suite of programs [22].

Gaussian-3 (G3) based theory, the most recent in the Gaussian-n series, provides improved accuracy over the earlier G2 and G1 methods [19]. However, further modifications have been made in G3 theory to improve the accuracy for large nonhydrogen systems containing third-row atoms such as hypervalent SF_6 and PF_5 molecules [2]. These modifications, in the form of B3LYP/6-31G(2df,p) geometry, B3LYP/6-31G(2df,p) zero-point energy and g polarization function in the G3Large basis set for third-row atoms at the HF level, resulted in the G3X theory [1]. G3X theory and its variants have improved accuracy over G3 theory, however at the cost of 10%-15% additional computational time [1]. Despite their advances, there are still

some non-hydrogen molecules mainly involving the third-row atoms for which the heats of formation are outside the desired accuracy of 2 kcal/mol. A general and reliable systematic correction procedure is desirable to improve the predictive capability for the heats of formation of compounds involving all elements of first 3 rows of the periodic table.

In the 1980s, Bond Additivity Correction (BAC) procedures were developed for quantum chemical calculations based on the MP4 method [23,24]. Different variations of BAC-MP4 (BAC-MP4/6-311++G**, BAC-MP4 with HF geometry optimization, and BAC-MP2) were developed to reduce computational time or improve accuracy [25,26]. But, these procedures suffer from the same limitations as BAC-MP4, due to similar functional forms of the BAC corrections. Hence, BAC-G2 was developed to correct G2 methods to calculate energies for both small and large molecules [27]. This approach has also been extended to other levels of electron correlation and to a hybrid combination of MP2 and DFT methods. G3-based methods have proven to be computationally faster and more accurate than G2 methods. In this paper, we address the appropriateness and value of applying the BAC procedure to the G3-based methods. We have therefore developed new Bond Additivity Correction parameters for the G3-based methods, G3B3 and G3MP2B3. These methods use the B3LYP/6-31G(d) method as opposed to G3, which use HF and MP2 methods for the geometry optimization and frequency calculations. The B3LYP method not only enhances the consistency of optimized geometries but also provides consistency with the BAC-hybrid and BAC-DFT methods.

The BAC procedure involves the atomic, molecular and pair-wise bond corrections for the heats of formation of stable molecules as well as radicals and ions. BAC parameters have been obtained by minimizing the errors between the BAC-G3B3 predictions and experimental heats of formation for a 155-molecule reference set, containing a variety of molecules. Our

reference set is larger than the one used for calculating the BAC-G2 parameters, due to the greater accuracy of the G3 methods. In addition to the reference set, we also have a test set of compounds, which is used to test the predictive capabilities of BAC parameters computed using the reference set. The test set includes many neutrals, ions and transition state structures from the first three rows of the periodic table.

Like the BAC-G2 method, BAC-G3B3 and BAC-G3MP2B3 require parameters for each atom type, but not for each bond type as in the BAC-MP4 method. The BAC-MP4 method provided excellent thermochemistry for combustion and CVD systems, but could not treat ions. Furthermore, it was inadequate for systems with highly oxidized species involving SO_x's, NO_x's and PO_x's. The BAC-G2 method attempted to correct the discrepancies for halogens, but required large correction terms, which led to accumulated errors, particularly for the heats of atomization. The BAC-G3B3 and BAC-G3MP2B3 methods should provide a better base for these systems, since the G3 methods have smaller inherent and systematic errors. As we shall show, the BAC-G3B3 method provides the best estimates of thermochemistry for compounds involving the first 3 rows of the periodic table. Reasonably accurate experimental data is known for the thermochemistry of most of these compounds. Many of the compounds had been used earlier in the reference set to evaluate the BAC parameters for BAC-G2, BAC-MP4, BAC-MP2 and BAC-hybrid methods.

In this work, we compile an updated reference set of heats of formation for comparing thermochemical parameters and determining BAC parameters. The result of this work are sets of parameters defining the BAC-G3B3 and BAC-G3MP2B3 procedures along with comparisons with experimental and other theoretical approaches indicating the accuracy of BAC-G3B3 and

BAC-G3MP2B3 methods. The parameters developed have predictive capabilities that can be used for a variety of molecules.

6.2 BAC Procedure for Estimating Thermochemical Properties

In this section, we describe the BAC procedure for estimating the thermochemical properties: heat of formation, heat capacity, entropy and free energy of a molecule. The overall BAC procedure and the sequence of calculations are schematically shown in Figure 6.1.

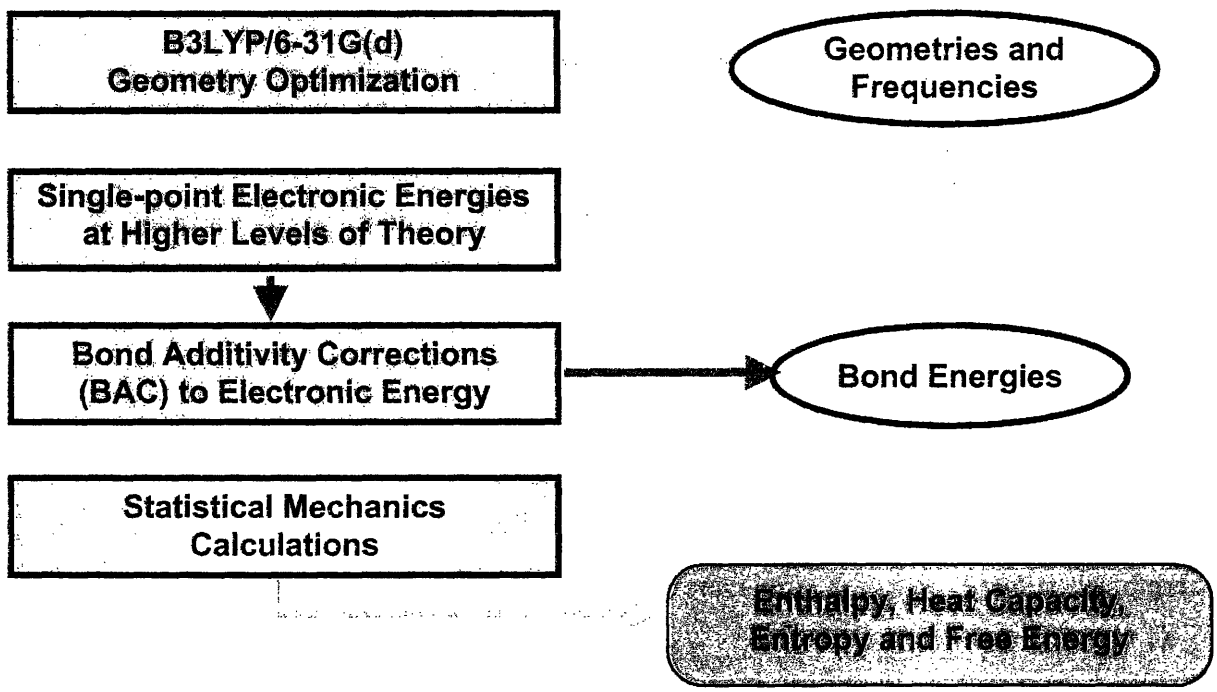

Figure 6.1 BAC Procedure for Estimating Thermochemical Properties

First, the molecular geometry is optimized and vibrational frequencies are calculated at B3LYP level of theory using the 6-31G(d) basis set. Next, single point calculations are performed at

increasing levels of theory and basis sets to obtain the raw electronic energy. BAC corrections are added to the raw electronic energy to determine the corrected electronic energy. The corrected energy is then used to derive the enthalpy, entropy, heat capacity and free energy of the molecule. In the following subsections, we describe the details of the BAC-G3B3 and BAC-G3MP2B3 procedure.

6.2.1 G3B3 and G3MP2B3 Electronic Structure Calculations

Electronic structure calculations are performed to obtain the geometry, vibrational frequencies, and electronic energy of a molecule. Within the G3 suite of methods, we have chosen the G3B3 and G3MP2B3 methods for applying the BAC procedure. The G3B3 and G3MP2B3 methods use the B3LYP level of theory with the 6-31G(d) basis set to determine the equilibrium geometry and vibrational frequencies. We chose the B3LYP method for greater consistency (only a single geometry optimization is needed) and accuracy. In addition, the B3LYP employs the same geometry and frequency calculations used by the BAC-hybrid and BAC-DFT procedures, ie. B3LYP/6-31G(d). The resulting vibrational frequencies are used subsequently to determine the zero point energy (ZPE) of the molecule derived from statistical mechanics (See Figure 6.1).

Having determined the structure and vibrational frequencies of the molecule, single-point electronic energy calculations are performed using a higher level of electronic structure theory that incorporates electron correlation. For the BAC-G3B3 method, we apply the G3B3 method, involving QCISD(T, E4T) with 6-31G(d) basis set, MP4 with 6-31G(2df,p) basis set, and MP2 with GT Large basis set. For the BAC-G3MP2B3 method, we apply the G3MP2B3 method, involving QCISD(T) with 6-31G(d) basis set and MP2 with GTMP2Large basis set. The

combination of geometry optimization, frequency calculation, and electronic energy calculation is performed as a single procedural step within the Gaussian® suite of programs using the keywords: G3B3 or G3MP2B3.

6.2.2 BAC Corrections to Electronic Energy

To correct for errors in electronic energy of the molecule, we had developed a set of empirical expressions collectively referred to as Bond Additivity Corrections [28]:

$$E_{BAC-Correction}(total) = E_{BAC-atom} + E_{BAC-molecule} + \sum_{ij} E_{BAC-bond}(A_i A_j), \quad (6.1)$$

where ij is summed over all the chemical bonds in the molecule. The total correction consists of three terms: 1. an atomic correction due to all the atoms that make up the molecule, 2. a molecular correction due to the molecule as a whole and 3. bond corrections due to all the bonds in the molecule. The correction terms are functions of the BAC parameters which are obtained by comparing the BAC predicted heats of formation with a reference set of experimental values.

There are 4 kinds of BAC parameters: 1. A_{atom} (atom correction), 2. B_{atom}, 3. A_{ii} (bond corrections) and 4. $K_{elec\text{-}pair}$ (electron pair correction). The atom and bond correction parameters depend on the types of atom, while the electron pair correction parameter depends on the molecular spin state. Physical meaning of these parameters and their respective contributions to the atomic, molecular and bond correction terms in Eq. 6.1 are briefly described in the following subsections.

Atomic Corrections

The atomic correction is summed over all the atoms making up the molecule:

$$E_{BAC-atom} = \sum_k A_k \,. \tag{6.2}$$

The atomic correction corrects errors in the intra-atomic electron correlation, which is due to the differences between atomic electronic configurations, charge and spin-orbit coupling, as well as core valence interactions and other relativistic effects. Atom parameters improve the accuracy of molecular predictions by shifting some of the systematic error into the calculation of constituent elements.

Molecular Corrections

Molecular correction (second term in Eq. 6.1) corrects the error from overall electronic structure of molecule:

$$E_{BAC-molecule} = E_{BAC-elec-pair} + E_{BAC-S2} \,. \tag{6.3}$$

$E_{BAC\text{-}clcc\text{-}pair}$ is the energy difference due to the spin of the molecule and the individual atoms comprising the molecule:

$$E_{BAC-elec-pair} = K_{elec-pair}(S_{molecule} - \sum_k S_k) \,. \tag{6.4}$$

$S_{molecule}$ and S_k are spin quantum numbers for the molecule and the k^{th} atom. (S for singlet, doublet, triplet and quartet are 0, 0.5, 1 and 1.5, respectively).

Errors due to the interaction of electrons in atoms and molecules are systematic, and depend on the way in which electron correlation is accounted for while computing the electronic energies of molecules. Size of the correlation error depends on the spin state of the molecule, and the errors are much larger when electrons are paired than when they are unpaired. Hence, the correction term involving $K_{elec\text{-}pair}$ describes the general case of electron pairing. It needs to be noted that the molecular correction term destroys the size consistency of quantum chemistry

methods. For example, the sum of the calculated energies for hydrogen and oxygen atoms is not the same as the energy of the hydroxyl radical when the 2 atoms are fixed at infinity.

The second term in Eq. 6.3, corresponding to $E_{BAC\text{-}S2}$, depends on the spin contamination, if present in the electronic wave function. For example, a doublet state may have a quartet-state spin contamination. The spin contamination term corrects the errors arising from the open-shell methods based on unrestricted Hartree-Fock (UHF). Since DFT methods tend not to have any significant instability, we do not include the unrestricted wave function spin correction.

Bond-wise Corrections

Bond-wise corrections address the systematic error from electron pairing not covered by the molecular correction term. Correction for each bond A-B in the molecule having neighbors C and D is:

$$E_{BAC-bond}(AB) = A_{AB}e^{(-\alpha R_{AB})} + \sum_{C} B_{CA} + \sum_{D} B_{DB} \,. \qquad (6.5)$$

The first correction term is a function of bond correction parameter (A_{AB}), exponent (α) and bond distance (R_{AB}). Due to the negative exponential dependence, the correction is more significant for molecules with shorter bond distances, which are common for unsaturated, dative and hypervalent bonds. This term is important for bonds between atoms in the second and third rows. Typical examples are PF_5 and SF_6, where the heavier *p*-block elements are attached to highly electronegative elements such as the halogens or oxygen. Hence, bond correction parameter A_{AB} plays an important role in correcting the errors in hypervalent compounds.

For the BAC-G3B3 and BAC-G3MP2B3 procedures, A_{AB} is set as the geometric mean of the A_{ii}s for the atoms A and B:

$$A_{AB} = \sqrt{A_{ii,A} \times A_{ii,B}} \,. \qquad (6.6)$$

A_{ii} is dependent on the atom type and not the bond type, and the bond dependence of the correction parameter A_{AB} comes from the geometric mean of the 2 A_{ii} s. The second and third terms (B_{CA} & B_{DB}) in Eq. 6.5 correct for the errors due to nearest neighbors. The correction for the nearest neighbors is the sum of the corrections for the individual neighboring atoms:

$$B_{CA} = B_C + B_A . \tag{6.7}$$

Due to B_{CA} and B_{DB}, the total bond-wise correction is not zero when the bond distance is infinity.

6.2.3 Thermochemical Properties

Having obtained the electronic energy of the molecule, we first calculate the electronic heat of atomization:

$$E_{atomization} = \sum_{i}^{n} E_i(atoms) - [E_{ab-initio}(molecule) + E_{ZPE}]. \tag{6.8}$$

Heat of atomization is subtracted from the sum of experimental heats of formation of the atoms to yield the uncorrected heat of formation at 0K:

$$\Delta H_{f0,uncorrected} = \sum_{atoms} \Delta H_{f0,atoms} - E_{atomization} . \tag{6.9}$$

The total BAC correction is subtracted from the uncorrected heat of formation to yield the corrected heat of formation at 0K:

$$\Delta H_{f0,BAC} = \Delta H_{f0,uncorrected} - E_{BAC\text{-}correction} . \tag{6.10}$$

Statistical mechanics is used to calculate the enthalpy, entropy and free energy of the molecule at desired temperature. The thermochemical properties as a function of temperature can be fit to form the NASA polynomial coefficients compatible with Chemkin thermodynamic database [28].

We obtain the error estimate or the confidence level of the heats of formation predicted by BAC-G3B3 and BAC-G3MP2B3 methods. We use the similarities between G3B3 and G3MP2B3 methods to obtain the error estimate (in kcal/mol):

$$Error_{BAC-G3B3} = \sqrt{1+(\Delta H_{BAC-G3B3} - \Delta H_{BAC-G3MP2B3})^2 + (\Delta H_{BAC-G3B3} - \Delta H_{Raw-G3B3})^2} \quad (6.11)$$

$$Error_{BAC-G3MP2B3} = \sqrt{1+(\Delta H_{BAC-G3B3} - \Delta H_{BAC-G3MP2B3})^2} \quad (6.12)$$

Since the raw G3B3 method is reasonably accurate in predicting the heats of formation for most molecules, it is used as one of the references while computing the error estimate. This helps one to identify molecules with consistently large errors due either to the raw G3B3 method or to large corrections within the BAC procedure. For large error estimates, further electronic energy calculations should be applied to the given molecule at higher levels of theory and basis sets; basis set extrapolations for small basis sets is not sufficient to identify the cause of the uncertainty.

6.2.4 Reference and Test Set of Molecules

The parameters for the BAC procedure are determined by fitting the calculated heats of formation to a reference set of experimental values. The reference set of molecules consists of open and closed shell compounds representing various chemical moieties, multireference configurations, isomers, and degrees of saturation. For the BAC-G3B3 and BAC-G3MP2B3 procedures, the reference set is an extension of the one used for calculating the BAC-G2 parameters. We created an extended test set to ascertain the predictive capability of the BAC methods. The test set extends the reference set to include ions as well as additional molecules involving third-row atoms, including Set A compounds [1] and the nonhydrogen species (triatomic and larger) used in the G3/99 test set [1,2] as well as PO_x compounds used to assess

the G3X2 theory [3,4]. Unlike the G2 method, the G3 methods provide more reliable and systematic treatment of the heats of formation for these additional third-row containing molecules.

Table D.1 in the appendix lists the heats of formation for the reference set used in the current work, along with comparison of the values used in the previous work. Table D.2 lists the heats of formation of compounds used in the extended test set. Experimental sources for the heats of formation are also cited in Tables D.1 and D.2. In Table 6.3, Section 3.2, we also list, for convenience, the experimental heats of formation (Column 2). Heats of formation of molecules in the reference set have been quite well established experimentally. Most of the experimental values for the reference set of molecules are the ones recently recommended by the IUPAC subcommittee [29]. The recommended values have been taken from evaluations or reviews. For compounds involving Si, P, S, Al and B atoms, experimental values are taken from other data sources. For some compounds, the updated values recommended by IUPAC subcommittee are significantly different from the ones used in fitting the BAC-G2 parameters [27], in particular, NH_2, HNO, CN, CH_2OH, CH_3CN, $CH_2CH{=}CH_2$ and CS. The differences in the experimental heats of formation are listed in Table D.3 in Appendix D.

6.3 Results and Discussion

In this section, we present the results and assess the performance of the BAC-G3B3 and BAC-G3MP2B3 methods for the thermochemical properties for various types of molecules. The assessment is made by comparing the predicted heats of formation against experimental data as well as values predicted by many theoretical methods for different classes of compounds both in the reference set and the extended test set of molecules.

6.3.1 BAC-G3B3 and BAC-G3MP2B3 Parameters

BAC parameters are obtained by minimizing the difference between BAC predicted heats of formation and established experimental values for the 155-molecule reference set. The resulting parameters for the BAC-G3B3 and BAC-G3MP2B3 are listed in Tables 6.1 and 6.2, respectively.

Table 6.1 BAC-G3B3 Parameters (kcal/mol.)

		$K_{elec\ pair}$ = 0.318	
Atom	A_{atom}	B_{atom}	A_{ii}
H	0.021	0.060	1.1500
B	0.050	0.010	1.1242
C	0.141	0.005	0.0000
N	0.278	0.054	0.0000
O	0.000	-0.024	45.8645
F	0.023	0.031	50.9352
Al	-0.70	-0.05	2.0000
Si	0.003	0.058	22.3296
P	-0.337	0.049	609.9930
S	-0.664	0.063	503.9800
Cl	0.146	0.046	1074.3082

Table 6.2 BAC-G3MP2B3 Parameters (kcal/mol.)

		$K_{elec\ pair}$ = 0.286	
Atom	A_{atom}	B_{atom}	A_{ii}
H	0.000	0.113	0.3259
B	0.030	0.004	1.3241
C	-0.230	0.002	0.0000
N	0.092	0.081	2.2571
O	0.000	0.031	68.4380
F	-0.080	0.110	59.0911
Al	-0.575	-0.050	1.0000
Si	-1.277	0.119	10.9056
P	-0.675	0.031	467.4820

S	-1.622	0.064	519.0579
Cl	-0.496	0.133	1172.3986

The BAC-G3B3 atom correction parameters are less than 1 kcal/mol for all the elements, unlike the BAC-G2 atom parameters some of which were greater than a kcal/mol (See Table 1 in Reference [27]). Specifically, BAC-G2 atom correction parameters for H, C, N, O and F were 0.485, 1.081, 1.498, -0.501 and -1.942 kcal/mol, while the corresponding BAC-G3B3 parameters are 0.021, 0.141, 0.278, 0.000 and 0.023. This indicates the overall accuracy of the G3B3 methods as compared to the G2 method, especially for compounds involving interactions between second and third row elements. Since G3MP2B3 is less accurate than G3B3, particularly for third-row elements, the atom correction parameters are considerably larger for the BAC-G3MP2B3 procedure.

$K_{elec\text{-}pair}$'s for BAC-G3B3 (0.318) and BAC-G3MP2B3 (0.286) are smaller than that for BAC-G2 (0.860). In BAC-G2, the $E_{BAC\text{-}elec\text{-}pair}$ correction terms were larger for molecules having many atoms, since the accumulation of spin quantum number for each atom resulted in a large net $E_{BAC\text{-}elec\text{-}pair}$ (See Eq. 6.4). However, these large corrections tended to be compensated by the large atomic corrections, $E_{BAC\text{-}atom}$ (Eq. 6.2). The $K_{elec\text{-}pair}$ and atom parameters are both small for BAC-G3B3 and BAC-G3MP2B3 methods. To some extent, errors due to electron pairs were accounted within raw G3 methods by means of the semi-empirical HLC parameters, which were fit using the experimental heats of formation [1]. The HLC parameters were helpful in correcting the errors separately due to unpaired and paired electrons in atoms and molecules. The $K_{elec\text{-}pair}$ computed in this work corrects the additional errors not covered by the HLC parameters.

6.3.2 Assessment of the BAC-G3B3 and BAC-G3MP2B3 Procedures for Reference-set of Molecules

Table 6.3 compares the heats of formation predicted by BAC-G3B3 and BAC-G3MP2B3 against those predicted by the raw G3B3 and raw G3MP2B3 methods and with the established experimental values (see Tables D.1 and D.2 in Appendix D for references to experimental data). The raw G3B3 and G3MP2B3 values are listed to help identify the deviations of raw energies from experimental values. For ready reference, the accuracies in the predicted heats of formation for the BAC-G3B3, BAC-G3MP2B3, and BAC-G2 methods (theory minus experiment) are listed in last 3 columns of the table. Some entries in raw G2 and BAC-G2 columns in Table 6.3 are blank since the corresponding molecules are newly added into the reference or test set.

Table 6.3 Comparison of Raw and BAC Predicted Heats of Formation against Experimental Values for Reference-set of Molecules

	Heat of Formation (kcal/mol.)									
								Error = Theory - Experiment		
Neutrals	**Experimental**	**Raw-G3B3**	**BAC-G3B3**	**Raw-G3MP2B3**	**BAC-G3MP2B3**	**Raw-G2**	**BAC-G2**	**BAC-G3B3**	**BAC-G3MP2B3**	**BAC-G2**
Reference Set										
C	171.3	171.2	171.1	171.2	171.4	171.2	170.1	-0.2	0.2	-1.2
CCl_4	-22.9	-23.1	-23.5	-24.8	-23.4	-25.8	-22.8	-0.6	-0.5	0.1
CF_4	-223.2	-223.2	-222.9	-223.1	-223.1	-228.6	-222.6	0.3	0.1	0.4
$CH_2\ ^1A_1$	102.5	101.7	102.0	101.4	102.0	101.3	101.2	-0.4	-0.4	-1.7
$CH_2\ ^3B_1$	93.4	92.2	92.2	92.0	92.3	94.6	93.6	-1.2	-1.1	-0.2
CH_2Cl_2	-22.8	-21.8	-22.0	-22.8	-22.2	-23.5	-21.7	0.8	0.6	1.1
CH_2F_2	-108.3	-108.2	-108.1	-108.2	-108.3	-110.9	-107.5	0.2	0.0	0.8
H_2CNH	21.6	21.0	21.3	20.8	21.2	20.6	20.4	-0.3	-0.4	-1.2
CH_2NH_2	35.7	36.2	36.0	36.5	36.2	36.8	36.4	0.3	0.5	0.7
CH_2O	-26.0	-27.0	-26.4	-27.0	-26.4	-28.1	-26.7	-0.5	-0.5	-0.8
CH_2OH	-4.3	-4.2	-4.1	-4.0	-3.9	-3.9	-3.7	0.2	0.4	-1.6
$CH_2(OH)_2$	-93.5	-94.5	-94.2	-93.9	-94.0	-95.9	-94.5	-0.7	-0.5	-1.0
CH_3	35.0	34.2	34.2	34.3	34.4	35.0	34.8	-0.8	-0.6	-0.1
CH_3Cl	-19.6	-19.2	-19.4	-19.6	-19.5	-20.6	-19.3	0.3	0.1	0.3
CH_3F	-55.6	-56.7	-56.7	-56.6	-56.8	-58.5	-56.4	-1.1	-1.2	-0.8
CH_3NH	42.4	42.5	42.4	42.7	42.4	42.9	42.6	0.0	0.0	0.2
CH_3NH_2	-5.5	-4.8	-5.1	-4.4	-5.2	-5.6	-5.2	0.4	0.3	0.3
CH_3NHNH_2	22.6	23.1	22.5	23.7	22.3	22.0	22.4	-0.1	-0.3	-0.2
CH_3NO_2	-17.9	-18.9	-18.5	-17.5	-18.2	-20.8	-18.8	-0.7	-0.3	-0.9
CH_3O	4.2	4.3	4.5	4.5	4.4	4.7	6.0	0.3	0.3	1.8
CH_3ONO	-15.6	-16.8	-16.0	-16.0	-16.2	-18.7	-16.5	-0.4	-0.6	-0.9
CH_3ONO_2	-28.6	-30.8	-29.8	-28.8	-29.4	-32.9	-29.6	-1.2	-0.8	-1.0

$CH_3OO\ ^2A''$	2.5	2.8	2.5	3.3	2.2	2.1	2.5	0.0	-0.4	0.0
CH_3OOH	-31.3	-30.8	-30.8	-30.1	-31.0	-32.0	-30.9	0.5	0.3	0.4
CH_3SH	-5.5	-5.0	-4.7	-6.0	-4.7	-5.5	-5.1	0.8	0.8	0.4
CH_3SiH_3	-6.9	-6.7	-7.6	-6.7	-7.7	-7.6	-6.3	-0.7	-0.7	0.6
CH_4	-17.9	-18.0	-18.1	-17.7	-18.0	-18.7	-18.0	-0.2	-0.1	-0.1
$CHCl_3$	-24.7	-23.6	-23.9	-25.1	-24.1	-25.8	-23.4	0.8	0.6	1.3
CHF_3	-166.9	-166.8	-166.6	-166.8	-166.8	-170.7	-166.0	0.3	0.1	0.7
CO	-26.4	-27.0	-26.6	-27.8	-27.0	-28.3	-27.1	-0.1	-0.6	-0.7
CO_2	-94.1	-95.7	-94.9	-95.5	-94.4	-96.8	-94.4	-0.8	-0.4	-0.3
CS	66.6	65.9	67.1	63.6	66.0	65.9	66.4	0.4	-0.6	1.4
CS_2	28.0	25.0	27.0	22.7	26.9	25.8	26.9	-1.0	-1.1	-1.1
HCN	32.3	30.6	31.0	30.5	31.3	31.1	30.7	-1.3	-1.0	-1.6
HCO	10.3	9.4	9.8	9.0	9.7	9.2	10.0	-0.5	-0.7	-0.1
HCOOH	-90.5	-91.1	-90.4	-90.7	-90.1	-92.6	-90.8	0.1	0.4	-0.2
HNCS	30.0	29.8	31.0	29.1	31.5	30.5	30.6	1.0	1.5	0.6
OCS	-34.0	-36.1	-34.6	-36.8	-34.2	-35.8	-34.1	-0.6	-0.3	-0.2
$CH\ ^4\Sigma-$	157.4	157.5	157.3	156.7	156.9	161.3	159.7	-0.1	-0.5	2.3
CH_3PH_2	-4.4	-3.5	-3.9	-4.1	-3.9	-4.4	-4.2	0.5	0.5	0.1
CCl_2F_2	-117.9	-118.3	-118.4	-118.9	-118.1	-122.9	-118.4	-0.5	-0.2	-0.5
$C\ ^5S$	267.7	267.8	267.4	267.9	267.9	268.1	266.2	-0.3	0.2	-1.5
CH_3OH	-48.2	-48.4	-48.3	-48.0	-48.2	-49.5	-48.5	-0.1	0.0	-0.3
$-CH_2CH_2O-$	-12.6	-13.0	-12.4	-12.7	-12.5	-14.0	-13.1	0.1	0.1	-0.6
$-CH_2CH_2S-$	19.7	18.8	19.3	17.8	19.4	18.7	18.9	-0.4	-0.3	-0.8
$C_2H\ ^2\Sigma+$	135.0	134.6	134.8	133.9	134.8	138.6	137.7	-0.2	-0.2	2.7
HCCH	54.5	54.2	54.7	53.7	54.7	55.7	55.1	0.2	0.3	0.6
HC(O)CHO	-50.7	-52.4	-51.3	-52.2	-51.0	-53.7	-51.7	-0.7	-0.3	-1.0
H_2CCH_2	12.5	12.2	12.5	11.6	12.3	12.6	12.3	0.0	-0.2	-0.2
C_2H_5	28.9	28.5	28.5	28.6	28.7	29.7	29.3	-0.4	-0.2	0.3
CH_2CO	-11.4	-12.5	-11.8	-12.6	-11.5	-12.2	-11.4	-0.4	-0.1	0.0
$CH_3CH_2NH_2$	-11.4	-11.6	-11.8	-11.2	-11.9	-12.3	-12.3	-0.5	-0.5	-0.9
CH_3CH_2OH	-56.1	-56.5	-56.4	-56.1	-56.3	-57.4	-56.7	-0.3	-0.2	-0.6
CH_3CH_2ONO	-24.8	-24.6	-23.7	-23.8	-23.9	-26.4	-24.6	1.1	0.9	0.3
CH_3CH_2SH	-11.0	-10.6	-10.3	-11.6	-10.2	-10.9	-10.9	0.7	0.8	0.1
CH_3CHO	-39.6	-40.2	-39.7	-40.0	-39.4	-41.1	-40.0	0.0	0.2	-0.3
CH_3CO	-2.4	-2.9	-2.5	-3.0	-2.4	-3.1	-2.3	-0.1	0.0	0.1
CH_3NHCH_3	-4.4	-3.9	-4.4	-3.4	-4.3	-4.9	-4.4	0.1	0.1	0.0
CH_3OCH_3	-44.0	-44.7	-44.2	-44.1	-44.3	-46.2	-44.2	-0.3	-0.3	-0.2
CH_3OOCH_3	-30.0	-29.7	-29.3	-28.7	-29.5	-31.6	-29.6	0.7	0.5	0.4
CH_3SCH_3	-8.9	-8.6	-8.2	-9.5	-8.3	-9.3	-8.0	0.7	0.6	0.9
$OS(CH_3)_2$	-36.1	-34.3	-35.4	-34.8	-35.6	-34.9	-36.0	0.7	0.5	0.1
$SiH_2(CH_3)_2$	-22.7	-21.3	-22.3	-21.2	-22.4	-21.8	-20.5	0.4	0.3	2.2
CH_3COOH	-103.3	-103.8	-103.2	-103.2	-102.6	-105.2	-103.5	0.0	0.6	-0.2
CH_3CH_3	-20.1	-20.3	-20.3	-20.0	-20.2	-20.8	-20.4	-0.2	-0.2	-0.3
$-CH_2CH_2CH_2-$	12.7	13.2	13.2	13.1	13.4	13.4	12.2	0.5	0.7	-0.5
$-CH_2OCH_2OCH_2O-$	-113.2	-114.1	-113.0	-112.7	-113.6	-116.3	-113.8	0.2	-0.4	-0.6
CH_2CCH_2	45.6	44.8	45.3	43.8	44.9	46.3	45.5	-0.4	-0.7	-0.1
CH_2CHCH_2	40.8	39.9	40.2	39.8	40.8	41.7	40.5	-0.6	-0.1	1.4
CH_3CCH	44.4	43.9	44.3	43.4	44.4	45.5	45.0	-0.1	0.0	0.6
$CH_3CH_2CH_3$	-25.0	-25.3	-25.3	-25.1	-25.2	-25.7	-25.7	-0.3	-0.2	-0.8
CH_3CH_2CHO	-44.8	-44.5	-44.0	-44.3	-43.7	-45.4	-44.6	0.8	1.1	0.2
CH_3CHCH_2	4.8	4.5	4.8	4.0	4.7	5.1	4.6	0.0	-0.2	-0.3
CH_3COCH_3	-51.9	-52.2	-51.8	-51.9	-51.4	-53.2	-52.3	0.1	0.5	-0.3
$CH_3CH_2CH_2CH_3$	-30.1	-30.3	-30.4	-30.2	-30.2	-30.7	-31.2	-0.3	-0.2	-0.8
$CH_2CHCHCH_2$	26.1	26.2	26.9	25.0	26.5	27.8	26.5	0.8	0.4	0.4
CH_3CCCH_3	34.7	34.9	35.1	34.5	35.3			0.4	0.6	
$CH_3CH(CH_3)_2$	-32.4	-32.3	-32.3	-32.2	-32.2	-32.8	-33.2	0.1	0.2	-0.8
C_6H_{12}	-29.5	-29.5	-30.2	-29.7	-30.2			-0.7	-0.7	
C_6H_6	19.8	20.1	20.9	18.1	20.6	23.4	20.4	1.1	0.8	0.6
OH	8.9	8.3	8.3	8.1	8.1	9.0	9.2	-0.6	-0.8	-0.2
H	52.1	52.1	52.1	52.1	52.1	52.1	51.6	-0.1	0.0	-0.5
HCl	-22.1	-21.7	-22.3	-22.4	-22.0	-22.5	-22.3	-0.2	0.1	-0.3
HF	-65.3	-65.3	-65.5	-65.5	-65.4	-66.2	-65.3	-0.2	-0.1	0.0
HN_3	70.3	70.0	70.3	70.4	70.7	69.8	69.2	-0.1	0.4	-1.2
HNO	27.0	25.4	25.9	25.3	25.4	24.5	25.3	-1.1	-1.6	1.5
$HO_2\ ^2A''$	3.5	3.0	2.4	3.2	2.0	3.3	2.9	-1.1	-1.5	-0.6
$HONO_2$	-32.3	-32.8	-32.2	-31.2	-31.9	-34.5	-32.1	0.1	0.4	0.2
HONO Cis	-18.3	-18.5	-18.0	-18.1	-18.3	-19.9	-18.6	0.4	0.1	-0.3
HONO Trans	-18.8	-19.1	-18.6	-18.7	-19.0	-20.5	-19.2	0.2	-0.1	-0.3
$NH\ ^3\Sigma-$	84.1	84.0	84.1	83.6	83.7	86.2	85.0	0.0	-0.4	0.9
HOCl	-18.7	-17.2	-18.5	-17.3	-18.4	-18.4	-18.8	0.2	0.3	-0.2

HNO ^{3}A"	45.5	43.5	43.7	43.7	43.5	45.1	45.0	-1.8	-2.0	-0.5
H_2	0.0	-0.5	-0.3	-1.1	-0.9	-1.1	-1.4	-0.3	-0.9	-1.4
H_2NF	-5.0	-6.2	-6.2	-5.9	-6.4	-7.4	-5.7	-1.2	-1.4	-0.7
H_2O	-57.8	-57.7	-57.9	-57.7	-57.9	-58.1	-58.0	-0.1	-0.1	-0.2
HOOH	-32.5	-32.0	-32.4	-31.7	-32.6	-32.4	-32.2	0.1	-0.1	0.3
NH_2	45.1	44.2	44.3	44.1	44.1	45.0	44.4	-0.8	-1.0	0.1
NH_3	-11.0	-10.4	-10.4	-10.2	-10.8	-10.9	-10.6	0.5	0.2	0.4
H_2NNH_2	22.8	24.1	23.7	24.5	23.4	23.6	23.9	1.0	0.6	1.1
ClO	24.3	26.6	25.1	26.7	25.3	26.4	25.3	0.8	1.0	1.0
FOF	5.9	6.6	5.8	7.2	5.8	5.3	5.2	-0.1	-0.1	-0.7
ClNO	12.4	13.1	13.5	12.4	12.8	11.6	13.2	1.2	0.4	0.9
NO $^3\Pi$	21.6	21.7	22.0	21.5	21.6	20.9	21.1	0.5	0.0	-0.5
N_2O	19.6	19.2	19.8	19.9	20.2	20.2	20.6	0.2	0.6	1.0
O	59.6	59.4	59.4	59.4	59.4	59.4	59.9	-0.1	-0.1	0.4
OClO	22.8	27.4	23.3	28.5	23.4	27.6	22.3	0.5	0.6	-0.5
$ClNO_2$	3.0	2.3	2.8	3.1	2.9	-0.2	2.4	-0.2	-0.1	-0.6
NO_2	7.9	7.5	8.1	8.3	8.2	7.2	8.4	0.2	0.2	0.5
O_2 $^3\Sigma$ -	0.0	-0.1	-1.0	0.4	-1.1	2.4	1.6	-1.0	-1.1	1.6
$FONO_2$	2.4	1.9	2.3	3.9	2.6	0.1	2.4	-0.1	0.2	0.0
NO_3 $^2B_2$	17.6	17.6	18.4	19.9	19.4	19.1	21.5	0.8	1.8	3.9
$ONNO_2$	19.8	19.5	20.4	20.3	19.7	18.4	21.0	0.6	-0.1	1.2
O_3 $^1A_1$	34.1	34.3	33.3	35.4	33.1	33.0	32.5	-0.8	-1.0	-1.6
O_2NNO_2	2.2	0.9	1.9	3.2	2.1	-0.4	3.2	-0.3	-0.1	1.0
NF_2	8.5	7.6	7.7	7.3	7.2	6.0	8.7	-0.8	-1.4	0.2
N	113.0	113.0	112.7	113.0	112.9	113.0	111.5	-0.3	-0.1	-1.5
FNNF Cis	17.9	17.4	17.7	17.6	17.6	14.6	17.6	-0.2	-0.3	-0.3
N_2	0.0	0.6	1.0	0.6	1.2	1.2	0.7	1.0	1.2	0.7
F	19.0	18.9	18.9	18.9	19.0	18.9	20.8	-0.1	0.0	1.9
F_2	0.0	1.2	0.7	1.4	1.0	0.3	-0.2	0.7	1.0	-0.2
Cl	29.0	29.0	28.8	29.0	29.5	29.0	29.8	-0.2	0.5	0.8
Cl_2	0.0	1.9	-0.4	0.7	-0.6	1.4	0.4	-0.4	-0.6	0.4
Si	107.6	107.4	107.4	107.4	108.6	107.4	107.3	-0.2	1.1	-0.3
$SiCl_4$	-158.2	-156.4	-158.7	-158.7	-158.6	-156.8	-158.4	-0.5	-0.4	-0.2
SiH_2 $^3B_1$	84.6	84.7	84.7	83.0	84.0	85.7	85.3	0.1	-0.6	0.7
SiH_3	46.4	46.7	46.4	45.7	46.1	46.6	46.9	0.0	-0.3	0.5
SiO	-24.6	-24.4	-24.1	-25.6	-24.1	-22.9	-22.6	0.5	0.5	2.0
SiO_2	-66.6	-67.7	-67.5	-69.6	-68.3	-66.6	-66.8	-0.9	-1.7	-0.2
SiS	27.6	26.7	27.7	24.3	27.5	27.7	27.6	0.1	-0.1	0.0
PH_2	32.8	32.3	32.3	31.4	32.0	32.8	32.3	-0.5	-0.8	-0.5
P	75.6	75.6	75.9	75.6	76.3	75.6	75.3	0.3	0.7	-0.3
PH $^3\Sigma$ -	56.8	55.7	56.0	54.7	55.5	57.6	57.2	-0.8	-1.3	0.4
P_2	34.2	34.8	34.4	33.9	34.5	35.6	34.2	0.3	0.3	0.0
PN	42.8	41.8	42.8	42.0	43.1	42.8	43.1	0.0	0.3	0.3
H_2S	-4.9	-4.6	-4.4	-5.7	-4.3	-4.9	-5.3	0.5	0.6	-0.4
S	66.2	66.1	66.8	66.1	67.7	66.1	65.9	0.5	1.5	-0.3
SH	34.2	33.7	34.3	32.9	34.5	34.4	34.0	0.1	0.3	-0.2
SO $^3\Sigma$ -	1.2	1.5	0.9	1.7	1.7	3.9	1.7	-0.3	0.5	0.5
SO_2	-70.9	-68.4	-70.6	-68.4	-70.8	-65.9	-70.2	0.3	0.1	0.7
SO_3	-94.6	-90.2	-94.3	-89.3	-94.3	-87.7	-95.2	0.3	0.2	-0.6
SiF_4	-386.0	-383.9	-385.3	-383.6	-384.8			0.7	1.2	
P_4	14.1	17.8	14.0	14.7	14.0			-0.1	-0.1	
PH_3	1.7	2.7	2.2	2.0	2.2	1.9	1.6	0.5	0.5	-0.1
$SiCl_2$	-40.3	-39.5	-40.0	-41.6	-39.6			0.3	0.7	
SF_6	-291.7	-283.0	-291.9	-281.3	-291.9			-0.2	-0.2	
ClSSCl	-4.0	-2.4	-4.7	-5.8	-5.3	-2.5	-5.9	-0.7	-1.4	-1.9
$(CH_3)_2SO_2$	-89.2	-86.2	-89.3	-85.0	-88.6			-0.1	0.6	
$(CH_3)_3CSH$	-26.2	-27.2	-26.9	-28.1	-26.6			-0.7	-0.4	
C_4H_8S	-8.2	-7.7	-7.7	-8.7	-7.7			0.5	0.5	
-CHCHSC(CH$_3$)CH-	20.0	19.5	19.1	17.2	17.9			-0.9	-2.1	
$C_5H_{10}S$	-15.2	-15.2	-15.4	-16.2	-15.1			-0.2	0.1	
$-CH_2SCH_2-$	19.6	18.8	19.3	17.8	19.4	18.7	18.9	-0.3	-0.2	-0.8
Cl_2SO_2	-84.8	-78.5	-84.6	-78.7	-84.6	-80.0	-86.1	0.2	0.2	-1.3
$C_{10}H_8$	36.1	34.9	36.3	31.8	36.1			0.2	0.0	
Additional Molecules for Test Set										
C_2Cl_6	-32.1	-38.9	-39.4	-40.9	-38.5	-43.5	-39.8	-7.3	-6.4	-7.7
C_2Cl_4	-3.0	-5.1	-5.2	-7.7	-5.2	-7.6	-4.7	-2.2	-2.2	-1.8
C_2F_4	-157.9	-161.8	-161.3	-162.0	-161.0	-165.7	-159.2	-3.4	-3.1	-1.3
$-CH_2CH_2NH-$	28.3	30.9	30.4	31.0	30.4	30.3	29.8	2.1	2.1	1.4
NCCN	73.8	71.9	72.5	72.3	73.9	74.7	73.6	-1.3	0.1	-0.3
$-CH=CHCH_2-$	66.2	68.1	68.4	67.4	68.3	68.9	67.5	2.2	2.1	1.3

$-CH_2CHCHCH_2-$	34.7	39.1	39.3	38.2	39.2	40.0	38.3	4.6	4.5	3.6
$-CH_2C(=CH_2)CH_2-$	47.9	46.0	46.3	45.3	46.3	47.3	45.6	-1.6	-1.6	-2.3
$CH_3CH_2NO_2$	-24.4	-26.0	-25.5	-24.6	-25.1	-28.5	-26.8	-1.1	-0.7	-2.4
CH_3CN	17.7	17.1	17.3	17.2	17.9	17.9	17.5	-0.4	0.2	2.2
CN	105.6	104.9	105.1	104.3	105.0	107.3	106.4	-0.5	-0.6	2.4
CO $^3\Pi$	114.3	110.4	110.6	109.5	110.0	112.1	112.3	-3.7	-4.3	-2.0
FNO	-15.7	-21.2	-20.7	-21.0	-21.0	-23.4	-20.9	-5.0	-5.3	-5.2
HNCO	-24.9	-29.2	-28.5	-28.8	-27.9	-29.6	-28.8	-3.6	-3.0	-3.9
HNNH Trans	50.9	48.3	48.5	48.1	48.2	47.8	47.4	-2.4	-2.7	-3.5
HOF	-23.5	-20.5	-21.0	-20.1	-20.9	-21.3	-21.1	2.5	2.6	2.3
$HOSO_2$	-92.0	-84.7	-88.1	-84.2	-88.2	-83.9	-90.4	3.9	3.8	1.6
$O=C(NH_2)_2$	-58.7	-55.7	-55.6	-54.4	-54.8	-56.9	-55.9	3.1	3.9	2.8
O_3 Cyclic	70.0	66.4	65.8	66.7	64.4	65.5	65.7	-4.2	-5.6	-4.3
$OHCH_2CH_2OH$	-93.9	-91.4	-91.2	-90.9	-90.9	-92.7	-91.6	2.7	3.0	2.3
SiH_3SiH_3	19.1	17.4	15.7	17.5	15.8	16.1	18.0	-3.4	-3.3	-1.1
SiH_2 $^1A_1$	64.8	63.0	63.3	62.7	64.0	62.3	62.8	-1.5	-0.8	-2.0
SiH_4	8.2	7.1	6.3	7.0	6.3	5.9	7.1	-1.9	-1.9	-1.1
ClOO	23.3	28.5	27.5	29.0	27.8	29.7	28.5	4.2	4.5	5.2
C_2H_3	71.8	70.2	70.4	69.8	70.6	72.6	71.7	-1.4	-1.2	-0.7
CH_2S	24.3	27.4	28.4	26.3	28.4	27.7	28.3	4.1	4.1	4.0
CH $^2\Pi$	142.5	141.0	141.1	140.4	141.0	141.9	141.2	-1.4	-1.5	-1.3
CH_2CHCCH	70.4	68.6	69.3	67.5	69.3			-1.1	-1.1	
HCCCCH	111	109.4	110.2	108.5	110.6	113.2	111.8	-0.8	-0.4	0.8
CH_3S ($^2A'$)	29.8	28.9	29.5	28.3	29.7	29.8	30.4	-0.3	-0.1	0.6
SCl_2	-4.2	-1.0	-3.2	-3.3	-3.7	-3.6	-8.4	1.0	0.5	-4.2
S_2	30.7	31.8	31.9	30.1	32.0	34.0	32.7	1.2	1.3	0.9
C_2H_5Cl	-26.8	-26.4	-26.5	-26.8	-26.6	-24.2	-26.5	0.3	0.2	0.0
PF_3	-229.1	-223.3	-227.0	-223.6	-226.8	-223.8	-233.5	2.1	2.3	-4.4
PCl_3	-69.0	-64.1	-68.4	-67.0	-69.2	-64.6	-68.8	0.6	-0.2	0.2
PCl_5	-86.1	-85.0	-93.3	-88.3	-93.9	-85.7	-93.8	-7.2	-7.8	-7.7
PF_5	-381.1	-372.5	-380.3	-372.2	-380.0	-374.5	-395.2	0.8	1.1	-14.1
PO	-9.0	-15.6	-16.5	-19.6	-20.3	-6.0	-8.8	-7.5	-11.3	0.2
PO_2 ($^2A_1$)	-69.6	-67.8	-70.4	-68.5	-71.1	-67.3	-71.3	-0.8	-1.5	-1.7
HOPO Cis	-112.4	-108.9	-111.0	-108.8	-110.9	-110.1	-111.8	1.4	1.5	0.6
$HOPO_2$	-171.4	-165.5	-169.6	-164.8	-169.3	-169.6	-171.9	1.8	2.1	0.5
$(HO)_2P$	-90.1	-87.1	-88.8	-87.1	-88.7	-86.6	-89.4	1.3	1.4	0.7
$(HO)_2PO$	-158.8	-154.2	-157.7	-154.0	-157.8			1.1	1.0	
$(HO)_3P$	-188.8	-184.4	-187.2	-183.8	-186.9	-184.8	-188.2	1.6	1.9	0.6
$CClF_3$	-169.2	-169.7	-169.6	-169.9	-169.5			-0.4	-0.3	
C_2F_6	-321.3	-323.2	-322.7	-322.7	-322.4			-1.4	-1.1	
$POCl_3$	-136.0	-129.0	-136.2	-130.3	-135.7			-0.2	0.2	
CF_3CN	-118.4	-120.6	-120.0	-120.3	-119.4			-1.6	-1.0	
ClF_3	-38.0	-34.9	-39.2	-33.3	-38.2			-1.2	-0.2	
AlH_3	30.8	30.5	31.7	31.1	31.9	28.8	29.0	0.9	1.1	-1.8
AlF_3	-289.0	-289.4	-288.2	-289.2	-288.3	-287.7	-296.9	0.8	0.7	-7.9
$AlCl_3$	-139.7	-141.7	-141.0	-142.3	-140.4	-142.5	-139.0	-1.3	-0.7	0.7
BH_3	21.0	23.2	23.2	24.9	24.7	22.3	20.2	2.2	3.7	-0.8
BF_3	-271.5	-272.5	-272.7	-271.8	-272.3	-269.4	-267.7	-1.2	-0.8	3.8
BCl_3	-96.7	-97.6	-98.3	-97.9	-97.3	-100.9	-116.4	-1.6	-0.6	-19.7
AlH	59.6	58.0	59.0	57.9	58.8	57.5	58.4	-0.6	-0.8	-1.2
AlF	-63.1	-65.6	-64.6	-65.4	-64.5	-64.9	-66.2	-1.5	-1.4	-3.1
AlCl	-12.2	-14.3	-13.5	-15.0	-13.7	-13.9	-13.9	-1.3	-1.5	-1.7
BH	106.6	103.5	103.7	103.4	103.7	103.3	102.6	-2.9	-2.9	-4.0
BF	-27.7	-27.2	-27.1	-27.6	-27.5	-27.9	-37.9	0.6	0.2	-10.2
BCl	41.2	41.6	41.5	40.5	41.0	40.1	34.9	0.3	-0.2	-6.4

Note that the difference is taken to be theory minus experiment, the reverse of the difference defined in G3 references [1,2,19,20].

A frequency distribution histogram of the errors (theory minus experiment) for the BAC-G3B3 and BAC-G3MP2B3 methods are shown in Figures 6.2 and 6.3. The 216 neutral molecules listed in Table 6.3 are used in the test set, 155 molecules in the reference set (denoted BAC-

G3B3 Ref), while the 61 additional molecules of Table 6.3 represent the extended set (denoted BAC-G3B3 Ext).

We performed a statistical analysis on the energy differences between theory and experiment for both the raw G3 and G2 energies and BAC corrected energies. The average, RMS and maximum errors in the heats of formation calculated for these methods are listed in Table 6.4.

Table 6.4 Overall Accuracy of raw and BAC Quantum Chemistry Methods

Method	Heat of Formation (kcal/mol.)		
	Average Error	**RMS Error**	**Maximum Error**
Reference Set[a]			
Raw-G3B3	0.82	1.37	8.73
BAC-G3B3	0.44	0.56	1.76
Raw-G3MP2B3	1.07	1.71	10.42
BAC-G3MP2B3	0.50	0.67	2.09
Raw-G2	1.34	1.90	6.80
BAC-G2	0.69	0.90	2.68
Test Set without ions[b]			
Raw-G3B3	1.38	2.16	8.73
BAC-G3B3	0.91	1.50	7.51
Raw-G3MP2B3	1.61	2.47	10.56
BAC-G3MP2B3	0.96	1.66	11.31
Test Set with ions[c]			
Raw-G3B3	1.32	2.04	8.73
BAC-G3B3	0.95	1.52	7.51
Raw-G3MP2B3	1.60	2.38	10.56
BAC-G3MP2B3	1.04	1.71	11.31
Set Containing only ions[d]			
Raw-G3B3	1.09	1.55	5.41
BAC-G3B3	1.13	1.60	5.60
Raw-G3MP2B3	1.57	2.00	5.20
BAC-G3MP2B3	1.40	1.85	5.70

[a]-155 molecules are used in the reference set
[b]-216 molecules are used in the test set with neutrals and without ions
[c]-273 molecules are used in the test set with ions
[d]-57 ions are used

We first discuss the results for the reference set, for which the accuracy of the experimental values is believed to be high. The results of the extended test set are discussed separately below. From the results of reference set in Tables 6.3 and 6.4, we observe the following:

a. Errors in the raw G3B3 and G3MP2B3 energies are less than the corresponding errors for the raw G2 method for most of the molecules. This indicates improved inherent accuracy of the G3-based methods.

b. The raw G3B3 energies are more accurate than the raw G3MP2B3 energies for most of the molecules. This is consistent with the higher-level quantum chemistry approaches used in G3B3 as opposed to G3MP2B3.

c. The BAC-G3B3 and BAC-G3MP2B3 energies are more accurate than the BAC-G2 energies for most of the molecules. The BAC-G3B3 energies are more accurate than the BAC-G3MP2B3 energies. The average, RMS and maximum errors in the heats of formation are the least for BAC-G3B3 method. Errors in BAC-G3B3 are significantly lower than those in BAC-G2, while they are slightly lower than BAC-G3MP2B3.

d. The BAC procedure significantly improves the accuracy of both the G3B3 and G3MP2B3 methods, and provides consistently excellent agreements with experiments. BAC-G3B3 has reduced the average error from 0.82 to 0.44 kcal/mol, and the RMS error from 1.37 to 0.56 kcal/mol.

e. The BAC-G3MP2B3 energies are approaching the accuracies of the BAC-G3B3 energies (average error of 0.50 vs 0.44 kcal/mol), making the G3MP2B3 method a very viable method for determining the heats of formation of molecular species, particularly for larger molecules for which the G3B3 method becomes computationally expensive.

g. While the average error for raw G3B3 is within a kcal/mol, the maximum error (8.73 kcal/mol) is high. BAC corrections have reduced the maximum errors considerably. There is a similar improvement in the maximum error for G3MP2B3 methods.

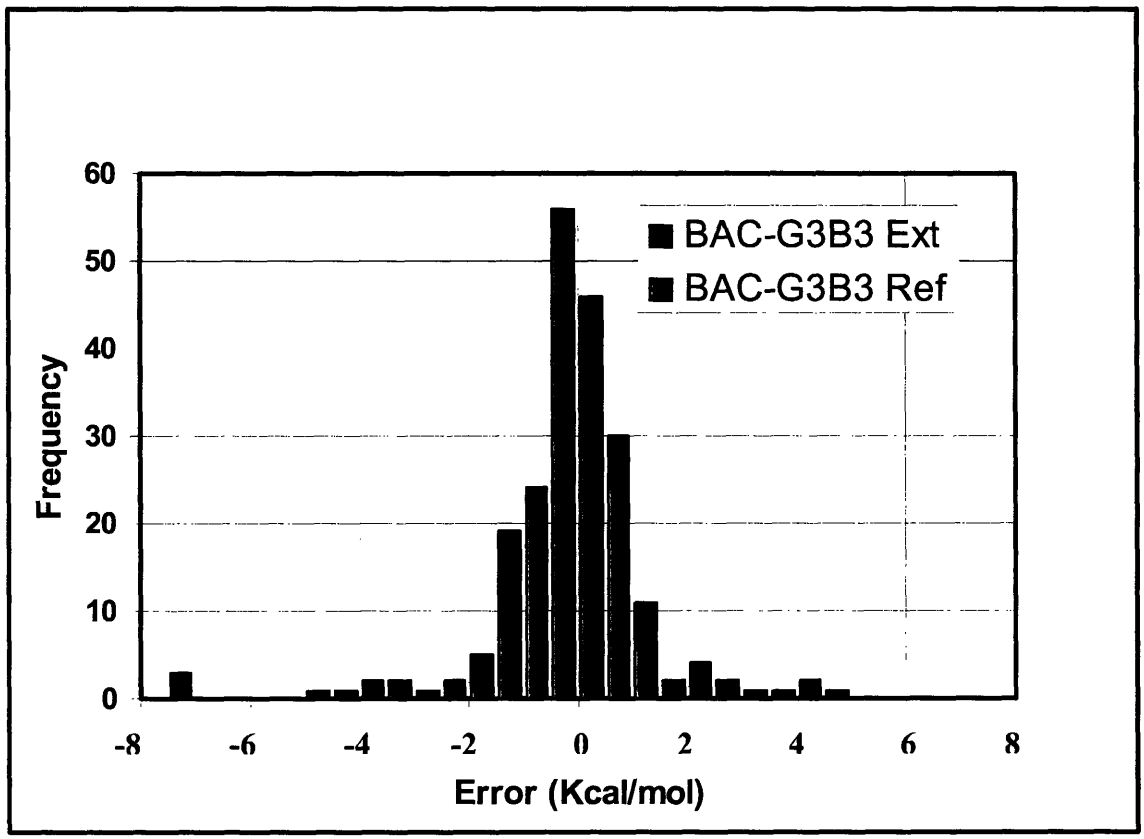

Figure 6.2 Frequency Distribution of Errors in BAC-G3B3 Predicted Heats of Formation of Neutrals

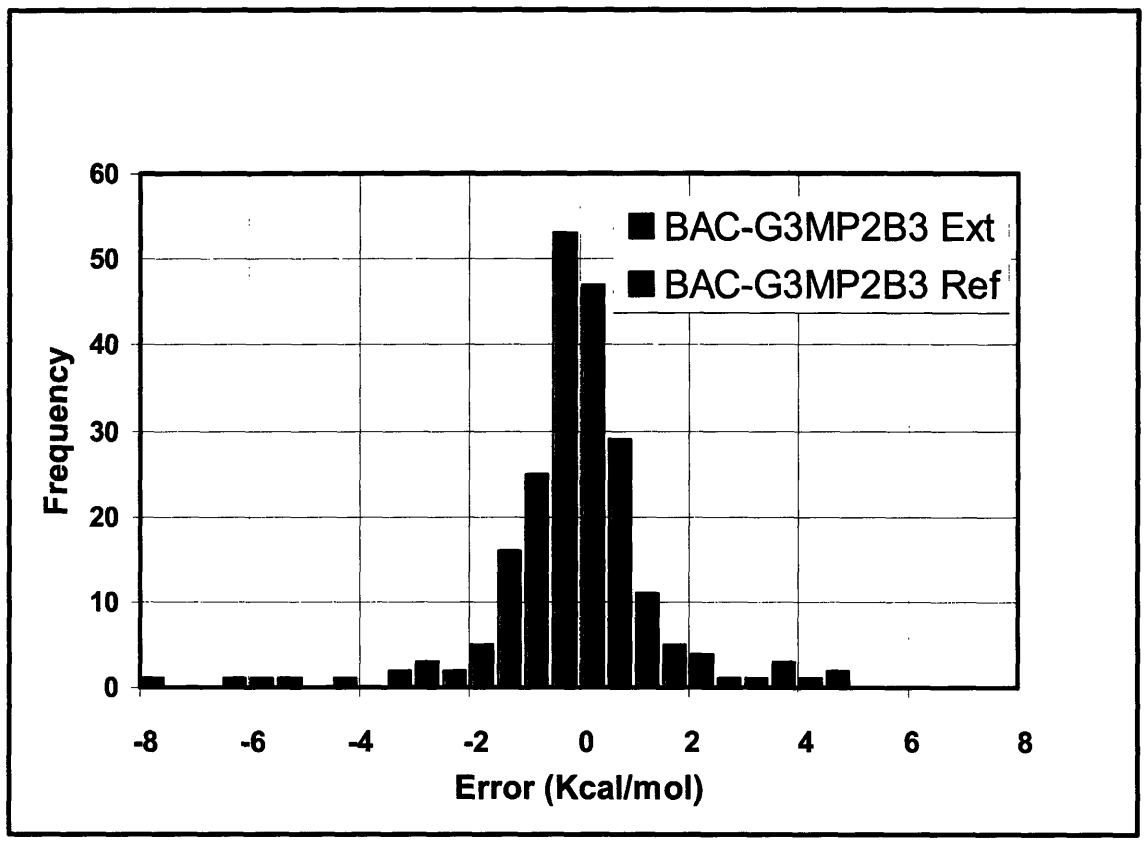

Figure 6.3 Frequency Distribution of Errors in BAC-G3MP2B3 Predicted Heats of Formation of Neutrals

The neutrals used in Figures 6.2 and 6.3 are from Table 6.3. The 216 neutral molecules include the 155 molecules in the reference set (BAC-G3MP2B3 Ref) and 61 additional molecules (BAC-G3MP2B3 Ext). Based on the reference set, the BAC-G3B3 method gives the best results. The BAC-G3B3 method is clearly preferable to BAC-G2 due to its greater accuracy. In addition, it is computationally faster. BAC-G3B3 can be applied to predict the heats of formation of large molecules with many atoms, which BAC-G2 could not handle. It should be noted that the BAC-G3MP2B3 also does remarkably well. BAC-G3MP2B3 is well suited to be applied to even larger molecules. As was the case for the BAC-G2 procedure, BAC-G3B3 and BAC-G3MP2B3 parameters depend only on the atoms, and not the pairs of atoms present in a molecule. Only a few reference compounds containing a given element are required to determine the BAC

parameters for all the compounds containing the element. This requires a reference set that is sufficiently large to define the parameters, but does not introduce artifacts in the parameters due to errors in the experimental heats of formation. Figures 6.4 and 6.5 show the frequency distribution of the errors (theory minus experiment) for the test set of 61 molecules. These figures are used to assess the predictive capabilities of the BAC-G3B3 and BAC-G3MP2B3 methods.

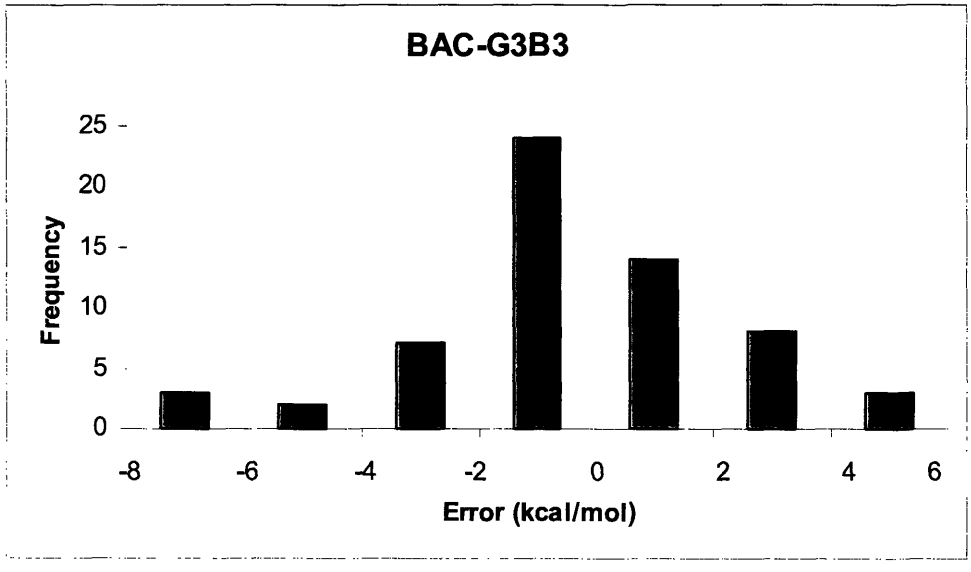

Figure 6.4 Frequency Distribution of Errors in BAC-G3B3 Predicted Heats of Formation of 61 Neutral Molecules in Test Set

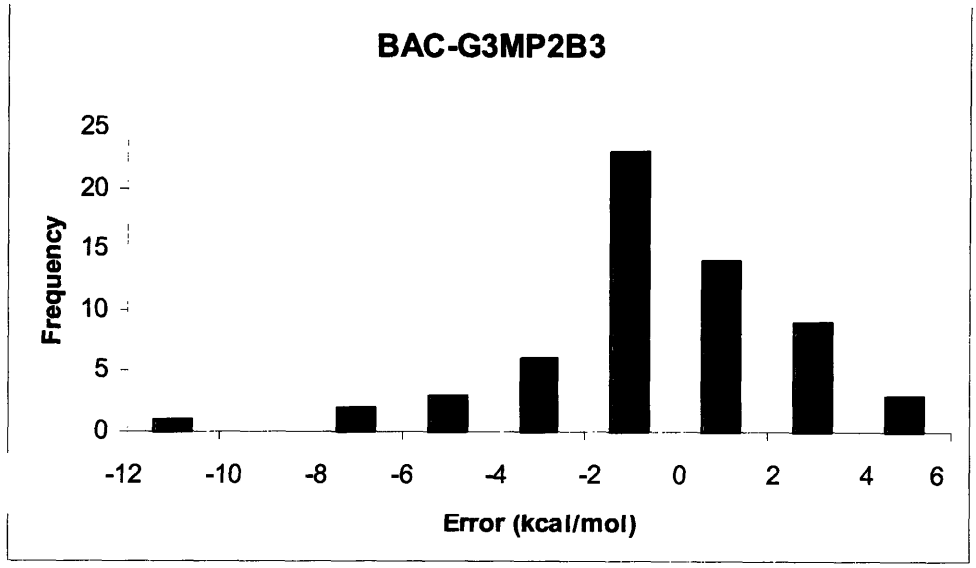

Figure 6.5 Frequency Distribution of Errors in the BAC-G3MP2B3 Predicted Heats of Formation of 61 Neutral Molecules in Test Set

BAC-G3B3 energies for molecules C_2Cl_6, PCl_6 and PO have errors between -8 and -6 kcal/mol., FNO and O_3 cyclic between -6 and -4 kcal/mol., while $-CH_2CHCHCH_2-$, ClOO and CH_2S have errors between 4 and 6 kcal/mol. BAC-G3MP2B3 energy for molecule PO has error between -12 and -10 kcal/mol., C_2Cl_6 and PCl_6 between -8 and -6 kcal/mol., $CO^{3\Pi}$, FNO and O_3 cyclic between -6 and -4 kcal/mol., while $-CH_2CHCHCH_2-$, ClOO and CH_2S have errors between 4 and 6 kcal/mol. In the following subsection, we discuss the larger test set and results for specific chemical groups that represent special concerns.

6.3.3 Assessment of the BAC-G3B3 and BAC-G3MP2B3 Procedures for Test Set of Molecules

In addition to the reference set, we have defined an extended test set of compounds used to test the predictive capabilities of BAC procedures. The test set includes additional neutrals, as well as ions and transition state structures from the first three rows of the periodic table, representing

diverse set of different chemical moieties. The test set includes molecules for which the accuracy of experimental values have not been as well validated and thus were not included in the reference set. Including such molecules in the reference set could have an adverse effect on defining the BAC parameters. In addition, the test set includes positive and negative ions for which the predictive capability of the BAC procedure has not yet been demonstrated.

To further discuss the accuracy of the BAC-G3B3, we have broken the discussion into several parts. First, we discuss the overall agreement between theory and experiment for the test set. Then we discuss those compounds for which the BAC-G2 procedure has difficulties. Then we discuss the set of compounds for which the G3 method has particular difficulty, involving interactions between second and third row elements, for which the G3X method was developed [1], with particular attention to the PO_x species. We then discuss special case of the boron and aluminum compounds, for which experimental data is sparse or lacking. Finally, we discuss the applicability of the BAC-G3B3 and BAC-G3MP2B3 procedures for cations and anions as well as for transition state structures.

First, we discuss the overall applicability of the BAC-G3B3 procedure for the test set. The average, RMS and maximum errors in the heats of formation for the test set for the BAC-G3B3 and BAC-G3MP2B3 procedures, along with the raw G3B3 and G3MP2B3 methods are listed in Table 6.4. We include an intermediate analysis for only the neutrals in the test set (excluding the anions and cations). Compared with the reference set, the errors for the larger test set are somewhat larger, as is to be expected. However, the errors are still quite small (average error of 0.91 and 0.96 vs 0.44 and 0.50 kcal/mol, and the RMS error of 1.50 and 1.66 vs 0.56 and 0.67 kcal/mol). One cause for the error can be due to the complex electron correlation interactions between the electrons within the molecule, indicating that higher levels of electronic

theory are still required. The other cause of error can be due to errors in the predicted experimental values.

Table 6.5 lists the compounds for which the BAC-G2 had deviations higher than 1 kcal/mol. The table includes compounds not only from original reference set used for BAC-G2 [27], but also from those in the extended test set.

Table 6.5 Errors in BAC Predicted Heats of Formation of Compounds with Highest Errors for BAC-G2 or BAC-G3B3

Molecule	Error in Heat of Formation (kcal/mol.)					
	BAC-G3B3	**Raw-G3B3**	**BAC-G3MP2B3**	**Raw-G3MP2B3**	**BAC-G2**	**Raw-G2**
Organic Compounds						
CH_2Cl_2	0.8	1.0	0.6	0.0	1.1	-0.7
CS_2	-1.0	-3.0	-1.1	-5.3	-1.1	-2.2
C	-0.2	-0.1	0.2	-0.1	-1.2	-0.1
H_2CNH	-0.3	-0.6	-0.4	-0.8	-1.2	-1.0
$CHCl_3$	0.8	1.1	0.6	-0.4	1.3	-1.1
CS	0.4	-0.7	-0.6	-3.0	1.4	-0.7
$C\ ^5S$	-0.3	0.1	0.2	0.3	-1.5	0.4
CH_2OH	0.2	0.1	0.4	0.3	-1.6	0.4
HCN	-1.3	-1.7	-1.0	-1.8	-1.6	-1.2
CH_2CHCH_2	-0.6	-0.9	-0.1	-1.0	1.4	0.9
$CH_2\ ^1A_1$	-0.4	-0.8	-0.4	-1.0	-1.7	-1.2
CH_3O	0.3	0.1	0.3	0.3	1.8	0.5
$CH\ ^4\Sigma-$	-0.1	0.1	-0.5	-0.7	2.3	3.9
$C_2H\ ^2\Sigma+$	-0.2	-0.4	-0.2	-1.1	2.7	3.6
$-CH_2CH_2NH-$	2.1	2.5	2.1	2.6	1.4	2.0
$-CH{=}CHCH_2-$	2.2	1.9	2.1	1.2	1.3	2.7
C_2Cl_4	-2.2	-2.2	-2.3	-4.8	-1.8	-4.6
$OHCH_2CH_2OH$	2.7	2.5	3.0	3.0	2.3	1.2
$O{=}C(NH_2)_2$	3.1	3.0	3.9	4.3	2.8	1.8
C_2F_4	-3.4	-3.9	-3.1	-4.1	-1.3	-7.8
HNCO	-3.7	-4.3	-3.1	-3.9	-3.9	-4.7
CO ($^3\Pi$)	-3.7	-3.9	-4.3	-4.8	-2.0	-2.3
CH_2S	4.1	3.1	4.1	2.0	4.0	3.4
$-CH_2CHCHCH_2-$	4.6	4.3	4.5	3.5	3.6	5.3
C_2Cl_6	-7.3	-6.8	-6.4	-8.8	-7.7	-11.4
Inorganic Compounds						

H_2NNH_2	1.0	1.3	0.6	1.7	1.1	0.8
HN_3	-0.1	-0.3	0.4	0.1	-1.2	-0.5
$ONNO_2$	0.6	-0.3	-0.1	0.5	1.2	-1.4
H_2	-0.3	-0.5	-0.9	-1.1	-1.4	-1.4
HNO	-1.1	-1.6	-1.6	-1.7	1.5	-2.5
N	-0.3	0.0	-0.1	0.0	-1.5	0.0
O_2 $^3\Sigma$ -	-1.0	-0.1	-1.1	0.4	1.6	2.4
O_3 $^1A_1$	-0.8	0.2	-1.0	1.3	-1.6	-1.1
F	-0.1	-0.1	0.0	-0.1	1.9	-0.1
SiO	0.5	0.2	0.5	-1.0	2	1.7
$SiH_2(CH_3)_2$	0.4	1.4	0.3	1.5	2.2	0.9
NO_3 $^2B_2$	0.8	0.0	1.8	2.3	3.9	1.5
PF_3	2.1	5.8	2.3	5.5	-4.4	5.3
HNNH trans	-2.4	-2.6	-2.7	-2.8	-3.5	-3.1
HOF	2.5	3.0	2.6	3.4	2.3	2.1
Si_2H_6	-3.4	-1.7	-3.3	-1.6	-1.1	-3
$HOSO_2$	3.9	7.3	3.8	7.8	1.6	8.1
O_3 cyclic	-4.2	-3.6	-5.6	-3.3	-4.3	-4.5
ClOO	4.2	5.2	4.5	5.7	5.2	6.4
FNO	-5.0	-5.5	-5.3	-5.3	-5.2	-7.7
PCl_5	-7.2	1.1	-7.8	-2.2	-7.7	0.4

From the table, we observe that the BAC-G3B3 procedure has addressed many of the errors for those species for which BAC-G2 is not accurate within 2 kcal/mol. In particular, highly oxidative species or species involving dative bonds (e,.g. NO_3, HN_3 etc.) have improved significantly. Other molecules in the table show consistent predicted values across the row, independent of the quantum chemistry method or whether BAC corrections are applied. This suggests that perhaps the experimental values may be in error. Further investigation of both the experimental and theoretical values to ascertain their accuracy is recommended. The recent changes in the recommended values of experimental heats of formation (see Table C.3 of the supplement) are, for the most part, supported by the findings of the BAC-G3B3 method.

Specifically, the NIST Computational Chemistry Comparison and Benchmark Database [30] has suggested alternative experimental heats of formation for some molecules whose heats of formation vary significantly from the experimental values used in this work. For example, the

following compounds have significant changes in experimental heats of formation (Table 6.6). Using the alternative heats of formation for those compounds would reduce the errors in the BAC-G3B3 predicted heats of formation. Those compounds would no longer be outliers (errors < 2 kcal/mol).

Table 6.6 Heats of Formation (kcal/mol.) Suggested by NIST Computational Chemistry Comparison and Benchmark Database

Compound	Alternative $H_{f,298K}$	This work $H_{f,298K}$
$-CH_2CH_2NH-$	30.1	28.3
$OHCH_2CH_2OH$	-92.6	-93.9
$O=C(NH_2)_2$	-56.6	-58.7
CH_2S	27.4	24.3
$-CH_2CHCHCH_2-$	37.5	34.7

The G3 method is known to have difficulties with elements of the third row, particularly when they involve hypervalent or dative bonding with elements of the second row, such as the sulfur-oxygen bond. The G3X method [1] was developed to remove some of the deficiencies in the G3 method, at the expense of increased computational time. In Table 6.7, we compare the results of the BAC-G3B3 procedure with the raw values for the G3 and G3X methods for the non-hydrogen species in the G3/99 test set suite [1,19]. Compounds containing C, N, O, F, Si, P, S and Cl atoms are included in the table. Boron and Aluminum compounds are discussed separately in Table 6.9.

Table 6.7 Errors in the BAC-G3B3 and G3X Predicted Heats of Formation for Selected Nonhydrogen Species in G3/99 Test Suite

	Deviations with Experiment (theory-experiment, kcal/mol.)			
Compounds	**G3X**	**Raw-G3**	**BAC-G3B3**	**Raw-G3B3**
CO_2	-1.7	-1.7	-0.8	-1.6
SO_2	0.7	2.5	0.3	2.5
CF_4	-0.1	-0.2	0.3	0.0

CCl_4	-0.9	-0.2	-0.6	-0.2
COS	-3.2	-2.1	-0.6	-2.1
CS_2	-3.3	-3.0	-1.0	-3.0
$SiCl_4$	0.6	1.8	-0.5	1.8
N_2O	-0.7	-0.4	0.2	-0.4
ClNO	0.5	0.8	1.2	0.7
F_2O	1.0	0.7	-0.1	0.7
C_2F_4	-4.3	-3.9	-3.4	-3.9
SO_3	1.5	4.4	0.3	4.4
SiF_4	-2.3	1.1	0.7	2.1
PF_3	1.9	4.8	2.1	5.8
O_3	0.4	0.8	-0.8	0.2
ClF_3	0.4	1.9	-1.2	3.1
C_2Cl_4	-2.7	-3.4	-2.2	-2.1
CF_3CN	-2.2	-1.8	-1.6	-2.2
PF_5	1.8	7.1	0.8	8.6
SF_6	0.5	6.2	-0.2	8.7
P_4	2.2	4.2	-0.1	3.7
SCl_2	1.9	2.0	1.0	3.2
$POCl_3$	2.3	3.1	-0.2	7.0
PCl_5	-1.7	-2.4	-7.2	1.1
Cl_2O_2S	2.6	4.4	0.2	6.3
PCl_3	3.3	3.2	0.6	4.9
Cl_2S_2	-0.5	-0.1	-0.7	1.6
$SiCl_2$	0.1	-0.4	0.3	0.8
CF_3Cl	-0.1	-1.2	-0.4	-0.5
C_2F_6	-1.8	-2.8	-1.4	-1.9

We see that the BAC-G3B3 does very well overall. This includes both unsaturated carbon-sulfur bonds, for which the sulfur is electronegative, and sulfur-oxygen bonds, for which the sulfur is electropositive. The halogenated compound hydrocarbons tend to have uniformly lower heats of formation than the experimental values, consistent with a recent recommendation [31] that the experimental values of these compounds should be lowered.

While the G3X is an improvement over the G3 method, Mackie et al. [32] has extended the G3X method to include even larger basis sets and applied the new method, denoted G3X2 to phosphorous oxides. A single g polarization function for the third-row G3Large basis set at the HF level, yielding a G3XLarge basis set. The B3LYP/6-31G(2df,p) step has replaced the

MP2(FU)/6-31G(d) method for geometry optimization and HF/6-31G(d) and MP2(FU)/6-31G(d) for the calculation of zero-point energies. G3X2 technique uses G3XLarge basis set expansion correction at the MP2(full) level instead of G3Large basis set at MP2(full) level. In Table 6.8, we have compared the enthalpies predicted by BAC-G3B3 against the values for G3X and G3X2 for the phosphorous oxide containing compounds. The results indicate a slight lowering of a couple of kcal/mol going from G3X to G3X2, consistent with the predicted values from the BAC-G3B3 and BAC-G2 procedures. This provides additional confirmation of the predictive capability of the BAC-G3B3 procedure for the phosphorous-oxide-containing species.

One of the dominant effects of the BAC procedure is to lower the energy relative to the raw G3B3 method for the bonding of P and S to the electronegative elements F, O, and Cl. This is achieved via the exponential term in the bond-wise additive correction given in Eq. 6.5. Figure 6.6 shows the resulting bond-additivity-correction contribution for selected bond types. This lowering of the energy, for instance, brings the heats of formation for SO_2, SO_3, Cl_2SO_2, SF_6, PF_3, PF_5, $POCl_3$, and PCl_3 into significantly better agreement with experiment (see Table 6.7). The addition of the extended basis sets in the G3X and G3X2 methods also tend to lower the energy (see Tables 6.7 and 6.8).

The results for the PO and PCl_5 molecules stand out from the molecules in Tables 6.7 and 6.8. For PO, the BAC-G3B3 and BAC-G3MP2B3 methods are predicting too low an energy (see Table 6.8). The discrepancy for the PO molecule most likely is a pathological artifact of the G3 method itself, since the BAC corrections for PO only amount to 0.9 kcal/mol. The G3B3 and G3MP2B3 predicted values are significantly different from the G3X, G3X2, and G2 results. Occasionally, one or more of the individual steps in Gaussian-n methods can diverge. For instance, the G1 method for $C_2H_4^+$ differs by more than 100.0 kcal/mol from the G2 and G2MP2

values. For PO, the results for the G3 and G3B3 differ by 7.1 kcal/mol for a tiny change in bond distance, going from 1.472 Å to 1.499 Å. The electronic calculation for PO has a convergence problem in the electronic wavefunction, leading to a discrepancy in the resulting estimates of the MP2 energy in the QCISD(T) step. The unusually large difference of 4.0 kcal/mol between the G3B3 and G3MP2B3 values (see Table 6.3), is indicative of a convergence problem in the G3 for the PO molecule.

The situation for the PCl_5 molecule is less clear. Our results suggest that the experimental value should be lower. Gurvich et al. [33] recommends a heat of formation of –90.0 rather than the -86.1 value taken from Chase et al. [34]. The lower experimental value is consistent with the above observed trends from the other levels of theory. Whether or not the experimental heat of formation should be further lowered, as predicted by the BAC-G3B3 and BAC-G2 values, needs to be further investigated. In general, it is difficult to determine when the G3 methods themselves are having pathological difficulties as opposed to experimental data.

Table 6.8 Heats of Formation of Phosphorus Oxides Predicted by BAC-G3B3, G3X and G3X2 Methods

Species	Heat of Formation (kcal/mol.)				
	G3X	**G3X2**	**BAC-G3B3**	**BAC-G2**	**Other Sources**
PO	-7.7	-9.0	-16.5 ± 4.0	-8.8	-6.7 [35], -5.6 [34]
PO_2	-67.6	-69.6	-70.4 ± 2.9	-71.3	-67.3 [35], -75.1 [36]
HOPO Cis	-110.3	-112.3	-111.0 ± 2.3	-111.8	-110.6 [37]
$HOPO_2$	-167.4	-170.5	-169.6 ± 4.2	-171.9	-168.8 [37]
$(HO)_2P$	-88.3	-90.1	-88.8 ± 1.9	-89.4	
$(HO)_2PO$	-156.4	-158.8	-157.7 ± 3.6	-157.9	-156.4
$(HO)_3P$	-186.4	-188.8	-187.2 ± 3.0	-188.2	

For $(HO)_2P$ and $(HO)_3P$, there is lack of experimental data

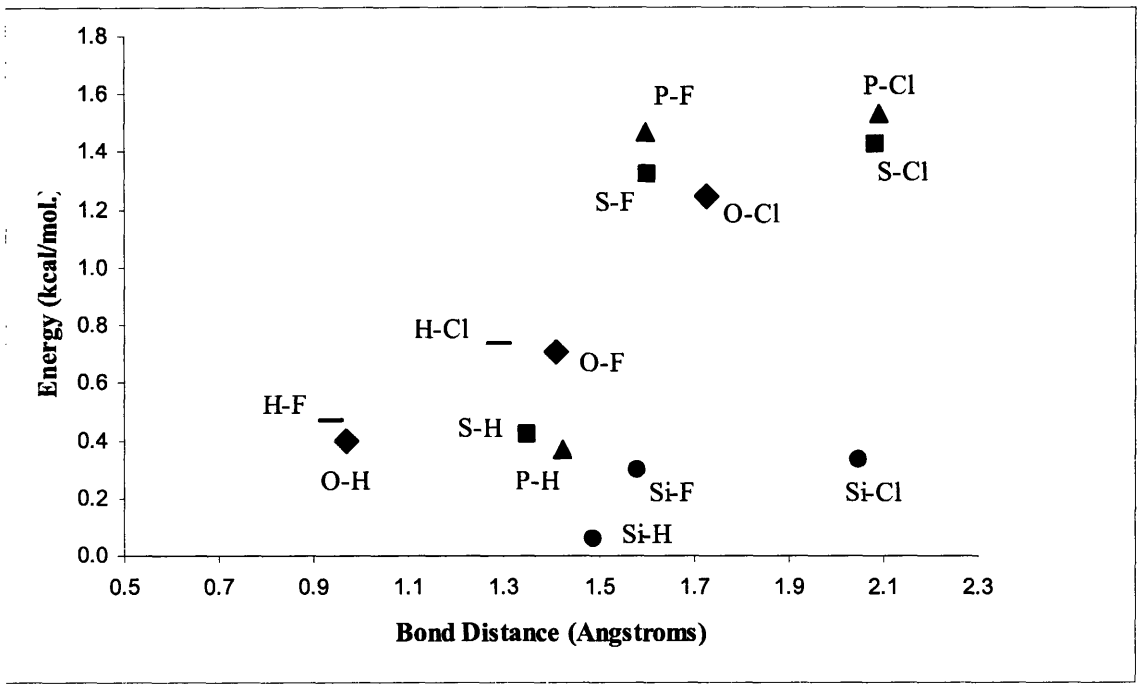

Figure 6.6 BAC Factor $A_{ij}e^{-\alpha Rij}$ for Chemical Bonds involving H, F, and Cl

In Figure 6.6, BAC-G3B3 parameters are used for illustration purposes. For all the cases, α is 3.0 A^{-1}. Each point in the plot corresponds to a typical unsaturated single-bond bond distance. Since A_{ii} for C and N are 0, the correction factor for bonds between H, F and Cl, and C or O is 0. We now address the thermochemistry for molecules containing boron and aluminum. Few aluminum and boron compounds exist for use in the reference set of molecules, due to the limited experimental data with reasonable uncertainties. In the reference set of molecules, AlH_3, AlF_3, $AlCl_3$, AlH, AlF and AlCl are used for aluminum compounds, while BH_3, BF_3 and BCl_3 are used for boron compounds. Since the two sets of compounds consist of limited types of atoms and bonds, they are not representative of various elements from the first 3 rows. The number of compounds are fewer than the total number of BAC parameters required for the BAC-G3B3 as well as BAC-G3MP2B3 methods. This introduces numerous choices of parameters or degrees of freedom that could address the errors for the few compounds. Hence, the B and Al

compounds are used only to estimate the BAC parameters for B and Al, respectively. This prevents the BAC parameters for the other atoms and the overall results to be biased by the considerable uncertainties in experimental data for these small number of Al and B compounds. Table 6.9 compares the BAC predicted heats of formation of Al and B compounds. Unless otherwise indicated in the table, the current experimental values are taken from Gurvich et al. [33]. We use the heat of formation of a BAC-G2 calculation for BH_3. Value recommended by Cox et al. [38] is used for BF_3.

Table 6.9 Predicted Heats of Formation for Al and B Compounds

Species	Heat of Formation (kcal/mol.)				
	BAC-G3B3	**BAC-G3MP2B3**	**BAC-G2**	**Experimental Value**	**Other Sources**
AlH_3	31.7	31.9	-1.8	30.8 ± 4.8	30.81 [35]
AlF_3	-288.2	-288.3	-7.9	-289.0 ± 0.7	-289.0 ± 0.6 [36]
$AlCl_3$	-141.0	-140.4	-7.7	-139.7 ± 1.2	-139.7 ± 0.7 [36]
AlH	59.0	58.8	-1.2	59.6 ± 0.8	61.9 ± 4.8 [36]
AlF	-64.5	-64.5	1.0	-63.1 ± 0.7	-63.5 ± 0.8 [36]
AlCl	-13.7	-13.7	-1.7	-12.2 ± 0.7	-12.3 ± 1.5 [36]
BH_3	23.2	24.7	24.1	21 ± 2.4	25.5 ± 2.4 [36], 23.80 [39]
BF_3	-272.7	-272.3	-267.7	-271.5 ± 0.2 [38]	-271.420 [34], -271.65 [40]
BCl_3	-98.4	-97.3	-98.3	-96.68 ± 0.31	-96.3 ± 0.5 [36], -97.50 [39], -96.31 [40]
BH	103.7	103.7	104.6	106.6 ± 1.7	105.8 ± 2.0 [36], 108.24 [39], 73.8 [40]
BF	-27.1	-27.5		-27.7 [34]	-27.7 [40]
BCl	41.5	41.0	42.0	41.2 ± 6.0	33.8 ± 4 [36], 36.01 [39], 33.80 [40]

For AlH_3, there is lack of experimental data, the vale mentioned in the table is an estimate from theory

Next, we report the results for anions and cations. The errors in the predicted heats of formation are reported in Table 6.10. We have defined the heats of formation to follow the ion

convention rather than the electron convention [41-43] in which the heat capacity of the electron is ignored. Thus, the heat of formation of a positive ion is taken to be the heat of formation of the neutral molecule plus the ionization potential, while the heat of formation of a cation is taken to be the heat of formation of the neutral molecule minus the electron affinity. Overall, the results for the ions provide excellent agreement with experiment, as can be seen from the statistical error analysis in Table 6.4. The resulting errors in the heats of formation can be due either to the neutral molecule heat of formation or to measurements in the ionization potential or electron affinity. Since the geometries of the ions are very similar to those of the neutral molecules (excluding proton affinities), most of BAC corrections for a given ion-neutral pair tend to cancel. Thus, the BAC results are very similar to the excellent results provided by the raw G3B3 and G3MP2B3 methods themselves.

Table 6.10 Comparison of Errors in Predicted Heats of Formation for Ions

Ions	Heat of Formation (kcal/mol.)					
	Experimental Energies		Predicted Heat of Formation (kcal/mol.)			
	$H_{f,298K}$ of Neutral	Electron Affinity	BAC-G3B3	BAC-G3MP2B3	Raw-G3B3	Raw-G3MP2B3
Anions						
P	75.6	17.2	1.0	2.5	0.5	1.7
S	66.2	47.9	0.6	1.3	-0.2	-0.5
CH	142.5	28.6	0.0	0.4	0.0	0.0
CH_2	93.4	15.0	1.0	0.6	0.8	0.2
CH_3	35.0	1.8	2.2	1.2	2.0	0.9
SiH_2	64.8	25.9	-0.6	-0.1	-0.7	-1.3
SiH_3	46.4	32.5	-0.1	0.1	0.0	-0.5
PH	56.8	23.8	0.6	0.9	0.1	-0.1
PH_2	32.8	29.3	-0.2	-0.6	-0.4	-1.4
SH	33.3	54.4	2.0	1.6	1.3	-0.3
C_2	200.2	75.5	-2.9	-3.8	-3.1	-4.6
CF_2	-43.5	4.1	-2.3	-2.1	-2.5	-2.7
SO_2	-70.9	25.5	0.6	1.1	2.1	2.6
C_2H	135.0	68.5	0.6	-0.8	0.1	-1.9

C_2H_3	71.8	15.4	-1.0	-2.4	-1.4	-3.3
C_3H_5	40.8	10.9	0.2	-1.1	-0.3	-2.2
CHO	10.3	7.2	0.0	-0.7	-0.6	-1.5
CHF	30.0	12.5	5.6	5.7	5.4	5.2
CH_3O	4.2	36.2	1.3	0.6	0.9	0.5
CH_3S	29.8	43.1	0.0	-0.6	-0.8	-2.2
CH_2S	24.3	10.7	4.5	4.3	3.6	2.3
C_2H_3O	80.6	42.1	1.3	0.8	0.8	0.1
OH	8.9	42.2	0.8	0.2	0.7	0.0
F	19.0	78.4	-0.3	-0.5	-0.4	-0.7
O	59.6	33.7	2.6	3.0	2.4	2.8
C	171.3	29.1	1.1	3.5	1.4	3.4
Cl	29.0	83.4	-0.1	-1.1	-0.2	-1.7
Cl_2	0.0	55.1	0.4	0.1	0.8	-0.7
O_2	0.0	10.1	1.1	1.8	1.5	2.6
CN	105.6	89.0	-0.7	-1.3	-1.1	-2.1
H_2N	45.1	17.8	1.3	-0.2	1.0	-0.3
HN	84.1	8.8	4.5	4.3	4.4	4.0
	$H_{f,298K}$ of Neutral	**Ionization Potential**	**BAC-G3B3**	**BAC-G3MP2B3**	**Raw-G3B3**	**Raw-G3MP2B3**
Cations						
Si	107.6	187.9	-0.5	-0.3	-0.6	-1.7
S	66.2	238.9	-1.4	-1.9	-1.9	-3.3
CH_4	-17.9	291.0	2.6	2.9	2.8	3.3
NH_3	-11.0	234.8	-0.4	-0.2	-0.1	0.5
SiH_4	8.2	253.7	-1.2	-3.1	0.2	-1.3
PH	56.8	234.1	0.3	-0.7	-0.2	-1.6
PH_2	32.8	226.5	-0.4	-0.7	-0.5	-1.5
SH	34.2	239.1	-1.1	-1.9	-1.5	-3.4
$SH_2(^2B_1)$	-4.9	241.4	-0.3	-0.6	-0.4	-1.8
$N_2\ ^2\Sigma$	0.0	359.3	1.0	1.1	0.7	0.7
O_2	0.0	278.3	-0.7	-0.9	0.4	1.1
S_2	30.7	215.8	0.8	0.9	1.0	-0.7
O	59.6	313.9	-1.4	-1.9	-1.3	-1.8
N	113.0	335.3	-0.8	-1.4	-0.7	-1.4
F	19.0	401.7	-0.7	-0.1	-0.5	0.0
C	171.3	259.7	-1.2	-1.9	-1.2	-2.2
Cl	29.0	299.1	-1.8	-1.5	-1.5	-1.9
OH	8.9	300.2	-2.5	-3.2	-2.3	-3.1
H_2O	-57.8	291.0	-0.7	-0.6	-0.3	-0.3
H_2	0.0	355.7	-0.4	-0.1	-0.5	-0.2
HCCH	54.5	262.9	0.6	1.1	0.3	0.2
H_2CCH_2	12.5	242.4	0.5	1.3	0.3	0.8
CO	-26.4	323.1	0.1	-0.2	-0.3	-0.8
HCO	10.3	187.7	-0.4	-0.1	-1.0	-0.9
HCl	-22.1	294.0	-1.0	-0.6	-0.3	-0.8

In Table 6.11, we compare the applicability of the BAC-G3B3 and BAC-G3MP2B3 procedures with previous BAC procedures [27] for determining activation energies for reactions. The activation energy represents the difference between the heats of formation of the transition state structure and reactants. Since errors can occur (or cancel) due to the accuracy of either the transition state structure or the reactants, we also provide the absolute heat of formation of the transition state structure. In Table 6.11, first row for each column is the difference in the heats of formation of the transition state and the reactants. The corresponding raw G3B3 and G3MP2B3 values are given in parentheses. The second row represents the heats of formation of the transition state structure itself.

Table 6.11 Activation Energies (kcal/mol.) Predicted by Different BAC Procedures

Reaction	BAC-G3B3	BAC-G3MP2B3	BAC-G2	BAC-Hybrid	BAC-DFT	BAC-MP4
$H_2 + H \Leftrightarrow H + H_2$	8.0 (8.3)	7.6 (8.0)	9.2	8.7	7.6	8.8
	59.8	58.8	59.7	60.9	59.7	60.9
$CH_4 + OH \Leftrightarrow CH_3 + H_2O$	3.2 (3.6)	3.4 (4.0)	5.0	1.6	-0.5	3.2
	-6.6	-6.5	-3.8	-6.7	-9.8	-5.1
$H_2 + O \Leftrightarrow H + OH$	8.1 (8.5)	7.5 (8.6)	12.1	9.8	4.9	10.5
	67.2	66.6	70.6	69.4	66.0	70.3
$NH_3 + O \Leftrightarrow NH_2 + OH\ ^3A'$	9.1 (9.5)	9.4 (9.8)	12.2	11.4	2.8	12.2
	58.1	58.0	61.5	59.8	53.8	61.1
$NH_3 + O \Leftrightarrow NH_2 + OH\ ^3A''$	7.8 (8.2)	8.1 (8.5)	10.1	10.5	1.2	9.8
	56.8	56.7	59.4	58.9	52.2	58.7
$C_2H_4 + H \Leftrightarrow C_2H_5$	-0.9 (-0.6)	-1.3 (-0.7)	2.3	1.9	1.2	2.9
	63.7	63.1	66.2	67.7	66.1	67.3
$H + CO \Leftrightarrow HCO$	1.0 (1.0)	0.5 (0.7)	2.4	2.4	-4.6	2.4
	26.5	25.6	26.9	27.3	23.0	25.7
$C_2H_5 \Leftrightarrow C_2H_5$	39.8 (40.3)	39.1 (40.0)	40.6	39.9	38.7	42.3
	68.3	67.8	69.9	69.5	66.9	71.1
$HCN \Leftrightarrow HNC$	44.1 (45.3)	42.5 (44.5)	44.4	47.9	47.1	45.1
	75.1	73.8	75.1	78.3	78.9	76.9
$C_2H_5NO_2 \Leftrightarrow C_2H_4 + HONO$	45.9 (47.1)	44.8 (46.6)	48.3	46.4	41.3	48.5
	20.4	19.7	21.5	20.4	16.7	23.7
$C_2H_5Cl \Leftrightarrow C_2H_4 + HCl$	57.6 (58.1)	56.4 (57.5)	59.0	61.8	52.2	70.5

	31.1	29.8	32.1	34.9	24.0	43.3

Since the BAC corrections are small for the BAC-G3B3 and BAC-G3MP2B3 procedures and most of the BAC corrections cancel in the determination of the activation energy, the BAC-G3B3 and BAC-G3MP2B3 results are nearly identical to the raw G3B3 and G3MP2B3 results. For the most, the BAC-G3B3 and BAC-G3MP2B3 activation energies are very similar to each other, but slightly lower than the BAC-G2 results. Part of the differences may be due to the use of the B3LYP method for optimizing the geometry and determining the frequencies. The same geometries and frequencies are used in the BAC-G3B3 and BAC-G3MP2B3 procedures as for the BAC-Hybrid and BAC-DFT procedures.

6.4 Summary

We have developed the Bond Additivity Correction (BAC) procedure for the G3B3 and G3MP2B3 quantum chemistry methods to improve the accuracy of predicted thermochemical properties of open and closed shell molecules containing elements from first 3 rows of the periodic table. BAC-G3B3 and BAC-G3MP2B3 parameters have been developed for atomic, molecular and bond-wise corrections to heats of formation of molecules.

The usefulness of BAC procedure has been assessed by comparing the heats of formation predicted by the BAC-G3B3 and BAC-G3MP2B3 procedure against experimental values for a 273-molecule test set containing various chemical moieties, multireference configurations, isomers and degrees of saturation. BAC corrections have significantly improved the overall accuracy as well as the accuracy for specific compounds. For the reference set, the average error for the BAC-G3B3 results is 0.44 kcal/mol compared to 0.82 kcal/mol for the raw G3B3. For

the extended test set with neutrals, average error for the BAC-G3B3 results is 0.91 kcal/mol compared to 1.38 kcal/mol for the raw G3B3.

Compared to former BAC-MP4 and BAC-G2 methods, BAC-G3B3 provides better estimates of thermochemistry for compounds involving the first 3 rows of periodic table, consistent with the improved accuracy of the G3 methods themselves. Some of the molecules need to be reinvestigated experimentally and theoretically, since the reported experimental values in literature may not be sufficiently accurate. In particular, better experimental data needs to be determined for the B, Al and P compounds in order to determine the true predictive capability of the BAC procedure for these compounds.

References

1. L. A. Curtiss, P. C. Redfern, K. Raghavachari and J. A. Pople (2001). Gaussian-3X (G3X) theory: Use of improved geometries, zero-point energies, and Hartree–Fock basis sets. *Journal of Chemical Physics*, 114, 108-117.
2. L. A. Curtiss, K. Raghavachari, P. C. Redfern and J. A. Pople (2000). Assessment of Gaussian-3 and density functional theories for a larger experimental test set. *Journal of Chemical Physics*, 112, 7374-7383.
3. J. C. Mackie, G. B. Bacskay and N. L. Haworth (2002). Reactions of phosphorus-containing species of importance in the catalytic recombination of H + OH: Quantum chemical and kinetic studies. *Journal of Physical Chemistry A,* 106, 10825-10830.
4. N. L. Haworth, G. B. Bacskay and J. C. Mackie (2002). The role of phosphorus dioxide in the h + oh recombination reaction: ab initio quantum chemical computation of thermochemical and rate parameters. *Journal of Physical Chemistry A*, 106, 1533-1541.
5. T. H. Dunning (1989). Gaussian basis sets for use in correlated molecular calculations. I. The atoms boron through neon and hydrogen. *Journal of Chemical Physics*, 90, 1007-1023.
6. R. A. Kendall, T. H. Dunning and R. J. Harrison (1992). Electron affinities of the first-row atoms revisited. Systematic basis sets and wave functions. *Journal of Chemical Physics*, 96, 6796-6806.
7. T. Arai (1960). General analysis of various methods of atoms in molecules. *Reviews in Modern Physics*, 32, 370-400.
8. G. A. Petersson, A. Bennett, T. G. Tensfeldt, M. A. Al-Laham, W. A. Shirley and J. Mantzaris (1988). A complete basis set model chemistry. I. The total energies of closed-shell atoms and hydrides of the first-row elements. *Journal of Chemical Physics*, 89, 2193-2218.
9. G. A. Petersson and M. A. Al-Laham (1991). A complete basis set model chemistry. II. Open-shell systems and the total energies of the first-row atoms. *Journal of Chemical Physics*, 94, 6081-6090.
10. D. E. Woon and T. H. Dunning (1993). Gaussian basis sets for use in correlated molecular calculations. III. The atoms Aluminum through Argon. *Journal of Chemical Physics*, 98, 1358-1371.
11. B. J. Lynch and D. G. Truhlar (2003). Robust and affordable multicoefficient methods for thermochemistry and thermochemical kinetics: the mccm/3 suite and sac/3. *Journal of Physical Chemistry A*, 107, 3898-3906.
12. Y. Zhao, B. J. Lynch and D. G. Truhlar (2004). Development and assessment of a new hybrid density functional model for thermochemical kinetics. *Journal of Physical Chemistry A*, 108, 2715-2719.
13. Y. Zhao, B. J. Lynch and D. G. Truhlar (2004). Doubly hybrid DFT: new multi-coefficient correlation and density functional methods for thermochemistry and thermochemical kinetics. *Journal of Physcial Chemistry A*, 108, 4786-4791.
14. P. L. Fast, M. L. Sanchez and D. G. Truhlar (1999). Multi-coefficient Gaussian-3 method for calculating potential energy surfaces. *Chemical Physics Letters*, 306, 407-410.
15. J. A. Pople, M. Head-Gordon, D. J. Fox, K. Raghavachari and L. A. Curtiss (1989). Gaussian-1 theory: A general procedure for prediction of molecular energies. *Journal of Chemical Physics*, 90, 5622-5629.

16. L. A. Curtiss, C. Jones, G. W. Trucks, K. Raghavachari and J. A. Pople (1990). Gaussian-1 theory of molecular energies for second-row compounds. *Journal of Chemical Physics*, 93, 2537-2545.
17. L. A. Curtiss, K. Raghavachari, G. W. Trucks and J. A. Pople (1991). Gaussian-2 theory for molecular energies of first- and second-row compounds. *Journal of Chemical Physics*, 94, 7221-7230.
18. L. A. Curtiss and K. Raghavachari, (1993). Gaussian-2 theory using reduced Møller–Plesset orders. *Journal of Chemical Physics*, 98, 1293-1298.
19. L. A. Curtiss, K. Raghavachari, P. C. Redfern, V. Rassolov and J. A. Pople (1998). Gaussian-3 (G3) theory for molecules containing first and second-row atoms. *Journal of Chemical Physics*, 109, 7764-7776.
20. L. A. Curtiss, P. C. Redfern, K. Raghavachari, V. Rassolov and J. A. Pople (1999). Gaussian-3 theory using reduced Møller-Plesset order. *Journal of Chemical Physics*, 110, 4703-4709.
21. A. G. Baboul, L. A. Curtiss, P. C. Redfern and K. Raghavachari (1999). Gaussian-3 theory using density functional geometries and zero-point energies. *Journal of Chemical Physics*, 110, 7650-7657.
22. M. J. Frisch, G. W. Trucks, H. B. Schlegel, G. E. Scuseria, M. A. Robb, J. R. C. J. A. Montgomery, T. Vreven, K. N. Kudin, J. C. Burant, J. M. Millam, S. S. Iyengar, J. Tomasi, V. Barone, B. Mennucci, M. Cossi, G. Scalmani, N. Rega, G. A. Petersson, H. Nakatsuji, M. H. M. Ehara, K. Toyota, R. Fukuda, J. Hasegawa, M. Ishida, T. Nakajima, Y. Honda, O. Kitao, H. Nakai, M. Klene, X. Li, J. E. Knox, H. P. Hratchian, J. B. Cross, C. Adamo, J. Jaramillo, R. Gomperts, R. E. Stratmann, O. Yazyev, A. J. Austin, R. Cammi, C. Pomelli, J. W. Ochterski, P. Y. Ayala, K. Morokuma, G. A. Voth, P. Salvador, J. J. Dannenberg, V. G. Zakrzewski, S. Dapprich, A. D. Daniels, M. C. Strain, O. Farkas, D. K. Malick, A. D. Rabuck, K. Raghavachari, J. B. Foresman, J. V. Ortiz, Q. Cui, A. G. Baboul, S. Clifford, J. Cioslowski, B. B. Stefanov, G. Liu, A. Liashenko, P. Piskorz, I. Komaromi, R. L. Martin, D. J. Fox, T. Keith, M. A. Al-Laham, C. Y. Peng, A. Nanayakkara, M. Challacombe, P. M. W. Gill, B. Johnson, W. Chen, M. W. Wong, C. Gonzalez and J. A. Pople (2003). Gaussian 03, Revision A.1; Gaussian, Inc.: Pittsburgh PA.
23. P. Ho and C. F. Melius (1990). Theoretical study of the thermochemistry of fluorosilanes (SiF_n and SiH_nF_m) compounds and hexafluorodisilane. *Journal of Physical Chemistry*, 94, 5120-5127.
24. C. F. Melius (1990). In *Chemistry and Physics of Energetic Materials*; Bulusu, S. N., Ed.; Kluwer Academic Publishers: Dorderecht; pp 21.
25. M. R. Zachariah and C. F. Melius (1997). Theoretical calculation of thermochemistry for molecules in the Si-P-H system. *Journal of Physical Chemistry*, 101, 913-918.
26. B. C. Garrett, M. L. Koszykowski, C. F. Melius and M. J. Page (1990). Theoretical calculations of the thermal rate constants for the gas-phase chemical reactions hydrogen atom + ammonia .dblarw. hydrogen + amidogen and deuterium atom + ammonia-d3 .dblarw. deuterium + amidogen-d2. *Journal of Physical Chemistry*, 94, 7096-7106.
27. C. F. Melius and M. D. Allendorf (2000). Bond additivity corrections for quantum chemistry methods. *Journal of Physical Chemistry*, 104, 2168-2177.
28. R. J. Kee, F. M. Rupley and J. A. Miller (1987). *The Chemkin Thermodynamic Data Base; Report: SAND-87-8215*; Sandia National Laboratories: Albuquerque, NM.
29. http://www.iupac-kinetic.ch.cam.ac.uk/Thermo2003.pdf, 2004.

30. *NIST Computational Chemistry Comparison and Benchmark Database, NIST Standard Reference Database Number 101, http://srdata.nist.gov/cccbdb*, May 2004; Vol. Release 10.
31. J. A. Manion (2002). Evaluated enthalpies of formation of the stable closed shell c1 and c2 chlorinated hydrocarbons. *Journal of Physical and Chemical Reference Data*, 31, 123-172.
32. J. C. Mackie, G. B. Bacskay and N. L. Haworth (2002). Reactions of phosphorus-containing species of importance in the catalytic recombination of H + OH: quantum chemical and kinetic studies. *Journal of Physical Chemistry A*, 106, 10825-10830.
33. L. V. Gurvich, I. V. Veyts and C. B. Alcock (1994). *Thermodynamic Properties of Individual Substances*; CRC Press: Boca Raton, FL, Vol. 3.
34. M. W. Chase (1998). *Fourth Edition, Journal of Physical and Chemical Reference Data, Monograph 9*, 1.
35. L. V. Gurvich, I. V. Veyts and C. B. Alcock (1989). *Thermodynamic Properties of Individual Substances*, Fouth Edition ed.; Hemisphere Pub. Co.: New York, 1989.
36. M. W. Chase, Jr., C. A. Davies, J. R. Downey, Jr., D. J. Frurip, R. A. McDonald and A. N. Syverud (1985). JANAF Thermochemical Tables. Third Edition. Part II, chromium-zirconium. *Journal of Physical and Chemical Reference Data*, 14.
37. D. L. Hildenbrand and K. H. Lau (1994). Thermochemical properties of gaseous POBr and some H–P–O species. *Journal of Chemical Physics*, 100, 8373-8376.
38. J. D. Cox, D. D. Wagman and V. A. Medvedev (1984). *CODATA Key Values for Thermodynamics*; Hemisphere Publishing Corp.: New York, Vol. 1.
39. M. F. Guest, J. B. Pedley and M. J. Horn (1969). Selected values of chemical thermodynamic properties: Part-1. *Journal of Chemical Thermodynamics*, 1, 345.
40. I. Barin and O. Knacke (1973). *Thermochemical properties of inorganic substances*; Springer-Verlag: Berlin, New York.
41. S. G. Lias, J. E. Bartmess, J. F. Liebman, J. L. Holmes, R. D. Levin and W. G. Mallard. *NIST Chemistry WebBook, NIST Standard Reference Database Number 69*; National Institute of Standards and Technology: Gaithersburg MD, 20899, March 2003.
42. S. G. Lias, R. D. Levin and S. A. Kafafi. *NIST Chemistry WebBook, NIST Standard Reference Database Number 69*; National Institute of Standards and Technology: Gaithersburg MD, 20899, March 2003.
43. S. G. Lias and J. F. Liebman. *NIST Chemistry WebBook, NIST Standard Reference Database Number 69*; National Institute of Standards and Technology: Gaithersburg MD, 20899, March 2003.

Chapter 7: Selectivity in Heterogeneous Catalytic Epoxidation of Ethylene

This chapter presents the important factors affecting branching ratio and selectivity for ethylene epoxidation on silver. Section 7.2 presents the surface mechanism with coverage-dependent activation energies of surface reactions and preexponential factor for the reaction of oxametallacycle to acetaldehyde. Section 7.3 discusses important reactions influencing branching ratio and selectivity with expressions to explain how gas transport across the catalyst boundary layer and surface chemistry affect the selectivity of epoxidation. Section 7.4 compares selectivities predicted by the surface mechanism against data for experimental and industrial reactors. Section 7.5 shows the effect in heat of formation of oxametallacycle on yield and selectivity of epoxide. Section 7.6 includes the sensitivity and uncertainty analyses for the rate parameters of surface mechanism.

7.1 Introduction

Ethylene oxide, an important raw material for several commodity chemicals, is commercially produced by the partial oxidation of ethylene on silver catalyst. The worldwide production capacity of ethylene oxide exceeds 22 billion pounds per annum [1]. In ethylene epoxidation, surface reactions are thought to follow two pathways:

$$C_2H_4 + 1/2\ O_2 \Leftrightarrow C_2H_4O \qquad \Delta H = -25.2 \text{ kcal/mol}$$

$$C_2H_4 + 3\ O_2 \Leftrightarrow 2\ CO_2 + 2\ H_2O \qquad \Delta H = -318.0 \text{ kcal/mol}$$

Former pathway is the partial oxidation resulting in epoxide, while latter is total combustion resulting in carbon dioxide. Based on the above reaction scheme, selectivity is defined as the molar percentage of reacted ethylene that forms epoxide:

$$S_{epoxide} = \frac{F_{epoxide,out}}{\left(F_{ethylene,in} - F_{ethylene,out}\right)}. \quad (7.1)$$

Conversion is the percentage of ethylene reacted:

$$x_{ethylene} = \frac{\left(F_{ethylene,in} - F_{ethylene,out}\right)}{F_{ethylene,in}}. \quad (7.2)$$

Yield is the product of selectivity and conversion:

$$Y_{epoxide} = x_{ethylene} \times S_{epoxide}. \quad (7.3)$$

Current process for ethylene oxide is based on 50-year old technology and there is constant motivation to improve the process. Improving yield and selectivity will not only increase profits through ethylene oxide production but also address climatic problems by reducing carbon dioxide emission. Current research in epoxide is in understanding the surface mechanism of epoxidation on silver. Important surface species had been spectroscopically identified and characterized in epoxidation reactions [2-7]. Selectivity was explained only on the basis of two forward reactions of oxametallacycle to epoxide and acetaldehyde [6]. Considering same preexponential factor for the two forward reactions, branching ratio between epoxide and acetaldehyde was thought to depend only on the difference in activation energies of the forward reactions.

Selectivity depends not only on the 2 forward reactions but also the reverse reaction of epoxide to oxametallacycle, since the reaction of oxametallacycle to epoxide is in equilibrium and reverse reaction is favored by fast surface kinetics and transport resistance of epoxide across the boundary layer from catalyst surface to gas phase. Preexponential factor of the reaction to acetaldehyde is expected to be less than that of the reaction to epoxide due to rearrangement of

C-H and C-O bonds and migration of H from α- to β-carbon in oxametallacycle while forming acetaldehyde.

In this work, we account for the branching of oxametallacycle and lower preexponential factor for the second branching reaction. We identify the significance of oxametallacycle-epoxide equilibrium and reverse reaction of epoxide. The role and thermodynamic stabilities of surface, subsurface oxygen and bulk silver oxide and the reactive form of oxygen on catalyst surface are discussed. Having put together a coverage-dependent and thermodynamically consistent surface mechanism, we have validated the kinetic model against experimental and plant conditions for epoxidation. Sensitivity analysis is performed to identify the effect of preexponentials and thermodynamic parameters including zero-coverage heats of chemisorption and coverage coefficients of surface species on ethylene oxide concentrations.

We use predictive kinetics to explain the selectivity of epoxidation. There could be many postdictive mathematical models and multiple choices of rate parameters that would fit and reproduce the literature data well. It is essential to use predictive kinetics from first principles and essential physics of surface reactions to have reasonable chance of making accurate extrapolations for a broad range of reactor conditions, not limited to the data available in literature. Kinetic and transport parameters in our work are not fitted from experimental data, but either calculated or taken from literature based on first principles.

7.2 Surface Mechanism and Rate Parameters of Ethylene Oxidation on Silver

In this section, we present the surface mechanism and rate parameters of epoxide reactions. First, the importance of coverage dependence in the rate parameter of epoxidation reactions is discussed. Next, the different surface reactions in the mechanism are explained. Stability in different forms of oxygen and active form of oxygen are analyzed. Dissociative adsorption of oxygen, adsorption of ethylene, formation of surface oxametallacycle, and branching of oxametallacycle to form epoxide and acetaldehyde are discussed with respect to the kinetics and thermodynamics of epoxidation process. Finally, DFT method used to calculate the preexponential factor of oxametallacycle to acetaldehyde is presented.

7.2.1 Coverage Dependence in Rate Parameters of Surface Reactions

In literature, many surface experiments are conducted under ultra high vacuum (UHV) conditions to study the structure of single crystal catalyst surfaces in the presence and absence of chemisorbed species. At UHV conditions, the reaction probability is low ($\sim 10^{-4}$, [8]) and the amount of ethylene oxide produced from reaction between ethylene and oxygen may be too small to be measured. Typically, high pressure (pressures $\sim 10^3$ to 10^5 torr) conditions are used to produce measurable amounts of ethylene oxide from the reaction between ethylene and oxygen on a silver catalyst in a high-pressure reaction cell. Following this, the reactants are pumped off the reaction cell rapidly and the catalyst sample is transferred in a short time ($\sim$ 20 s) to a UHV cell where the catalyst is subjected to different surface techniques [9-13] and silver catalyst surface composition, surface structure, adsorbate arrangements, reaction pathways, and core electronic levels of the adsorbates and surfaces are probed. Results of UHV may not be directly applicable to high pressure catalytic reactors, unless surface coverages at high pressures

(which are of practical interest) can be duplicated at vacuum at temperatures which are high enough. At low pressures, there may be negligible interactions among different adsorbates and surface coverage may have negligible effect on the chemisorption enthalpies of surface species. However, at high pressures significant adsorbate-adsorbate interactions would signify the dependence of chemisorption enthalpies on coverages. In this work, coverage dependence is accounted for the chemisorption enthalpies of adsorbed species. Self coverage dependence in the heat of chemisorption of oxygen is particularly important since DFT calculations showed that atomic oxygen is 5 kcal/mol less stable on 0.25 ML than on 0.11 ML oxygen covered silver [14].

7.2.2 Dissociative Oxygen Adsorption and Different Forms of Oxygen

Oxygen molecule dissociatively adsorbs on silver surface to form surface oxygen:

$$O_2 + 2\ AG(S) \Leftrightarrow 2\ O(S) \qquad (S1)$$

In literature, stabilities of molecular, surface, subsurface oxygen, and silver oxide have been studied. Low desorption temperature (170K, [15]) and low chemisorption enthalpy of molecular oxygen (10.0 kcal/mol, [16,17]) indicated that molecular oxygen was not stable on silver. Surface atomic oxygen was found by XPS when molecular oxygen dissociatively adsorbed on Ag(110) even at low temperature (130K) for a dosage of 1100 L O_2 [18]. Engelhardt and Menzel investigated the adsorption of oxygen on Ag(110), Ag(111) and Ag(100) surfaces through LEED and AES by measuring work function changes and kinetics at and above room temperature for O_2 partial pressures up to 10^{-5} Torr [19]. High desorption temperatures (550 and 660K on Ag(111) Ag(110), [9,15] and high heat of chemisorption (~ 80 kcal/mol [19]) suggested that atomic oxygen was stable on the surface.

Backx et al. observed different desorption peaks for oxygen when they ran several cycles of oxygen adsorption at room temperatures followed by TPD analysis [15]. First contact of a clean Ag(111) surface with oxygen followed by TPD analysis gave a desorption peak at around 600K. Desorption peak was 70% larger, when a second cycle of adsorption followed by TPD was undertaken. For a further six cycles, the peak continued to increase and desorption peak for the final cycle was observed at around 880K. A desorption peak at 900K was observed by Bowker et al [20].

These temperatures are much higher than the typical temperatures at which surface atomic oxygen is observed to desorb from the surface. This might indicate the presence of subsurface oxygen in silver. Backx et al. used TPD study to show that adsorbed atomic oxygen diffuses into the subsurface region above 423K and does not desorb or diffuse into the bulk until above 723K [15]. However, the saturation subsurface oxygen is limited to a few (~ 2) monolayers, as observed from experiments by Campbell [9]. He dosed 1400 Torr oxygen on Ag(111) at 443K for 640 seconds; only two monolayers desorbed during a subsequent TPD experiment. Subsurface oxygen has been characterized in several other studies using XPS and TPD [16,17,21].

Some researchers have hypothesized that subsurface oxygen weakens the binding of surface oxygen, increasing the amount of oxygen taking part in epoxidation process, while some have considered subsurface oxygen not to affect the surface reaction mechanism. Former hypothesis was in agreement with the results of van den Hoek et al. [22] whose Hartree-Fock-Slater calculations showed that the subsurface oxygen decreases the binding of atomic oxygen on Ag(110). However, Pawela-Crew et al. used near-edge adsorption fine structure analysis (NEXAFS) to show that subsurface oxygen does not affect the orientation of molecular oxygen

on silver [23]. They observed a similar shape in the NEXAFS spectra of molecular oxygen with and without the presence of subsurface oxygen. Since the epoxidation conditions are very different from the experimental conditions at low partial pressures, the nature and even the presence of subsurface oxygen may be quite different in the two cases. The obtained phase diagram revealed that surface oxygen actuated silver as the partial oxidation catalyst.

Experimental evidence in the phase diagram showed that subsurface oxygen is more stable than Ag_2O. Subsurface oxygen did not involve simple dissolution of oxygen in the bulk, but a separate species that could be spectroscopically characterized. The phase diagram (T, P plot) had a well-shaped curve for subsurface oxygen. For higher doses of O_2, subsurface oxygen was found which led to well-shaped P, T curves (drop in P with respect to T, a minimum P and increase in P). For low doses, only silver oxide was observed at much lower temperatures. The P, T curve for silver oxide was a straight line.

Using the standard states of silver and molecular oxygen, the heat of formation of silver oxide is calculated as 7.4 kcal/mol, which is significantly lower than the heat of chemisorption of surface oxygen (25.0 kcal/mol). Heat of chemisorption of surface oxygen with respect to molecular oxygen has been derived from heat of chemisorption of surface oxygen with respect to atomic oxygen (84, 81.15, 78.62 kcal/mol [14,24]). The above thermodynamic analysis shows that the three forms of oxygen in the decreasing order of stability are: surface oxygen, subsurface oxygen and silver oxide. Despite the differing stabilities, different forms of oxygen could co-exist if chemical potential of O_2 were sufficient to saturate all the surface sites with atomic O, convert bulk silver to silver oxide and fill up subsurface sites with oxygen.

The binding energy of surface oxygen with respect to atomic oxygen is 3.27 eV (= 75.4 kcal/mol). Hence, the binding energy with respect to molecular oxygen is 15.9 kcal/mol.

By including the change in entropy, Gibbs free energy of the dissociative adsorption of oxygen to form surface oxygen is estimated as -13.4 kcal/mol. Reported binding energy of subsurface oxygen with respect to atomic oxygen is 2.93 eV, while the binding energy with respect to molecular oxygen is -8.1 kcal/mol.

Equilibrium partitioning would reveal the degree of co-existence of the 3 phases due to the following 3 reactions:

$Ag + 1/2\ O_2 \Leftrightarrow O(S)$ $\Delta G_1 = -13.4$ kcal/mol. $K_{p1} = 720{,}477.8$

$Ag + 1/2\ O_2 \Leftrightarrow O^{sb}$ $\Delta G_2 = 1.9$ kcal/mol. $K_{p2} = 0.2$

$2Ag + 1/2\ O_2 \Leftrightarrow Ag_2O$ $\Delta G_3 = 0.5$ kcal/mol. $K_{p3} = 1.7$

Changes in free energies and equilibrium constants of above reactions indicate that the equilibrium between silver and oxygen favors surface oxygen over subsurface oxygen and bulk silver oxide. At 1 bar P_{O2}, surface oxygen coverage is considerable.

Li et al. conducted extensive DFT calculations to identify surface oxygen as the most stable and reactive active oxygen species for epoxidation conditions corresponding to industrial reactors [25]. Silver oxide is 0.5 kcal/mol less stable than silver and oxygen, if the partial pressure of O_2 is 1 bar and the temperature is 500K which corresponds to the nominal operating temperature for industrial epoxidation reactor. Silver oxide is more stable than silver, if the partial pressure is increased and temperature is decreased. The issue is whether active site on silver catalyst is silver or silver oxide and equilibrium between silver and silver oxide is O_2 P-dependent and T-dependent. Using the reported chemisorption energies for subsurface and surface oxygen [25], the heat of chemisorption of surface oxygen with respect O_2 is calculated to be 1.6 kcal/mol. Subsurface oxygen lowers the binding energy of surface oxygen. Enthalpy of formation or the hypothetical chemisorption enthalpy of subsurface oxygen has been derived

from the difference in binding energies in the presence and absence of subsurface oxygen. Surface oxygen is 13.4 kcal/mol less stable when subsurface oxygen is present.

7.2.3 Subsurface Oxygen vs. Silver Oxide

To help provide insight into the remarkable catalytic behavior of the oxygen/silver system for heterogeneous oxidation reactions, purely subsurface oxygen, and structures involving both on-surface and subsurface oxygen, as well as oxide-like structures at the Ag(111) surface was studied by Li et al. for a wide range of coverages and adsorption sites using DFT [26]. It was found that adsorption on the surface in fcc sites is energetically favorable for low coverages, while for higher coverage a thin surface-oxide structure is energetically favorable. This structure was proposed to correspond to the experimentally observed (434) phase. With increasing O concentrations, thicker oxide-like structures resembling compressed $Ag_2O(111)$ surfaces were energetically favored. Due to the relatively low thermal stability of these structures, and the very low sticking probability of O_2 at Ag(111), their formation and observation might require the use of atomic oxygen or ozone, O_3 and low temperatures. Diffusion of O into the subsurface region was also investigated at low coverage (~0.11 ML), and the effect of surface Ag vacancies in the adsorption of atomic oxygen and ozone-like species. The most stable oxide of silver, Ag_2O, however, thermally decomposed at 460K and at atmospheric pressure, making this seem unlikely the energy barriers for O penetration through the surface. From a recent trend study of oxygen adsorption and incorporation at the basal planes of Ru, Rh, Pd, and Ag, Li et al. [27] found that the coverage at which the onset of oxygen occupation of subsurface sites correlated closely with that predicted at which bulk oxide formation begins, and that this occurs at progressively lower

coverages for the metals more to the right side of the periodic table. The energy cost for lattice distortion was found to play a key role, where it was greater for the metals more to the left side of the periodic table (Ru and Rh). With regard to pure free-electron-like metals, the O/Al(111) and O/Mg(0001) systems were investigated as well by first-principles calculations. Experimental evidence indicated that the (111) orientation was an important crystal face for real silver catalysts since at high temperatures, facets with this face resulted [28,29] presumably due to the fact that it had the lowest surface energy. There were only two ordered phases of oxygen on Ag(111) that were reported; the (434) [30] and (A33A3)R30° structures [28,31]. The latter actually exhibited a superstructure given in matrix notation as (2631; 21326). The (434) structure had recently been investigated by STM, where the atomic structure was proposed to involve a thin surface-oxide layer [32,33]. It was furthermore proposed that at low coverage (u50.0560.03 ML), O atoms occupied subsurface octahedral sites below the first Ag layer.

Compared to pure surface oxygen adsorption, which exhibited a strong decrease in adsorption energy with increasing coverage, pure subsurface adsorption exhibited a weak dependence on the coverage, where the octahedral site was favored for all of the investigated coverage range of 0.11 to 1 ML. Comparing the adsorption energies of surface and subsurface oxygen, it was found that the former was energetically favored over the latter for coverages up to around 1/2 a monolayer, whereafter the pure subsurface structures were preferred. The energetically favorable structures involving both surface and subsurface oxygen had a lower density of states at the Fermi energy and involved less ionic O atoms as compared to the energetically unfavorable structures. The presence of subsurface oxygen modified the surface oxygen-silver bond significantly. Depending on the adsorption site, it could either stabilize or destabilize the surface oxygen and vice versa. The energetically most favorable structures,

however, stabilized the surface oxygen. On the basis of the energetics of all the calculated structures, it was found that at low coverages oxygen preferred to stay on the surface in fcc site. With increasing coverage a thin (434) surface oxide was energetically favorable, and for higher concentrations, the calculations predicted the formation of oxide-like structures very similar to $Ag_2O(111)$. We proposed that with the use of atomic oxygen or ozone and low temperatures, such thicker oxide-like films might be observed experimentally.

7.2.4 Subsurface Oxygen in Transition Metal Surfaces

Li et al. presented a DFT trend study addressing the incorporation of oxygen into the basal plane of the late 4d transition metals from Ru to Ag [27]. Occupation of subsurface sites was always connected with a significant distortion of the host lattice, rendering it initially less favorable than surface chemisorption. Penetration into the surface started only after a critical coverage, which was found to be very similar to those above which the bulk oxide phase became thermodynamically more stable, suggesting that the initial incorporation of O actuated the formation of a surface oxide on TM surfaces. King and coworkers proposed that the critical coverage, at which the transition between a chemisorbed phase and the appearance of an oxidic film occurs is thermodynamically, not kinetically determined [33]. Below the critical coverage, the heat of formation of chemisorbed phase was higher than the heat of formation of oxide. Repulsive interactions between the O adatoms drived the differential heat of adsorption down sharply with increasing coverage, until at the critical coverage it is equal to that of the formation of an oxide film.

Li et al. found that incorporation of O into the subsurface region was initially always less stable than surface chemisorption, largely due to the additional cost of distorting the substrate lattice and breaking metal bonds [27]. With increasing surface coverage, this preference decreased due to repulsive interactions within the more densely packed electronegative O adlayer. Above a certain critical O coverage, occupation of subsurface sites then became more favorable compared to a continued filling of the on-surface sites. Incorporation commenced already at low surface coverages for the case of Ag; the coverages were similar to the critical coverages for oxide formation, obtained with King's thermodynamic model. This suggested that the initial incorporation of subsurface O is the "bottle-neck" in the oxidation sequence of these metal surfaces. This incorporation is strongly dependent on lattice deformation properties, the ease of oxide formation follows similar trends as the bulk cohesive energy or the bulk modulus. The oxidation of TMs commences with the dissociative chemisorption of O_2 at highly coordinated sites on the surface, possibly preceded by molecular physisorption at low temperatures. Additionally, a marked decrease of surface binding energy, E_b with coverage was observed. This reflected a repulsive interaction within the more and more densely packed electronegative overlayer. The decrease in surface binding energy translates into a steeply decreasing differential heat of adsorption, which was compared with the experimental heat of formation of the most stable bulk oxide phase of the respective metal, H_f. Following King's thermodynamic argument [33], the critical surface coverage for the transition to the oxide phase, is given once the differential heat of adsorption has fallen below the value of H_f.

7.2.5 Function of Silver as an Oxidation Catalyst

Li et al. performed DFT calculations taking into account temperature and partial pressure to present a comprehensive picture of the behavior and interaction of oxygen and Ag(111) [25]. This provided valuable insight into the function of silver as an oxidation catalyst. The obtained phase diagram revealed the most stable species present in a given environment and thus identified active oxygen species. In particular, for the conditions of ethylene epoxidation, a thin oxide-like structure is most stable, suggesting that such atomic O species were actuating the catalysis, in contrast to hitherto proposed molecular-like species.

To help understand the high activity of silver as an oxidation catalyst, e.g., for the oxidation of ethylene to epoxide and the dehydrogenation of methanol to formaldehyde, the interaction and stability of many different oxygen species at the Ag(111) surface was studied for a wide range of coverages. Through calculation of the free energy, as obtained from DFT and accounting the temperature and partial pressure via the oxygen chemical potential, the phase diagram of O/Ag(111) was obtained. The results revealed that a thin surface-oxide structure was most stable for the temperature and pressure range of ethylene epoxidation. For higher temperatures, low coverages of chemisorbed oxygen were most stable, which could also play a role in oxidation reactions. For temperatures greater than about 775K there were no stable oxygen species, except for the possibility of O atoms adsorbed at under coordinated surface sites including surface imperfections and defects. At low temperatures (400K) and atmospheric pressure, provided kinetic limitations can be overcome, thicker oxide-like structures were predicted. Due to their low thermal stability, however, they could be ruled out as playing an important role in the heterogeneous reactions under technical conditions. Bulk dissolved oxygen and molecular ozone-like species adsorbed at a surface vacancy, as have been proposed in the literature, were found to be energetically unfavorable.

We have calculated coverage-dependent thermodynamically consistent activation energies for forward and reverse reactions based on the coverage-dependent heat of chemisorption of oxygen from experimental data [16, 26 and 34]:

$$Q_O(\theta_{C2H4}) = 84.0 + 3.6\,\theta_{C2H4} - 35.7\,\theta_O.$$

Self coverage-dependence in the heat of chemisorption of oxygen is particularly important since atomic oxygen is found to be 5 kcal/mol less stable on 0.25 ML than on 0.11 ML oxygen covered silver.

The calculated activation energies of the forward and reverse reactions are 0.0 and $49.0 + 7.2\theta_{C2H4} - 71.4\theta_O$ kcal/mol. Difference between the activation energies results in reaction enthalpy: $- 49.0 - 7.2\theta_{C2H4} + 71.4\theta_O$, which is consistent with the reaction and oxygen chemisorption enthalpy measured from TPD experiments [10]. Experimental binding energy for surface oxygen with respect to O_2 is - 11 kcal/mol and the derived binding energy with respect to O is - 70.56 kcal/mol. Energy with respect to O is consistent with the oxygen chemisorption enthalpy.

7.2.6 Ethylene Adsorption

Ethylene is known to adsorb weakly on silver [35-37].

$$C_2H_4 + AG(S) \Leftrightarrow C_2H_4(S) \qquad (S2)$$

Low temperatures (130 and 155K [11,34]) of desorption and low chemisorption enthalpy (8.9 kcal/mol, [11], TDS on clean Ag(110) surface for an exposure of 10^{-6} mbar sec. of ethylene) have been reported in literature. The coverage-dependent heat of chemisorption of ethylene is [34]:

$$Q_{C2H4}(\theta_O) = 8.9 + 3.6\,\theta_O.$$

This is used to estimate the coverage-dependent activation energies of forward and reverse reactions: 0.0 and $8.9 + 3.6\theta_O$ kcal/mol, respectively.

7.2.7 Formation of Oxametallacycle and Branching to Epoxide and Acetaldeyhde

Reaction between adsorbed ethylene and oxygen results in the formation of surface oxametallacycle [6]:

$$C_2H_4(S) + O(S) \Leftrightarrow H_2COCH_2(S) \qquad (S3)$$

Figure 7.1 describes the geometry of oxametallacycle, epoxide and acetaldehyde. Oxygen and carbon atoms in oxametallacycle are bound to Ag atoms on the catalyst surface, and the hydrocarbon part of oxametallacycle is geometrically closer to epoxide than acetaldehyde. Oxametallacycle undergoes ring closing via an additional bond between oxygen and β-carbon to form epoxide, while H migrates from α- to β-carbon and single bond between α-carbon and oxygen shortens for double bond to form acetaldehyde.

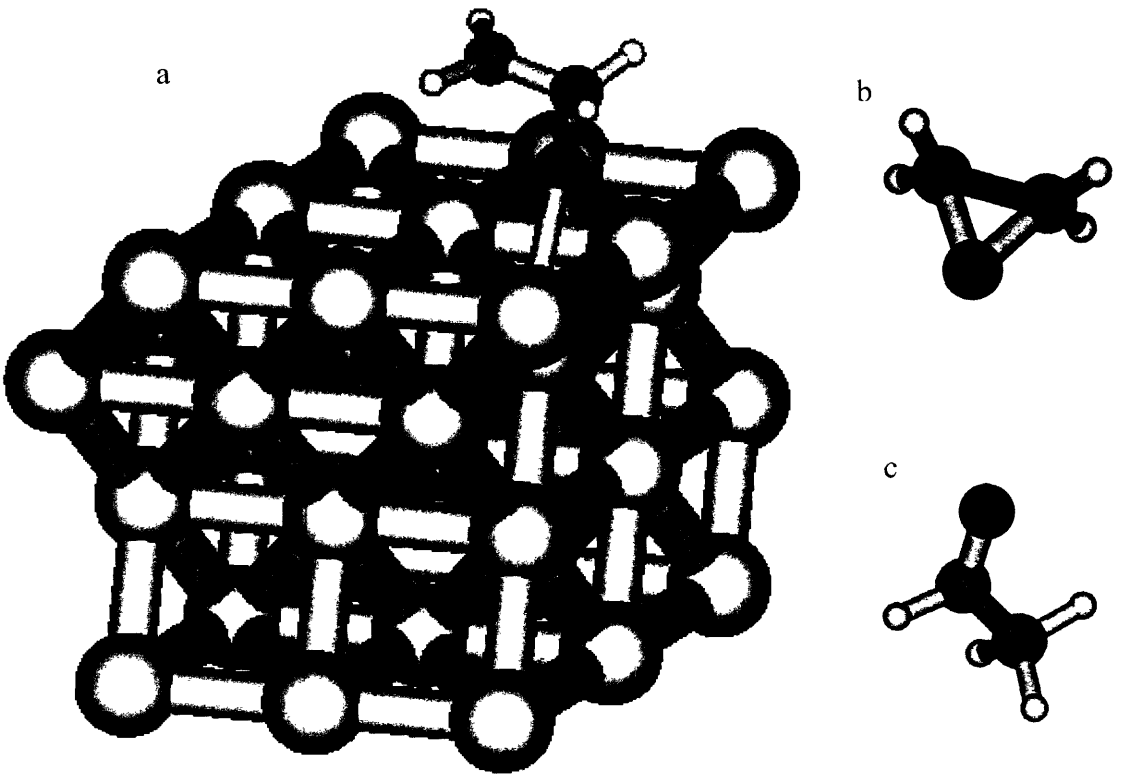

Figure 7.1 Geometry of (a) Surface Oxametallacycle having O-C-C Backbone with O and C bound to Ag atoms (b) Epoxide (c) Acetaldehyde

In Figure 7.1, silver surface is represented by a 3×3 unit cell with 4 layers of silver atoms. Using DFT, Linic and Barteau estimated the heat of formation of oxametallacycle and the activation energy of forward reaction of Step S3 (14.9 kcal/mol). We add coverage dependence of surface oxygen and surface ethylene to this coverage-independent activation energy, since adsorbed oxygen and ethylene react to form oxametallacycle:

$$14.9 - 32.1\theta_O + 3.6\theta_{C2H4}.$$

We calculate activation energy of the reverse reaction based on thermodynamic consistency with respect to enthalpy (-25.2 kcal/mol) of the overall reaction: $1/2\ O_2 + C_2H_4 \Leftrightarrow C_2H_4O$. Oxametallacycle branches to form ethylene oxide and acetaldeyhde:

$$H_2COCH_2(S) \Leftrightarrow C_2H_4O + 2\ AG(S) \qquad (S4)$$

$$H_2COCH_2(S) \rightarrow CH_3CHO + 2\ AG(S) \qquad (S5)$$

First reaction is reversible and activation energy of the reverse reaction is 5 kcal/mol less than that of the forward reaction (16.0 and 11.0 kcal/mol [6]). We calculate the preexponential factor for the reaction of surface oxametallacycle leading to acetaldehyde (Step S5) using Density Functional Theory (DFT).

7.2.8 Calculation of Preexponential Factor of Oxametallacycle Reaction to Acetaldehyde

We use Guassian98® suite of programs and apply DFT to obtain the analytical second derivatives or the vibrational frequencies of the transition state leading to acetaldehyde. DFT describes how the ground state electron density and total energy can be obtained by solving a set of one-electron Schrödinger equations (the Kohn-Sham equations). Becke 1988 and Perdew 1986 non-hybrid GGA, BP86 is used for exchange and correlation energies [38], Dunning/Huzinaga valence double-zeta, d95v basis set with single first polarization functions is used for C, H, O atoms [39] and LANL2DZ basis set with LANL2 ECP data is used for silver [40-42]. Silver atoms are allowed to move in the cluster calculation, and 4 silver atoms attached to the hydrocarbon part are used in frequency calculation. Twenty seven vibrational frequencies are computed for the hydrocarbon-silver system consisting of 11 atoms. Since there are 7 atoms in the hydrocarbon part, 14 frequency modes are used for calculating the vibrational partition function of the transition state. When N is the number of atoms in a molecule, people normally use 3N-7 frequencies in a TS because 1 of the frequencies is negative (the reaction coordinate) and 6 of the frequencies are zero (3 translations and 3 rotations). In this case, however, 6

vibrational frequencies of the modes that hold the OMME onto the silver surface are neglected when calculating the vibrational partition function. The 6 computed frequencies are 74, 89, 104, 120, 171 and 220 cm^{-1}. If the DFT-predicted frequencies for oxametallacycle were available for the 6 modes holding the hydrocarbon part to the silver surface, then it would be worthwhile to compare them against our calculated frequencies for oxametallacycle. If any of the frequencies change significantly, then the A-factor would be significantly different if the lower frequencies were included. There are subtle unresolved issues with the low frequency modes that correspond to the surface atoms. Normal modes corresponding to bond stretch, scissor, twist, wag and ring deformations are identified in oxametallacycle. Vibrational frequencies of oxametallacycle and transition state are included in Appendix E. Negative frequency corresponding to reaction coordinate or saddle point for the transition state is -342.92 cm^{-1}. Vibrational frequencies of the transition state are used to calculate the vibrational partition function:

$$Q_v = \prod_{i=1}^{s} \frac{1}{1 - e^{(-\frac{h\nu_i}{k_B T})}}, \tag{7.4}$$

where s is the number of vibrational modes. There are 3N-6 vibrational modes for stable species. The total partition function which is a product of the translational, rotational and vibrational partition functions is used to calculate the preexponential factor:

$$A = \frac{RT}{h} \frac{Q_{TS}}{Q_{Oxametallacycle}}. \tag{7.5}$$

The translational partition function cancels out completely for the transition state and oxametallacycle, since they have the same mass. The moments of inertia of the TS and OMME are assumed to be similar, and hence rotational partition function does not contribute significantly.

Our calculated preexponential factor for forward reaction of oxametallacycle to acetaldehyde is 4.22×10^{12} s^{-1}, which is lower than the theoretical maximum of 10^{13} s^{-1} due to a

decrease in entropy of the oxametallacycle when it changes geometry to form the transition state. It is to be noted that the calculated preexponential factor is an order of magnitude lower than the preexponential factor (4.00×10^{13} s^{-1}, [43]) for the reaction of oxametallacyle to ethylene oxide. The optimized geometry of transition state and significant displacement of hydrogen atom (0.9A°) from α- to β-carbon and shortening of the C-O single bond indicates the change in geometry from oxametallacyle to acetaldehyde.

Table 7.1 lists the reactions S1 through S5 in the surface mechanism with coverage-dependent activation energies. The surface mechanism is thermodynamically consistent since linear combination of the enthalpies of 5 elementary reactions lead to the enthalpy of the overall epoxidation reaction.

Table 7.1 Surface Mechanism and Coverage-Dependent Thermodynamically Consistent Activation Energies for Epoxidation on Silver

Step #	Reaction	Activation Energies (kcal/mol)	
		E_f	E_r
S1	$O_2 + 2\ AG(S) \Leftrightarrow 2\ O(S)$	0.0	$49.0 + 7.2\theta_{C2H4} - 71.4\theta_O$
S2	$C_2H_4 + AG(S) \Leftrightarrow C_2H_4(S)$	0.0	$8.9 + 3.6\theta_O$
S3	$C_2H_4(S) + O(S) \Leftrightarrow H_2COCH_2(S)$	$14.9 - 32.1\theta_O + 3.6\theta_{C2H4}$	12.5
S4	$H_2COCH_2(S) \Leftrightarrow C_2H_4O + 2\ AG(S)$	16.0	11.0
S5	$H_2COCH_2(S) \Leftrightarrow CH_3CHO + 2\ AG(S)$	15.7	41.1

Coverage dependence for oxygen: $Q_O(\theta_{C2H4}) = 84.0 + 3.6\ \theta_{C2H4} - 35.7\ \theta_O$ [16,26,34];
Coverage dependence for ethylene: $Q_{C2H4}(\theta_O) = 8.9 + 3.6\ \theta_O$ [34]
Heat of formation of oxametallacycle: H_f(OMME) = -18.5 [6]

7.3 Branching Ratio and Selectivity of Epoxide

In this section, expressions for branching ratio and selectivity of epoxide based on the two parallel branching reactions of oxametallacycle and the reverse reaction of epoxide (see Figure

7.2) are derived. Next, the effect of surface chemistry with the reverse reaction of epoxide on branching ratio and selectivity of epoxide is analyzed. Then, we explain the trends in selectivity when the conversion changes.

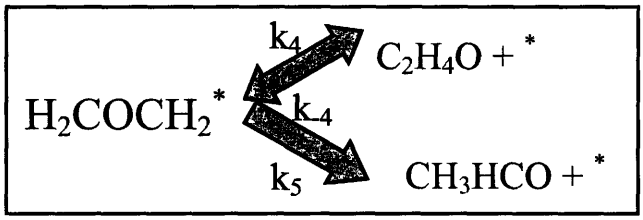

Figure 7.2 Branching of Oxametallacycle and Reversibility of Ethylene Oxide

Branching ratio is derived as:

$$BR = \frac{k_4}{k_5} \times (1 - \frac{P_{C2H4O,surface}}{K_{eq,4}} \times \frac{\theta_v}{\theta_{OMME}}), \quad (7.6)$$

where k_4 and k_5 are the rate constants of the forward reactions, $K_{eq,4}$ is the equilibrium constant of the first reaction, $P_{C2H4O,surfacc}$ is the partial pressure of ethylene oxide at the catalyst surface and θ_{OMME} and θ_v are surface coverages of oxametallacycle and vacancy. Selectivity is related to branching ratio:

$$S_{epoxide} = \frac{BR}{BR+1}. \quad (7.7)$$

7.3.1 Effect of Surface Chemistry and Transport on Branching Ratio and Selectivity

Rate parameters of forward reactions, and hence surface chemistry affect the branching of oxametallacycle to epoxide and acetaldehyde:

$$\frac{k_4}{k_5} = \frac{A_4 \exp(-\frac{E_{f,4}}{RT})}{A_5 \exp(-\frac{E_{f,5}}{RT})}. \qquad (7.8)$$

A_5 has been calculated to be an order-of-magnitude lower than A_4 (see Section 7.2.8). The term involving equilibrium constant in Eq. 7.6 signifies the reversibility of epoxide to oxametallacycle.

$P_{C2H4O,surface}$, which is the partial pressure of epoxide at the surface could be quite different from the partial pressure at the bulk gas phase due to resistance to transport of ethylene oxide and other gas molecules across the catalyst boundary layer. The transport resistance favors the reverse reaction of epoxide which in turn reduces the branching ratio.

Due to diffusional resistance in the boundary layer, the partial pressure of epoxide in bulk gas phase is lower than the partial pressure at the surface, and the pressure difference is derived as:

$$P_{C2H4O,bulk} = P_{C2H4O,surface} - \frac{\delta}{D}(N_{flux})RT, \qquad (7.9)$$

where δ is boundary layer thickness, D is diffusivity of epoxide and N_{flux} is the molar flux of epoxide per unit area of the catalyst surface. Transport resistance to epoxide reduces its partial pressure in the bulk, decreasing the overall throughput or yield. Rate of the reverse reaction may be comparable to that of the forward reaction unless ethylene oxide is taken away from the catalyst surface by fast stream of bulk gas flowing through the reactor.

For an experimental microreactor, it is easy to estimate the partial pressure difference between ethylene oxide at the bulk and the interface from Eq. 7.9. Using a boundary layer thickess $\delta = 50$ μm, diffusion coefficient $D = 10^{-5}$ m^2/s, $R = 8.314$ J/mol/K, $T = 512$ K and molar epoxide flux $N_{flux} = 2\times10^{-6}$ $mol/m^2/s$ (as seen from reactor simulations), the partial pressure

difference is estimated as 0.04 bar. This is about 30% of the total partial pressure of ethylene oxide, based on the predicted 90% selectivity and 95% conversion of an inlet stream of ethylene at 0.15 bar (3% mole fraction, 5 bar total pressure).

Brauer [44] devised an empirical correlation describing the velocity field around a spherical particle for a broad range of application, being valid for $0 < \mathrm{Re} < 3\times10^5$:

$$\frac{D}{\delta} = \left\{2 + f_k \frac{(\mathrm{Re}\,Sc)^{1.7}}{1+(\mathrm{Re}\,Sc)^{1.2}}\right\}\frac{D}{d_p}, \tag{7.10}$$

in which

$$f_k = \frac{0.66}{\left\{1+(0.84Sc^{1/6})^3\right\}^{1/3}}. \tag{7.11}$$

For typical industrial epoxidation reactors corresponding to a flow rate of 3000 GHSV (7.5 ms^{-1}), catalyst pellet diameter of 10 mm, diffusivity of 1×10^{-5} m^2s^{-1} and kinematic viscosity of 1.46×10^{-5} m^2s^{-1}, the Re and Sc are 7500 and 1.46. Using Eqs. 7.10 and 7.11, the boundary layer thickness is calculated as 145 μm. For a molar epoxide flux of 2×10^{-6} $mol/m^2/s$, the partial pressure difference for the industrial reactor is estimated as 0.12 bar. This is about 24% of the total partial pressure of ethylene oxide, based on 80% selectivity and 10% conversion of an inlet ethylene stream of 6.25 bar (25% mole fraction, 25 bar total pressure).

7.3.2 Decrease of Selectivity with Increase in Conversion

Eqs. 7.6 and 7.7 for branching ratio and selectivity explain the experimentally observed trend of decreasing selectivity with increasing conversion. Increasing conversion of oxametallacycle increases partial pressure of epoxide at the surface resulting in an increase in the rate of reverse reaction of epoxide.

N_{flux} is proportional to the rate of conversion of ethylene in epoxidation reactor. Increase in the rate of reverse reaction and molar flux of epoxide due to increase in conversion result in the decrease of branching ratio and selectivity. Inclusion of reverse reaction leads to physically observable decrease of selectivity with increase in conversion, while the omission would have led to constant branching ratio and selectivity irrespective of changes in conversion:

$$BR' = \frac{k_4}{k_5}. \tag{7.12}$$

Figure 7.3 shows how the predicted selectivity varies with conversion for experimental conditions in a microreactor [45]. The operating conditions of the microreactor used are: 5 bar total pressure, 0.124 s reactor residence time, 5 L/h gas flow and 3% C_2H_4, 16.5% O_2 and rest N_2 in the reactor feed.

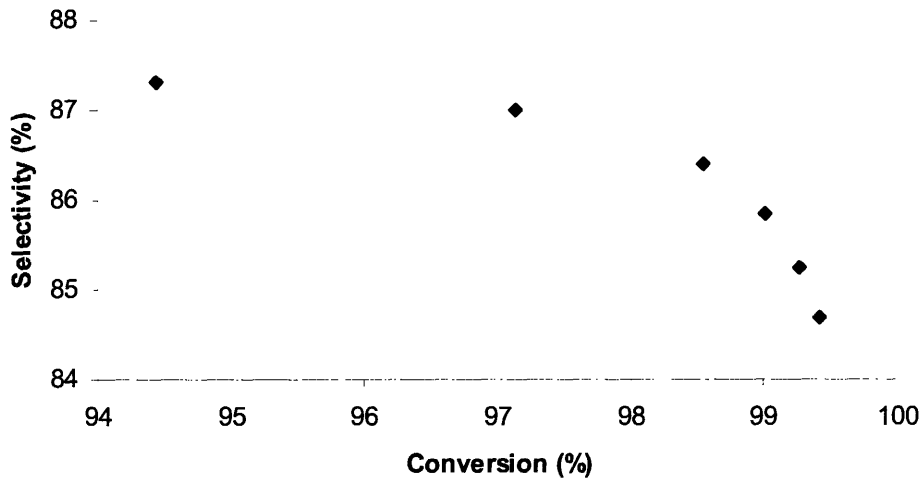

Figure 7.3 Variation of Predicted Selectivity with Conversion for Microreactor Conditions

From Figure 7.3, we observe that the predicted selectivity decreases with conversion. The selectivity drops abruptly as the conversion goes from 97% to 99%. Figure 7.4 plots $\frac{P_{C2H4O,surface}}{K_{eq,4}}\frac{\theta_v}{\theta_{OMME}}$, the second term from Eq. 7.6, as a function of conversion. This term signifies the importance of reverse reaction of ethylene oxide to oxametallacycle.

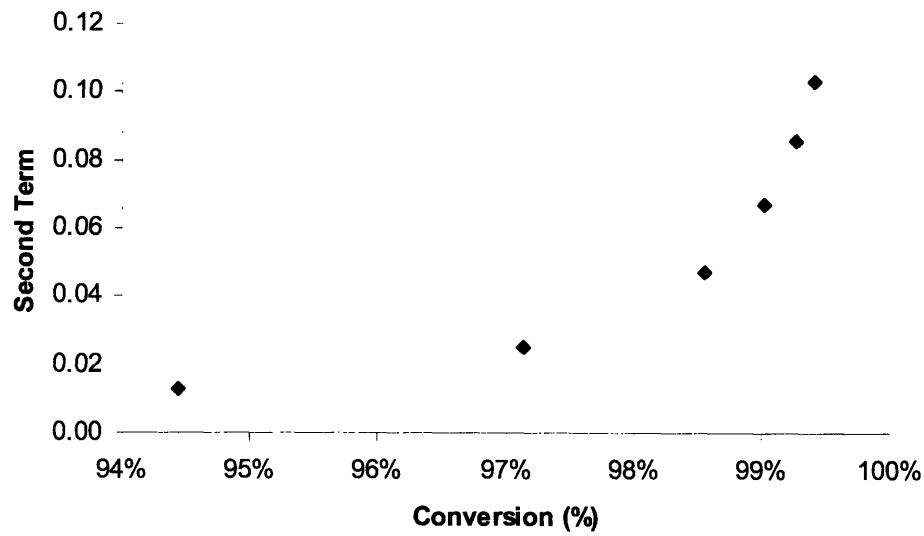

Figure 7.4 Variation of Second Term with Conversion for Microreactor Conditions

From Figure 7.4, we observe that the second term signifying the reverse reaction of EO stays at a low value until about 97% conversion where it starts raising significantly. Due to a low inlet C_2H_4 pressure (0.15 bar), EO partial pressure at the surface stays low (0.09 bar, based on the computed P-difference due to boundary layer) for all the conversions. However, θ_{ommc} decreases significantly after about 97% conversion increasing the $\frac{\theta_v}{\theta_{omme}}$ ratio. From this point, the reverse reaction of EO to OMME becomes kinetically significant compared to the forward reactions of OMME to EO and CH_3CHO, and selectivity is no longer governed only by the 2 forward

reactions. The site fraction of OMME decreases since it is increasingly consumed in the acetaldehyde channel. Until 97% conversion, the 2 forward reactions of OMME are only important and the selectivity stays fairly constant.

7.4 Validation of Surface Mechanism for Experimental and Plant Conditions

Kestenbaum et al. measured the selectivities to ethylene oxide in microreactors for different operating temperatures, total pressures and molar flow rates of reactants [45]. Series of experiments were conducted for varying temperatures on a Laser-LIGA catalyst at 5 bar total pressure, reactor residence time of 0.124 s, 5 L/h gas flow and 3% C_2H_4, 16.5% O_2 and N_2 as inerts in the feed to reactor. Our surface mechanism and transport model predicts the conversions, selectivities and yields for the operating conditions in the microreactor geometry (Figure 7.5). Plug flow is assumed to model the microreactor. Diffusional transport of gas species across the boundary layer is modeled by using elementary reactions with the rates functions of transport coefficients and boundary layer thickness. The rate constant of reaction leading to interfacial gas phase concentration from bulk is given by:

$$k_{diffusion,bulk-to-\mathrm{int}erface} = \frac{D}{\delta}. \tag{7.13}$$

Rate constant of the reverse reaction leading to bulk concentration is given by:

$$k_{diffusion,\mathrm{int}erface-to-bulk} = k_{diffusion,bulk-to-\mathrm{int}erface} \times K_{eq,diffusion}, \tag{7.14}$$

where

$$K_{eq,diffusion} = \frac{V_{bulk}}{V_{\mathrm{int}erface}}, \tag{7.15}$$

is the ratio between the bulk volume in gas phase to volume in the interface. This ratio is used to balance the total number of moles of any gas species between the bulk and interface, despite

change in volumes of the 2 phases. Bulk and interfacial volumes are based on the length scales of catalyst and boundary layer, respectively. For the experimental microreactor, the thickness is same as the channel height since the boundary layer extends all the way to the top of microreactor channel. Hence, the ratio between bulk and interfacial volume is unity. For the industrial reactor, the boundary layer thinkess as seen from simulations is 145 μm, which is less than typical diameter (10 mm) of catalyst pellets used [46]. Hence, bulk-to-intefacial volume ratio is 71.4. The kinetic rate constants for forward and reverse reactions involving the gas species at interface are adjusted by the bulk-to-interface volume ratio:

$$k_f = k_{f,kinetic} \times \frac{V_{bulk}}{V_{interface}}, \tag{7.16}$$

and

$$k_r = k_{r,kinetic} \times \frac{V_{bulk}}{V_{interface}}. \tag{7.17}$$

To simulate the transport of gases and reaction of gas and surface species, the Aurora application of CHEMKIN® software package is used.

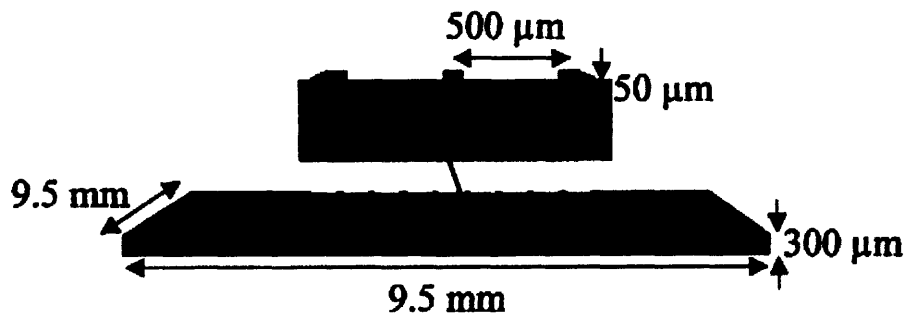

Figure 7.5 Geometry of Microreactor used for Experimental Conditions

Operating conditions for microreactor simulations are 5 bar total pressure, 0.124 s reactor residence time, 5 L/h gas flow and 3% C_2H_4, 16.5% O_2 and rest N_2 in the reactor feed. Temperature is varied from 420 to 660K. Given the inlet mole fractions in the microreactor, we predict the ethylene conversion at different temperatures (Figure 7.6a). Conversion increases

with temperature since more ethylene and oxygen reacts as the temperature increases. Variation of yield is studied for a broad range of temperature, since a non-monotonic response is expected in the yield. This is confirmed as shown in Figure 7.6b.

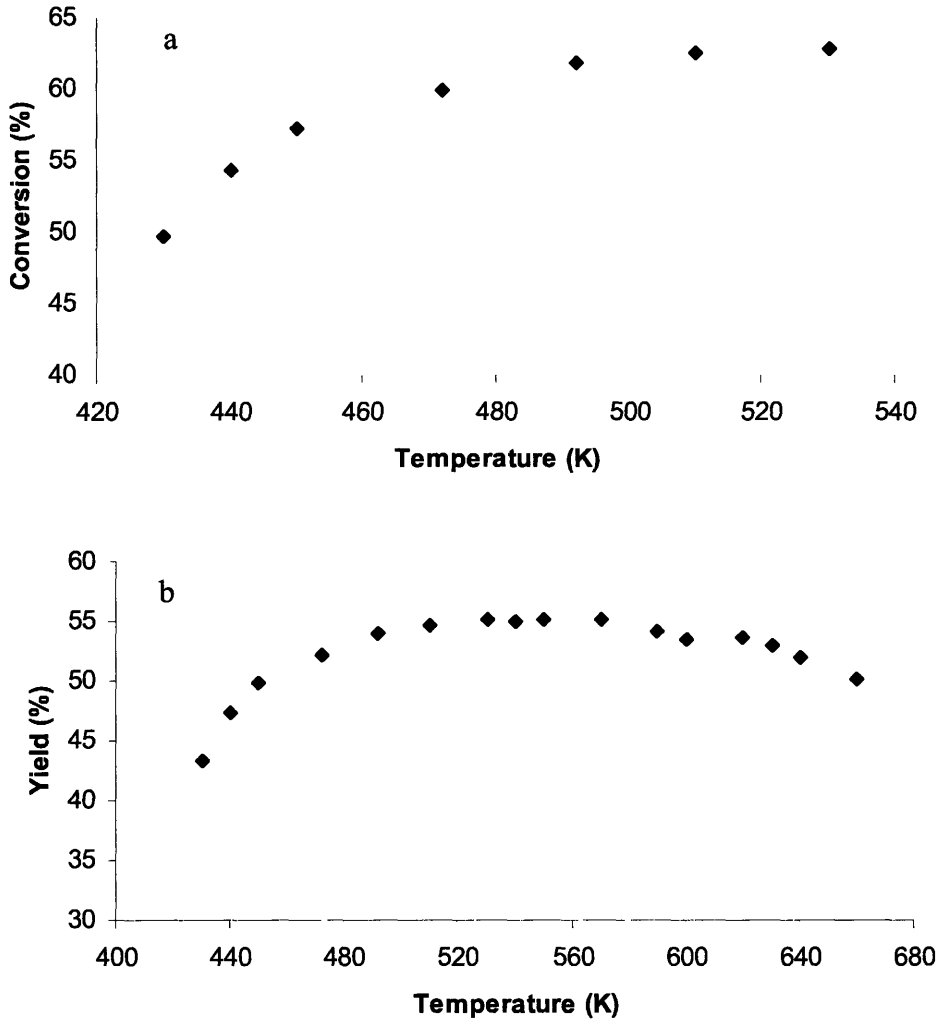

Figure 7.6 Variation of (a) Conversion and (b) Yield with Temperature

From Figure 7.6b, we observe that the yield peaks with temperature. Yield is a product of conversion and selectivity. Conversion increases while selectivity decreases with temperature. Selectivity decreases with temperature due to a small difference (~ 0.3 kcal/mol) in activation energies of the 2 forward reactions: one leading to epoxide and the other leading to acetaldehyde. Reverse reaction of epoxide becomes favorable as the temperature increases due to increase in conversion.

Our surface mechanism along with the transport model predicts a selectivity of 85%, while the selectivity measured from the experiment was 65% at 239 °C. Predictive selectivities are little off the values measured in experiments, nevertheless our model is completely predictive and none of the kinetic and transport parameters is adjusted to fit the experimental data. The comparison between the model and experiments and the agreement between them are significant, given the possibility of systematic errors and uncertainties in the measurement of concentrations at the reactor outlet.

We have simulated an industrial epoxidation reactor for the nominal operating conditions (see Table 7.2). The industrial reactor is usually of the shell and tube type comprising several thousand mild steel or stainless steel tubes, 20-50 mm inside diameter. Tube lengths are in the range 6-12 mm and the silver catalyst is in the form of 3-10 mm diameter particles [46]. Typical selectivity observed in ethylene oxide plants for unpromoted silver catalyst is in the range 75-80%.

Table 7.2 Nominal Plant Conditions for Ethylene Oxide Process

Pressure	25 atm
Temperature	500K
Residence Time	5 seconds
Mole Fractions	
Ethylene	0.25
Oxygen	0.25
Methane	0.50

Figure 7.7 shows the variation of selectivity with conversion for plant conditions.

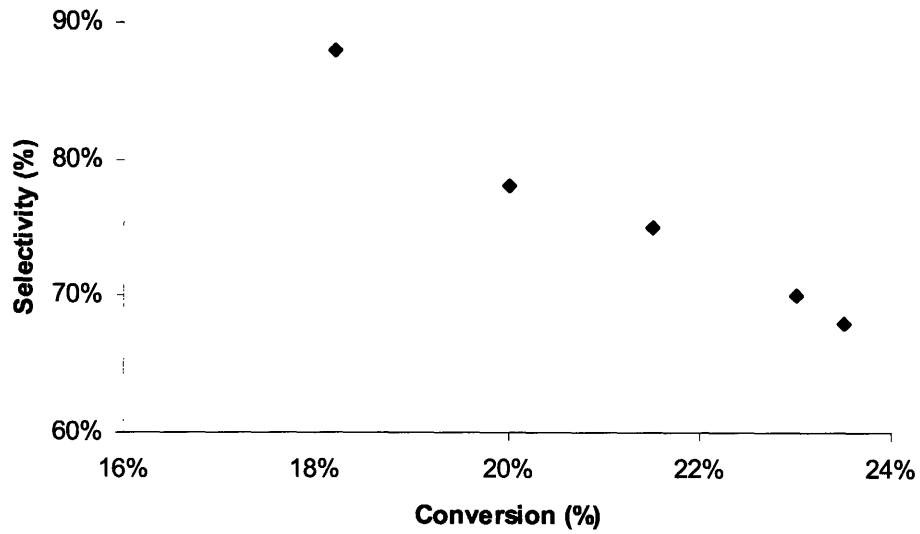

Figure 7.7 Variation of Selectivity with Conversion predicted for Plant Conditions

Figure 7.8 plots $\frac{P_{C2H4O,surface}}{K_{eq,4}}\frac{\theta_v}{\theta_{OMME}}$, the second term from Eq. 7.6, as a function of conversion.

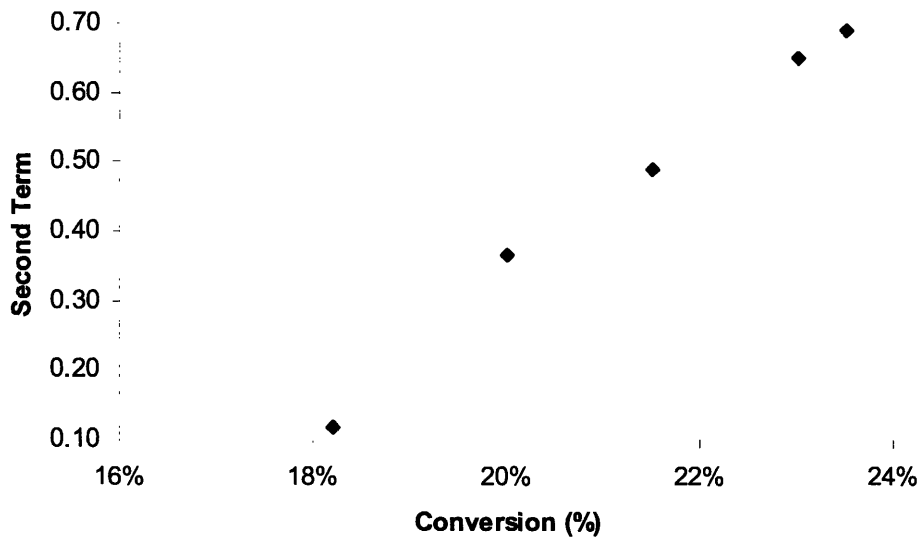

Figure 7.8 Variation of Second Term with Conversion for Plant Conditions

From Figure 7.8, we observe that second term signifying the reverse reaction of ethylene oxide changes significantly and becomes very large for plant conditions. Due to a higher inlet C_2H_4 pressure (6.25 bar), the total EO partial pressure stays at a higher value (0.50 bar) for the plant conditions relative to the microreactor conditions (0.13 bar). Based on the boundary layer calculations, the ethylene oxide partial pressure at the surface is 0.31 bar for plant conditions, while it is 0.09 bar for microreactor conditions. This results in significant reverse reaction of ethylene oxide to oxametallacycle, and the site fraction of OMME decreases since it is further consumed to form acetaldehyde under plant conditions. The $\frac{\theta_v}{\theta_{omme}}$ ratio for plant conditions is much higher than the ratio for microreactor conditions. Hence, the 2 factors, higher interfacial partial pressure of EO and higher ratio between site fractions of vacancy and oxametallacycle explain the early falloff in the selectivity-conversion curve for the plant conditions.

7.5 Effect of Heat of Formation of Oxametallacycle on Yield and Selectivity

Oxametallacycle is an important surface intermediate in the ethylene epoxidation reactions. Surface energetics and heat of formation of oxametallacycle affects the activation energies of 2 parallel reactions of oxametallacycle to form epoxide and acetaldehyde. Figure 7.9 is the reaction coordinate diagram showing activation energies (in kcal/mol) for the 2 reactions.

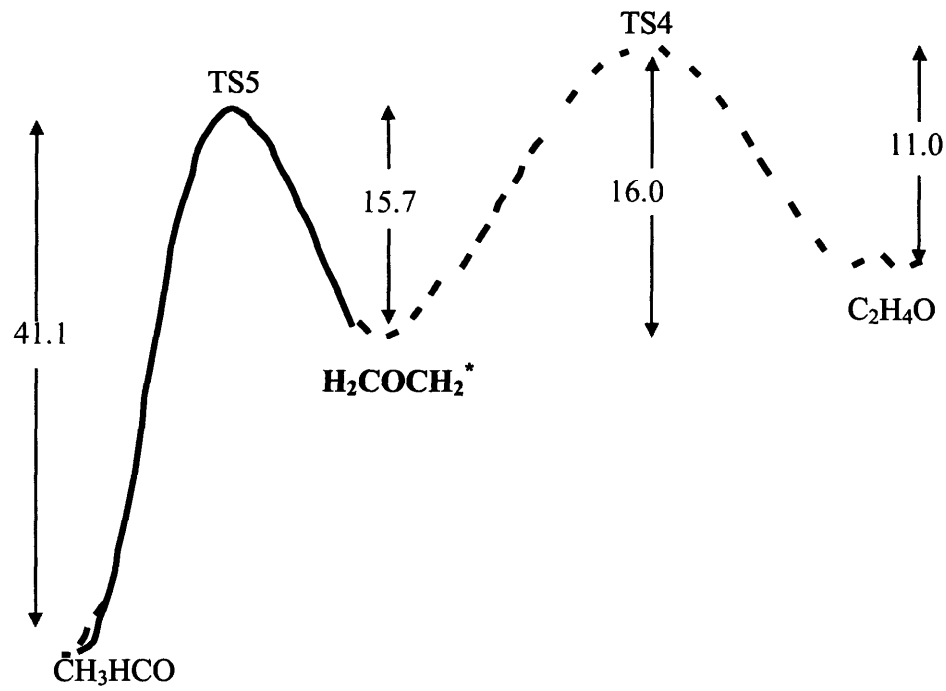

Figure 7.9 Reaction Coordinate Diagram for Oxametallacycle Reactions

Increasing the heat of formation of oxametallacycle decreases the activation energy of forward reaction leading to epoxide. Since this reaction is reversible, increase in the heat of formation of oxametallacycle shifts the ethylene oxide equilibrium towards the forward direction. Increase in the heat of formation of oxametallacycle also decreases the activation energy of the reaction leading to acetaldehyde, however this does not affect the acetaldehyde equilibrium since the reaction proceeds only in the forward direction. Overall, increase in the heat of formation of oxametallacyle is expected to increase the selectivity and yield of ethylene oxide process. Figure 7.10 shows the variation of predicted selectivity and yield with increase in heat of formation of oxametallacycle. Industrial plant conditions are used to simulate the selectivities.

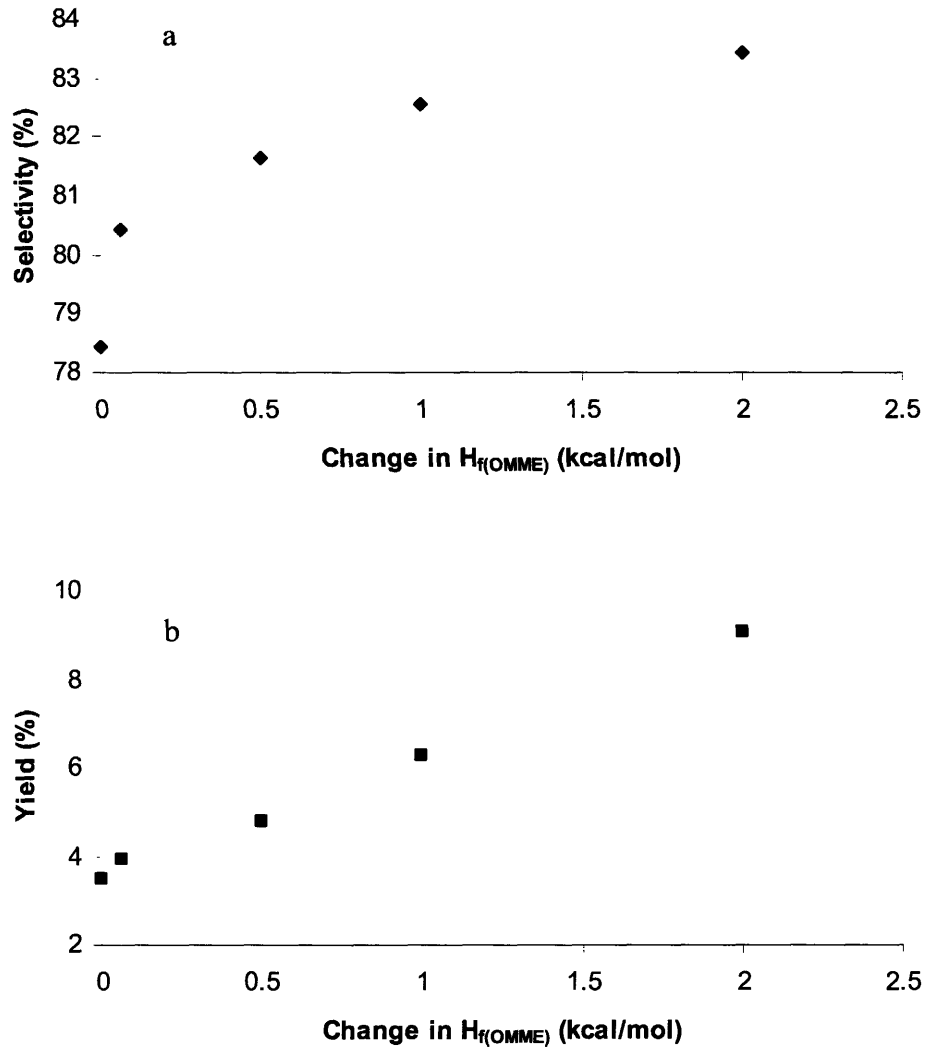

Figure 7.10 Effect of Heat of Formation of Oxametallacycle on (a) Selectivity and (b) Yield of Epoxide

From Figures 7.10a and 7.10b, we see that the selectivity and yield increases with the increase in the heat of formation of oxametallacyle. This not only signifies the sensitivity of oxametallacycle but also offers an insight into the role of promoters or trace metals in increasing the yield and selectivity of ethylene oxide. These compounds are expected to change the heat of formation of surface intermediates. And a small change in the heat of formation of

oxametallacyle is predicted to improve the yield and selectivity significantly as seen from Figure 7.10. Now an important question arises as to the direction of change in the heat of formation of oxametallacyle.

In oxametallacycle, the α-C and O atoms are bound to the silver catalyst. Since oxygen is a contact atom for both oxametallacycle and surface oxygen, adsorbate-surface interactions for the 2 surface species are expected to be similar. Surface oxygen is known to become less stable when trace amounts of chlorine in the form of 1,2-dichloroethane is added to the silver catalyst. Due to similar adsorbate-surface interactions, oxametallacyle is also expected to be less stable in the presence of chlorine. Hence, the heat of formation of oxametallacyle would increase in the presence of chlorine. This would offer a thermodynamic insight into the promoter effect of chlorine in ethylene epoxidation.

7.6 Sensitivity and Uncertainty Analysis

Preexponential factors and activation energies of the forward and reverse reactions are the kinetic parameters whose values may be uncertain. Some of the preexponential factors are reported from experimental data in the literature, while the rest are calculated using quantum chemistry methods. The coverage-dependent activation energies are based on chemisorption enthalpies of surface species, which are dependent on the enthalpies at zero coverages and the coverage coefficients of surface species. These values are obtained from experimental data in low-pressure studies. Due to possible uncertainties in experimental measurements as well as quantum chemistry calculations, we perform a first-order sensitivity analysis followed by a detailed uncertainty analysis to identify key preexponential factors, zero-coverage chemisorption enthalpies and coverage coefficients of surface species.

7.6.1 Sensitivity Analysis

Sensitivity analysis is performed by solving a set of adjoint differential equations corresponding to the sensitivity of species concentrations with respect to the parameters. From the 5-step mechanism, the rates of elementary reactions are expressed below:

$$r_1 = k_{f,1}[O_2]\theta_v^2 C_t^2 - k_{r,1}\theta_o^2 C_t^2, \tag{7.18}$$

$$r_2 = k_{f,2}[C_2H_4]\theta_v C_t - k_{r,2}\theta_{C2H4} C_t, \tag{7.19}$$

$$r_3 = k_{f,3}\theta_{C_2H_4}\theta_O C_t^2 - k_{r,3}\theta_{OMME}\theta_v C_t^2, \tag{7.20}$$

$$r_4 = k_{f,4}\theta_{OMME} C_t - k_{r,4}[C_2H_4O]\theta_v C_t, \tag{7.21}$$

and

$$r_5 = k_{f,5}\theta_{OMME} C_t - k_{r,5}[CH_3CHO]\theta_v C_t, \tag{7.22}$$

where k_f, k_r are the rate constants of forward and reverse reactions, θ the coverage of surface species and C_t the surface site density. The concentrations of gas phase species are expressed in mol/cm^3, while site density is expressed in mol/cm^2. Set of ODEs for the rates of production of gas and surface species is given below:

$$\frac{d[O_2]}{dt} = -r_1, \tag{7.23}$$

$$\frac{d[C_2H_4]}{dt} = -r_2, \tag{7.24}$$

$$\frac{d[C_2H_4O]}{dt} = r_4, \tag{7.25}$$

$$\frac{d[CH_3CHO]}{dt} = r_5, \tag{7.26}$$

$$\frac{d\theta_O}{dt} = (2r_1 - r_3)/C_t, \tag{7.27}$$

$$\frac{d\theta_{C_2H_4}}{dt} = (r_2 - r_3)/C_t, \tag{7.28}$$

$$\frac{d\theta_{OMME}}{dt} = (r_3 - r_4 - r_5)/C_t, \tag{7.29}$$

and

$$\frac{d\theta_v}{dt} = (-2r_1 - r_2 + r_3 + r_4 + r_5)/C_t. \tag{7.30}$$

Eqs. 7.23 through 7.30 can be represented as:

$$\frac{d\underline{y}}{dt} = \underline{f}(\underline{y}, \underline{p}, t), \tag{7.31}$$

where $\underline{y}$ is the vector of solution variables: $[O_2]$, $[C_2H_4]$, $[C_2H_4O]$, $[CH_3CHO]$, θ_O, θ_{C2H4}, θ_{OMME} and θ_v. $\underline{p}$ is the vector of parameters which include the preexponential factors, zero-coverage limit chemisorption enthalpies and coverage coefficients of surface species. The adjoint differential equations for sensitivity analysis can be derived as:

$$\frac{\partial}{\partial t}\left(\frac{\partial y_l}{\partial p_i}\right) = \frac{\partial f_l}{\partial y_l} \times \frac{\partial y_l}{\partial p_i} + \frac{\partial f_l}{\partial p_i}, \tag{7.32}$$

where y_l is the l^{th} solution variable, f_l is the rate of production of y_l, and p_i is the i^{th} parameter. The sensitivity of variable y_l with respect to parameter p_i is defined as: $\frac{\partial y_l}{\partial p_i}$. This is normalized with respect to the solution variable and parameter resulting in log-sensitivity: $\frac{\partial \ln y_l}{\partial \ln p_i} = \frac{p_i}{y_l}\frac{\partial y_l}{\partial p_i}$.

The set of differential equations (Eqs. 7.23 through 7.30) and the adjoint set corresponding to Eq. 7.32 for all the solution variables are simulated using MATLAB version 6.5. Figure 7.11 shows the logarithmic sensitivity of ethylene oxide concentration to the preexponential factors of the forward reactions in the 5-step surface mechanism. For Figure 7.11, the logarithmic sensitivity is $\frac{\partial \ln EO}{\partial \ln A_{f,i}} = \frac{A_{f,i}}{EO}\frac{\partial EO}{\partial A_{f,i}}$ for i^{th} reaction.

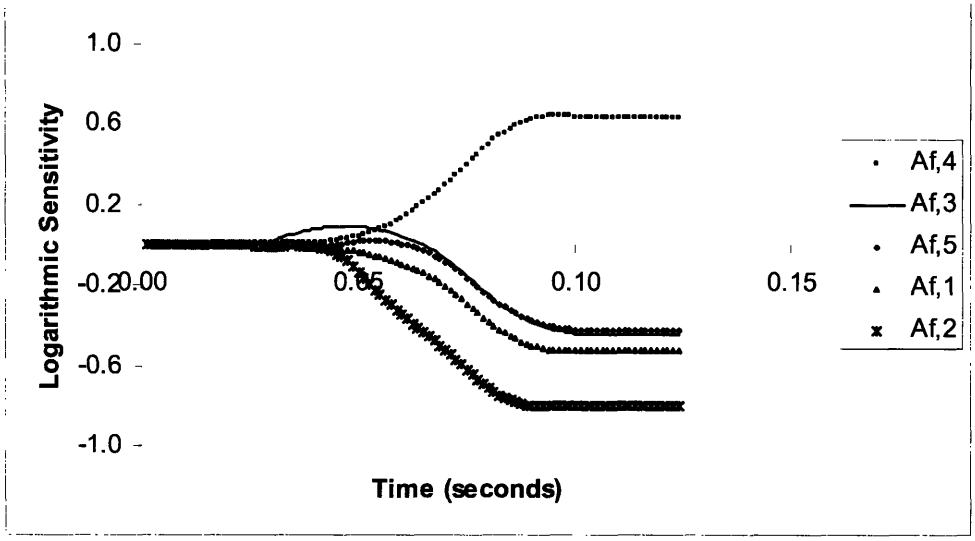

Figure 7.11 Logarithmic Sensitivity of EO Respect to A-factors of Forward Reactions

From Figure 7.11, we observe that the sensitivity of ethylene oxide concentration with respect to preexponential factor of the 4th forward reaction is positive, while those with respect to other preexponential factors are negative. Step 4 results in the formation of ethylene oxide from oxametallacycle. Increase in the rate of Step 4 increases the surface concentration of oxametallacycle and the gas concentration of ethylene oxide. Hence, an increase in the preexponential factor of the step results in an increase in the ethylene oxide concentration and consequently a positive sensitivity. Increasing the preexponential factor of Step 5 favors the branching of oxametallacycle towards acetaldehyde; hence, a negative sensitivity for ethylene oxide concentration. Steps 1 and 2 result in the adsorption of oxygen and ethylene, which react through Step 3 to form surface oxametallacycle. Thus, these 3 steps increase the conversion of oxametallacycle, and hence the partial pressure of epoxide at the surface. This in turn, increases the rate of reverse reaction of epoxide. Hence, sensitivities of ethylene oxide concentration with respect to the preexponential factors of forward reactions of the 3 steps are negative. Ethylene

oxide concentration is the most sensitive to preexponential factor of Step 2, next to that of Step 4.

Figure 7.12 shows the logarithmic sensitivity of ethylene oxide concentration to zero-coverage chemisorption enthalpies and coverage coefficients of surface species.

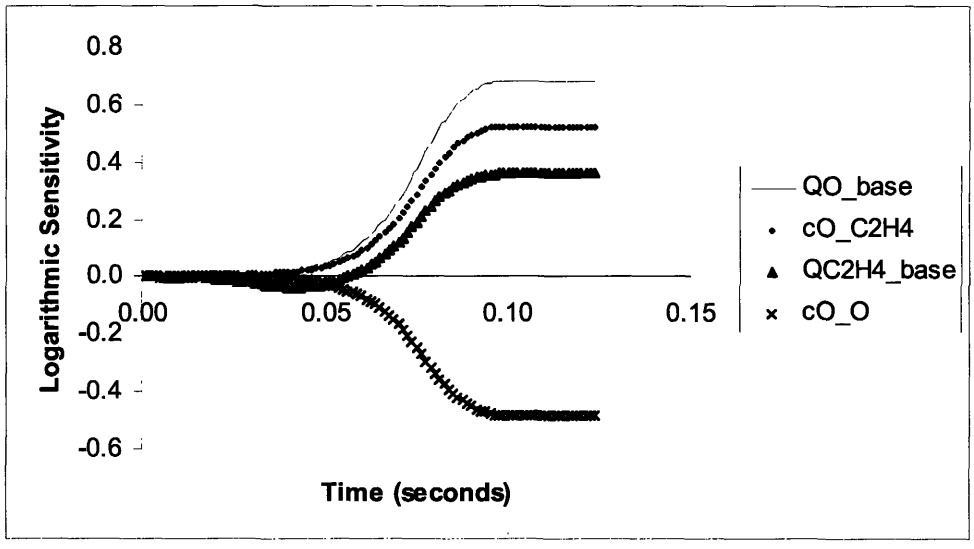

Figure 7.12 Logarithmic Sensitivity of EO Respect to Thermodynamic Parameters

The thermodynamic parameters considered are the zero-coverage limit heats of chemisorption of surface oxygen and ethylene (Q_{O_base} and Q_{C2H4_base}), and coverage-dependent coefficients for surface oxygen and ethylene (c_{O_C2H4} and c_{O_O}). From Figure 7.12, we observe that the sensitivities with respect to the coverage coefficient of oxygen on ethylene, chemisorption enthalpy of ethylene and oxygen are positive, while sensitivity with respect to coverage coefficient of oxygen on oxygen is negative.

Surface oxygen is stabilized in the presence of ethylene. Increasing chemisorption enthalpy of ethylene stabilizes surface ethylene, while chemisorption enthalpy of oxygen stabilizes surface oxygen. So, surface oxygen and ethylene are favored by increasing the coverage coefficient of oxygen on ethylene, chemisorption enthalpies of ethylene and oxygen.

This in turn favors the formation of oxametallacycle and its reaction to ethylene oxide. As a result, the log-sensitivity of ethylene oxide concentration with respect to the 3 parameters is positive. Surface oxygen reduces its own stability, as evident from the negative coefficient for the self-coverage dependence of oxygen. Hence, an increase in the coverage coefficient decreases the ethylene oxide concentration.

From Figures 7.11 and 7.12, we have identified the preexponential factors of forward reactions of Steps 2, 4, heat of chemisorption of oxygen at zero coverage, the coverage-dependent coefficient of oxygen on ethylene and coverage coefficient of oxygen on oxygen to be the main parameters affecting the sensitivities of ethylene oxide concentrations. In general, sensitivity analysis investigates the local effect of small changes in the kinetic and thermodynamic parameters on model outputs around nominal parameter points. More complete information on the effects of parameters can be obtained by performing uncertainty analysis, which takes into account the entire range and probability density function (PDF) of parameters to give the PDF and uncertainty in the ethylene oxide concentrations.

7.6.2 Uncertainty Analysis

To characterize the uncertainty in preexponential factors, chemisorption enthalpy and coverage coefficients, we use a uniform probability distribution function (PDF) with nominal parameter value being the mean, and upper and lower bounds differing from the nominal value. An uncertainty analysis method, Deterministic Equivalent Modeling Method (DEMM) developed by Tatang, has proven to be computationally more efficient than the existing sampling techniques such as Monte Carlo and Latin Hyper Cube sampling [47]. DEMM estimates the PDF of model outputs, given the PDF of parameters. Both parameters and outputs are expressed as random

variables, which are in turn represented by expansions of functionals of known PDFs. The functionals called polynomial chaos expansions (PCE) were introduced by Wiener to develop series expansion for random variables in a way analogous to traditional Fourier series representations [47]. The series expansions consist of orthogonal polynomials characteristic of the PDF of parameters. Parameter θ with a uniform PDF ~ U[a, b] can be represented by PCE as:

$$\theta = \theta_0 \times P_0(\xi) + \theta_1 \times P_1(\xi), \tag{7.33}$$

where ξ is a random variable with uniform PDF ~ U[0,1]. $P_0(\xi)$ and $P_1(\xi)$ are Legendre polynomials of order 0 and 1 respectively. Coefficients of the PCE, θ_0 and θ_1 are given by:

$$\theta_0 = a, \tag{7.34}$$

and

$$\theta_1 = b - a. \tag{7.35}$$

All uncertain parameters are expressed as PCEs of random variables with known coefficients. Output PCEs contain unknown coefficients, which are solved by minimization of mean-weighted residuals (MWR). Weights in MWR are chosen using orthogonal collocation for black box models; in these models, outputs are not explicitly expressed in terms of parameters. Coefficients of PCEs in the outputs characterize the uncertainty propagated through the model. In literature, DEMM has been applied to study the uncertainties propagated in several chemical engineering problems [47,49,50].

Based on sensitivity analysis, we select the preexponential factor of forward reactions of Steps 2 and 4 ($A_{f,2}$ and $A_{f,4}$), zero-coverage chemisorption enthalpy of oxygen (Q_{O_base}), coverage-coefficient of oxygen on ethylene (C_{O_C2H4}) and oxygen (C_{O_O}) as uncertain kinetic parameters; we analyze the uncertainties propagated in the ethylene oxide concentrations.

Nominal values of the preexponential factors are 2.1×10^{11} $cm^3/mol/s$ and 4.0×10^{13} /s. Nominal value of the zero-coverage chemisorption enthalpy is 84.0 kcal/mol, while those of coverage coefficients of oxygen on ethylene and oxygen are 3.6 and -35.7, respectively. Preexponential factors typically have errors within 100-1000% of the nominal value, while heats of chemisorption are accurate within 5 kcal/mol. To model the uncertainty in preexponential factors, we use uniform probability density function with nominal value as the mean value, lower and upper bounds being 1/10 and 10 times the nominal value, respectively. 5 kcal/mol is used as the standard deviation for the uniform distribution in chemisorption enthalpies and coverage coefficients. The parameters are expressed as first order PCEs of corresponding random variable with uniform distribution:

$$A_{f2} = A_{f2,0} \times P_0(\xi_1) + A_{f2,1} \times P_1(\xi_1), \tag{7.36}$$

$$A_{f4} = A_{f4,0} \times P_0(\xi_2) + A_{f4,1} \times P_1(\xi_2), \tag{7.37}$$

$$Q_{O\_base} = Q_{O\_base,0} \times P_0(\xi_6) + Q_{O\_base,1} \times P_1(\xi_6), \tag{7.38}$$

$$C_{O\_C2H4} = C_{O\_C2H4,0} \times P_0(\xi_7) + C_{O\_C2H4,1} \times P_1(\xi_7), \tag{7.39}$$

and

$$C_{O\_O} = C_{O\_O,0} \times P_0(\xi_8) + C_{O\_O,1} \times P_1(\xi_8), \tag{7.40}$$

where $P_0(\xi)$ (= 1) and $P_1(\xi)$ (= $\sqrt{\frac{3}{2}}\xi$) are the zeroth and first order orthonormal Legendre polynomials. Using nominal values of the parameters, we calculate the coefficients (Table 7.3) of two terms in the PCE for each of the 10 parameters.

Table 7.3 Coefficients of Polynomial Chaos Expansion

Parameter (Units)	Mean Value	θ_0	θ_1
A_{f2} ($cm^3/mol/s$)	2.1×10^{11}	2.1×10^{10}	2.08×10^{12}

A_{f4} (/s)	4.0×10^{13}	4.0×10^{12}	3.96×10^{14}
Q_{O_basc} (kcal/mol)	84.0	75.3	17.3
C_{O_C2H4} (kcal/mol)	3.6	-5.1	17.3
C_{O_O} (kcal/mol)	-35.7	-27.0	-17.3

To analyze the uncertainty propagated, we express the selectivity as PCEs of the 8 random variables:

$$S = S_0 + \sum_{i=1}^{8} S_i P_1(\xi_i). \tag{7.41}$$

From the above PCEs, we derive algebraic expressions for the mean, μ and standard deviation, σ of selectivity:

$$\mu_S = S_0, \tag{7.42}$$

and

$$\sigma_S = \sqrt{\frac{\sum_{i=1}^{8} S_i^2}{2}}. \tag{7.43}$$

The unknown coefficients in the PCEs are solved by minimization of mean-weighted residuals (MWR). Weights in MWR are chosen using orthogonal collocation. Collocation points are obtained by solving roots of the Legendre polynomial with an order one higher than that used for characterizing the uncertainty in the heats of chemisorption. In this case, we use roots of the third order Legendre polynomial: $P_3(\xi)$ $(= \sqrt{\frac{7}{2}}(\frac{5\xi^3 - 3\xi}{2}))$ to construct collocation points.

The solved coefficients of the PCE characterize the uncertainty propagated through the model. The mean and standard deviation (as error bar) of selectivity are plotted in Figure 7.13. Variance analysis explains the contributions of uncertainties in the parameters to uncertainty of predicted selectivities.

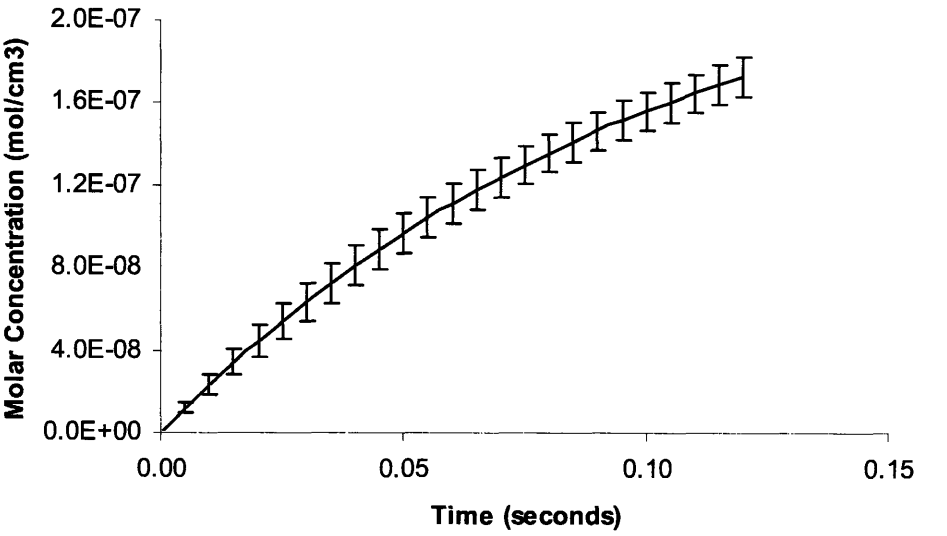

Figure 7.13 Mean and Standard Deviation of Ethylene Oxide Concentration with Reaction Time

Figures 7.14 & 7.15 show the contributions for the 2 forward preexponential factors, zero-coverage heat of chemisorption of oxygen and coverage coefficients. Uncertainty is plotted as standard deviation in molar concentration of ethylene oxide (in mol/cm^3).

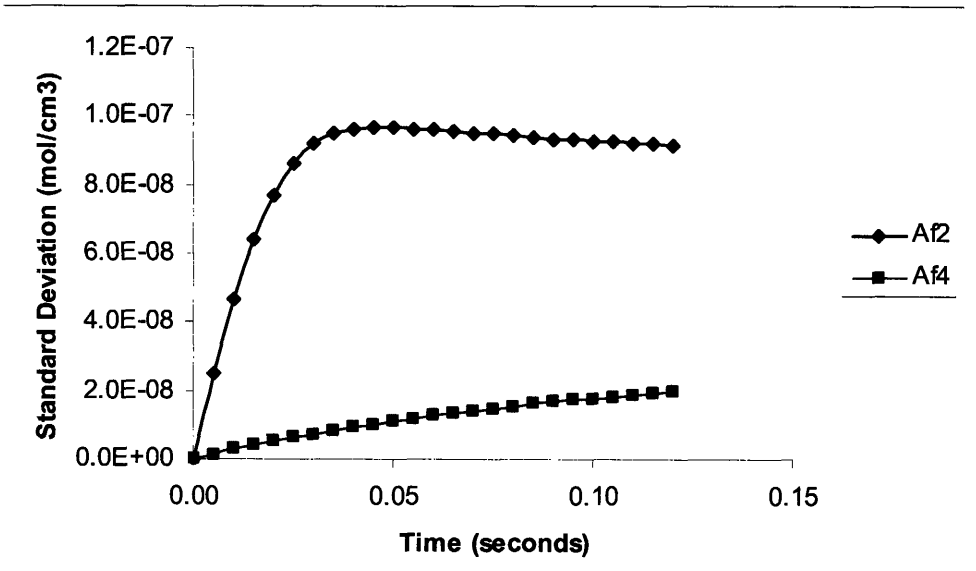

Figure 7.14 Uncertainty Contribution in the Forward A-factors of Reactions leading to Ethylene Adsorption and Epoxide Formation (Steps 2 and 4)

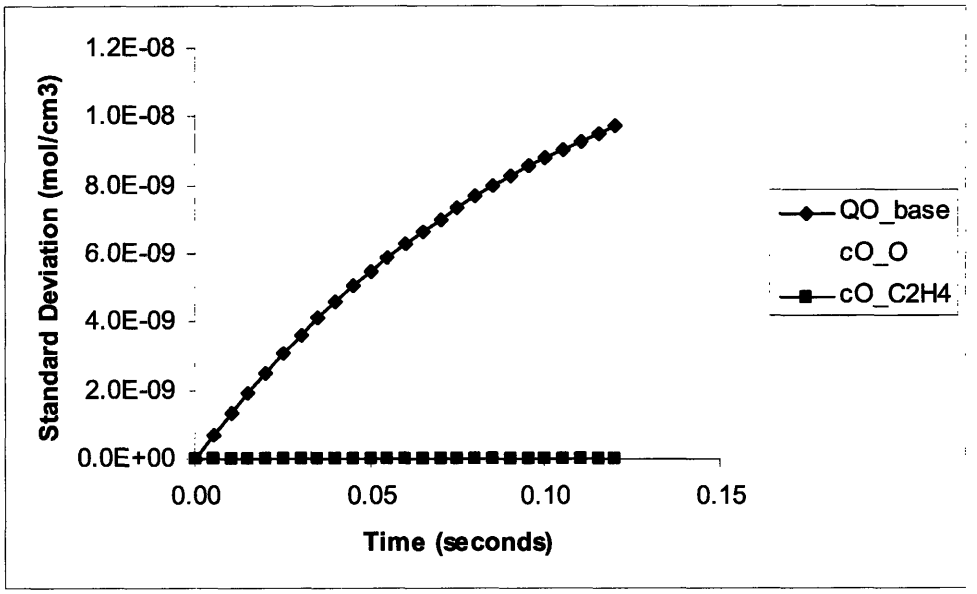

Figure 7.15 Uncertainty Contribution in Chemisorption Enthalpy of Oxygen, Coverage Coefficients of Oxygen and Ethylene

From Figures 7.14 & 7.15, we observe that the uncertainties due to preexponential factor of reaction of oxametallacycle leading to surface ethylene is the greatest; about an order-of-magnitude lower than the actual concentrations of epoxide predicted. Zero-coverage chemisorption enthalpy of oxygen (Q_{O_basc}) is the next important uncertain parameter followed by self-coverage coefficient of oxygen (C_{O_O}). The uncertainties in these 2 parameters increase with reaction time similar to a variation in ethylene oxide concentration.

7.7 Summary

Current research in surface mechanism for silver-catalyzed epoxidation of ethylene has motivated this chapter on explaining the selectivity to epoxide. We have contributed significantly in understanding the reversible equilibrium between oxametallacycle and epoxide, and the lower A-factor for acetaldehyde formation relative to epoxide formation to explain the observed EO selectivities for experimental conditions. Equilibrium between surface oxametallacycle and epoxide and comparable rates of forward and reverse reactions in the equilibrium suggests that reverse reaction affects selectivity. Equation for branching ratio which considers the reversible epoxide equilibrium and the ratio between site fractions of vacancy and oxametallacycle explain the decreasing selectivity with increasing conversion. Falloff in selectivity-conversion curve for the industrial plant reactors occurs earlier than the experimental microreactors. This is attributed to the kinetically significant reverse reaction of ethylene oxide to oxametallacycle for the plant conditions even at low conversions. For the experimental microreactor, the reverse reaction becomes important only at high conversions; until this point selectivity stays fairly constant since it is governed only by the 2 forward reactions of oxametallacycle. Rearrangement of C-H and C-O bonds in oxametallacycle and migration of H

from α- to β-carbon in oxametallacycle while forming acetaldehyde suggests a lower preexponential factor for the reaction. Density Functional Theory (DFT) predicts a preexponential factor of 4.22×10^{12} s^{-1}, which is an order-of-magnitude lower than the preexponential factor for reaction to epoxide (4.00×10^{13} s^{-1}). Our thermodynamically consistent surface mechanism includes coverage-dependent activation energies for dissociative adsorption of oxygen, ethylene and formation and branching of oxametallacycle to epoxide and acetaldehyde. Selectivities, conversions and yields predicted by the mechanism are validated against literature data for experimental and industrial epoxidation conditions. Increasing selectivities and yields with increase in heat of formation of oxametallacycle offers a thermodynamic and operational insight into the role of chlorine as a promoter in epoxidation. This work identifies surface atomic oxygen as the reactive form of oxygen in epoxidation and oxygen covered silver as active phase of silver catalyst.

References

1. M. C. J. Bradford and D. X. Fuentes (2002). A possible role for surface carbon during ethylene epoxidation over silver catalysts. *Catalysis Communications*, 3, 51-60.
2. G. S. Jones, M. Mavrikakis, M. A. Barteau and J. M. Vohs (1998). First synthesis, experimental and theoretical vibrational Spectra of an oxametallacycle on a metal surface. *Journal of American Chemical Society*, 120, 3196-3204.
3. S. Linic and M. A. Barteau (2002). Formation of a stable surface oxametallacycle that produces ethylene oxide, *Journal of American Chemical Society*, 124 (2), 310-315.
4. J. W. Medlin, M. Mavrikakis and M. A. Barteau (1999). Stabilities of substituted oxametallacycle intermediates: Implications of regioselectivity of epoxide ring opening and olefin epoxidation. *Journal of Physical Chemistry B*, 103, 11169-11175.
5. J. W. Medlin and M. A. Barteau (2001). The formation of epoxides from reactions of oxametallacylces on Ag(110): A density functional theory study. *Journal of Physical Chemistry B*, 105, 10054-10061.
6. S. Linic and M. A. Barteau (2003). Control of ethylene epoxidation selectivity by surface oxametallacycles. *Journal of American Chemical Society*, 125, 4034-4035.
7. J. W. Medlin, M. A. Barteau and J. M. Vohs (2000). Stabilities of substituted oxametallacycle intermediates: Implications of regioselectivity of epoxide ring opening and olefin epoxidation. *Journal of Molecular Catalysis A*, 163, 129-145.
8. R. A. van Santen and H. P. C. E. Kuipers (1987). The mechanism of ethylene epoxidation. *Advances in Catalysis*, 35, 265-321.
9. C. T. Campbell (1985). The selective epoxidation of ethylene catalyzed by Ag(111): A comparison with Ag(110). *Journal of Catalysis*, 94, 436-444.
10. C. T. Campbell (1986). Chlorine promoters in selective ethylene epoxidation over Ag(111): A comparison with Ag(110). *Journal of Catalysis*, 99, 28-38.
11. C. T. Campbell and M. T. Paffett (1984). The role of chlorine promoters in catalytic ethylene epoxidation over the Ag(110) surface. *Applications of Surface Science*, 19, 28-42.
12. C. T. Campbell and B. E. Koel (1985). Chlorine promotion of selective ethylene oxidation over Ag(110): Kinetics and mechanism. *Journal of Catalysis*, 92, 272-283.
13. R. M. Grant and R. M. Lambert (1985). A single crystal study of the silver-catalyzed selective oxidation and total oxidation of ethylene. *Journal of Catalysis,* 92, 364-375.
14. W. Li, C. Stampfl and M. Scheffler (2002). *Physical Review B*, 65, 1-19.
15. C. Backx, C. P. M. de Groot and P. Biloen (1981). Adsorption of oxygen on Ag(110) studied by high resolution ELS and TPD. *Surface Science*, 104, 300-317.
16. M. A. Barteau and R. J. Madix (1980). The adsorption of molecular oxygen species on Ag(110). 97, 101-110.
17. C. T. Campbell (1985). Atomic and molecular oxygen adsorption on Ag(111). *Surface Science,* 157 (1), 43-60.
18. C. T. Campbell and M .T. Paffett (1984). The interactions of O_2, CO, and CO_2 with Ag(110). *Surface Science*, 143, 517-535.
19. H. A. Engelhardt and D. Menzel (1976). Adsorption of oxygen on silver single crystal surfaces. *Surface Science*, 57, 591-618.
20. M. Bowker, P. Pudney and G. Roberts (1989). Oxygen adsorption on silver powder. 85, 2635-2640.

21. R. W. Joyner and M. W. Roberts (1979). A study of the adsorption of oxygen on silver at high pressure by electron spectroscopy. *Chemical Physical Letters*, 60, 459-462.
22. P. J. van den Hoenk, E. J. Baerends and R. A. van Santen (1989). Chemisorption and dissociation of O_2 on Ag(110). *Surface Science*, 221, L791-L799.
23. J. Pawela-Crew, R. J. Madix and J. Stohr (1995). The effect of subsurface oxygen on the orientation of molecular oxygen on Ag(110). *Surface Science*, 339, 23-28.
24. E. Shustorovich (1990). The Bond-Order conservation approach to chemisorption and heterogeneous catalysis: Applications and implications. *Advances in Catalysis*, 37, 101-163.
25. W. Li, C. Stampfl and M. Scheffler (2003). Why is a noble metal catalytically active? The role of the O-Ag interaction in the function of silver as an oxidation catalyst. Los Alamos National Laboratory, Preprint Archive, Condensed Matter, 1-4, arXiv:cond-mat/0305297.
26. W. Li, C. Stampfl and M. Scheffler (2003). Why is a noble metal catalytically active? The role of the O-Ag interaction in the function of silver as an oxidation catalyst. *Physical Review B*, 67, 1-16.
27. M. Todorova, W. X. Li, M. V. Ganduglia-Pirovano, C. Stampfl, K. Reuter and M. Scheffler (2002). Role of subsurface oxygen in oxide formation at transition metal surfaces. *Physical Review Letters*, 89, 1-4.
28. X. Bao, G. Lehmpfuhl, G. Weinberg, R. Schlogl and G. Ertl (1992). Variation of the morphology of silver surfaces by thermal and catalytic etching. *Journal of Chemical Society, Faraday Transactions*, 88, 865-872.
29. A. Nagy, G. Mestl, D. Herein, G. Weinberg, E. Kitzelmann and R. Schlogl (1999). The correlation of subsurface oxygen diffusion with variations of silver morphology in the silver-oxygen system. *Journal of Catalysis,* 182, 417-429.
30. M. Todorova, W. X. Li, M. V. Ganduglia-Pirovano, C. Stampfl, K. Reuter and M. Scheffler (2002). Role of subsurface oxygen in oxide formation at transition metal surfaces. *Physical Review Letters*, 89, 1-4.
31. X. Bao, M. Muhler, Th. Schedel-Niedrig and R. Schlogl (1996). Coadsorption of nitric oxide and oxygen on the Ag(110) surface. *Physical Review B*, 54, 2249-2262.
32. C. I. Carlisle, D.A. King, M. L. Bocquet, J. Cerda′ and P. Sautet (2000). Imaging the surface and the interface atoms of an oxide film on Ag{111} by scanning tunneling microscopy: experiment and theory. *Physical Review Letters*, 84, 3899-3902.
33. C. I. Carlisle, T. Fujimoto, W.S. Sim and D.A. King (2000). Atomic imaging of the transition between oxygen chemisorption and oxide film growth on Ag{1 1 1}. *Surface Science,* 470, 15-31.
34. B. Kruger and C. Benndorf (1986). Ethylene and ethylene-oxide adsorption on Ag(110). *Surface Science*, 178, 704-715.
35. T. E. Felter, W. H. Weinberg, P. A. Zhdan and G. K. Boresknov (1980). An XPS and UPS investigation of the adsorption of ethylene on the (111) surface of silver. *Surface Science,* 97, L313-L319.
36. A. E. Marcinowsky and J. M. Berty (1973). Ethylene adsorption on oxygenated silver. Evidence for two types of chemisorbed oxygen. *Journal of Catalysis*, 29, 494-499.
37. J. Mikami, S. Satoh and H. Kobayashi (1970). Studies on the catalytic oxidation of ethylene by means of the pulse technique. *Journal of Catalysis*, 18, 265-270.
38. A. D. Becke (1988). Density-functional exchange-energy approximation with correct asymptotic behavior. *Physical Review A: Atomic, Molecular, and Optical Physics*, 38, 3098-3100.

39. T. H. Dunning, Jr. and P. J. Hay (1976). Modern Theoretical Chemistry, Ed., H. F. Schaefer III, Plenum: New York. 1-28.
40. P. J. Hay and W. R. Wadt (1985). Ab initio effective core potentials for molecular calculations. Potentials for the transition metal atoms scandium to mercury. *Journal of Chemical Physics,* 82, 270-283.
41. W. R. Wadt and P. J. Hay (1985). Ab initio effective core potentials for molecular calculations. Potentials for main group elements sodium to bismuth. *Journal of Chemical Physics,* 82, 284-298.
42. P. J. Hay and W. R. Wadt (1985). Ab initio effective core potentials for molecular calculations. Potentials for potassium to gold including the outermost core orbitals. *Journal of Chemical Physics,* 82, 299-310.
43. S. Linic and M. A. Barteau (2003). Construction of a reaction coordinate and a microkinetic model for ethylene epoxidation on silver from DFT calculations and surface science experiments. *Journal of Catalysis*, 214, 200-212.
44. H. Brauer (1985). Transport Processes through the Interface of Particles, in H. J. Rehm and G. Reed (eds.), Biotechnology, Vol. 2, Fundamentals of Biochemical Engineering, Verlag Chemie, Weinheim.
45. H. Kestenbaum, A. Lange de Oliviera, W. Schmidt and F. Schuth (2002). Silver-catalyzed oxidation of ethylene to ethylene oxide in a microreaction system. Industrial Engineering and Chemistry Research, 41, 710-719.
46. B. K. Hodnett (2000). Heterogeneous Catalytic Oxidation: Fundamental and technological aspects of the selectivbe and total oxidation of organic compounds. John Wiley and Sons, West Sussex, England.
47. M. Tatang (1995). Direct incorporation of uncertainty in chemical and environmental engineering systems. Chemical Engineering; Massachusetts Institute of Technology.
48. N. Wiener (1938). The homogeneous chaos. American Journal of Mathematics, 60, 897-936.
49. B. K. Pun (1998). Treatment of uncertainties in atmospheric chemical systems: A combined modeling and experimental approach. Chemical Engineering, Massachusetts Institute of Technology.
50. C. Wang (1999). Parametric uncertainty analysis for complex engineering systems. Chemical Engineering, Massachusetts Institute of Technology: Cambridge.

Chapter 8: Development of an Extensive Ethylene Oxide Mechanism

This chapter presents the development of an extensive ethylene oxide (EO) reaction mechanism. In Section 8.2, we describe the methods available in literature for systematically generating mechanisms for gas phase reactions. In Section 8.3, we describe the Decomposition Tree Approach which uses an algorithm for generating mechanisms given an incomplete list of reactive species [1]. The approach uses domain knowledge to define different reaction possibilities, builds a decompostion tree to identify missing species, and systematically generates elementary reactions. In Section 8.4, we apply the Decomposition Tree Approach to generate an extensive EO mechanism. Starting with ethylene and oxygen as the reactants and the observed products: ethylene oxide, acetaldehyde, water, carbon dioxide and propene, we use the decomposition tree to find possible chemical routes. In Section 8.5, we compare selectivity and conversion predicted by the extensive EO mechanism against the predictions of other literature mechanisms.

8.1 Introduction

Many algorithms for automatic mechanism generation are developed in literature, primarily for homogeneous gas phase reaction systems. Typical in these approaches, sensitivity and rate-of-production analyses are used to screen unimportant reactions. Rate based species selection methodologies with information on the rates-of-formation of species are employed to identify

kinetically important reactions. Information from available lab-scale experiments and plant-scale reactors about observed products should also be used in the construction of reaction mechanism. In this work, we systematize the development of surface reaction mechanism by considering information from experiments and plant data. This approach is implemented for generating reactions in silver-catalyzed ethylene epoxidation.

8.2 Mechanism Generation

There is an extensive literature that describes methods for systematically generating mechanisms for gas phase reactions. Gasteiger et al. developed a program EROS [2], Blurock et al. set up a software system to manage, manipulate and generate reaction data [3], Glaude et al. developed a computer-aided design mechanism [4], and Warth et al. used advanced software based on referenced canonical treelike description of molecules [5]. Woo et al. established a quantitative link between measurable experimental changes and kinetics analysis to explain the behavior of styrene-based polymers in binary mixtures during pyrolysis [6]. The developed algorithms for automatic generation were based on graph theory [3,7-21]. Molecular species designated by graphs were identified by their vertices, with edges and subgraphs internal representations for a given class of reaction. Klinke et al. extended the tools of mechanism generation to handle heterogeneous Fischer-Tropsch synthesis on Ni(111) and Co(0001) surfaces [22]. Bounaceur applied a computer aided design of comprehensive primary and simplified secondary mechanisms in the case of alkanes pyrolysis by writing systematically all the generic reactions: initiations, isomerizations, decompositions by ß-scission, metatheses, additions and terminations [23]. Battin-Leclerc used EXGAS, the system for automatic generation of detailed mechanism in modeling ignition delays of butynes and generic reactions for the oxidation of alkenes [24].

Valdes-Perez applied artificial intelligence principles to the problem of inferring simple reaction mechanisms that were consistent with available experimental evidence. The interactive computer program MECHEM based on a combinatorial heuristic search, was applied to methane and alkane conversion chemistry [25]. An algorithm was introduced that can generate reaction-pathway hypotheses for computer-assisted elucidation. The algorithm used stoichiometry as a basis to construct reaction pathway and conjectures reaction intermediates, products and their molecular formulas. These conjectured species had a degree of plausibility when the algorithm was used systematically to search for the simplest pathways consistent with given experimental evidence [26].

Matheu et al. presented a fast, automated method for computing pressure dependence of rate constants on-the-fly during automated mechanism generation for a series of pressure-dependent reactions through cycloalkyl radical intermediates, including systems with over 90 isomers and 200 accessible product channels [27]. Grenda constructed automated computational mechanism-generation technique for methane pyrolysis following a detailed set of elementary reactions, estimated required reaction, and constructed a kinetic model which agreed well with experimental data for several species [28]. Matheu et al. predicted the observed autocatalysis and concentration profiles by employing pressure-dependent reactions generally and systematically during computerized mechanism construction with rate constants computed for chemically or thermally activated pressure-dependent reactions [29].

The above methods presented in literature generate surface mechanisms by predicting the rates of elementary surface reactions and screening unimportant reactions, species based on rates and sensitivity analysis. However, Decomposition Tree Approach developed by Achilles [1] was based on algorithm for hypothesizing mechanisms given an incomplete list of reactive species.

The algorithm provided alternative explanations of the observations of species, and served as a basis for hypothesizing species that may be missing from the original list. Using the observations as guideline for developing systematic algorithm, procedures for representing and ordering molecular structrures were presented to enable the automatic generation of missing species and possible reactions. Natural constraints on allowable combinations of possible reactions were translated into an integer programming formulation. By following the algorithm for solving integer program, all mechanistic hypotheses consistent with the constraints could be identified in the order of their complexity based on the implementation and physical nature of the process.

8.3 Summary of Achilles' Decomposition Tree Approach

This secion, an extended excerpt from Achilles' doctoral thesis [1], explains the decomposition tree approach with details on:

1. Matrix representation of molecules.
2. Matrix representation of bond breaking.
3. Decompostion Tree showing the hierarchy of species.
4. Classification of types of reactions.
5. Process of mechanism generation.

8.3.1 Representation of Molecules using Unique Connection Table

A compact, simple, umambiguous, and unique representation of the molecule is necessary to give complete information on its toplogy and geometric structure. Connection tables, a form of unambiguous representation, are matrices that explicitly represent the interconnections or bonds

among individual atoms. A list of codes is required for the elements and bond types. Multigraph or bond matrix is a connection table treating a molecule as set of balls (atoms) and sticks (bonds). It records the formal bond orders that exist between each atom. Connection tables can be compactly stored by computer due not only to upper triangle symmetry but also sparsity with few non-zero elements for large molecules. Connection tables could be conveniently converted to IUPAC notation to reference physical property databases, if needed to extract the heats of formation, entropies and heat capacities.

Leaving hydrogen atoms out of the connection tables and assuming all other atoms to have complete vacancies prevents the representation of reactive species with missing hydrogen species. Adding the hydrogen atom to a connection table, however, exacerbates the problem of establishing rules for choosing a unique ordering for species in a connection table. Typically, a unique connection table is formed from a diagram of the molecule with each atom numbered arbitrarily and the atom to atom bonds entered into the table.

Sorting algorithm is developed in the Decomposition Tree Approach for uniquely ordering the atoms in a connection table that depends only on the bond structure of molecule. An atom is ordered first by its element type (according to a user specified list), then by their calculated number, and finally by the ordering of the atoms connected to it. Bond number, a concept created for the sorting algorithm, is actually a set of numbers that represents the number of different types of bonds each atom has with other atoms. The highest priority bond types are placed first in a list of bond types, and one bond number is considered greater than another if it has a larger number of higher priority bond types. Atoms with the highest bond numbers are placed first in the connection table, and atoms with lower numbers are placed in decreasing order.

The element list places the carbon atoms first and the hydrogen atoms last. Next, the bond numbers for the carbon atoms are calculated. Typically, single and double bonds appear in the bond list. For example in acetaldehyde (CH_3CHO), the 2 C atoms have a set of six numbers in its bond indices that represent the number of carbon-carbon double bonds, carbon-carbon single bonds, carbon-hydrogen double bonds (always zero), carbon-hydrogen single bonds, carbon-oxygen single bonds, and carbon-oxygen double bonds, respectively. The carbons are completely ordered by the bond numbers, and rearrangement according to structural relationship begins. The hydrogen atom attached to C_2 is first placed in the H group, since C_2 is first in the hydrogen group. All the remaining hydrogens are sorted in a similar manner, and the final ordering is at the bottom of Figure 8.1.

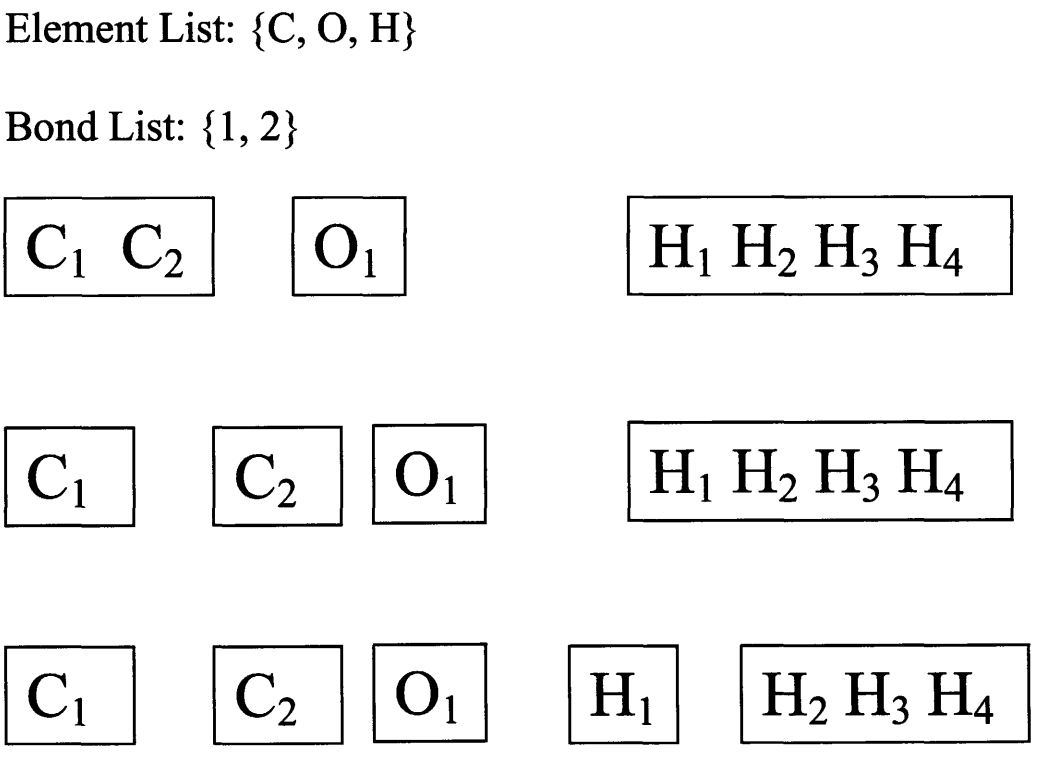

Figure 8.1 Trace of Sorting Algorithm for Acetaldehyde

Some groups contain more than one atom, when an atom is structurally indistinguishable from another, and it makes no difference what order they are placed in the connection table. As a result of implementing the ordering algorithm, molecules can be uniquely identified quickly. Additionally, atoms in a similar structural and chemical environment are grouped together, and structural symmetry is identified as well. If the connection table is to be used for physical property calculations for the original molecule, then the additional advantages are quite helpful. In Figure 8.1, the hydrogen atoms H_2, H_3 and H_4 are structurally indistinguishable from each other as indicated by their final grouping in the sorting algorithm.

8.3.2 Representation of Molecules after Breaking Bonds

Breaking bonds using a connection table representation is trivial. First, the bond to be broken is removed from the connection table. Second, an arbitrary atom is chosen and all of the atoms still connected to it make up one of the substructures' connection table. The remaining atoms obviously belong to the second substructure. Both connection tables are reordered using the sorting algorithm, and the process is complete. Figure 8.2 shows the tables before and after breaking the carbon-carbon single bond in acetaldehyde.

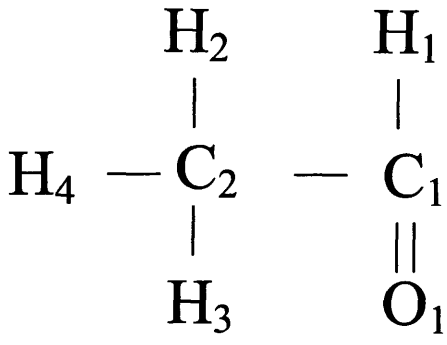

	C_1	C_2	O_1	H_1	H_2	H_3	H_4
C_1	1	1	2	1	0	0	0
C_2	1	1	0	0	1	1	1
O_1	2	0	3	0	0	0	0
H_1	1	0	0	7	0	0	0
H_2	0	1	0	0	7	0	0
H_3	0	1	0	0	0	7	0
H_4	0	1	0	0	0	0	7

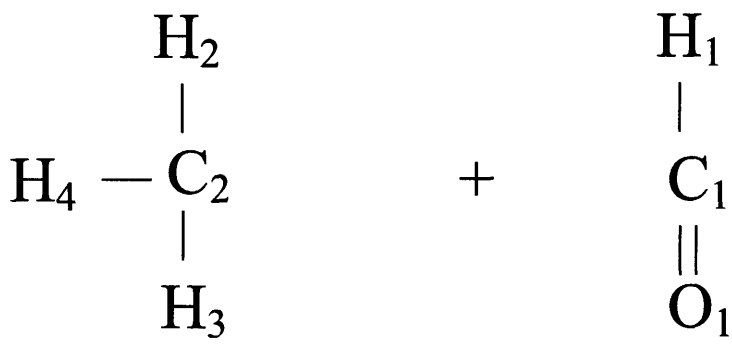

	C_2	H_2	H_3	H_4
C_2	1	1	1	1
H_2	1	7	0	0
H_3	1	0	7	0
H_4	1	0	0	7

	C_1	O_1	H_1
C_1	1	2	1
O_1	2	3	1
H_1	1	0	7

Figure 8.2 Connection Tables for Acetaldehyde and Two Molecules Formed after Breaking C-C Single Bond

8.3.3 Decomposition Tree Showing the Hierarchy of Species

A set of species is organized by their structural relationships, and the symbolic representation is similar to a directed graph or di-graph. Each molecule is a node, and the nodes are organized into levels by the number of elements in each molecule. The largest molecules are placed at the top-most level. An arc in a decomposition tree points from a large molecule to a smaller one indicating that the smaller molecule is a substructure of the larger one. Every arc must have a

partner so that the 2 smaller molecules are pointed to combine to form the larger one. If an arc does not have an explicit partner, then it is its own partner, which occurs when a molecule's structure can be split into 2 identical substructures. Figure 8.3 shows the algorithm for building a decomposition tree if the procedure begins with a partial list of species and their structures.

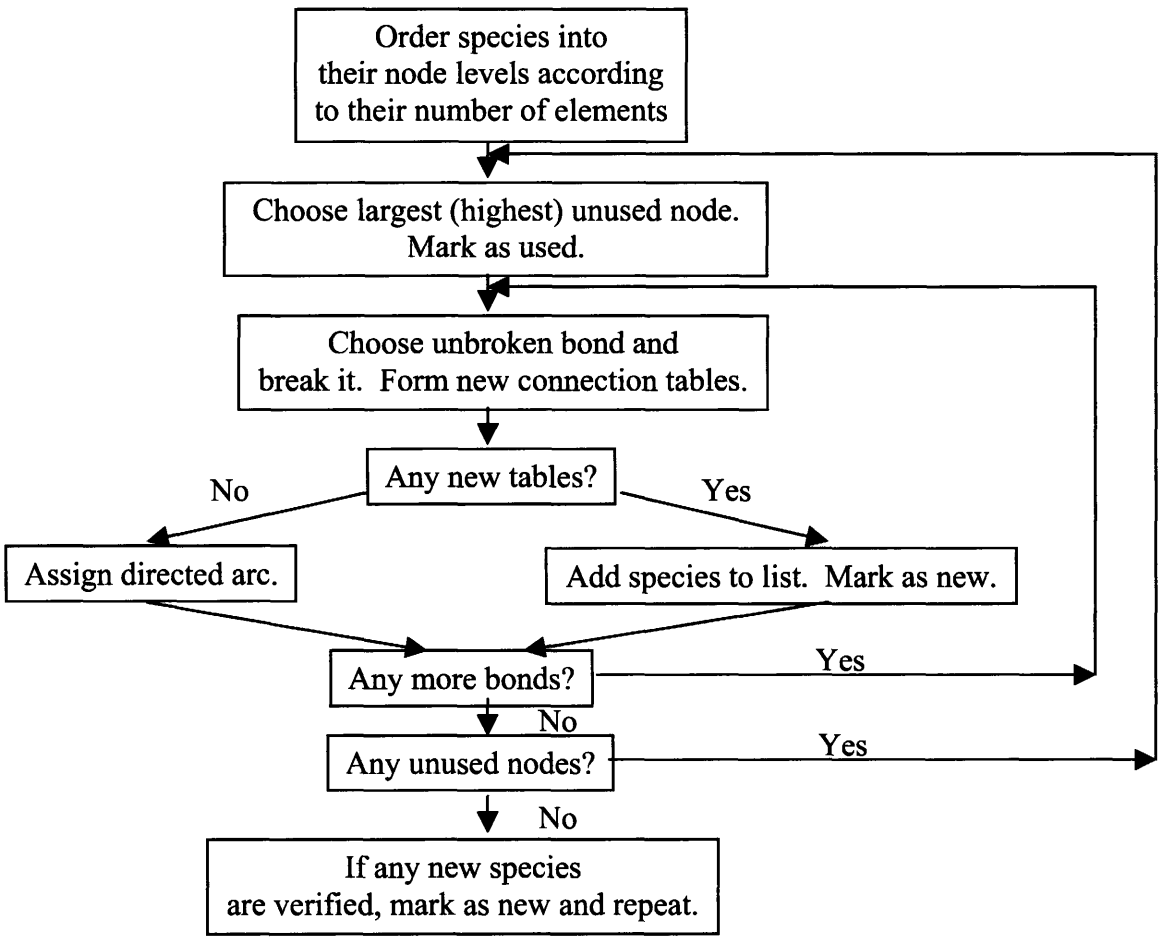

Figure 8.3 Algorithm for Building a Decomposition Tree [1]

There are 2 distinct phases that need to interact with experimental or theoretical verification of the existence of species: decomposing known species and hypothesizing new species. If a species arises from the breaking of a bond of a known species which is not in the original list, it is entered into the tree and directed arcs can point to, not from, the new species. If

a new species can physically exist and it is verified as participating in the reaction system being modeled, it is decomposed into substructures as well.

Species that participate in the reaction system and are known to have incomplete valencies (such as intermediates) are combined structurally with all other species to suggest additional missing species. As before, the new species is included in the tree and decomposed into substructures it can be verified. The success of this approach relies on knowing the structure for all of the species. In the case of a structurally unknown molecule, all the stoichiometric subsets of the molecule's molecular formula can be considered as possible species. This naturally leads to a large number of species, so every effort should be made to determine a molecule's structure before applying the Decomposition Tree Approach. The decomposition tree with the complete list of species is shown for the H_2-O_2 explosion reaction system, since this system is relatively small and not many species are generated from the base set of molecules: H_2 and O_2 as reactants and H_2O as product. Figure 8.4 shows the iterative construction of the decomposition tree for this reaction system.

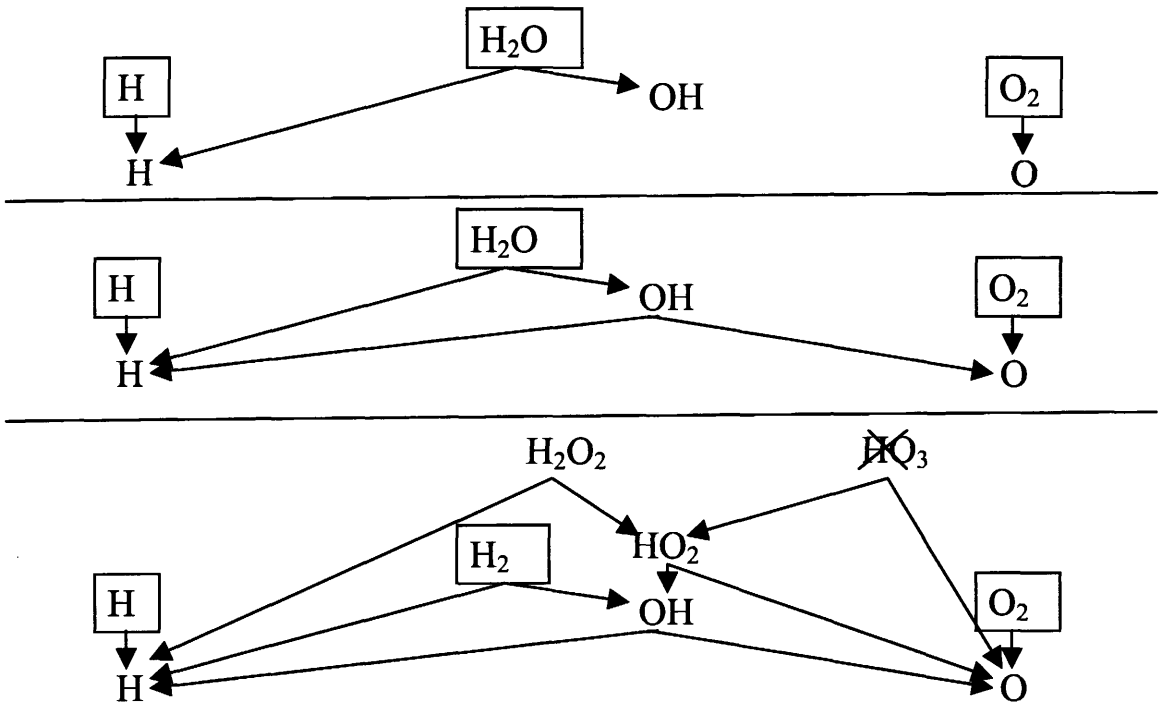

Figure 8.4 Iterative Construction of Decomposition Tree for H_2-O_2 System

8.3.4 Classification of Types of Reactions

The Decomposition Tree Approach defines an elementary reaction as a structural change of a molecule or molecules in which one chemical bond is broken and/or formed. Table 8.1 lists the four classes of elementary reactions which represent the changes that can take place with the breaking and/or formation of one chemical bond.

Table 8.1 Four classes of Elementary Reactions

Reaction Type	Number	Reaction Scheme
Isomerization	1	A ⇔A*
Decomposition	2	AB ⇔ A+B
Addition	3	A + B ⇔ AB
Exchange	4	AB + C ⇔ AC + B

8.3.5 Process of Mechanism Generation

The decomposition tree which consists of reactants and products relates reactive species to each other by their structure, and defines the complete list of possible reactions. Table 8.2 lists the 4 classes of reactions generated for the H_2-O_2 reaction system.

Table 8.2 Elementary Surface Reactions for H_2-O_2 Explosion Reaction System

Reaction Type	Number	Reaction
Decomposition/ Addition	1	$H_2 \Leftrightarrow H + H$
	2	$O_2 \Leftrightarrow O + O$
	3	$H_2O \Leftrightarrow H + OH$
	4	$H + O \Leftrightarrow OH$
	5	$H + O_2 \Leftrightarrow HO_2$
	6	$H + HO_2 \Leftrightarrow H_2O_2$
	7	$O + OH \Leftrightarrow HO_2$
	8	$OH + OH \Leftrightarrow H_2O_2$
Exchange	9	$OH + O \Leftrightarrow O_2 + H$
	10	$OH + H \Leftrightarrow H_2 + O$
	11	$OH + HO_2 \Leftrightarrow H_2O + O_2$
	12	$OH + OH \Leftrightarrow H_2O + O$
	13	$OH + OH \Leftrightarrow HO_2 + H$
	14	$OH + H_2O \Leftrightarrow H_2O_2 + H$
	15	$OH + H_2O_2 \Leftrightarrow H_2O + HO_2$
	16	$H_2 + HO_2 \Leftrightarrow H + H_2O_2$
	17	$2\ HO_2 \Leftrightarrow O_2 + H_2O_2$
	18	$H_2O + O \Leftrightarrow H + HO_2$
	19	$H_2O + H \Leftrightarrow H_2 + OH$
	20	$HO_2 + H \Leftrightarrow H_2 + O_2$
	21	$HO_2 + O \Leftrightarrow OH + O_2$
	22	$HO_2 + OH \Leftrightarrow H_2O_2 + O$

The elementary mechanism shown in Table 8.2 includes more reactions than the kietic mechanism predicted by Li et al [30]. Three reactions (Reactions 7, 8 and 18) from Table 8.2 are missing in the mechanism published by Li et al.

8.3.6 Screening Criteria

Since the goal of Decomposition Tree Approach is to generate reaction mechanisms for systems with many species, the main concern is controlling growth in the number of reactions and number of species. To include or eliminate surface species and reactions from the mechanism, screening criteria should be chosen based on:

1. Experimental knowledge showing the presence of species.
2. Thermodynamic principles underlying the stability of chemical species.
3. Kinetic rate rules indicating the reactivity of species.

Chemical species observed in experimental and industrial reactors should be included in the mechanism under appropriate reaction conditions. Species generated using the Decomposition Tree Approach not reported in literature, are screened based on thermodynamic principles.

As a thermodynamic screening criterion, species with heats of chemisorption less than a cutoff vale are excluded from the mechanism. The criterion assumes that species with heats of chemisorption above the cutoff value are considered thermodynamically stable under the reaction conditions. Ofcourse, the number of species in a reaction mechanism decreases with cutoff value, and adequate care should be taken to include all the important species in the mechanism.

In addition to thermodynamic screening, rate-based algorithm can be used to identify important reactions that produce and consume species. This prevents some species from accumulating in the mechanism, since additional reactions that consume the species are identified.

8.4 Decomposition Tree Approach for Ethylene Oxide Mechanism

8.4.1 Knowledge of Species from Experimental and Industrial Reactors

Ethylene and oxygen are the reactants and ethylene oxide is the desirable product in silver-catalyzed epoxidation of ethylene. Besides ethylene oxide, acetaldehyde, water, carbon dioxide and propene are generally the products observed in experimental and industrial epoxidation reactors. Surface oxamatellacycles were observed during the reaction between adsorbed ethylene and oxygen [31]. Acetate intermediates were detected when acetaldehyde was fed over oxygen-dosed Ag(110) [32]. Stuve and Madix studied the adsorption and reaction of water on clean and oxygen-covered Ag(110) surfaces using high resolution electron energy loss spectroscopy (EELS), temperature programmed desorption (TPD), and X-ray photoelectron (XPS) spectroscopy [33]. Reaction of adsorbed H_2O with pre-adsorbed oxygen to produce adsorbed hydroxyl groups was observed by EELS in the temperature range 205 to 255K. The hydroxyl groups recombined at 320K to yield both a TPD water peak at 320K and adsorbed atomic oxygen. Formation and decomposition of silver acetates is a possible route for the formation of CO_2. Surface hydroxyl species are key sources for the formation of water on silver catalyst.

8.4.2 Decomposition Tree for Ethylene Oxide Mechanism

Figure 8.5 shows the decomposition tree for the C_2H_4-O_2-Ag (EO) reaction system. Starting with 6 species: C_2H_4, O_2 and Ag as reactants, C_2H_4O and CH_3CHO as products, and $H_2COCH_2(S)$ as surface intermediate, first application of the tree building algorithm suggests including 12 new species: O, H, CH_2, HCO, H_2CO, CH_3, $HCCH_2$, $OCH_2(S)$, $HC(O)CH_2$, H_2CCHO, H_3CCO, H_3CCH, $HCOCH_2(S)$, $H_2COCH(S)$. Some of the new species are known to

occur and participate in the epoxidation chemistry, so they are added to the tree. While rest of these species included in the tree are evaluated based on a thermodynamic screening criteria (Section 8.4.6).

The algorithm for decomposition tree is applied multiple times for the additional set of species generated. Several new directed arcs are drawn and new species are identified. The decomposition tree method forces experimental evidence to limit the number of species that exist in the reaction system, and prevents the infinite chain of generated molecules.

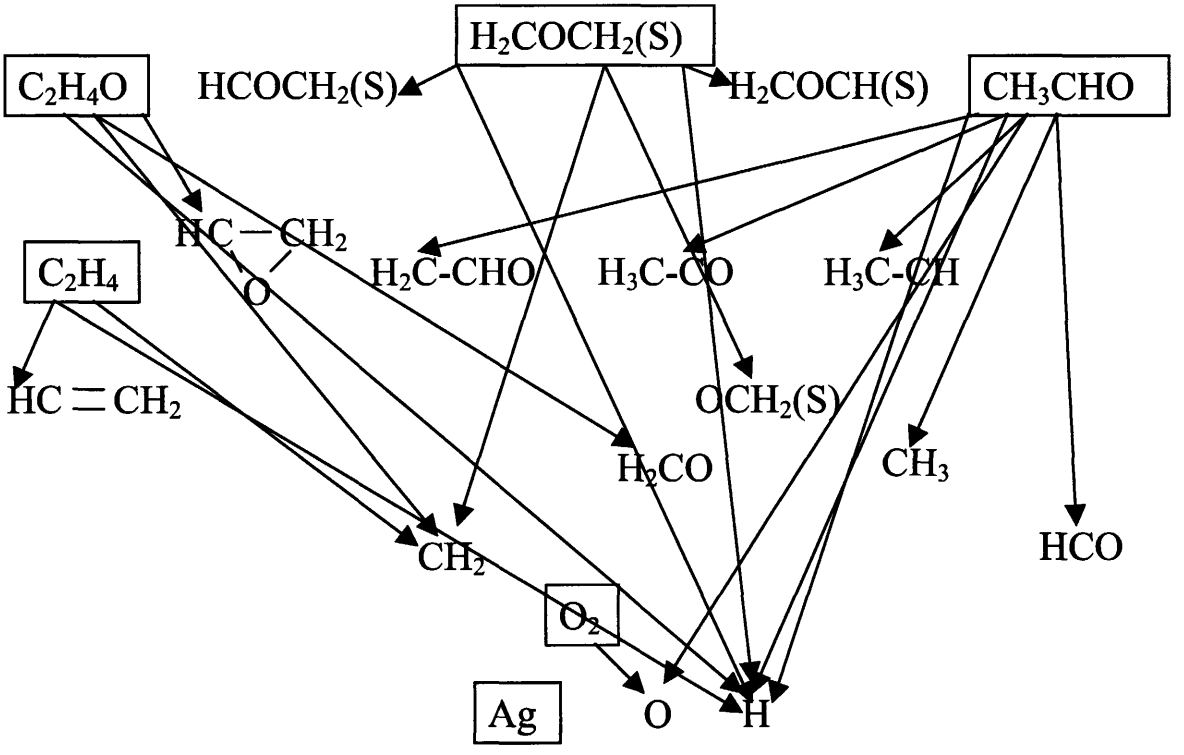

Figure 8.5 First Application of Decomposition Tree for C_2H_4-O-Ag Reaction System [1]

8.4.3 Subset of Generated Molecules in Ethylene Oxide Mechanism

Tables 8.3 through 8.7 list the subset of molecules generated from the 6 reactants, products and intermediates based on bond connectivities among the atoms in each molecule. In the subset, molecules are arranged in the decreasing order of number of atoms. Table 8.5 lists the molecules generated from C_2H_4O, which is a cyclic compound. Some of the generated compounds are cyclic, so they are indicated by the word "cyclic." Structures of some generated molecules in Table 8.5 are explained here for clarity. H_2C-CH_2-O has the O attached to only one of the C's. This is the ring opened structure of epoxide containing all the 7 atoms. Cyclic (HC-O-CH_2) has the cyclic C-O-C ring, with one H attached to a C and two H's attached to the second C. O-CH-CH_2 has the O single bonded to a C which is attached to one H. HC-CH_2-O has the O single bonded to the C which is attached to two H's. Cyclic (C-O-CH_2) has the C-O-C ring with the 2 H's attached to one of the C's. Cyclic (HC-O-CH) has the ring with one H attached to each of the 2 C's. O-CH-CH has the O single bonded to one of the C's. C-CH_2-O has the O single bonded to C which is attached to 2 H's. H_2C-O has the O single bonded to C. (C-O-CH) has the cyclic C-O-C ring with H attached to one of the C's. H_2C-O has the O single bonded to C. O-CH-C has the O single bonded to C attached to 1 H. Cyclic (C-O-C) has the C-O-C ring. Table 8.6 lists the molecules generated from CH_3CHO. In the table, H_2C-CHO, H_3C-CO, HC-CHO, H_2C-CO, HC-CO, C-CHO, HCO, C-CO, CO have C=O double bonds. Table 8.7 lists the molecules generated from surface oxametallacycle. HC-CH_2-Ag(O) has both O and Ag single bonded to C attached to 2 H's. H_2C-CH-Ag(O) has both O and Ag single bonded to C attached to 1 H. C-CH_2-O(Ag) has both O and Ag single bonded to C attached to 2 H's. HC-CH-O(Ag) has both O and Ag single bonded to C attached to 1 H. H_2C-C-O(Ag) has both O and Ag single bonded to C that is not attached to any H. H_2C-O(Ag) has both O and Ag single bonded to C. C-CH-O(Ag)

has O and Ag atoms single bonded to C attached to 1 H. HC-C-O(Ag) has O and Ag single bonded to C which is not attached to any H. HC-O(Ag) has O and Ag attached to C. C-C-O(Ag) has both O and Ag attached to one of the 2 C's.

Table 8.3 Subset of Molecules Generated from C_2H_4

Number of Atoms	Species
5	$CH{=}CH_2$
4	$H_2C{=}C$
	H-C=C-H
3	H-C-H
	C=C-H
2	C-H
	C=C
1	H
	C

Table 8.4 Subset of Molecules Generated from O_2

Number of Atoms	Species
1	O

Table 8.5 Subset of Molecules Generated from C_2H_4O

Number of Atoms	Species
7	H_2C-CH_2-O
6	cyclic (HC-O-CH_2)
	O-CH-CH_2
	HC-CH_2-O
	H_2C-CH_2
5	cyclic (C-O-CH_2)
	cyclic (HC-O-CH)
	HC-CH_2
	O-C-CH_2
	O-CH-CH
	C-CH_2-O
4	H_2C-O
	C-CH_2
	cyclic (C-O-CH)
	HC-CH
	O-C-CH
	O-CH-C
3	HC-O
	HCH
	C-CH
	cyclic (C-O-C)
	C-C-O
2	CH
	C-O
	C-C
1	H
	C
	O

Table 8.6 Subset of Molecules Generated from CH_3CHO

Number of Atoms	Species
6	H_2C-CHO
	H_3C-CO
	H_3C-CH
5	HC-CHO
	H_2C-CO
	H_2C-CH
	H_3C-C
4	CH_3
	C-CH_2

	HC-CO
	C-CHO
3	CH_2
	HCO
	C-CO
	C-CH
2	CO
	CH
	C-C
1	C
	H
	O

Table 8.7 Subset of Molecules Generated from $H_2COCH_2(S)$

Number of Atoms	Species
8	$H_2C\text{-}CH_2\text{-}O\text{-}Ag$
	$H_2C\text{-}CH_2\text{-}Ag\text{-}O$
7	$HCOCH_2(S)$
	$H_2COCH(S)$
	$H_2C\text{-}CH_2(O)$
	$H_2C\text{-}CH_2\text{-}O$
	$HC\text{-}CH_2\text{-}Ag(O)$
	$H_2C\text{-}CH\text{-}O\text{-}Ag$
	$H_2C\text{-}CH\text{-}Ag(O)$
	$H_2C\text{-}CH\text{-}Ag\text{-}O$
	$HC\text{-}CH_2\text{-}O\text{-}Ag$
6	$HCOCH(S)$
	$H_2COC(S)$
	$COCH_2(S)$
	$HC\text{-}CH_2\text{-}O$
	$H_2C\text{-}CH\text{-}O$
	$C\text{-}CH_2\text{-}O(Ag)$
	$C\text{-}CH_2\text{-}O\text{-}Ag$
	$HC\text{-}CH\text{-}O(Ag)$
	$HC\text{-}CH_2\text{-}Ag$
	$H_2C\text{-}C\text{-}O(Ag)$
	$H_2C\text{-}CH\text{-}Ag$
	$HC\text{-}CH\text{-}O\text{-}Ag$
	$H_2C\text{-}C\text{-}O\text{-}Ag$
	$C\text{-}CH_2\text{-}Ag\text{-}O$
	$H_2C\text{-}C\text{-}Ag\text{-}O$
	$HC\text{-}CH\text{-}Ag\text{-}O$
5	$OCH_2(S)$
	$H_2C\text{-}O\text{-}Ag$
	$H_2C\text{-}O(Ag)$
	$HC\text{-}CH\text{-}Ag$
	$H_2C\text{-}CH$
	$H_2C\text{-}C\text{-}Ag$
	$H_2C\text{-}Ag\text{-}O$
	$COCH(S)$
	$HCOC(S)$
	$HC\text{-}CH\text{-}O$
	$C\text{-}CH_2\text{-}O$
	$H_2C\text{-}C\text{-}O$
	$C\text{-}CH\text{-}O(Ag)$
	$C\text{-}CH_2\text{-}Ag$
	$C\text{-}CH\text{-}O\text{-}Ag$
	$HC\text{-}C\text{-}O(Ag)$
	$C\text{-}CH\text{-}O\text{-}Ag$
	$HC\text{-}C\text{-}O\text{-}Ag$
	$C\text{-}CH\text{-}Ag\text{-}O$
	$HC\text{-}C\text{-}Ag\text{-}O$
4	$OCH(S)$
	$HC\text{-}O(Ag)$
	$H_2C\text{-}O$
	$H_2C\text{-}Ag$
	$HC\text{-}O\text{-}Ag$
	$HC\text{-}Ag\text{-}O$

Note that species like H_2O, OH and HO_2 are not listed in Tables 8.3 through 8.7 since they are not formed when any bond breaks in the 6 reactants, products and intermediate. However, they are produced when small molecules/atoms like H, O, H_2 and O_2 combine to form a larger molecule. So, they are eventually included after addition reactions are generated in the ethylene oxide mechanism.

8.4.4 Generation of Reactions

Starting with the subset of molecules listed in Tables 8.3 through 8.7, elementary surface reactions that fit into the 4 reaction classes are identified and they are listed in Table 8.8. New molecules due to the reactions are added to the existing set of molecules which are presented in Tables 8.3 through 8.7.

Table 8.8 Elementary Surface Reactions for Ethylene Epoxidation System

Reaction Type	Number	Reaction
Isomerization	1	$H_2COCH_2(S) \Leftrightarrow C_2H_4O(S)$
	2	$H_2COCH_2(S) \Leftrightarrow CH_3CHO(S)$
	3	$HCOCH_2(S) \Leftrightarrow H_2COCH(S)$
	4	$HCOCH_2(S) \Leftrightarrow HC\text{-}CH_2\text{-}O\text{-}Ag$
	5	$HCOCH_2(S) \Leftrightarrow HC\text{-}CH_2\text{-}Ag\text{-}O$
	6	$H_2COCH(S) \Leftrightarrow H_2C\text{-}CH\text{-}O\text{-}Ag$
	7	$H_2COCH(S) \Leftrightarrow H_2C\text{-}CH\text{-}Ag\text{-}O$
	8	$HC\text{-}CH_2\text{-}Ag(O) \Leftrightarrow H_2C\text{-}CH\text{-}Ag(O)$
	9	$HC\text{-}CH_2\text{-}Ag(O) \Leftrightarrow H_3C\text{-}C\text{-}Ag(O)$
	10	$H_2C\text{-}CH\text{-}O\text{-}Ag \Leftrightarrow H_3C\text{-}C\text{-}O\text{-}Ag$
	11	$H_2C\text{-}CH\text{-}O\text{-}Ag \Leftrightarrow HC\text{-}CH_2\text{-}O\text{-}Ag$
	12	$H_2C\text{-}CH\text{-}O\text{-}Ag \Leftrightarrow H_2C\text{-}CH\text{-}O(Ag)$
	13	$H_2C\text{-}CH\text{-}O\text{-}Ag \Leftrightarrow H_2C\text{-}CH\text{-}Ag(O)$
	14	$H_2C\text{-}CH\text{-}Ag(O) \Leftrightarrow H_3C\text{-}C\text{-}Ag(O)$
	15	$H_2C\text{-}CH\text{-}Ag\text{-}O \Leftrightarrow H_3C\text{-}C\text{-}Ag\text{-}O$
	16	$H_2C\text{-}CH\text{-}Ag\text{-}O \Leftrightarrow H_2C{=}CH\text{-}Ag\text{-}O$
	17	$H_2C\text{-}CH\text{-}Ag\text{-}O \Leftrightarrow H_2C\text{-}CH(O)\text{-}Ag$
	18	$H_2C\text{-}CH\text{-}Ag\text{-}O \Leftrightarrow HC\text{-}CH_2\text{-}Ag\text{-}O$
	19	$HC\text{-}CH_2\text{-}O\text{-}Ag \Leftrightarrow H_2C\text{-}CH\text{-}O\text{-}Ag$

20 $HC\text{-}CH_2\text{-}O\text{-}Ag \Leftrightarrow H_2C{=}CH\text{-}O\text{-}Ag$
21 $HC\text{-}CH_2\text{-}O\text{-}Ag \Leftrightarrow H_2C\text{-}CH\text{-}O(Ag)$
22 $HCOCH(S) \Leftrightarrow H_2COC(S)$
23 $HCOCH(S) \Leftrightarrow H_2C{=}CO(S)$
24 $HCOCH(S) \Leftrightarrow HC\text{-}CH\text{-}O\text{-}Ag$
25 $HCOCH(S) \Leftrightarrow HC\text{-}CH\text{-}Ag\text{-}O$
26 $HCOCH(S) \Leftrightarrow HC{=}CH\text{-}O\text{-}Ag$
27 $HCOCH(S) \Leftrightarrow HC{=}CH\text{-}Ag\text{-}O$
28 $H_2COC(S) \Leftrightarrow HCOCH(S)$
29 $H_2COC(S) \Leftrightarrow H_2C{=}CO(S)$
30 $H_2COC(S) \Leftrightarrow H_2C\text{-}C\text{-}O\text{-}Ag$
31 $H_2COC(S) \Leftrightarrow H_2C\text{-}C\text{-}Ag\text{-}O$
32 $HC\text{-}CH\text{-}Ag\text{-}O \Leftrightarrow HC{=}CH\text{-}Ag\text{-}O$
33 $HC\text{-}CH\text{-}Ag\text{-}O \Leftrightarrow H_2C\text{-}C\text{-}Ag\text{-}O$
34 $HC\text{-}CH\text{-}Ag\text{-}O \Leftrightarrow HC\text{-}CH\text{-}O(Ag)$
35 $OCH_2(S) \Leftrightarrow H_2C\text{-}O\text{-}Ag$
36 $OCH_2(S) \Leftrightarrow O\text{-}CH_2\text{-}Ag$
37 $OCH_2(S) \Leftrightarrow H_2C\text{-}Ag\text{-}O$
38 $H_2C\text{-}O\text{-}Ag \Leftrightarrow O\text{-}CH_2\text{-}Ag$
39 $HC\text{-}CH\text{-}Ag \Leftrightarrow H_2C\text{-}C\text{-}Ag$
40 $HC\text{-}CH\text{-}Ag \Leftrightarrow C\text{-}CH_2\text{-}Ag$
41 $HC\text{-}CH\text{-}Ag \Leftrightarrow HC{=}CH\text{-}Ag$
42 $H_2C\text{-}C\text{-}Ag \Leftrightarrow HC\text{-}CH\text{-}Ag$
43 $H_2C\text{-}C\text{-}Ag \Leftrightarrow H_2C{=}C\text{-}Ag$
44 $COCH(S) \Leftrightarrow HCOC(S)$
45 $COCH(S) \Leftrightarrow C\text{-}O\text{-}CH(Ag)$
46 $COCH(S) \Leftrightarrow C\text{-}O\text{-}CH\text{-}Ag$
47 $HCOC(S) \Leftrightarrow C\text{-}O\text{-}CH(Ag)$
48 $HCOC(S) \Leftrightarrow C\text{-}O\text{-}CH\text{-}Ag$
49 $C\text{-}CH\text{-}O(Ag) \Leftrightarrow HC\text{-}C\text{-}O(Ag)$
50 $C\text{-}CH\text{-}O(Ag) \Leftrightarrow HC\text{-}C\text{-}Ag\text{-}O$
51 $C\text{-}CH\text{-}O(Ag) \Leftrightarrow HC{=}C\text{-}Ag\text{-}O$
52 $C\text{-}CH\text{-}O\text{-}Ag \Leftrightarrow HC{=}C\text{-}Ag(O)$
53 $C\text{-}CH\text{-}O\text{-}Ag \Leftrightarrow HC{=}C\text{-}O(Ag)$
54 $C\text{-}CH\text{-}O\text{-}Ag \Leftrightarrow C\text{-}CH\text{-}Ag\text{-}O$
55 $C\text{-}CH_2\text{-}Ag \Leftrightarrow HC{=}CH\text{-}Ag$
56 $C\text{-}CH_2\text{-}Ag \Leftrightarrow H_2C{=}C\text{-}Ag$
57 $HC\text{-}C\text{-}O(Ag) \Leftrightarrow HC\text{-}C\text{-}Ag\text{-}O$
58 $HC\text{-}C\text{-}O(Ag) \Leftrightarrow HC{=}C\text{-}Ag\text{-}O$
59 $HC\text{-}C\text{-}O(Ag) \Leftrightarrow C\text{-}CH\text{-}Ag\text{-}O$
60 $HC\text{-}C\text{-}O(Ag) \Leftrightarrow HC{=}C\text{-}Ag\text{-}O$
61 $HC\text{-}C\text{-}O(Ag) \Leftrightarrow HC{=}C\text{-}Ag(O)$
62 $HC\text{-}C\text{-}O(Ag) \Leftrightarrow HC{=}C\text{-}O(Ag)$
63 $HC\text{-}C\text{-}O\text{-}Ag \Leftrightarrow HC\text{-}C\text{-}O(Ag)$
64 $HC\text{-}C\text{-}O\text{-}Ag \Leftrightarrow C\text{-}CH\text{-}O(Ag)$
65 $HC\text{-}C\text{-}O\text{-}Ag \Leftrightarrow HC{=}C\text{-}Ag\text{-}O$

66 HC-C-O-Ag ⇔ C-CH-Ag-O
67 HC-C-O-Ag ⇔ HC=C-Ag(O)
68 HC-C-O-Ag ⇔ HC=C-O(Ag)
69 HC-C-O-Ag ⇔ HC-C-Ag-O
70 HC-C-O-Ag ⇔ HC-C-O(Ag)
71 C-CH-Ag-O ⇔ HC-C-Ag-O
72 C-CH-Ag-O ⇔ C=CH-Ag-O
73 C-CH-Ag-O ⇔ HC=C-Ag-O
74 C-CH-Ag-O ⇔ HC≡C-Ag-O
75 HC-C-Ag-O ⇔ C=CH-Ag-O
76 HC-C-Ag-O ⇔ HC=C-Ag-O
77 HC-C-Ag-O ⇔ HC≡C-Ag-O
78 HC=C-Ag-O ⇔ C=CH-Ag-O
79 HC=C-Ag-O ⇔ HC≡C-Ag-O
80 HC≡C-Ag-O ⇔ C=CH-Ag-O
81 OCH(S) ⇔ CH-O-Ag
82 OCH(S) ⇔ O-CH-Ag
83 HC-O(Ag) ⇔ CH-O-Ag
84 CH-O-Ag ⇔ HC-O(Ag)
85 HC-Ag-O ⇔ CH-O-Ag
86 HC-Ag-O ⇔ HC-O(Ag)
87 C-CH-Ag ⇔ HC-C-Ag
88 C-CH-Ag ⇔ HC=C-Ag
89 C-CH-Ag ⇔ HC≡C-Ag
90 C-CH-Ag ⇔ C=CH-Ag
91 C-CH-Ag ⇔ C≡CH-Ag
92 HC-C-Ag ⇔ HC=C-Ag
93 HC-C-Ag ⇔ HC≡C-Ag
94 HC-C-Ag ⇔ C=CH-Ag
95 HC-C-Ag ⇔ C≡CH-Ag
96 HC=C-Ag ⇔ C=CH-Ag
97 HC=C-Ag ⇔ C≡CH-Ag
98 HC≡C-Ag ⇔ C=CH-Ag
99 HC≡C-Ag ⇔ C≡CH-Ag
100 C=CH-Ag ⇔ C≡CH-Ag
101 COC(S) ⇔ C-O-C(Ag)
102 COC(S) ⇔ C-O-C-Ag
103 C-C-O(Ag) ⇔ C-C-O-Ag
104 C-C-O(Ag) ⇔ C-C-Ag-O
105 C-C-O(Ag) ⇔ C≡C(O)-Ag
106 C-C-O(Ag) ⇔ C=C(O)-Ag
107 C-C-O(Ag) ⇔ C-C(O)-Ag
108 C-C-O(Ag) ⇔ C≡C-Ag-O
109 C-C-O(Ag) ⇔ C=C-Ag-O
110 C-C-O(Ag) ⇔ C-C-Ag-O
111 C-C-O-Ag ⇔ C-C-Ag-O

	112	C-C-O-Ag ⇔ C≡C(O)-Ag
	113	C-C-O-Ag ⇔ C=C(O)-Ag
	114	C-C-O-Ag ⇔ C-C(O)-Ag
	115	C-C-O-Ag ⇔ C≡C-Ag-O
	116	C-C-O-Ag ⇔ C=C-Ag-O
	117	C-C-O-Ag ⇔ C-C-Ag-O
	118	C-C-Ag-O ⇔ C≡C(O)-Ag
	119	C-C-Ag-O ⇔ C=C(O)-Ag
	120	C-C-Ag-O ⇔ C-C(O)-Ag
	121	C-C-Ag-O ⇔ C≡C-Ag-O
	122	C-C-Ag-O ⇔ C=C-Ag-O
	123	C-C-Ag-O ⇔ C-C-Ag-O
	124	C≡C(O)-Ag ⇔ C=C(O)-Ag
	125	C≡C(O)-Ag ⇔ C-C(O)-Ag
	126	C≡C(O)-Ag ⇔ C≡C-Ag-O
	127	C≡C(O)-Ag ⇔ C=C-Ag-O
	128	C≡C(O)-Ag ⇔ C-C-Ag-O
	129	C=C(O)-Ag ⇔ C-C(O)-Ag
	130	C=C(O)-Ag ⇔ C≡C-Ag-O
	131	C=C(O)-Ag ⇔ C=C-Ag-O
	132	C=C(O)-Ag ⇔ C-C-Ag-O
	133	C-C(O)-Ag ⇔ C≡C-Ag-O
	134	C-C(O)-Ag ⇔ C=C-Ag-O
	135	C-C(O)-Ag ⇔ C-C-Ag-O
	136	C≡C-Ag-O ⇔ C=C-Ag-O
	137	C≡C-Ag-O ⇔ C-C-Ag-O
	138	C=C-Ag-O ⇔ C-C-Ag-O
	139	OC(S) ⇔ C-O-Ag
	140	OC(S) ⇔ O-C-Ag
	141	O-C-Ag ⇔ O=C-Ag
	142	O-C-Ag ⇔ O-C-Ag
	143	C-O-Ag ⇔ O=C-Ag
	144	C-O-Ag ⇔ C-O(Ag)
	145	C-Ag-O ⇔ C-O-Ag
	146	C-Ag-O ⇔ O=C-Ag
	147	C-Ag-O ⇔ O-C-Ag
	148	C-C-Ag ⇔ C=C-Ag
	149	C-C-Ag ⇔ C≡C-Ag
Decomposition / Addition	1	$H_2COCH_2(S) \Leftrightarrow HCOCH_2(S) + H$
	2	$H_2COCH_2(S) \Leftrightarrow H_2COCH(S) + H$
	3	$H_2COCH_2(S) \Leftrightarrow CH_2 + OCH_2(S)$
	4	$H_2COCH_2(S) \Leftrightarrow H_2C\text{-}CH_2\text{-}O + Ag$
	5	$H_2COCH_2(S) \Leftrightarrow H_2C\text{-}CH_2\text{-}Ag + O$
	6	$H_2C\text{-}CH_2\text{-}O\text{-}Ag \Leftrightarrow H_2C\text{-}CH\text{-}O\text{-}Ag + H$
	7	$H_2C\text{-}CH_2\text{-}O\text{-}Ag \Leftrightarrow CH_2 + CH_2\text{-}O\text{-}Ag$

8	$H_2C\text{-}CH_2\text{-}O\text{-}Ag \Leftrightarrow HC\text{-}CH_2\text{-}O\text{-}Ag + H$
9	$H_2C\text{-}CH_2\text{-}O\text{-}Ag \Leftrightarrow H_2C\text{-}CH_2 + Ag\text{-}O$
10	$H_2C\text{-}CH_2\text{-}O\text{-}Ag \Leftrightarrow H_2C\text{-}CH_2\text{-}O + Ag$
11	$H_2C\text{-}CH_2\text{-}Ag\text{-}O \Leftrightarrow H_2C\text{-}CH_2\text{-}Ag + O$
12	$H_2C\text{-}CH_2\text{-}Ag\text{-}O \Leftrightarrow CH_2 + CH_2\text{-}Ag\text{-}O$
13	$H_2C\text{-}CH_2\text{-}Ag\text{-}O \Leftrightarrow HC\text{-}CH_2\text{-}Ag\text{-}O + H$
14	$H_2C\text{-}CH_2\text{-}Ag\text{-}O \Leftrightarrow H_2C\text{-}CH\text{-}Ag\text{-}O + H$
15	$H_2C\text{-}CH_2\text{-}Ag\text{-}O \Leftrightarrow H_2C\text{-}CH_2 + Ag\text{-}O$
16	$HCOCH_2(S) \Leftrightarrow COCH_2(S) + H$
17	$HCOCH_2(S) \Leftrightarrow HCOCH(S) + H$
18	$HCOCH_2(S) \Leftrightarrow CH + OCH_2(S)$
19	$HCOCH_2(S) \Leftrightarrow HC\text{-}CH_2\text{-}O + Ag$
20	$HCOCH_2(S) \Leftrightarrow HC\text{-}CH_2\text{-}Ag + O$
21	$HCOCH_2(S) \Leftrightarrow HC\text{-}CH_2 + Ag\text{-}O$
22	$H_2COCH(S) \Leftrightarrow HCOCH(S) + H$
23	$H_2COCH(S) \Leftrightarrow H_2COC(S) + H$
24	$H_2COCH(S) \Leftrightarrow CH_2 + OCH(S)$
25	$H_2COCH(S) \Leftrightarrow HC\text{-}CH_2 + Ag\text{-}O$
26	$H_2COCH(S) \Leftrightarrow H_2C\text{-}CH\text{-}Ag + O$
27	$H_2COCH(S) \Leftrightarrow H_2C\text{-}CH\text{-}O + Ag$
28	$H_2C\text{-}CH_2\text{-}Ag \Leftrightarrow H_2C\text{-}CH_2 + Ag$
29	$H_2C\text{-}CH_2\text{-}Ag \Leftrightarrow CH_2 + H_2C\text{-}Ag$
30	$H_2C\text{-}CH_2\text{-}Ag \Leftrightarrow HC\text{-}CH_2\text{-}Ag + H$
31	$H_2C\text{-}CH_2\text{-}Ag \Leftrightarrow H_2C\text{-}CH\text{-}Ag + H$
32	$H_2C\text{-}CH\text{-}O\text{-}Ag \Leftrightarrow HC(O)\text{-}CH_2 + Ag$
33	$H_2C\text{-}CH\text{-}O\text{-}Ag \Leftrightarrow HC\text{-}CH_2 + Ag\text{-}O$
34	$H_2C\text{-}CH\text{-}O\text{-}Ag \Leftrightarrow HC\text{-}CH\text{-}O\text{-}Ag + H$
35	$H_2C\text{-}CH\text{-}O\text{-}Ag \Leftrightarrow H_2C\text{-}C\text{-}O\text{-}Ag + H$
36	$CH_2\text{-}O\text{-}Ag \Leftrightarrow H_2C\text{-}O + Ag$
37	$CH_2\text{-}O\text{-}Ag \Leftrightarrow CH_2 + Ag\text{-}O$
38	$CH_2\text{-}O\text{-}Ag \Leftrightarrow HC\text{-}O\text{-}Ag + H$
39	$HC\text{-}CH_2\text{-}O\text{-}Ag \Leftrightarrow HC\text{-}CH_2(O) + Ag$
40	$HC\text{-}CH_2\text{-}O\text{-}Ag \Leftrightarrow H_2C\text{-}CH + Ag\text{-}O$
41	$HC\text{-}CH_2\text{-}O\text{-}Ag \Leftrightarrow C\text{-}CH_2\text{-}O\text{-}Ag + H$
42	$HC\text{-}CH_2\text{-}O\text{-}Ag \Leftrightarrow HC\text{-}CH\text{-}O\text{-}Ag + H$
43	$H_2C\text{-}CH_2\text{-}Ag \Leftrightarrow H_2C\text{-}CH_2 + Ag$
44	$H_2C\text{-}CH_2\text{-}Ag \Leftrightarrow CH_2 + H_2C\text{-}Ag$
45	$CH_2\text{-}Ag\text{-}O \Leftrightarrow H_2C\text{-}Ag + O$
46	$CH_2\text{-}Ag\text{-}O \Leftrightarrow CH_2 + Ag\text{-}O$
47	$CH_2\text{-}Ag\text{-}O \Leftrightarrow HC\text{-}Ag\text{-}O + H$
48	$HC\text{-}CH_2\text{-}Ag\text{-}O \Leftrightarrow HC\text{-}CH_2\text{-}Ag + O$
49	$HC\text{-}CH_2\text{-}Ag\text{-}O \Leftrightarrow HC\text{-}CH_2 + Ag\text{-}O$
50	$HC\text{-}CH_2\text{-}Ag\text{-}O \Leftrightarrow H + C\text{-}CH_2\text{-}Ag\text{-}O$
51	$HC\text{-}CH_2\text{-}Ag\text{-}O \Leftrightarrow CH + H_2C\text{-}Ag\text{-}O$
52	$HC\text{-}CH_2\text{-}Ag\text{-}O \Leftrightarrow HC\text{-}CH\text{-}Ag\text{-}O + H$
53	$H_2C\text{-}CH\text{-}Ag\text{-}O \Leftrightarrow H + HC\text{-}CH\text{-}Ag\text{-}O$

54 $H_2C\text{-}CH\text{-}Ag\text{-}O \Leftrightarrow CH_2 + HC\text{-}Ag\text{-}O$

55 $H_2C\text{-}CH\text{-}Ag\text{-}O \Leftrightarrow H_2C\text{-}C\text{-}Ag\text{-}O + H$

56 $H_2C\text{-}CH\text{-}Ag\text{-}O \Leftrightarrow H_2C\text{-}CH + Ag\text{-}O$

57 $H_2C\text{-}CH\text{-}Ag\text{-}O \Leftrightarrow H_2C\text{-}CH\text{-}Ag + O$

58 $COCH_2(S) \Leftrightarrow COCH(S) + H$

59 $COCH_2(S) \Leftrightarrow C + OCH_2(S)$

60 $COCH_2(S) \Leftrightarrow C\text{-}CH_2\text{-}O + Ag$

61 $COCH_2(S) \Leftrightarrow C\text{-}CH_2\text{-}Ag + O$

62 $COCH_2(S) \Leftrightarrow C\text{-}CH_2 + Ag\text{-}O$

63 $HCOCH(S) \Leftrightarrow COCH(S) + H$

64 $HCOCH(S) \Leftrightarrow CH + OCH(S)$

65 $HCOCH(S) \Leftrightarrow HC\text{-}CH + Ag\text{-}O$

66 $HCOCH(S) \Leftrightarrow HC\text{-}CH\text{-}O + Ag$

67 $HCOCH(S) \Leftrightarrow HC\text{-}CH\text{-}Ag + O$

68 $OCH_2(S) \Leftrightarrow OCH(S) + H$

69 $OCH_2(S) \Leftrightarrow CH_2 + Ag\text{-}O$

70 $OCH_2(S) \Leftrightarrow O + H_2C\text{-}Ag$

71 $HC\text{-}CH_2\text{-}Ag \Leftrightarrow H_2C\text{-}CH + Ag$

72 $HC\text{-}CH_2\text{-}Ag \Leftrightarrow C\text{-}CH_2\text{-}Ag + H$

73 $HC\text{-}CH_2\text{-}Ag \Leftrightarrow HC\text{-}CH\text{-}Ag + H$

74 $HC\text{-}CH_2\text{-}Ag \Leftrightarrow CH + H_2C\text{-}Ag$

75 $HCOCH(S) \Leftrightarrow COCH(S) + H$

76 $HCOCH(S) \Leftrightarrow HCOC(S) + H$

77 $HCOCH(S) \Leftrightarrow CH + OCH(S)$

78 $HCOCH(S) \Leftrightarrow CH_2 + Ag\text{-}O$

79 $H_2COC(S) \Leftrightarrow HCOC(S) + H$

80 $H_2COC(S) \Leftrightarrow CH_2 + OC(S)$

81 $H_2COC(S) \Leftrightarrow C\text{-}CH_2 + Ag\text{-}O$

82 $H_2COC(S) \Leftrightarrow O\text{-}C\text{-}CH_2 + Ag$

83 $OCH(S) \Leftrightarrow OC(S) + H$

84 $OCH(S) \Leftrightarrow HC\text{-}O + Ag$

85 $OCH(S) \Leftrightarrow HC\text{-}Ag + O$

86 $H_2C\text{-}CH\text{-}Ag \Leftrightarrow HC\text{-}CH\text{-}Ag + H$

87 $H_2C\text{-}CH\text{-}Ag \Leftrightarrow H_2C\text{-}C\text{-}Ag + H$

88 $H_2C\text{-}CH\text{-}Ag \Leftrightarrow H_2C\text{-}CH + Ag$

89 $H_2C\text{-}CH\text{-}Ag \Leftrightarrow CH_2 + HC\text{-}Ag$

90 $H_2C\text{-}Ag \Leftrightarrow CH_2 + Ag$

91 $H_2C\text{-}Ag \Leftrightarrow HC\text{-}Ag + H$

92 $HC\text{-}CH\text{-}O\text{-}Ag \Leftrightarrow C\text{-}CH\text{-}O\text{-}Ag + H$

93 $HC\text{-}CH\text{-}O\text{-}Ag \Leftrightarrow HC\text{-}C\text{-}O\text{-}Ag + H$

94 $HC\text{-}CH\text{-}O\text{-}Ag \Leftrightarrow HC\text{-}CH + Ag\text{-}O$

95 $HC\text{-}CH\text{-}O\text{-}Ag \Leftrightarrow CH + HC\text{-}O\text{-}Ag$

96 $HC\text{-}CH\text{-}O\text{-}Ag \Leftrightarrow HC(O)\text{-}CH + Ag$

97 $CH\text{-}Ag \Leftrightarrow C\text{-}Ag + H$

98 $CH\text{-}Ag \Leftrightarrow CH + Ag$

99 $H_2C\text{-}C\text{-}O\text{-}Ag \Leftrightarrow CH_2 + C\text{-}O\text{-}Ag$

100 $H_2C\text{-}C\text{-}O\text{-}Ag \Leftrightarrow HC\text{-}C\text{-}O\text{-}Ag + H$

101 $H_2C\text{-}C\text{-}O\text{-}Ag \Leftrightarrow C\text{-}CH_2 + Ag\text{-}O$

102 $H_2C\text{-}C\text{-}O\text{-}Ag \Leftrightarrow O\text{-}C\text{-}CH_2 + Ag$

103 $CH\text{-}O\text{-}Ag \Leftrightarrow HC\text{-}O + Ag$

104 $CH\text{-}O\text{-}Ag \Leftrightarrow CH + Ag\text{-}O$

105 $CH\text{-}O\text{-}Ag \Leftrightarrow C\text{-}O\text{-}Ag + H$

106 $C\text{-}CH_2\text{-}O\text{-}Ag \Leftrightarrow C + H_2C\text{-}O\text{-}Ag$

107 $C\text{-}CH_2\text{-}O\text{-}Ag \Leftrightarrow C\text{-}CH_2 + Ag\text{-}O$

108 $C\text{-}CH_2\text{-}O\text{-}Ag \Leftrightarrow C\text{-}CH\text{-}O\text{-}Ag + H$

109 $C\text{-}CH_2\text{-}O\text{-}Ag \Leftrightarrow C\text{-}CH_2\text{-}O + Ag$

110 $HC\text{-}CH_2\text{-}Ag \Leftrightarrow C\text{-}CH_2\text{-}Ag + H$

111 $HC\text{-}CH_2\text{-}Ag \Leftrightarrow HC\text{-}CH\text{-}Ag + H$

112 $HC\text{-}CH_2\text{-}Ag \Leftrightarrow HC\text{-}CH_2 + Ag$

113 $HC\text{-}CH_2\text{-}Ag \Leftrightarrow CH + H_2C\text{-}Ag$

114 $Ag\text{-}O \Leftrightarrow Ag + O$

115 $C\text{-}CH_2\text{-}Ag\text{-}O \Leftrightarrow C\text{-}CH_2\text{-}Ag + O$

116 $C\text{-}CH_2\text{-}Ag\text{-}O \Leftrightarrow C\text{-}CH_2 + Ag\text{-}O$

117 $C\text{-}CH_2\text{-}Ag\text{-}O \Leftrightarrow C + H_2C\text{-}Ag\text{-}O$

118 $C\text{-}CH_2\text{-}Ag\text{-}O \Leftrightarrow C\text{-}CH\text{-}Ag\text{-}O$

119 $CH_2\text{-}Ag\text{-}O \Leftrightarrow H_2C\text{-}Ag + O$

120 $CH_2\text{-}Ag\text{-}O \Leftrightarrow CH_2 + Ag\text{-}O$

121 $CH_2\text{-}Ag\text{-}O \Leftrightarrow HC\text{-}Ag\text{-}O + H$

122 $HC\text{-}CH\text{-}Ag\text{-}O \Leftrightarrow HC\text{-}CH\text{-}Ag + O$

123 $HC\text{-}CH\text{-}Ag\text{-}O \Leftrightarrow HC\text{-}CH + Ag\text{-}O$

124 $HC\text{-}CH\text{-}Ag\text{-}O \Leftrightarrow CH + HC\text{-}Ag\text{-}O$

125 $HC\text{-}CH\text{-}Ag\text{-}O \Leftrightarrow C\text{-}CH\text{-}Ag\text{-}O + H$

126 $HC\text{-}CH\text{-}Ag\text{-}O \Leftrightarrow HC\text{-}C\text{-}Ag\text{-}O + H$

127 $HC\text{-}Ag\text{-}O \Leftrightarrow C\text{-}Ag\text{-}O + H$

128 $HC\text{-}Ag\text{-}O \Leftrightarrow CH + Ag\text{-}O$

129 $HC\text{-}Ag\text{-}O \Leftrightarrow HC\text{-}Ag + O$

130 $H_2C\text{-}C\text{-}Ag\text{-}O \Leftrightarrow H_2C\text{-}C\text{-}Ag + O$

131 $H_2C\text{-}C\text{-}Ag\text{-}O \Leftrightarrow C\text{-}CH_2 + Ag\text{-}O$

132 $H_2C\text{-}C\text{-}Ag\text{-}O \Leftrightarrow CH_2 + C\text{-}Ag\text{-}O$

133 $H_2C\text{-}C\text{-}Ag\text{-}O \Leftrightarrow HC\text{-}C\text{-}Ag\text{-}O + H$

134 $H_2C\text{-}CH\text{-}Ag \Leftrightarrow HC\text{-}CH_2 + Ag$

135 $H_2C\text{-}CH\text{-}Ag \Leftrightarrow H_2C\text{-}C\text{-}Ag + H$

136 $H_2C\text{-}CH\text{-}Ag \Leftrightarrow CH_2 + HC\text{-}Ag$

137 $H_2C\text{-}CH\text{-}Ag \Leftrightarrow HC\text{-}CH\text{-}Ag + H$

138 $COCH(S) \Leftrightarrow C + OCH(S)$

139 $COCH(S) \Leftrightarrow COC(S) + H$

140 $COCH(S) \Leftrightarrow HC(O)\text{-}C + Ag$

141 $COCH(S) \Leftrightarrow C\text{-}CH\text{-}Ag + O$

142 $C\text{-}CH_2\text{-}Ag \Leftrightarrow C\text{-}CH_2 + Ag$

143 $C\text{-}CH_2\text{-}Ag \Leftrightarrow C + H_2C\text{-}Ag$

144 $C\text{-}CH_2\text{-}Ag \Leftrightarrow C\text{-}CH\text{-}Ag + H$

145 $H_2C\text{-}Ag \Leftrightarrow CH_2 + Ag$

146 $H_2C\text{-}Ag \Leftrightarrow HC\text{-}Ag + H$
147 $HCOC(S) \Leftrightarrow COC(S) + H$
148 $HCOC(S) \Leftrightarrow CH + OC(S)$
149 $HCOC(S) \Leftrightarrow HC\text{-}C\text{-}O + Ag$
150 $HCOC(S) \Leftrightarrow HC\text{-}C\text{-}Ag + O$
151 $OC(S) \Leftrightarrow C\text{-}O + Ag$
152 $OC(S) \Leftrightarrow O\text{-}Ag + C$
153 $OC(S) \Leftrightarrow C\text{-}Ag + O$
154 $H_2C\text{-}C\text{-}Ag \Leftrightarrow C\text{-}CH_2 + Ag$
155 $H_2C\text{-}C\text{-}Ag \Leftrightarrow CH_2 + C\text{-}Ag$
156 $H_2C\text{-}C\text{-}Ag \Leftrightarrow HC\text{-}C\text{-}Ag + H$
157 $C\text{-}CH\text{-}O\text{-}Ag \Leftrightarrow HC(O)\text{-}C + Ag$
158 $C\text{-}CH\text{-}O\text{-}Ag \Leftrightarrow C\text{-}CH + Ag\text{-}O$
159 $C\text{-}CH\text{-}O\text{-}Ag \Leftrightarrow C + HC\text{-}O\text{-}Ag$
160 $C\text{-}CH\text{-}O\text{-}Ag \Leftrightarrow C\text{-}C\text{-}O\text{-}Ag + H$
161 $HC\text{-}C\text{-}O\text{-}Ag \Leftrightarrow HC\text{-}C\text{-}O + Ag$
162 $HC\text{-}C\text{-}O\text{-}Ag \Leftrightarrow C\text{-}CH + Ag\text{-}O$
163 $HC\text{-}C\text{-}O\text{-}Ag \Leftrightarrow CH + C\text{-}O\text{-}Ag$
164 $HC\text{-}C\text{-}O\text{-}Ag \Leftrightarrow C\text{-}C\text{-}O\text{-}Ag + H$
165 $CH\text{-}O\text{-}Ag \Leftrightarrow HC\text{-}O + Ag$
166 $CH\text{-}O\text{-}Ag \Leftrightarrow CH + O\text{-}Ag$
167 $CH\text{-}O\text{-}Ag \Leftrightarrow C\text{-}O\text{-}Ag + H$
168 $C\text{-}Ag \Leftrightarrow C + Ag$
169 $C\text{-}O\text{-}Ag \Leftrightarrow C\text{-}O + Ag$
170 $C\text{-}O\text{-}Ag \Leftrightarrow C + Ag\text{-}O$
171 $CH_2\text{-}O\text{-}Ag \Leftrightarrow H_2C\text{-}O + Ag$
172 $CH_2\text{-}O\text{-}Ag \Leftrightarrow CH_2 + Ag\text{-}O$
173 $CH_2\text{-}O\text{-}Ag \Leftrightarrow HC\text{-}O\text{-}Ag + H$
174 $C\text{-}CH\text{-}Ag\text{-}O \Leftrightarrow C\text{-}CH\text{-}Ag + O$
175 $C\text{-}CH\text{-}Ag\text{-}O \Leftrightarrow C\text{-}CH + Ag\text{-}O$
176 $C\text{-}CH\text{-}Ag\text{-}O \Leftrightarrow C + HC\text{-}Ag\text{-}O$
177 $C\text{-}CH\text{-}Ag\text{-}O \Leftrightarrow C\text{-}C\text{-}Ag\text{-}O + H$
178 $HC\text{-}C\text{-}Ag\text{-}O \Leftrightarrow HC\text{-}C\text{-}Ag + O$
179 $HC\text{-}C\text{-}Ag\text{-}O \Leftrightarrow C\text{-}CH + O\text{-}Ag$
180 $HC\text{-}C\text{-}Ag\text{-}O \Leftrightarrow CH + C\text{-}Ag\text{-}O$
181 $HC\text{-}C\text{-}Ag\text{-}O \Leftrightarrow C\text{-}C\text{-}Ag\text{-}O + H$
182 $C\text{-}Ag\text{-}O \Leftrightarrow C\text{-}Ag + O$
183 $C\text{-}Ag\text{-}O \Leftrightarrow C + O\text{-}Ag$
184 $COC(S) \Leftrightarrow C + OC(S)$
185 $COC(S) \Leftrightarrow C\text{-}C\text{-}O + Ag$
186 $COC(S) \Leftrightarrow C\text{-}C\text{-}Ag + O$
187 $C\text{-}CH\text{-}Ag \Leftrightarrow C\text{-}CH + Ag$
188 $C\text{-}CH\text{-}Ag \Leftrightarrow C\text{-}C\text{-}Ag + H$
189 $C\text{-}CH\text{-}Ag \Leftrightarrow C + HC\text{-}Ag$
190 $HC\text{-}C\text{-}Ag \Leftrightarrow C\text{-}CH + Ag$
191 $HC\text{-}C\text{-}Ag \Leftrightarrow CH + C\text{-}Ag$

192 HC-C-Ag ⇔ C-C-Ag + H
193 C-C-O-Ag ⇔ C-C-O + Ag
194 C-C-O-Ag ⇔ C-C + Ag-O
195 C-C-O-Ag ⇔ C-O-Ag + C
196 C-C-Ag-O ⇔ C-C-Ag + O
197 C-C-Ag-O ⇔ C-C + Ag-O
198 C-C-Ag-O ⇔ C + C-Ag-O
199 C-C-Ag ⇔ C-C + Ag
200 C-C-Ag ⇔ C-Ag + C
201 HC-CH-O(Ag) ⇔ HC-CH-O + Ag
202 HC-CH-O(Ag) ⇔ C-CH-O(Ag) + H
203 HC-CH-O(Ag) ⇔ HC-C-O(Ag) + H
204 HC-CH-O(Ag) ⇔ CH + O-CH-Ag
205 HC-CH-O(Ag) ⇔ HC-CH-Ag + O
206 H_2C-O(Ag) ⇔ HC-O(Ag) + H
207 H_2C-O(Ag) ⇔ H_2C-O + Ag
208 H_2C-O(Ag) ⇔ H_2C-Ag + O
209 H_2C-C-O(Ag) ⇔ H_2C-C-O + Ag
210 H_2C-C-O(Ag) ⇔ H_2C-C-Ag + O
211 H_2C-C-O(Ag) ⇔ HC-C-O(Ag) + H
212 H_2C-C-O(Ag) ⇔ CH_2 + C-O(Ag)
213 C-CH_2-O(Ag) ⇔ C + H_2C-O(Ag)
214 C-CH_2-O(Ag) ⇔ C-CH-O(Ag) + H
215 C-CH_2-O(Ag) ⇔ C-CH_2-O + Ag
216 C-CH_2-O(Ag) ⇔ C-CH_2-Ag + O
217 HC-CH-Ag ⇔ C-CH-Ag + H
218 HC-CH-Ag ⇔ HC-C-Ag + H
219 HC-CH-Ag ⇔ HC-CH + Ag
220 HC-CH-Ag ⇔ CH + HC-Ag
221 C-CH-O(Ag) ⇔ C + O-CH-Ag
222 C-CH-O(Ag) ⇔ C-C-O(Ag) + H
223 C-CH-O(Ag) ⇔ HC(O)-C + Ag
224 C-CH-O(Ag) ⇔ C-CH-Ag + O
225 HC-C-O(Ag) ⇔ C-C-O(Ag) + H
226 HC-C-O(Ag) ⇔ CH + C-O(Ag)
227 HC-C-O(Ag) ⇔ HC-C-Ag + O
228 HC-C-O(Ag) ⇔ HC-C-O + Ag
229 HC-O(Ag) ⇔ C-O(Ag) + H
230 HC-O(Ag) ⇔ HC-Ag + O
231 HC-O(Ag) ⇔ HC-O + Ag
232 C-C-O(Ag) ⇔ C + C-O(Ag)
233 C-C-O(Ag) ⇔ C-C-O + Ag
234 C-C-O(Ag) ⇔ C-C-Ag + O
235 O-C-Ag ⇔ C-O + Ag
236 O-C-Ag ⇔ C-Ag + O
237 C_2H_4(S) ⇔ $(Ag_2)H_2C{=}CH(Ag_2)$ + H

238 $C_2H_4(S) \Leftrightarrow (Ag_2)H_2C{=}CH_2(Ag) + Ag$

239 $(Ag_2)H_2C{=}CH(Ag_2) \Leftrightarrow (Ag_2)HC{=}CH(Ag_2) + H$

240 $(Ag_2)H_2C{=}CH(Ag_2) \Leftrightarrow (Ag_2)H_2C{=}C(Ag_2) + H$

241 $(Ag_2)H_2C{=}CH(Ag_2) \Leftrightarrow (Ag)H_2C{=}CH(Ag_2) + Ag$

242 $(Ag_2)H_2C{=}CH(Ag_2) \Leftrightarrow (Ag_2)H_2C{=}CH(Ag) + Ag$

243 $(Ag_2)H_2C{=}CH(Ag_2) \Leftrightarrow (Ag_2)HC{=}CH_2(Ag) + H$

244 $(Ag_2)H_2C{=}CH_2(Ag) \Leftrightarrow (Ag_2)HC{=}CH_2(Ag) + H$

245 $(Ag_2)H_2C{=}CH_2(Ag) \Leftrightarrow (Ag)H_2C{=}CH_2(Ag) + Ag$

246 $(Ag_2)H_2C{=}CH_2(Ag) \Leftrightarrow (Ag_2)H_2C{=}CH(Ag) + H$

247 $(Ag_2)H_2C{=}CH_2(Ag) \Leftrightarrow (Ag_2)H_2C{=}CH_2 + Ag$

248 $(Ag)H_2C{=}CH(Ag_2) \Leftrightarrow H_2C{=}CH(Ag_2) + Ag$

249 $(Ag)H_2C{=}CH(Ag_2) \Leftrightarrow (Ag)HC{=}CH(Ag_2) + H$

250 $(Ag)H_2C{=}CH(Ag_2) \Leftrightarrow (Ag)H_2C{=}CH(Ag) + Ag$

251 $(Ag)H_2C{=}CH(Ag_2) \Leftrightarrow (Ag)H_2C{=}C(Ag_2) + H$

252 $(Ag)H_2C{=}CH(Ag_2) \Leftrightarrow H_2C(Ag) + HC(Ag_2)$

253 $(Ag_2)HC{=}CH(Ag_2) \Leftrightarrow (Ag)HC{=}CH(Ag_2) + Ag$

254 $(Ag_2)HC{=}CH(Ag_2) \Leftrightarrow (Ag_2)C{=}CH(Ag_2) + H$

255 $(Ag_2)HC{=}CH(Ag_2) \Leftrightarrow HC(Ag_2) + HC(Ag_2)$

256 $(Ag_2)H_2C{=}CH(Ag) \Leftrightarrow (Ag)H_2C{=}CH(Ag) + Ag$

257 $(Ag_2)H_2C{=}CH(Ag) \Leftrightarrow (Ag)HC{=}CH(Ag_2) + H$

258 $(Ag_2)H_2C{=}CH(Ag) \Leftrightarrow (Ag_2)H_2C{=}CH + Ag$

259 $(Ag_2)H_2C{=}CH(Ag) \Leftrightarrow (Ag_2)H_2C{=}C(Ag) + H$

260 $(Ag_2)HC{=}CH_2(Ag) \Leftrightarrow (Ag)H_2C{=}C(Ag_2) + H$

261 $(Ag_2)HC{=}CH_2(Ag) \Leftrightarrow (Ag)H_2C{=}CH(Ag) + Ag$

262 $(Ag_2)HC{=}CH_2(Ag) \Leftrightarrow (Ag)HC{=}CH(Ag_2) + H$

263 $(Ag_2)HC{=}CH_2(Ag) \Leftrightarrow H_2C{=}CH(Ag_2) + Ag$

264 $(Ag_2)HC{=}CH_2(Ag) \Leftrightarrow HC(Ag_2) + H_2C(Ag)$

265 $(Ag)H_2C{=}CH_2(Ag) \Leftrightarrow (Ag)H_2C{=}CH(Ag) + H$

266 $(Ag)H_2C{=}CH_2(Ag) \Leftrightarrow (Ag)H_2C{=}CH_2 + Ag$

267 $(Ag)H_2C{=}CH_2(Ag) \Leftrightarrow (Ag)H_2C{=}CH(Ag) + H$

268 $(Ag)H_2C{=}CH_2(Ag) \Leftrightarrow (Ag)H_2C{=}CH_2 + Ag$

269 $(Ag)H_2C{=}CH_2(Ag) \Leftrightarrow H_2C(Ag_2) + H_2C(Ag)$

270 $(Ag_2)H_2C{=}C(Ag_2) \Leftrightarrow (Ag_2)C{=}CH(Ag_2) + H$

271 $(Ag_2)H_2C{=}C(Ag_2) \Leftrightarrow (Ag)H_2C{=}C(Ag_2) + Ag$

272 $(Ag_2)H_2C{=}C(Ag_2) \Leftrightarrow (Ag_2)H_2C{=}C(Ag) + Ag$

273 $(Ag_2)H_2C{=}C(Ag_2) \Leftrightarrow H_2C(Ag_2) + C(Ag_2)$

274 $(Ag)H_2C{=}CH(Ag_2) \Leftrightarrow H_2C{=}CH(Ag_2) + Ag$

275 $(Ag)H_2C{=}CH(Ag_2) \Leftrightarrow (Ag)HC{=}CH(Ag_2) + H$

276 $(Ag)H_2C{=}CH(Ag_2) \Leftrightarrow (Ag)H_2C{=}CH(Ag) + Ag$

277 $(Ag)H_2C{=}CH(Ag_2) \Leftrightarrow (Ag)H_2C{=}C(Ag_2) + H$

278 $(Ag)H_2C{=}CH(Ag_2) \Leftrightarrow H_2C(Ag) + HC(Ag_2)$

279 $(Ag_2)H_2C{=}CH(Ag) \Leftrightarrow (Ag)H_2C{=}CH(Ag) + Ag$

280 $(Ag_2)H_2C{=}CH(Ag) \Leftrightarrow (Ag)HC{=}CH(Ag_2) + H$

281 $(Ag_2)H_2C{=}CH(Ag) \Leftrightarrow (Ag_2)H_2C{=}CH + Ag$

282 $(Ag_2)H_2C{=}CH(Ag) \Leftrightarrow (Ag_2)H_2C{=}C(Ag) + H$

283 $(Ag_2)C{=}CH_2(Ag) \Leftrightarrow (Ag)C{=}CH_2(Ag) + Ag$

284 $(Ag_2)C=CH_2(Ag) \Leftrightarrow (Ag)HC=C(Ag_2) + H$

285 $(Ag_2)C=CH_2(Ag) \Leftrightarrow (Ag_2)C=CH_2 + Ag$

286 $(Ag_2)C=CH_2(Ag) \Leftrightarrow C(Ag_2) + H_2C(Ag)$

287 $(Ag)HC=CH_2(Ag) \Leftrightarrow HC=CH_2(Ag) + Ag$

288 $(Ag)HC=CH_2(Ag) \Leftrightarrow (Ag)C=CH_2(Ag) + H$

289 $(Ag)HC=CH_2(Ag) \Leftrightarrow (Ag)HC=CH(Ag) + H$

290 $(Ag)HC=CH_2(Ag) \Leftrightarrow (Ag)HC=CH_2 + Ag$

291 $(Ag)HC=CH_2(Ag) \Leftrightarrow HC\text{-}Ag + H_2C(Ag)$

292 $(Ag_2)HC=CH(Ag) \Leftrightarrow (Ag)HC=CH(Ag) + Ag$

293 $(Ag_2)HC=CH(Ag) \Leftrightarrow (Ag)HC=C(Ag_2) + H$

294 $(Ag_2)HC=CH(Ag) \Leftrightarrow (Ag)C=CH(Ag_2) + H$

295 $(Ag_2)HC=CH(Ag) \Leftrightarrow HC=CH(Ag_2) + Ag$

296 $(Ag_2)HC=CH(Ag) \Leftrightarrow HC(Ag_2) + HC\text{-}Ag$

297 $(Ag_2)HC=CH_2 \Leftrightarrow (Ag_2)C=CH_2 + H$

298 $(Ag_2)HC=CH_2 \Leftrightarrow (Ag)HC=CH_2 + Ag$

299 $(Ag_2)HC=CH_2 \Leftrightarrow HC=CH(Ag_2) + H$

300 $(Ag_2)HC=CH_2 \Leftrightarrow HC(Ag_2) + CH_2$

301 $H_2C=CH_2(Ag) \Leftrightarrow HC=CH_2(Ag) + H$

302 $H_2C=CH_2(Ag) \Leftrightarrow (Ag)HC=CH_2 + H$

303 $H_2C=CH_2(Ag) \Leftrightarrow H_2C=CH_2 + Ag$

304 $H_2C=CH_2(Ag) \Leftrightarrow H_2C + H_2C(Ag)$

305 $(Ag)H_2C=CH_2 \Leftrightarrow H_2C=CH_2 + Ag$

306 $(Ag)H_2C=CH_2 \Leftrightarrow (Ag)HC=CH_2 + H$

307 $(Ag)H_2C=CH_2 \Leftrightarrow HC=CH_2(Ag) + H$

308 $(Ag)H_2C=CH_2 \Leftrightarrow H_2C(Ag) + CH_2$

309 $(Ag_2)H_2C=C(Ag) \Leftrightarrow (Ag)C=CH_2(Ag) + Ag$

310 $(Ag_2)H_2C=C(Ag) \Leftrightarrow (Ag)C=CH(Ag_2) + H$

311 $(Ag_2)H_2C=C(Ag) \Leftrightarrow (Ag_2)H_2C=C + Ag$

312 $(Ag_2)H_2C=C(Ag) \Leftrightarrow H_2C(Ag_2) + C(Ag)$

313 $(Ag_2)H_2C=CH \Leftrightarrow (Ag_2)H_2C=C + H$

314 $(Ag_2)H_2C=CH \Leftrightarrow HC=CH_2(Ag) + Ag$

315 $(Ag_2)H_2C=CH \Leftrightarrow HC=CH(Ag_2) + H$

316 $(Ag_2)H_2C=CH \Leftrightarrow H_2C(Ag_2) + CH$

317 $(Ag)C=CH_2(Ag) \Leftrightarrow C=CH_2(Ag) + Ag$

318 $(Ag)C=CH_2(Ag) \Leftrightarrow (Ag)C=CH(Ag) + H$

319 $(Ag)C=CH_2(Ag) \Leftrightarrow H_2C=C\text{-}Ag + Ag$

320 $(Ag)C=CH_2(Ag) \Leftrightarrow C(Ag) + H_2C(Ag)$

321 $(Ag)HC=C(Ag_2) \Leftrightarrow HC=C(Ag_2) + Ag$

322 $(Ag)HC=C(Ag_2) \Leftrightarrow (Ag)C=C(Ag_2) + H$

323 $(Ag)HC=C(Ag_2) \Leftrightarrow (Ag)C=CH(Ag) + Ag$

324 $(Ag)HC=C(Ag_2) \Leftrightarrow HC\text{-}Ag + C(Ag_2)$

325 $(Ag_2)C=CH_2 \Leftrightarrow H_2C=C\text{-}Ag + Ag$

326 $(Ag_2)C=CH_2 \Leftrightarrow HC=C(Ag_2) + H$

327 $(Ag_2)C=CH_2 \Leftrightarrow C(Ag_2) + CH_2$

328 $HC=CH_2(Ag) \Leftrightarrow C=CH_2(Ag) + H$

329 $HC=CH_2(Ag) \Leftrightarrow HC=CH\text{-}Ag + H$

330 $HC{=}CH_2(Ag) \Leftrightarrow CH{=}CH_2 + Ag$

331 $HC{=}CH_2(Ag) \Leftrightarrow CH + H_2C(Ag)$

332 $(Ag)HC{=}CH(Ag) \Leftrightarrow HC{=}CH\text{-}Ag + Ag$

333 $(Ag)HC{=}CH(Ag) \Leftrightarrow (Ag)C{=}CH(Ag) + H$

334 $(Ag)HC{=}CH(Ag) \Leftrightarrow (Ag)HC + (Ag)HC$

335 $(Ag)HC{=}CH_2 \Leftrightarrow H_2C{=}C(Ag) + H$

336 $(Ag)HC{=}CH_2 \Leftrightarrow HC{=}CH_2 + Ag$

337 $(Ag)HC{=}CH_2 \Leftrightarrow HC{=}CH(Ag) + H$

338 $(Ag)HC{=}CH_2 \Leftrightarrow HC\text{-}Ag + CH_2$

339 $(Ag)C{=}CH(Ag_2) \Leftrightarrow C{=}CH(Ag_2) + Ag$

340 $(Ag)C{=}CH(Ag_2) \Leftrightarrow (Ag)C{=}CH(Ag) + Ag$

341 $(Ag)C{=}CH(Ag_2) \Leftrightarrow (Ag)C{=}C(Ag_2) + H$

342 $(Ag)C{=}CH(Ag_2) \Leftrightarrow C(Ag) + HC(Ag_2)$

343 $HC{=}CH(Ag_2) \Leftrightarrow C{=}CH(Ag_2) + H$

344 $HC{=}CH(Ag_2) \Leftrightarrow HC{=}C(Ag_2) + H$

345 $HC{=}CH(Ag_2) \Leftrightarrow HC{=}CH\text{-}Ag + Ag$

346 $HC{=}CH(Ag_2) \Leftrightarrow CH + HC(Ag_2)$

347 $(Ag_2)H_2C{=}C \Leftrightarrow C{=}CH_2(Ag) + Ag$

348 $(Ag_2)H_2C{=}C \Leftrightarrow C{=}CH(Ag_2) + H$

349 $(Ag_2)H_2C{=}C \Leftrightarrow H_2C(Ag_2) + C$

350 $C{=}CH_2(Ag) \Leftrightarrow H_2C\text{-}Ag + C$

351 $C{=}CH_2(Ag) \Leftrightarrow H_2C{=}C + Ag$

352 $C{=}CH_2(Ag) \Leftrightarrow C{=}CH\text{-}Ag + H$

353 $H_2C{=}C(Ag) \Leftrightarrow CH_2 + C\text{-}Ag$

354 $H_2C{=}C(Ag) \Leftrightarrow HC{=}C\text{-}Ag + H$

355 $H_2C{=}C(Ag) \Leftrightarrow C{=}CH_2 + Ag$

356 $(Ag)C{=}CH(Ag) \Leftrightarrow C{=}CH(Ag) + Ag$

357 $(Ag)C{=}CH(Ag) \Leftrightarrow (Ag)C{=}C(Ag) + H$

358 $(Ag)C{=}CH(Ag) \Leftrightarrow HC{=}C(Ag) + Ag$

359 $HC{=}C(Ag_2) \Leftrightarrow C(Ag_2) + CH$

360 $HC{=}C(Ag_2) \Leftrightarrow C{=}C(Ag_2) + H$

361 $HC{=}C(Ag_2) \Leftrightarrow HC{=}C(Ag) + Ag$

362 $(Ag)C{=}C(Ag_2) \Leftrightarrow C{=}C(Ag_2) + Ag$

363 $(Ag)C{=}C(Ag_2) \Leftrightarrow C\text{-}Ag + C(Ag_2)$

364 $(Ag)C{=}C(Ag_2) \Leftrightarrow (Ag)C{=}C(Ag) + Ag$

365 $HC{=}CH(Ag) \Leftrightarrow CH + HC\text{-}Ag$

366 $HC{=}CH(Ag) \Leftrightarrow C{=}CH\text{-}Ag + H$

367 $HC{=}CH(Ag) \Leftrightarrow HC{=}CH + Ag$

368 $HC{=}CH(Ag) \Leftrightarrow HC{=}C\text{-}Ag + H$

369 $C{=}CH(Ag_2) \Leftrightarrow HC(Ag_2) + C$

370 $C{=}CH(Ag_2) \Leftrightarrow C{=}CH(Ag) + Ag$

371 $C{=}CH(Ag_2) \Leftrightarrow C{=}C(Ag_2) + H$

372 $(Ag_2)H_2C \Leftrightarrow H_2C(Ag) + Ag$

373 $(Ag_2)H_2C \Leftrightarrow HC(Ag_2) + H$

374 $H_2C(Ag) \Leftrightarrow CH_2 + Ag$

375 $H_2C(Ag) \Leftrightarrow HC\text{-}Ag + H$

	376	$C{=}CH(Ag) \Leftrightarrow HC(Ag) + C$
	377	$C{=}CH(Ag) \Leftrightarrow C{=}C(Ag) + H$
	378	$C{=}CH(Ag) \Leftrightarrow C{=}CH + Ag$
	379	$HC{=}C(Ag) \Leftrightarrow C{=}C\text{-}Ag + H$
	380	$HC{=}C(Ag) \Leftrightarrow C{=}CH + Ag$
	381	$HC{=}C(Ag) \Leftrightarrow CH + C\text{-}Ag$
	382	$(Ag)C{=}C(Ag) \Leftrightarrow C{=}C\text{-}Ag + Ag$
	383	$(Ag)C{=}C(Ag) \Leftrightarrow C(Ag) + C(Ag)$
	384	$C{=}C(Ag_2) \Leftrightarrow C + C(Ag_2)$
	385	$C{=}C(Ag_2) \Leftrightarrow C{=}C\text{-}Ag + Ag$
	386	$HC(Ag_2) \Leftrightarrow C(Ag_2) + H$
	387	$HC(Ag_2) \Leftrightarrow HC\text{-}Ag + Ag$
	388	$HC(Ag) \Leftrightarrow CH + Ag$
	389	$HC(Ag) \Leftrightarrow C\text{-}Ag + H$
	390	$C{=}C(Ag) \Leftrightarrow C\text{-}Ag + C$
	391	$C{=}C(Ag) \Leftrightarrow C{=}C + Ag$
	392	$C(Ag_2) \Leftrightarrow C\text{-}Ag + Ag$
	393	$C_2H_4(S) \Leftrightarrow C_2H_3 + H(S)$
	394	$C_2H_4(S) \Leftrightarrow C_2H_2 + H_2(S)$
	395	$C_2H_4(S) \Leftrightarrow C_2H + H_3(S)$
	396	$C_2H_4(S) \Leftrightarrow C_2 + H_4(S)$
	397	$C_2H_4(S) \Leftrightarrow CH_4 + C(S)$
	398	$C_2H_4(S) \Leftrightarrow CH_3 + CH(S)$
	399	$C_2H_4(S) \Leftrightarrow CH_2 + CH_2(S)$
	400	$C_2H_4(S) \Leftrightarrow CH + CH_3(S)$
	401	$C_2H_4(S) \Leftrightarrow C + CH_4(S)$
	402	$H_2COCH_2(S) \Leftrightarrow C_2H_4O + Ag$
	403	$H_2COCH_2(S) \Leftrightarrow CH_3CHO + Ag$
	404	$C_2H_4O(S) \Leftrightarrow C_2H_4(S) + O$
	405	$C_2H_4O(S) \Leftrightarrow C_2H_4 + O(S)$
	406	$C_2H_4O(S) \Leftrightarrow C_2H_3 + OH(S)$
	407	$CH_3COO(S) \Leftrightarrow CH_3(S) + CO_2$
	408	$H_2O(S) \Leftrightarrow H_2O + Ag(S)$
	409	$C_3H_6(S) \Leftrightarrow C_3H_6 + Ag(S)$
	410	$O_2 + 2\ Ag \Leftrightarrow 2\ O(S)$
	411	$C_2H_4 + Ag \Leftrightarrow C_2H_4(S)$
	412	$C_2H_4O + Ag \Leftrightarrow C_2H_4O(S)$
	413	$CH_3CHO + Ag \Leftrightarrow CH_3CHO(S)$
	414	$O(S) + C_2H_4(S) \Leftrightarrow H_2COCH_2(S)$
	415	$CO_2 + Ag(S) \Leftrightarrow CO_2(S)$
	416	$C_3H_6 + Ag(S) \Leftrightarrow C_3H_6(S)$
	417	$H_2O + Ag(S) \Leftrightarrow H_2O(S)$
Exchange	1	$CH_3CHO + O(S) + Ag(S) \Leftrightarrow CH_3COO(S) + H(S)$
	2	$CH_3CHO + O(S) + Ag(S) \Leftrightarrow OH(S) + CH_3CO(S)$
	3	$OH(S) + OH(S) \Leftrightarrow H_2O + O(S) + Ag(S)$

4	$C_2H_6 + O(S) + Ag(S) \Leftrightarrow C_2H_5(S) + OH(S)$
5	$CH_3CO(S) + O(S) \Leftrightarrow CH_3COO(S) + Ag(S)$
6	$H(S) + O(S) \Leftrightarrow OH(S) + Ag(S)$
7	$H(S) + OH(S) \Leftrightarrow H_2O(S) + Ag(S)$
8	$CH_3(S) + O(S) \Leftrightarrow CH_2(S) + OH(S)$
9	$CH_2(S) + O(S) \Leftrightarrow CH(S) + OH(S)$
10	$CH(S) + O(S) \Leftrightarrow CO(S) + H(S)$
11	$CO(S) + O(S) \Leftrightarrow CO_2(S) + Ag(S)$
12	$CH_3(S) + C_2H_4(S) \Leftrightarrow C_3H_6(S) + H(S)$

8.4.5 Estimation of Heats of Formation and Chemisorption

The change in free energy, enthalpy as well as entropy of reactions are functions of activity of each species. If the activity values are available, it is trivial to estimate the changes in free energy and enthalpy of reactions to determine which direction a reaction proceeds. If experimental data is not available or activity values cannot be calculated, a cutoff value is used in place of activity values. Since enthalpy and entropy values depend strongly on temperature, values are typically tabulated at the standard temperature and pressure (298K and 1 atm) and adjusted to the desired temperature by heat capacity contributions.

Unless the experimental heats of chemisorption is readily available from literature, the values are computed using Bond Order Conservation approach based on the formulas derived for mono-, di- and polyatomic adsorbates (Chapter 4). The heats of chemisorption are then subtracted from the heats of formation of gas phase species to give the values for surface species. The enthalpies of gas phase species are available in NIST kinetics webbook.

8.4.6 Screening Criteria for Ethylene Epoxidation

Surface science experiments were conducted in literature to identify different surface intermediates: surface oxygen O(S); ethylene $C_2H_4(S)$; oxametallacycle $H_2COCH_2(S)$; hydroxyl

radical OH(S); acetate $CH_3COO(S)$ and water $H_2O(S)$. Hence, these species and participating reactions are included in the EO mechanism. Figure 8.6 shows how the thermodynamic cutoff affects the number of species in the surface mechanism.

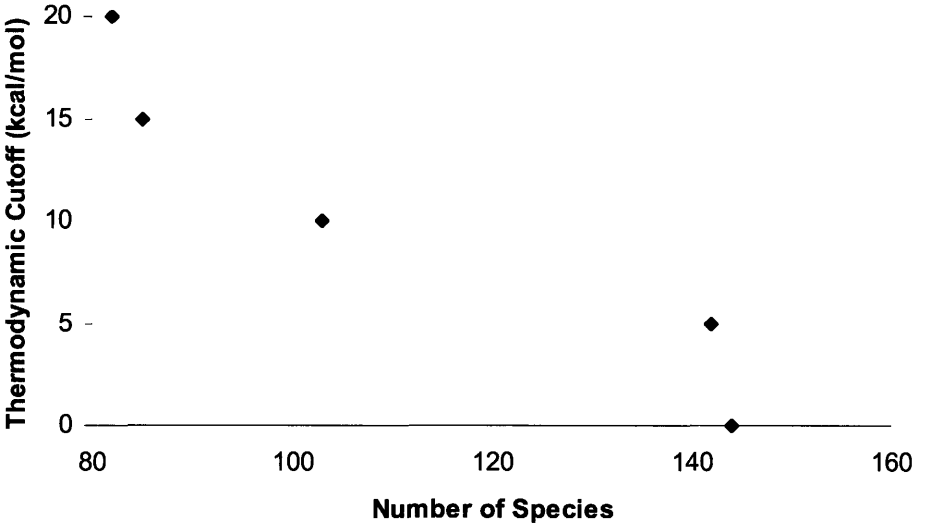

Figure 8.6 Number of Surface Species with Cutoff Heat of Chemisorption

There are about 40 species whose heats of chemisorption fall within 5 and 10 kcal/mol. For the current discussion, a cutoff value of 20 kcal/mol is used; species with chemisorption enthalpies above this value are thought to be stable on the surface. Table 8.9 lists species in the final surface mechanism.

Table 8.9 List of Species in the Surface Mechanism

Number	Species
1	H
2	O
3	C
4	Ag(S)
5	O(S)
6	AgO
7	CH

8	CO
9	CC
10	H(S)
11	O_2
12	CH_2
13	OC(S)
14	HCO
15	CAg(S)
16	CCH
17	CCO
18	CAg_2
19	HC-Ag
20	C=CH
21	H_2O
22	CO_2
23	OH(S)
24	CH(S)
25	CO(S)
26	C=C-Ag
27	CCH_2
28	OCH(S)
29	HCAg(S)
30	COC(S)
31	HCCO
32	CCAg(S)
33	OCAg(S)
34	$C=CH_2$
35	$C=CAg_2$
36	HC=CH
37	C=CHAg
38	HC=CAg
39	C=CAg(S)
40	CH_3
41	$CH_2(S)$
42	$CO_2(S)$
43	O-CH-Ag
44	$H_2O(S)$
45	$Ag_2C(S)$
46	H_2CAg
47	HCOC(S)
48	$OCCH_2$
49	COCH(S)
50	$HCAg_2(S)$
51	C_2H_3
52	HC=C-Ag(S)
53	HC=CHAg

54	Ag_2H_2C
55	$CH_4(S)$
56	C_2H_4
57	$H_2COC(S)$
58	CCHOAg(S)
59	HC-C-O-Ag(S)
60	$AgC{=}CHAg(S)$
61	$AgC{=}CAg_2(S)$
62	$HC{=}CAg_2(S)$
63	$C{=}CH_2Ag(S)$
64	$H_2C{=}CAg(S)$
65	$C_2H_4(S)$
66	C_2H_4O
67	CH_3CHO
68	$AgHC{=}CAg_2(S)$
69	$AgC{=}CHAg_2(S)$
70	$CH_3CO(S)$
71	$H_2COCH_2(S)$
72	$AgC{=}CH_2Ag(S)$
73	$AgH_2C{=}CAg_2(S)$
74	$Ag_2H_2C{=}CAg(S)$
75	$Ag_2C{=}CH_2Ag(S)$
76	$Ag_2HC{=}CHAg(S)$
77	$Ag_2HC{=}CH_2(S)$
78	$H_2C{=}CH_2Ag(S)$
79	$Ag_2HC{=}CH_2Ag(S)$
80	$AgH_2C{=}CHAg_2(S)$
81	$Ag_2H_2C{=}CHAg(S)$
82	$Ag_2H_2C{=}CH_2Ag(S)$

Table 8.10 shows the final surface mechanism. In general, collision theory and transition state theory are used to estimate the preexponentials for surface reactions generated in the EO mechanism. For Type 1 surface reactions, where a gas phase species (A) directly collides with the adsorbed species (B^*) or the vacant catalytic sites resulting in reactions, collision theory is used to set the upper bound while transition state theory is used for the lower bound. For Type 2 reactions where 2 surface species (A^* and B^*) react with each other, lower bound is given by transition state theory while upper bound is given by surface diffusion. For Type 3 reactions, where an adsorbed species (A^*) dissociatively desorbs to form gas and surface species, upper and

lower bounds of preexponential factors are calculated using transition state theory by considering mobile transition state and reactant, respectively. Details of the equations used to calculate bounds are provided in Chapter 4 (Section 4.2.6). Reactions 1 through 4 and 94 form the 5-step mechanism explained in Chapter 7. Preexponential factors for Reactions 1-3 and 94 are from Linic and Barteau and that for Reaction 4 is from our DFT calculations as explained in Chapter 7. Bond order conservation approach is used to estimate the activation energies of surface reactions (Section 4.2.4), except for Reactions 1-3 and 94 for which experimental heats of chemisorption are used.

Table 8.10 Final Surface Mechanism for Ethylene Epoxidation

No.	Reactions	A-factors (mol-cm-s units)		Activation Energies (kcal/mol)	
		Forward	Reverse	Forward	Reverse
Addition / Decomposition Reactions					
1	$O_2 + 2Ag(S) \Leftrightarrow 2O(S)$	9.87×10^{26}	3.80×10^{26}	0.0	49.0
2	$C_2H_4 + Ag(S) \Leftrightarrow C_2H_4(S)$	2.08×10^{11}	1.00×10^{13}	0.0	8.9
3	$H_2COCH_2(S) \Leftrightarrow C_2H_4O^* + Ag(S)$	4.00×10^{13}	1.67×10^{13}	16.0	11.0
4	$H_2COCH_2(S) \Leftrightarrow CH_3CHO^* + Ag(S)$	4.22×10^{12}	1.00×10^{13}	15.7	41.1
5	$H_2COC(S) \Leftrightarrow HCOC(S) + H$	1.00×10^{13}	1.00×10^{13}	135.7	0.0
6	$H_2COC(S) \Leftrightarrow CH_2 + OC(S)$	1.00×10^{13}	1.00×10^{13}	111.5	0.0
7	$H_2COC(S) \Leftrightarrow CCH_2 + AgO$	1.00×10^{13}	1.00×10^{13}	148.8	0.0
8	$H_2COC(S) \Leftrightarrow OCCH_2 + Ag(S)$	1.00×10^{13}	1.00×10^{13}	62.8	0.0
9	$OCH(S) \Leftrightarrow OC(S) + H$	1.00×10^{13}	1.00×10^{13}	15.3	0.0
10	$OCH(S) \Leftrightarrow HCO + Ag(S)$	1.00×10^{13}	1.00×10^{13}	38.1	0.0
11	$OCH(S) \Leftrightarrow HCAg(S) + O$	1.00×10^{13}	1.00×10^{13}	198.9	0.0
12	$HCAg(S) \Leftrightarrow CAg(S) + H$	1.00×10^{13}	1.00×10^{13}	136.4	0.0
13	$AgO \Leftrightarrow Ag(S) + O$	1.00×10^{13}	1.00×10^{13}	48.6	0.0
14	$COCH(S) \Leftrightarrow C + OCH(S)$	1.00×10^{13}	1.00×10^{13}	143.6	0.0
15	$COCH(S) \Leftrightarrow COC(S) + H$	1.00×10^{13}	1.00×10^{13}	91.2	0.0
16	$COCH(S) \Leftrightarrow HC(O)\text{-}C + Ag(S)$	1.00×10^{13}	1.00×10^{13}	0.0	0.0
17	$HCOC(S) \Leftrightarrow COC(S) + H$	1.00×10^{13}	1.00×10^{13}	91.2	0.0
18	$HCOC(S) \Leftrightarrow CH + OC(S)$	1.00×10^{13}	1.00×10^{13}	77.5	0.0
19	$HCOC(S) \Leftrightarrow HCCO + Ag(S)$	1.00×10^{13}	1.00×10^{13}	0.0	0.0
20	$OC(S) \Leftrightarrow CO + Ag(S)$	1.00×10^{13}	1.00×10^{13}	38.1	0.0
21	$OC(S) \Leftrightarrow AgO + C$	1.00×10^{13}	1.00×10^{13}	283.8	0.0

22	$OC(S) \Leftrightarrow CAg(S) + O$	1.00×10^{13}	1.00×10^{13}	211.0	0.0
23	$CCHOAg(S) \Leftrightarrow HC(O)\text{-}C + Ag(S)$	1.00×10^{13}	1.00×10^{13}	0.0	0.0
24	$CCHOAg(S) \Leftrightarrow CCH + AgO$	1.00×10^{13}	1.00×10^{13}	162.0	0.0
25	$HC\text{-}C\text{-}O\text{-}Ag(S) \Leftrightarrow HCCO + Ag(S)$	1.00×10^{13}	1.00×10^{13}	0.0	0.0
26	$HC\text{-}C\text{-}O\text{-}Ag(S) \Leftrightarrow CCH + AgO$	1.00×10^{13}	1.00×10^{13}	125.0	0.0
27	$CAg(S) \Leftrightarrow C + Ag(S)$	1.00×10^{13}	1.00×10^{13}	87.0	0.0
28	$COC(S) \Leftrightarrow C + OC(S)$	1.00×10^{13}	1.00×10^{13}	67.8	0.0
29	$COC(S) \Leftrightarrow CCO + Ag(S)$	1.00×10^{13}	1.00×10^{13}	29.4	0.0
30	$COC(S) \Leftrightarrow CCAg(S) + O$	1.00×10^{13}	1.00×10^{13}	196.7	0.0
31	$CCAg(S) \Leftrightarrow CC + Ag(S)$	1.00×10^{13}	1.00×10^{13}	24.1	0.0
32	$CCAg(S) \Leftrightarrow CAg(S) + C$	1.00×10^{13}	1.00×10^{13}	79.4	0.0
33	$OCAg(S) \Leftrightarrow CO + Ag(S)$	1.00×10^{13}	1.00×10^{13}	20.6	0.0
34	$OCAg(S) \Leftrightarrow CAg(S) + O$	1.00×10^{13}	1.00×10^{13}	193.6	0.0
35	$Ag_2H_2C{=}CH_2Ag(S) \Leftrightarrow Ag_2HC{=}CH_2Ag(S) + H$	1.00×10^{13}	1.00×10^{13}	99.6	0.0
36	$Ag_2H_2C{=}CH_2Ag(S) \Leftrightarrow Ag_2H_2C{=}CHAg(S) + H$	1.00×10^{13}	1.00×10^{13}	99.6	0.0
37	$AgH_2C{=}CHAg_2(S) \Leftrightarrow AgH_2C{=}CAg_2(S) + H$	1.00×10^{13}	1.00×10^{13}	100.5	0.0
38	$Ag_2H_2C{=}CHAg(S) \Leftrightarrow Ag_2H_2C{=}CAg(S) + H$	1.00×10^{13}	1.00×10^{13}	100.5	0.0
39	$Ag_2HC{=}CH_2Ag(S) \Leftrightarrow AgH_2C{=}CAg_2(S) + H$	1.00×10^{13}	1.00×10^{13}	100.5	0.0
40	$Ag_2H_2C{=}CAg_2(S) \Leftrightarrow Ag_2C{=}CHAg_2(S) + H$	1.00×10^{13}	1.00×10^{13}	103.4	0.0
41	$Ag_2C{=}CH_2Ag(S) \Leftrightarrow AgHC{=}CAg_2(S) + H$	1.00×10^{13}	1.00×10^{13}	120.2	0.0
42	$Ag_2HC{=}CHAg(S) \Leftrightarrow AgHC{=}CAg_2(S) + H$	1.00×10^{13}	1.00×10^{13}	99.6	0.0
43	$Ag_2HC{=}CHAg(S) \Leftrightarrow AgC{=}CHAg_2(S) + H$	1.00×10^{13}	1.00×10^{13}	99.6	0.0
44	$Ag_2HC{=}CH_2(S) \Leftrightarrow Ag_2C(S) + CH_2 + H$	1.00×10^{13}	1.00×10^{13}	22.0	0.0
45	$Ag_2HC{=}CH_2(S) \Leftrightarrow HCAg_2(S) + CH_2$	1.00×10^{13}	1.00×10^{13}	143.8	0.0
46	$H_2CCH_2Ag \Leftrightarrow C_2H_4 + Ag(S)$	1.00×10^{13}	1.00×10^{13}	5.6	0.0
47	$H_2C{=}CH_2Ag(S) \Leftrightarrow CH_2 + H_2CAg$	1.00×10^{13}	1.00×10^{13}	164.8	0.0
48	$Ag_2H_2C{=}CAg(S) \Leftrightarrow AgC{=}CHAg_2(S) + H$	1.00×10^{13}	1.00×10^{13}	120.2	0.0
49	$AgC{=}CH_2Ag(S) \Leftrightarrow AgC{=}CHAg(S) + H$	1.00×10^{13}	1.00×10^{13}	120.2	0.0
50	$AgHC{=}CAg_2(S) \Leftrightarrow AgC{=}CAg_2(S) + H$	1.00×10^{13}	1.00×10^{13}	139.1	0.0
51	$Ag_2C{=}CH_2(S) \Leftrightarrow HC{=}CAg_2(S) + H$	1.00×10^{13}	1.00×10^{13}	111.9	0.0
52	$Ag_2C{=}CH_2(S) \Leftrightarrow CAg_2 + CH_2$	1.00×10^{13}	1.00×10^{13}	209.4	0.0
53	$AgC{=}CHAg_2(S) \Leftrightarrow AgC{=}CAg_2(S) + H$	1.00×10^{13}	1.00×10^{13}	139.1	0.0
54	$C{=}CH_2Ag(S) \Leftrightarrow H_2C{=}C + Ag(S)$	1.00×10^{13}	1.00×10^{13}	24.1	0.0
55	$H_2C{=}CAg(S) \Leftrightarrow CH_2 + CAg(S)$	1.00×10^{13}	1.00×10^{13}	128.1	0.0
56	$H_2C{=}CAg(S) \Leftrightarrow HC{=}C\text{-}Ag(S) + H$	1.00×10^{13}	1.00×10^{13}	93.5	0.0
57	$H_2C{=}CAg(S) \Leftrightarrow C{=}CH_2 + Ag(S)$	1.00×10^{13}	1.00×10^{13}	5.6	0.0
58	$AgC{=}CHAg(S) \Leftrightarrow AgC{=}CAg + H$	1.00×10^{13}	1.00×10^{13}	139.1	0.0
59	$HC{=}CAg_2(S) \Leftrightarrow CAg_2 + CH$	1.00×10^{13}	1.00×10^{13}	199.3	0.0
60	$HC{=}CAg_2(S) \Leftrightarrow C{=}CAg_2 + H$	1.00×10^{13}	1.00×10^{13}	138.3	0.0
61	$HC{=}CHAg \Leftrightarrow CH + HC\text{-}Ag$	1.00×10^{13}	1.00×10^{13}	210.3	0.0
62	$HC{=}CHAg \Leftrightarrow HC{=}CH + Ag(S)$	1.00×10^{13}	1.00×10^{13}	10.8	0.0
63	$HC{=}CHAg \Leftrightarrow HC{=}C\text{-}Ag(S) + H$	1.00×10^{13}	1.00×10^{13}	98.7	0.0
64	$Ag_2H_2C \Leftrightarrow HCAg_2(S) + H$	1.00×10^{13}	1.00×10^{13}	84.4	0.0
65	$H_2CAg \Leftrightarrow CH_2 + Ag(S)$	1.00×10^{13}	1.00×10^{13}	12.9	0.0

66	$H_2CAg \Leftrightarrow HC\text{-}Ag + H$	1.00×10^{13}	1.00×10^{13}	84.4	0.0
67	$C{=}CHAg \Leftrightarrow HCAg + C$	1.00×10^{13}	1.00×10^{13}	179.8	0.0
68	$C{=}CHAg \Leftrightarrow C{=}CAg(S) + H$	1.00×10^{13}	1.00×10^{13}	125.0	0.0
69	$C{=}CHAg \Leftrightarrow C{=}CH + Ag(S)$	1.00×10^{13}	1.00×10^{13}	10.8	0.0
70	$HC{=}CAg \Leftrightarrow C{=}CH + Ag(S)$	1.00×10^{13}	1.00×10^{13}	24.1	0.0
71	$HC{=}CAg \Leftrightarrow CH + C\text{-}Ag(S)$	1.00×10^{13}	1.00×10^{13}	136.3	0.0
72	$C{=}CAg_2 \Leftrightarrow C + CAg_2$	1.00×10^{13}	1.00×10^{13}	142.4	0.0
73	$HCAg_2(S) \Leftrightarrow CAg_2 + H$	1.00×10^{13}	1.00×10^{13}	87.7	0.0
74	$HCAg \Leftrightarrow CH + Ag(S)$	1.00×10^{13}	1.00×10^{13}	30.3	0.0
75	$HCAg \Leftrightarrow CAg(S) + H$	1.00×10^{13}	1.00×10^{13}	24.7	0.0
76	$C{=}CAg(S) \Leftrightarrow CAg(S) + C$	1.00×10^{13}	1.00×10^{13}	79.4	0.0
77	$C_2H_4(S) \Leftrightarrow C_2H_3 + H(S)$	1.00×10^{13}	1.00×10^{13}	66.1	0.0
78	$C_2H_4(S) \Leftrightarrow CH_3 + CH(S)$	1.00×10^{13}	1.00×10^{13}	29.9	0.0
79	$C_2H_4(S) \Leftrightarrow CH_2 + CH_2(S)$	1.00×10^{13}	1.00×10^{13}	87.4	0.0
80	$C_2H_4(S) \Leftrightarrow C + CH_4(S)$	1.00×10^{13}	1.00×10^{13}	166.4	0.0
81	$H_2O(S) \Leftrightarrow H_2O + Ag(S)$	1.00×10^{13}	1.00×10^{13}	0.0	0.0
82	$C_3H_6(S) \Leftrightarrow C_3H_6 + Ag(S)$	1.00×10^{13}	1.00×10^{13}	5.6	0.0
83	$C_2H_4O + Ag(S) \Leftrightarrow C_2H_4O(S)$	1.00×10^{13}	1.00×10^{13}	5.0	3.0
84	$C_2H_4 + Ag(S) \Leftrightarrow C_2H_4(S)$	1.00×10^{13}	1.00×10^{13}	0.0	7.6
85	$CH_3COO(S) \Leftrightarrow CH_3(S) + CO_2$	1.00×10^{13}	1.00×10^{13}	0.0	94.1
86	$CO_2 + Ag(S) \Leftrightarrow CO_2(S)$	1.00×10^{13}	1.00×10^{13}	95.5	0.0
Isomerization Reactions					
87	$H_2COCH2(S) \Leftrightarrow C_2H_4O(S)$	1.00×10^{13}	1.00×10^{13}	2.0	0.0
88	$H_2COCH2(S) \Leftrightarrow CH_3CHO(S)$	1.00×10^{13}	1.00×10^{13}	0.0	25.6
89	$H_2COC(S) \Leftrightarrow H_2C{=}CO(S)$	1.00×10^{13}	1.00×10^{13}	0.0	44.9
90	$OCH(S) \Leftrightarrow O\text{-}CH\text{-}Ag$	1.00×10^{13}	1.00×10^{13}	28.2	0.0
91	$COC(S) \Leftrightarrow C\text{-}O\text{-}C\text{-}Ag$	1.00×10^{13}	1.00×10^{13}	7.8	0.0
92	$CCAg(S) \Leftrightarrow C{=}C\text{-}Ag$	1.00×10^{13}	1.00×10^{13}	14.0	0.0
Exchange Reactions					
93	$CH_3CHO + O(S) + Ag(S) \Leftrightarrow OH(S) + CH_3CO(S)$	1.00×10^{22}	1.00×10^{18}	0.0	0.0
94	$C_2H_4(S) + O(S) \Leftrightarrow H_2COCH_2(S) + Ag(S)$	1.90×10^{26}	9.50×10^{27}	14.9	12.5
95	$OH(S) + OH(S) \Leftrightarrow H_2O + O(S) + Ag(S)$	1.00×10^{18}	1.00×10^{22}	0.0	57.2
96	$H(S) + O(S) \Leftrightarrow OH(S) + Ag(S)$	1.00×10^{18}	1.00×10^{18}	0.0	0.0
97	$OH(S) + Ag(S) \Leftrightarrow H(S) + O(S)$	1.00×10^{18}	1.00×10^{18}	11.6	0.0
98	$H(S) + OH(S) \Leftrightarrow H_2O(S) + Ag(S)$	1.00×10^{18}	1.00×10^{18}	0.0	3.8
99	$CH_2(S) + O(S) \Leftrightarrow CH(S) + OH(S)$	1.00×10^{18}	1.00×10^{18}	26.2	0.0
100	$CH(S) + O(S) \Leftrightarrow CO(S) + H(S)$	1.00×10^{18}	1.00×10^{18}	0.0	0.0
101	$CH_3CO(S) + O(S) \Leftrightarrow CH_3COO(S) + Ag(S)$	1.00×10^{18}	1.00×10^{18}	0.0	11.6
102	$CH_3(S) + C_2H_4(S) \Leftrightarrow C_3H_6(S) + H(S)$	1.00×10^{18}	1.00×10^{18}	9.6	0.0

8.5 Results

Important gas species produced in the extensive EO mechanism are C_2H_4O, CH_3CHO, H_2O, CO_2 and C_3H_6. Important surface intermediates generated are O(S), C_2H_4(S), H_2COCH_2(S), C_2H_4O(S), CH_3CHO(S), CO_2(S), H_2O(S), CH_3COO(S), C_3H_6(S) and OH(S). Predictions of the extensive EO mechanism are compared against data for different operating conditions corresponding to microreactor experiments available in literature [34]. As mentioned in Chapter 7, microreactor experiments and surface studies played a great role in understanding selectivity and identifying surface species in epoxidation. The surface science studies helped understand the stability of various intermediates, while reactor experiments helped measure the concentrations of various products produced. Series of experiments were conducted for varying temperatures on a Laser-LIGA catalyst at 5 bar, reactor residence time of 0.124 s, 5 L/h gas flow and 3% C_2H_4, 16.5% O_2 and N_2 as inerts in the feed to reactor. The extensive EO mechanism predicts a selectivity of 84% which is comparable to that predicted by the 5-step mechanism (Chapter 7). Conversion (0.5%) for the extensive mechanism is lower than that of the 5-step mechanism (95%), since additional surface species generated in the extensive mechanism occupies catalyst surface which reduce the sites available for ethylene conversion. There is little change in selectivity because the parallel branching and selectivity of oxametallacycle to epoxide and acetaldehyde are not affected by additional surface reactions resulting in series burning of acetaldehyde to form carbon dioxide. Hence, the effect of additional surface species generated by the extensive mechanism is more pronounced on conversion than selectivity. Figure 8.7 shows the variation of conversion with reactor temperature.

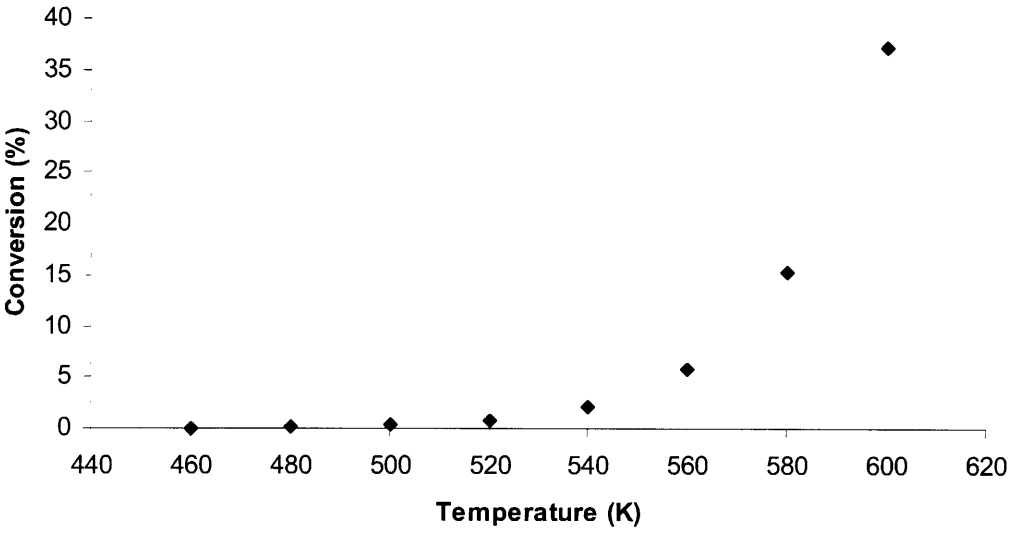

Figure 8.7 Variation of Predicted Conversion with Temperature for the Extensive EO Mechanism

As expected, conversion increases with temperature for the extensive mechanism. We also observe that conversion goes up remarkably after a temperature of 540K. As the temperature increases and the catalyst gets heated, additional surface species start desorbing resulting in increase of sites available for reaction. Figure 8.8 shows how the selectivity decreases with temperature.

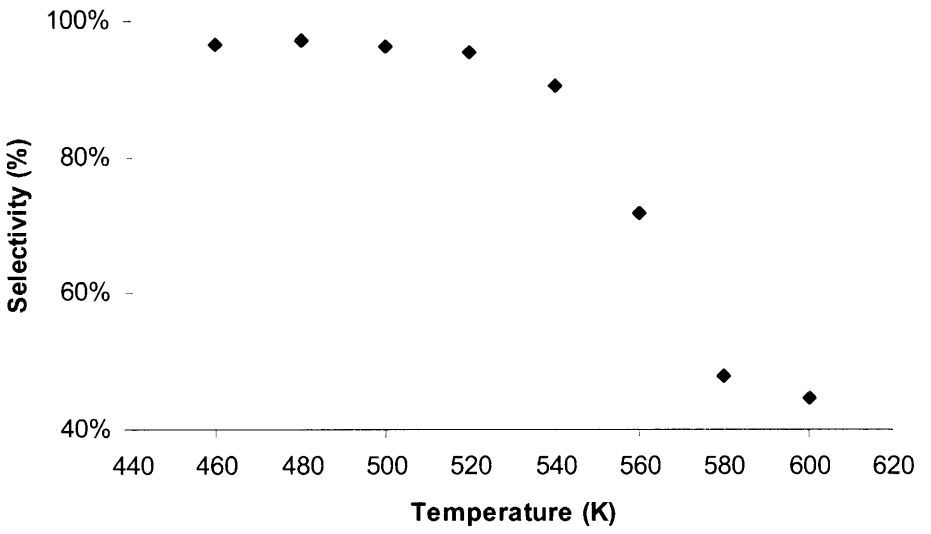

Figure 8.8 Variation of Predicted Selectivity with Temperature for the Extensive EO Mechanism

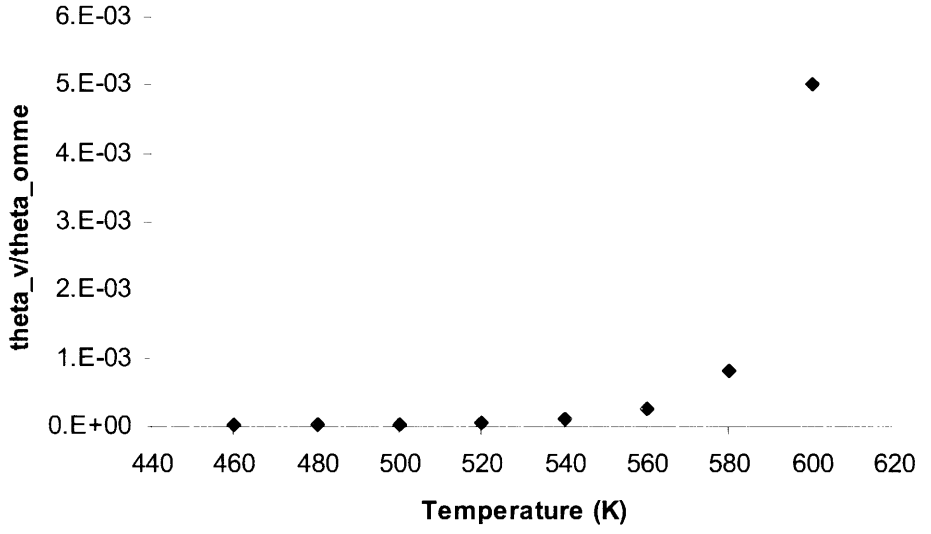

Figure 8.9 Variation of the Site-fraction Ratio with Temperature for the Extensive EO Mechanism

Though the site-fraction ratio is much less than 1, the overall value of the second term signifying reversibility (Eq. 7.6, Chapter 7) is comparable to 1, when the selectivity starts to fall off in Figure 8.9.

The extensive mechanism predicts formation of H_2O, CO_2 and C_3H_6 in addition to the 2 products, C_2H_4O and CH_3CHO. Formation and further reactions of water with hydroxyl radicals confirm the experimental findings for water on silver surface [33]. The reaction of adsorbed H_2O with pre-adsorbed oxygen to produce adsorbed hydroxyl groups was observed by EELS in the temperature range 205 to 255K. The predicted concentration of H_2O and CO_2 balance each other as expected, since the overall stoichiometry for complete oxidation of ethylene results in equal moles of the 2 compounds. C_3H_6 was observed in some industrial epoxidation reactors. Surface acetates were experimentally observed when acetaldehyde was fed over oxygen-dosed Ag(110) [32].

Surface species generated by the extensive EO mechanism includes species reported in the elementary mechanism published by Stegelmann et al. [35]. Table 8.11 lists the reactions with rate parameters for this elementary mechanism. The rate and thermodynamic parmaters are calculated using statistical thermodynamics from parameters of gas phase molecules and adsorbates. All parameters for gas phase molecules are extracted from standard thermodynamics data bases including NIST database. For surface species, some vibrational frequencies are taken from spectroscopic measurements like EELS, IR and Raman or DFT calculations, while the rest are assigned realistic values by guessing. Ground state energies are determined by simulation of TPD experiments and measurements of sticking coefficients, while rate constants are detemined from sticking measurements, TPD/TPR experiments, and steady-state kinetics on Ag(111). The enthalpy reported in Table 8.11 is the standard enethalpy of formation at 298K, to calculate the ground state energy of a species the sum of translational, rotational and vibrational energies are subtracted from the total enthalpy.

Table 8.11 Elementary Surface Mechanism Published by Stegelmann et al. [35]

No.	Reactions	A-factors (s^{-1} units)		Activation Energies (kJ/mol)	
		Forward	Reverse	Forward	Reverse
1	$O_2 + {}^* \Leftrightarrow O_2{}^*$	2.71×10^{5}	1.1×10^{12}	5.7	47.3
2	$O_2{}^* + {}^* \Leftrightarrow 2O^*$	4.0×10^{12}	8.0×10^{14}	75.0	157.5
3	$O_2 + 2O^* \Leftrightarrow 2OAgO(S)$	2.0×10^{7}	1.3×10^{15}	20.0	96.9
4	$C_2H_4 + O^* \Leftrightarrow C_2H_4AgO(S)$	7.2×10^{7}	2.2×10^{11}	0.0	37.1
5	$C_2H_4AgO(S) + OAgO(S) \Leftrightarrow H_2COCH_2AgO(S) + O^*$	9.0×10^{14}	5.3×10^{14}	112.0	183.3
6	$C_2H_4O + O^* \Leftrightarrow C_2H_4OAgO(S)$	1.95×10^{8}	4.8×10^{12}	0.0	39.1
7	$H_2COCH_2AgO(S) \Leftrightarrow C_2H_4OAgO(S)$	1.13×10^{13}	2.11×10^{12}	95.0	93.5
8	$H_2COCH_2AgO(S) \Leftrightarrow CH_3CHOAgO(S)$	9.0×10^{12}	4.5×10^{10}	95.0	204.3
9	$CH_3CHO + O^* \Leftrightarrow CH_3CHOAgO(S)$	2.9×10^{13}	2.6×10^{9}	4.4	4.4
10	$CH_3CHOAgO(S) + 6O^* \Leftrightarrow 2CO_2{}^* + 4OH^* + Ag(S)$	2.0×10^{20}	5.3×10^{13}	11.0	791.6
11	$C_2H_4 + Ag(S) \Leftrightarrow C_2H_4Ag(S)$	7.2×10^{7}	2.2×10^{11}	0.0	30.1
12	$C_2H_4AgO(S) + O^* \Leftrightarrow CH_2CHOHAgO(S) + {}^*$	4.0×10^{11}	3.1×10^{14}	32.0	42.8
13	$CH_2CHOHAgO(S) + O^* \Leftrightarrow CH_2CHOAgO(S) + OH^*$	2.6×10^{13}	1.3×10^{9}	86.0	106.1
14	$CH_2CHOAgO(S) + 5O^* \Leftrightarrow 2CO_2{}^* + 3OH^* + Ag(S)$	1.0×10^{20}	5.5×10^{13}	0.0	906.6
15	$2OH^* \Leftrightarrow H_2O^* + O^*$	1.4×10^{10}	1.0×10^{11}	65.6	50.0
16	$CO_2 + {}^* \Leftrightarrow CO_2{}^*$	3.6×10^{14}	1.0×10^{8}	0.0	0.0
17	$H_2O + {}^* \Leftrightarrow H_2O^*$	5.9×10^{14}	1.4×10^{9}	0.0	0.0

Surface species indicated by (S) signifies a metallic silver site, /O^* is a surface oxide site, and X^* and Y/O^* are an adsorbed species on metallic silver and surface oxide, respectively.

Figures 8.10-8.12 show how the conversion, selectivity and site fraction ratio between vacancy and oxametallacycle vary with temperature, as predicted by the Stegelmann mechanism [35].

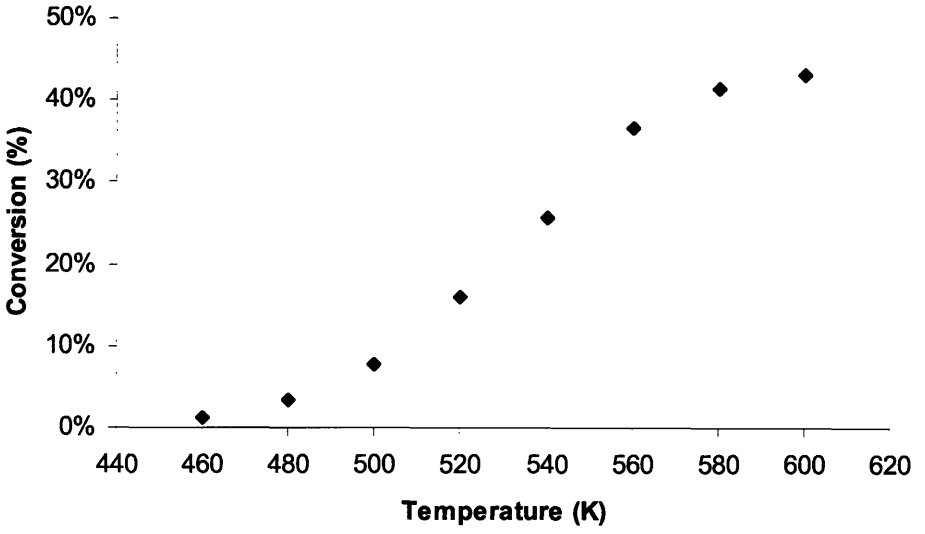

Figure 8.10 Variation of Predicted Conversion with Temperature for the Stegelmann Mechanism

Figure 8.11 Variation of Predicted Selectivity with Temperature for the Stegelmann Mechanism

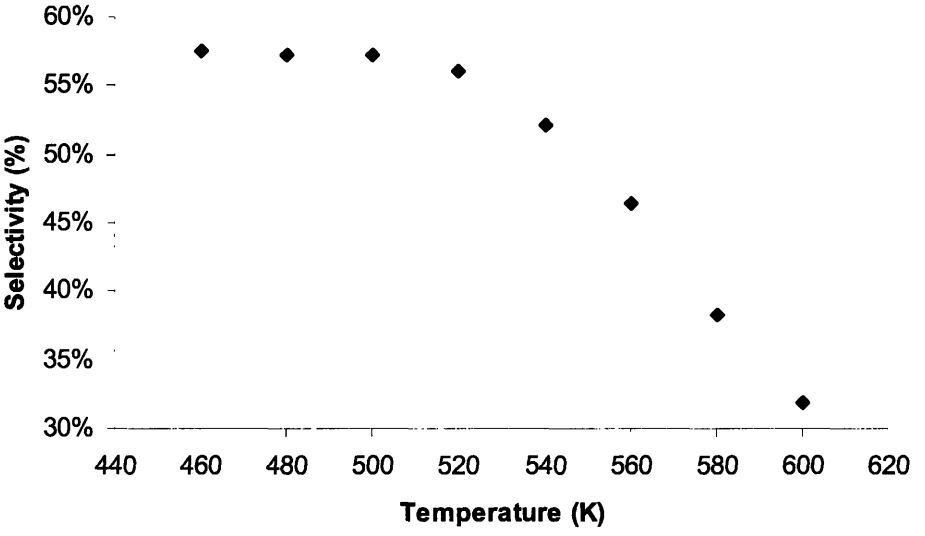

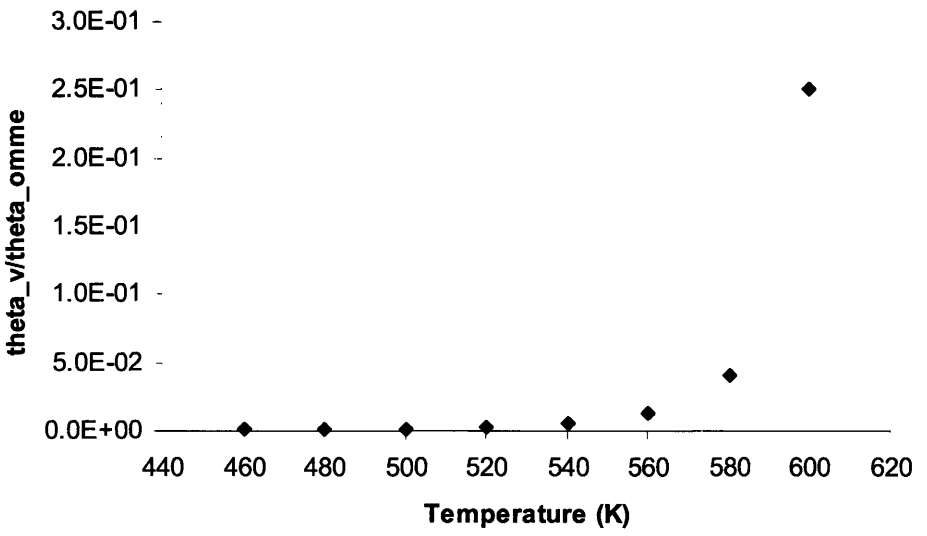

Figure 8.12 Variation of Predicted Site-fraction Ratio with Temperature for the Stegelmann Mechanism

Site-fraction ratio predicted by the Stegelmann mechanism is lower than that predicted by the extensive EO mechanism. This explains the lower predicted selectivity for the extensive EO mechanism.

8.6 Summary

In this chapter, we have applied the Decomposition Tree Approach for development of extenisve ethylene oxide (EO) mechanism. The EO mechanism extends the 5-step surface mechanism which was used in Chapter 7 to explain the selectivity and conversion observed in epoxidation reactors. Effect of additional species generated by the extensive mechanism is more pronounced on the conversion than the selectivity for EO as predicted for the microreactor conditions. Predicted selectivities are similar for the extensive and 5-step mechanisms, but conversion is significantly lower for the former than the latter. Conversion predicted by the extensive

mechanism increases, while selectivity decreases with temperature. Compared to the mechanism published by Stegelamann [35], the extensive EO mechanism predicts higher selectivity and the selectivity-conversion fall off occurs earlier in the conversion curve. This is attributed to the lower ratio of the site fractions between vacancy and oxametallacycle predicted by the extensive EO mechanism.

References

1. G. C. Achilles (1992). A systematic approach to mechanistic model building: developing and testing complex reaction mechanisms. Ph. D. Thesis, Carnegie Mellon University, Department of Chemical Engineering.
2. J. Gasteiger, M. Marsili, M. G. Hutchings, H. Saller, P. Rose and K. Rafeiner (1990). Models for the representation of knowledge about chemical reactions. *Journal of Chemical Informatics and Computer Science,* 30, 461-476.
3. E. S. Blurock (1995). Reaction system for modeling chemical reaction. *Journal of Chemical Informatics and Computer Science*, 35, 607-610.
4. P. A. Glaude, V. Warth, R. Fournet, F. Battin-Leclerc, G. Scacchi and G. M. Come (1998). Modelling of the oxidation of N-Octane and N-Decane using automatic generation of mechanisms. *International Journal of Chemical Kinetics*, 30, 949-959.
5. V. Warth, F. Battin-Leclerc, R. Fournet, P. A. Glaude, G. M. Co'me and G. Scacchi (2000). Computer based generation of reaction mechanisms for gas-phase oxidation. *Computational Chemistry (Oxford)*, 24, 541–560.
6. O. Sang Woo and L. J. Broadbelt (1998). Recovery of high-valued products from styrene-based polymers through coprocessing: Experiments and mechanistic modeling. *Cataysis Today*, 40, 121-140.
7. D. M. Matheu, W. H. Green, Jr. and J. M. Grenda (2003). Computational application of automated pressure-dependent mechanism generation: Reaction through cycloalkyl intermediates. *International Journal of Chemical Kinetics*, 35, 95-119.
8. L. J. Broadbelt, S. M. Stark and M. T. Klein (1994). Computer generated pyrolysis modeling: On-the-fly generation of species, reactions, and rates. *Industrial Engineering and Chemistry Research,* 33, 790-799.
9. L. J. Broadbelt, S. M. Stark and M. T. Klein (1995). Termination of computer-generated reaction mechanisms: Species rank-based convergence criterion. *Industrial Engineering and Chemistry Research*, 34, 2566-2573.
10. C. Chevalier, W. J. Pitz, J. Warnatz, C. K. Westbrook and H. Melenk (1992). Hydrocarbon ignition: Automatic generation of reaction mechanisms and applications to modeling of engine Shock. *Proceedings of the Combustion of Institute*, 24, 93-101.
11. S. J. Chinnick, D. L. Baulch and P. B. Ayscough (1988). An expert system for hydrocarbon pyrolysis reactions. *Chemometrics and Intelligent Laboratory Systems,* 5, 39-52.
12. A. M. Dean (1990). Detailed kinetic modeling of autocatalysis in methane pyrolysis. *Jounral of Physical Chemistry*, 94, 1432-1439.
13. M. Dente, S. Pierucci, S. E. Ranzi and G. Bussani (1992). New improvements in modeling kinetic schemes for hydrocarbon pyrolysis reactors. *Chemical Engineering Science*, 47, 2629-2634.
14. F. P DiMaio and P. G. Lignola (1992). KING. Kinetic Network Generator. *Chemical Engineering Science*, 51, 2713-2718.
15. W. H. Green, P. I. Barton, B. Bhattacharjee, D. M. Matheu, D. A. Schwer, J. Song, R. Sumathi, H. H. Carstensen, A. M. Dean and J. M. Grenda (2001). Computer construction of detailed chemical kinetic models for gas-phase reactors. *Industrial Engineering and Chemistry Research*, 40, 5362-5370.
16. J. M. Grenda, I. P. Androulakis and J. W. Bozzelli (2001). Combined use of automated kinetic mechanism Generation and reduction in the development of chemical reaction

models. *2nd Joint Meeting of the U.S. Sections of the Combustion Institute; The Combustion Institute.* Pittsburgh, PA.
17. J. M. Grenda, J. W. Bozzelli and A. M. Dean. Automated methods of treating chemically activated reactions in kinetic mechanism generation. *Eighth International Conference on Numerical Combustion.* Amelia Island, FL.
18. J. M. Grenda, A. M. Dean, W. H. Green, Jr. and P. K. Peczak (1998). Recent advances in automated kinetic mechanism generation. Presented at the Work-in-Progress Poster (Wipp) Session. *27th International Symposium on Combustion.* Boulder, CO.
19. D. M. Matheu, T. A. Lada, W. H. Green, Jr., A. M. Dean and J. M. Grenda (2001). Rate-based screening of pressure-dependent reaction networks. *Computer Physics and Communications,* 138, 237-249.
20. S. E. Prickett and M. L. Mavrovouniotis (1997). Construction of complex reaction systems Iii. An example: alkylation of olefins. *Computers in Chemical Engineering*, 21, 1325-1337.
21. A. S. Tomlin, T. Turanyi and M. J. Pilling (1997). Chapter 4: Mathematical tools for the construction, investigation and reduction of combustion mechanisms. In low-temperature combustion and autoignition. In: M. J. Pilling, ed. *Comprehensive Chemical Kinetics Series.* Vol. 35: Elsevier: Amsterdam.
22. D. J. Klinke and L. J. Broadbelt (1999). Construction of a mechanistic model of Fischer-Tropsch synthesis on Ni(111) and Co(0001) surfaces. *Chemical Engineering Science*, 54, 3379-3389.
23. R. Bounaceur, V. Warth, P. Marquaire, G. Scacchi, F. Domine', D. Dessort, B. Pradier and O. Brevart (2002). Modeling of hydrocarbons pyrolysis at low temperature. Automatic generation of free radicals mechanisms. *Journal of Analytical and Applied Pyrolysis*, 64, 103-122.
24. F. Battin-Leclerc (2002). Development of kinetic models for the formation and degradation of unsaturated hydrocarbons at high temperature. *Physical Chemistry and Chemical Physics*, 4, 2072-2078.
25. R. E. Valdes-Perez (1995). Computer-aided elucidation of reaction mechanisms: Partial oxidation of methane. in Methane and Alkane Conversion Chemistry, M.M. Bhasin and D.N. Slocum, eds., Plenum Press: New York.
26. R. E. Valdes-Perez (1992). Algorithm to generate reaction pathways for computer-assisted elucidation. *Journal of Computational Chemistry*, 13, 1079-1088.
27. D. M. Matheu, P. Aghalayam, W. H. Green, Jr. and J. M. Grenda (2002). Capturing pressure-dependence in automated mechanism generation for pyrolysis and combustion. *17th International Symposium on Gas Kinetics; IPTC.* Universita¨t Essen: Essen, Germany.
28. J. M. Grenda, I. P. Androulakis, A. M. Dean and W. H. Green, Jr. (2003). Application of computational kinetic mechanism generation to model the autocatalytic pyrolysis of methane. *Industrial & Engineering Chemistry Research*, 42, 1000-1010.
29. D. M. Matheu, A. M. Dean, J. M. Grenda and W. H. Green, Jr. (2003). Mechanism generation with integrated pressure dependence: A new model for methane pyrolysis. *Journal of Physical Chemistry A*, 107, 8552-8565.
30. J. Li, Z. Zhao, A. Kazakov and F. L. Dryer (2004). An updated comprehensive kinetic model of hydrogen combustion. *International Journal of Chemical Kinetics*, 36, 566-575.
31. S. Linic and M. A. Barteau (2003). Control of ethylene epoxidation selectivity by surface oxametallacycles. *Journal of American Chemical Society*, 125, 4034-4035.

32. A. G. Sault and R. J. Madix (1986a). The mechanism of acetate oxidation on Ag(110). *Surface Science*, 172, 598-614.
33. E. J. Stuve and R. J. Madix (1981). The adsorption and reaction of H2O on clean and oxygen covered Ag(110), *Surface Science*, 111, 11-25.
34. H. Kestenbaum, A. Lange de Oliviera, W. Schmidt, F. Schuth (2002). *Industrial Engineering and Chemistry Research*, 41, 710-719.
35. C. Stegelmann, N. C. Schiodt, C. T. Campbell and P. Stoltze (2004). Microkinetic modeling of ethylene oxidation over silver. *Journal of Catalysis*, 221, 630-649.

Chapter 9: Directions of Future Research

In this thesis, we have developed a computational methodology for estimating thermochemical and rate parameters, bond additivity corrections for advanced quantum chemistry methods and a surface mechanism for explaining yield and selectivity in ethylene epoxidation. More work needs to be done in the development of kinetic modeling in surface reactions, including:

- *Surface Chemistry Database of Rate Constants and Thermodynamic Parameters*

  Although computational methodologies have been developed in this work and there is an emerging literature for estimating thermochemical and rate parameters, a comprehensive kinetic database that compiles the parameters for a variety of surface reactions has not been developed yet. A database that includes reported kinetics results based on experiments and computational methods would be helpful to the catalyst community. The database should be designed for searching thermochemical and kinetics data based on specific species, reactions, and catalyst systems. Rate constant records for specified reactions can be found by searching the reaction database, while chemisorption enthalpies for species can be found by searching the thermo database. When queried, all rate constant and enthalpy records should be returned, with a link to details on the experimental measurements or theoretical calculations. Each rate constant record can contain the following information if available:

  1. Reactants and, if defined, reaction products.
  2. Rate parameters: preexponential factors, activation energies and their uncertainties.
  3. Temperature and pressure range of experiment or validity of theoretical calculation.

  Each enthalpy record can contain the following information:

1. Chemical species adsorbed.
2. Type of coordination.
3. Catalyst system.
4. Nature of binding sites or the surface morphology.
5. Chemisorption enthalpy at zero-coverage.
6. Coverage-dependent coefficients of other relevant species.
7. Temperature and pressure range of experiment or validity of theoretical calculation.

Figure 9.1 shows the structure of recommended surface chemistry database.

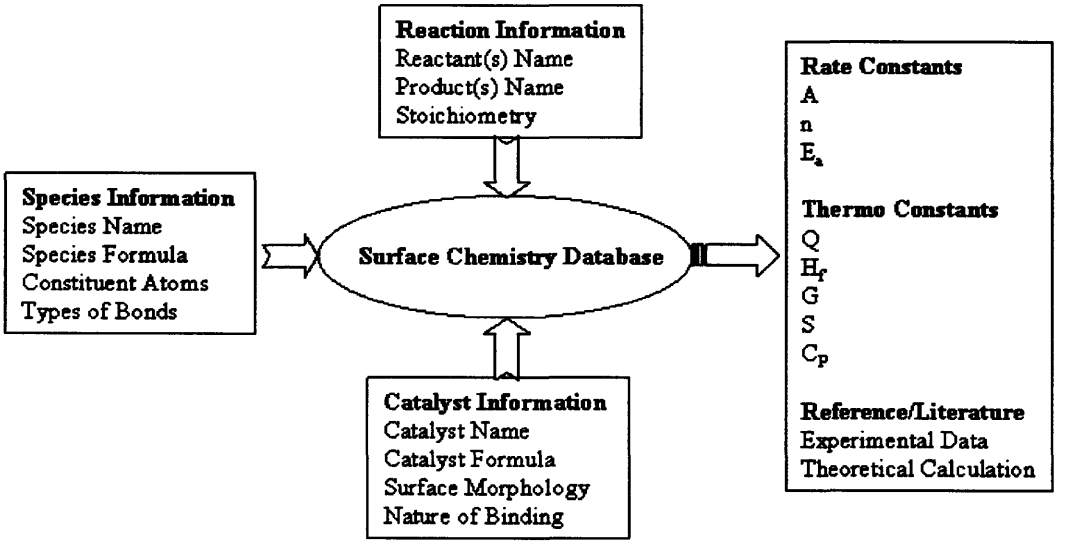

Figure 9.1 Structure for Surface Chemistry Database

- *Integration of Computational Methodologies with Reactor Modeling Software*

Our computational methodology helps in constructing surface reaction mechanisms, estimating rate and thermodynamic parameters using the Bond Order Conservation (BOC) approach for reactions on metals. This approach serves as a convenient first-order

approximation to a kinetic model for many catalytic process, and has the crucial advantage that one can be sure that a model constructed this way is thermodynamically consistent. For estimating the reaction barriers, the program uses the BOC approach which gives coverage-dependent activation energy as a nonlinear function of the chemisorption enthalpies. We recommend that the underlying equations to compute activation energies using BOC method be supplied as part of reactor modeling code. We recommend that 3 options be given to user of the code:

a) User sets the activation energy in one direction (possibly including linear coverage dependence); activation energy for the reverse is computed by the code using the coverage-dependent enthalpy of reaction.

b) User asks the code to estimate activation energy by BOC (UBI-QEP) method. The underlying equations needed to calculate the activation energies by BOC method can be supplied as part of the code.

c) User asks for BOC coverage dependence, but specifies most of the information required. Easier to implement than (b), but more demanding on the user.

- *Reinvestigation of Boron, Aluminum and Phosphorus compounds*

  Compared to former Bond Additivity Correction (BAC) procedures including, BAC-MP4 and BAC-G2 methods, BAC-G3B3 provides better estimates of thermochemistry for compounds involving the first 3 rows of periodic table, consistent with the improved accuracy of the composite G3-based quantum chemistry methods built into Gaussian® suite programs themselves. Some of the molecules need to be reinvestigated experimentally and theoretically, since the reported experimental values in literature are

not sufficiently accurate within 2-3 kcal/mol. and their values differ widely across different literature sources. In particular, better experimental data needs to be determined for the B, Al and P compounds: BH_3, BF_3, BCl_3, AlH_3, AlF_3, $AlCl_3$, PO, $P(OH)_3$ in order to determine the true predictive capability of the BAC procedure.

- *Deactivation Mechanism for Epoxidation Catalysts*

  Over the years deactivation of silver-based catalysts has been a subject of extensive research, with the aim of understanding its mechanism and improving catalyst stability. Several possible causes for catalyst deactivation, such as catalyst poisoning either by impurities [1,2] or by excess of chlorine-based promoters in the feed [3-5], accumulation of carbon deposits on catalyst surface [6-10], and increase of silver particles size [1,2,11-14] have been proposed. Deactivation kinetics of a commercial Ag/Al_2O_3 catalyst has been investigated using accelerated deactivation tests in a Berty-type gradientless recycle reactor. It has been shown that sintering is the main source for deactivation and deactivation kinetics can be described by a general power-law equation. Initial rates of ethylene oxide, carbon dioxide formation, and ethylene consumption have been measured with increasing temperature and oxygen concentration. However, no elementary kinetic model exists to explain the deactivation mechanism. It is recommended that a surface mechanism with elementary surface reactions be developed based on the observed experimental data. We recommend that the developed elementary reactions and overall stoichiometry be compared against the power-law model to test for validity. The predicted quantitative rates-of-production of surface species should be compared against experimental rates. The variation in size of silver particles due to sintering and effective

change in surface-to-volume ratio should be modeled using changes in surface site densities and number of active sites available for reactions.

- *Mechanism for Silver Chloride formation in Ethylene Epoxidation*

  Inside the epoxidation reactor, silver chloride is experimentally observed when chlorine is adsorbed on Ag(111) catalyst. Structural results explaining the role of silver chloride formed during chlorination of silver in catalytic reaction of ethylene epoxidation are presented [15]. The chloride nucleation on Ag(111) is found to occur on step edges and atomic terraces at low temperatures. Formation of silver clusters is hypothesized to explain a very high activity of chlorinated surface in ethylene epoxidation. A few ppm level of dichloroethane is found to have a much larger effect than thermal and oxygen-induced sintering of silver particles on catalyst stability under reaction conditions [16]. It is suggested that this effect is due to chloride-mediated intra-particle transport of silver. We recommend that a detailed surface mechanism modeling the underlying silver chloride reactions and the effect on activity of silver catalyst be developed. The characteristic time involved in formation of silver chloride crystals should be considered when modeling the nucleation mechanism. Theoretical calculations using quantum chemistry should be performed to compare the stability and reactivity of silver chloride against those of surface chlorine. It is recommended that activation energies of key reactions involving silver chloride be estimated to provide an insight into the chloride kinetics in epoxidation.

References

1. G. L. Montrasi, G. R. Tauszik, M. Solari and G. Leofanti (1983). Oxidation of ethylene to ethylene oxide: catalyst deactivation in an industrial run. *Applied Catalysis*, 5, 359-369.
2. E. P. S. Schouten, P. C. Borman and K. R. Westerterp (1996). Determination of the kinetics of ethene epoxidation. *Chemical Engineering and Processing*, 35, 43–55.
3. E. T. McBee, H. B. Hass and P. A. Wiseman (1945). Catalytic vapor phase oxidation of ethylene. *Industrial Engineering and Chemistry Research*, 37, 432–438.
4. S. A. Tan, R. B. Grant and R. M. Lambert (1986). Chlorine-oxygen interactions and the role of chlorine in ethylene oxidation over Ag(111). *Journal of Catalysis*, 100, 383–391.
5. K. L. Yeung, A. Gavriilidis, A. Varma and M. M. Bhasin (1998). Effects of 1,2 dichloroethane addition on the optimal silver catalyst distribution in pellets for epoxidation of ethylene. *Journal of Catalysis,* 174, 1–12.
6. J. T. Gleaves, A. G. Sault, R. J. Madix and J. R. Ebner (1990). Ethylene oxidation on silver powder: A tap reactor study. *Journal of Catalysis*, 121, 202–218.
7. I. E. Wachs and S. R. Kelemen (1981). The interaction of ethylene with surface carbonate and hydroxide intermediates on silver. *Journal of Catalysis*, 71, 78–87.
8. B. Grife, E. Blues and D. B. Smith (1984). Study of the effect of carbon dioxide on the catalytic properties of a silver catalyst in the oxidation of ethylene to ethylene oxide. *Applied Catalysis*, 10, 303–312.
9. S. A. Tan, R. B. Grant and R. M. Lambert (1987). Pressure dependence of ethylene oxidation kinetics and the effects of added CO_2 and Cs: A study on Ag(111) and Ag/α-Al_2O_3 catalysts. *Applied Catalysis*, 31, 159–177.
10. D. W. Park and G. Gau (1987). Ethylene epoxidation on a silver catalyst: Unsteady and steady state kinetics. *Journal of Catalysis*, 105, 81–94.
11. Y. Murakami, S. Komai and T. Hattori (1991). Accelerated sintering of platinum catalysts in reaction atmosphere for rapid estimation of catalyst life. *Studies in Surface Science and Catalysis*, 68, 645–652.
12. A. E. B. Presland, G. L. Price and D. L. Trimm (1972). Particle size effects during the sintering of silver oxidation catalysts. *Journal of Catalysis*, 26, 313–317.
13. X. E. Verykios, F. P. Stein and R. W. Coughlin (1980). Influence of metal crystallite size and morphology on selectivity and activity of ethylene oxidation catalyzed by supported silver. *Journal of Catalysis*, 66, 368–382.
14. G. B. Hoflund and D. M. Minahan (1996). Study of Cs-promoted, α-Alumina-supported silver, ethylene epoxidation catalysts: II. Effects of aging. *Journal of Catalysis*, 162, 48–53.
15. B. V. Andryushechkin, K. N. El'tsov, V. M. Shevlyuga, U. Bardi and A. Atrei. Local structure of thin AgCl films on silver surface. (2003). *Rossiiskaya Akademiya Nauk*, 59, 93-105.
16. S. Wodiunig, J. M. Keel, T. S. E. Wilson, F. W. Zemichael and R. M. Lambert (2003). AFM and XPS study of the sintering of realistic Ag/{0001}α-Al_2O_3 model catalysts under conditions of ethene epoxidation. *Catalysis Letters*, 87, 1-5.

Chapter 10: Conclusions

With the advancement of sophisticated surface science techniques and computational chemistry methodologies, developing surface mechanisms has become vital to understand the many complex surface reactions. As experimentalists and theoreticians get more information on the nature of surface species observed, it becomes increasingly important to integrate the existing knowledge with predictive kinetics to unravel the complex surface reactions. This thesis presents methodologies that serve as building blocks for generating elementary surface reactions and predicting kinetic parameters. Due to practical importance, the methodologies developed are tested for the heterogeneous catalytic partial oxidation of ethylene on silver. Various examples involving transition metal catalysts used in this thesis demonstrate the accuracy and computational efficiency of the methodologies developed.

Core of the thesis research is on development of tools that will estimate thermochemical and rate parameters, correct composite quantum chemistry methods for improved accuracy, build elementary surface mechanism by integrating knowledge from experiments and theory, and analyze sensitivities and uncertainties in the rate parameters of surface reactions. To achieve this goal, the following thesis works are performed:

- *Formulation of surface kinetics with coverage modifications for the thermodynamic and rate parameters.*

  A general, flexible and compact formulation accounting for thermodynamically consistent coverage-dependent surface kinetics is developed. A Software Requirements Specification (SRS) is prepared to modify the existing coverage-dependent functionality in CHEMKIN. Shifting the coefficients from reaction to thermo file of SURFACE

CHEMKIN enables the use of coverage dependence in the chemisorption enthalpies of surface species as well as activation energies of surface reactions. It has become easy to model the change in heats of formation of surface species and activation energies of surface reactions as the coverages evolve with time or distance along the reactor. Effectiveness of the modified approach is tested out on example problems involving silver-catalyzed ethylene epoxidation.

- *Integration of computational methodology as a software code that estimates coverage-dependent thermodynamic parameters and thermodynamically consistent rate parameters.*

  This thesis presents a new computational methodology for calculating temperature/coverage-dependent heats of formation, heat capacities and entropies. The direct extension of UBI-QEP approach treats polyatoms as pseudo diatoms which is a combination of 2 groups of atoms. Based on the extended UBI-QEP theory, chemisorpion enthalpy of each group is derived as a function of mono-coordinated chemisorption enthalpy and reduced sum of dissociation energies of atoms bound to the contact atom. However, the extended UBI-QEP equations don't predict chemisorption enthalpies that match with experimental data. Hence, we empirically modify the equations and replace the reduced sum by the regular sum of bond dissociation energies to predict chemisorption enthalpies of polyatomics. The predicted chemisorption enthalpies agree within 3 kcal/mol of experimental values for mono-, di- and polyatomic adsorbates coordinated via on-top, bridge and hollow sites with symmetric, asymmetric and chelating coordination structures on Ag(111), Ni(111), Ni(100), Ni(110), Pt(111),

Pd(111), Ag(110), Pd(110), Ag(100), Au(100) and Au(111) catalysts. The predicted tight physical upper and lower bounds for A-factors are validated against literature values for different catalyst reaction systems. MATLAB-based computer program are developed that outputs the thermodynamic and kinetic parameters as a Chemkin® formatted surface input file useful for higher level reactor calculations.

- *Development of Bond Additivity Corrections (BAC) for complex G3B3 and G3MP2B3 quantum chemistry methods.*

  BAC-G3B3 and BAC-G3MP2B3 parameters are developed for atomic, molecular and bond-wise corrections to heats of formation of open and closed shell molecules containing elements from first 3 rows of the periodic table. Compared to former BAC-MP4 and BAC-G2 methods, BAC-G3B3 provides better estimates of thermochemistry for compounds involving the first 3 rows of periodic table, consistent with the improved accuracy of the G3 methods themselves. Using a reference set and extended test set of molecules, the improved accuracy of BAC procedures is assessed.

- *Development of an elementary surface mechanism to explain the selectivity in ethylene epoxidation.*

  A 5-step surface mechanism that includes the 2 parallel branching reactions of oxametallacycle to epoxide and acetaldehyde is used to explain the selectivity to epoxide. The reversible equilibrium between oxametallacycle-epoxide, and the lower A-factor for acetaldehyde formation relative to epoxide formation explains the observed EO selectivities for experimental conditions. Falloff in selectivity-conversion curve for the

industrial plant reactors occurs earlier than the experimental microreactors. This is attributed to the kinetically significant reverse reaction of ethylene oxide to oxametallacycle for the plant conditions even at low conversions. For the experimental microreactor, the reverse reaction becomes important only at high conversions; until this point selectivity stays fairly constant since it is governed only by the 2 forward reactions of oxametallacycle. Increase in the predicted selectivities and yields with heat of formation of oxametallacycle offers a thermodynamic and operational insight into the role of chlorine as a promoter in epoxidation. This work identifies surface atomic oxygen as the reactive form of oxygen in epoxidation and oxygen covered silver as active phase of silver catalyst.

- *Application of uncertainty analysis to identify the important thermodynamic and rate parameters leading to uncertainties in ethylene oxide concentrations.*
  Deterministic Equivalent Modeling Method (DEMM) is used to study the effect of uncertainties in thermochemical and rate parameters on uncertainties in the ethylene oxide concentrations. Out of the many parameters, rate constant of the forward reaction leading to surface ethylene is found to be the most important uncertain parameter, zero-coverage chemisorption enthalpy of oxygen is the next important uncertain parameter followed by the self-coverage coefficient of oxygen.

- *Decomposition Tree Approach for the Development of Extensive EO Mechanism.*
  Decomposition Tree Approach is used to develop an extenisve ethylene oxide (EO) mechanism which extends the 5-step surface mechanism to explain the selectivity and

conversion observed in epoxidation reactors. Predicted selectivities are similar for the extensive and 5-step mechanisms, but conversion is significantly lower for the former than the latter due to the effect of additional species generated by the extensive mechanism. Compared to the mechanism published by Stegelamann [35], the extensive EO mechanism predicts higher selectivity. This is supported by the lower ratio of the site fractions between vacancy and oxametallacycle predicted by the extensive EO mechanism.

Appendix A: Software Documentation

Computer Code for Calculation of Thermochemical and Thermodynamically Consistent Rate Parameters

A.1 Introduction

SURF_THERM_KIN is a software code for the estimation of thermodynamic and thermodynamically consistent rate parameters of surface reactions. The code is used to calculate the thermodynamic and rate parameters of surface reactions and surface species on transition metal catalysts. Molecular chemisorption enthalpies and NASA polynomial coefficients are the thermodynamic parameters of surface species, while preexponential factors and activation energies are the rate parameters of surface reactions. They form the thermodynamic and rate data of the SURFACE Chemkin input file. This file could be integrated with the core utilities of the SURFACE KINETICS package of Chemkin software.

There are 2 calculation modules in the Code:

Module 1: Thermodynamic parameters

Module 2: Rate parameters

For both the modules, the user inputs the necessary parameters in a Microsoft Excel spreadsheet.

A.2 Calculation of Thermodynamic Parameters

Table A.1 lists the input variables for calculation of thermodynamic parameters. For each variable, the definition, variable type and an example are given. $C_2H_4(S)$ adsorbed on silver is

chosen as an example. Ethylene is attached to silver catalyst via the 2 carbon atoms with a coordination number of 2.

Table A.1 Input Variables for Calculation of Thermodynamic Parameters

Variable	Definition	Variable Type	Units	Example
		Catalyst Properties		
Catalyst Material	Material Name of the Catalyst	String	N/A	SILVER
Metallicity	Unimetallic = 1, Bimetallic = 2	Flag	N/A	1
Site Density	Density of sites on the catalyst	Floating point	moles/cm^2	1.05E-14
Standard State Entropy of the Catalyst	Entropy of the catalyst at 298K and 1 atm	Floating point	cal/mol/K	10.2
		Adsorbate Properties listed by Each Species		
		Atomic Information		
Species	Name of the adsorbate species	String	N/A	$C_2H_4(S)$
Atomicity	Monoatomic = 1 Diatomic = 2 Polyatomic = 3	Flag	N/A	1
Elements	Names of elements in the adsorbate species	String	N/A	C, H, AG
		Adsorbate-Surface Bond Properties		
Number of Atoms Bound to Surface	Number of atoms in the adsorbate bound to the catalyst surface	Integer	N/A	2
		Atoms Bound to Surface		
Atom1	Name of the first atom	String	N/A	C

	bound to the surface			
Atom2	Name of the second atom bound to the surface	String	N/A	C
Monocoordinated Atomic Chemisorption Heats (Table A.4)				
Atom 1	Chemisorption heat of Atom 1	Floating point	kcal/mol.	48.0
Atom 2	Chemisorption heat of Atom 2	Floating point	kcal/mol.	48.0
Coordination Number	Table A.2	Flag	N/A	2
Binding Strength	Table A.3	Flag	N/A	1
Coordination Structure	symmetric=1, asymmetric=2, chelating=3	Flag	N/A	1
Gas Phase Information				
Dissociation Energy of Bonds in Gas Molecule (Table A.6)				
Bond 1	Dissociation energy of bond 1	Floating point	kcal/mol.	174.1
Bond 2	Dissociation energy of bond 2	Floating point	kcal/mol.	221.4
Bond 3	Dissociation energy of bond 3	Floating point	kcal/mol.	0.0
Standard State Thermodynamic Properties of the Gas Molecule				
Enthalpy	Standard state enthalpy	Floating point	kcal/mol.	12.5
Heat Capacity	Standard state heat capacity	Floating point	cal/mol./K	10.3
Entropy	Standard state entropy	Floating point	cal/mol./K	52.4

A.2.1 Flag Variables

There are 5 flag variables in the input corresponding to the metallicity of the catalyst, atomicity of the adsorbate species, coordination number of the binding between the adsorbate and the catalyst, binding strength between adsorbate and catalyst and coordination structure. Metallicity refers to the nature of composition of the catalyst with the flag variable set to 1 for unimetallic catalyst and 2 for bimetallic (alloy) catalyst. Atomicity refers to the number of atoms in the adsorbate and the flag variable is 1, 2, or 3 for mono-, di- and polyatomic adsorbates, respectively. Coordination number of the binding between adsorbate and catalyst refers to the number of surface sites to which the adsorbate atoms are bound, and the flag variables are set depending on the nature of coordination and the type of catalyst surface. Definitions for common coordination numbers are given in Table A.2.

Table A.2 Coordination Number and Nature of Binding Site

Nature of Binding Site	Coordination Number
on-top	1
bridge	2
fcc(111) hollow hcp(001)	3
fcc(100) hollow	4
bcc(100) hollow	5

Figures A.1 through A.4 show the different binding sites.

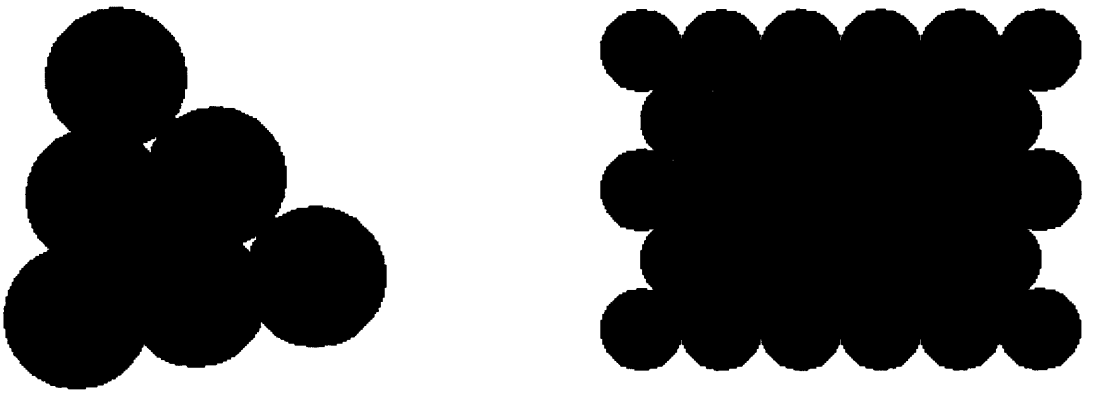

Figure A.1 Fcc(111) Unit Cell and Surface Plane

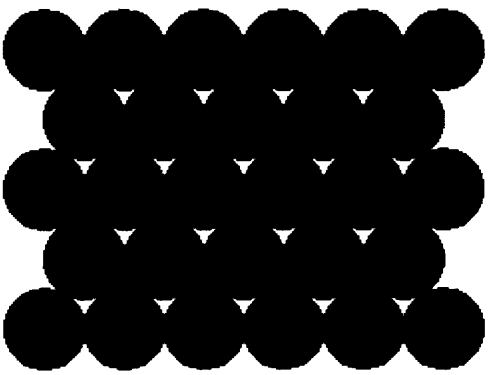

Figure A.2 Hcp(001) Unit Cell

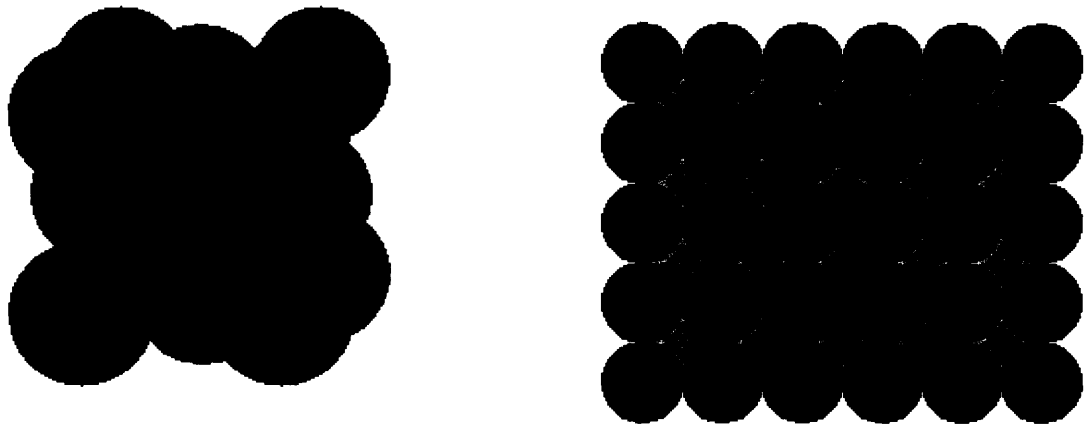

Figure A.3 Fcc(100) Unit Cell and Surface Plane

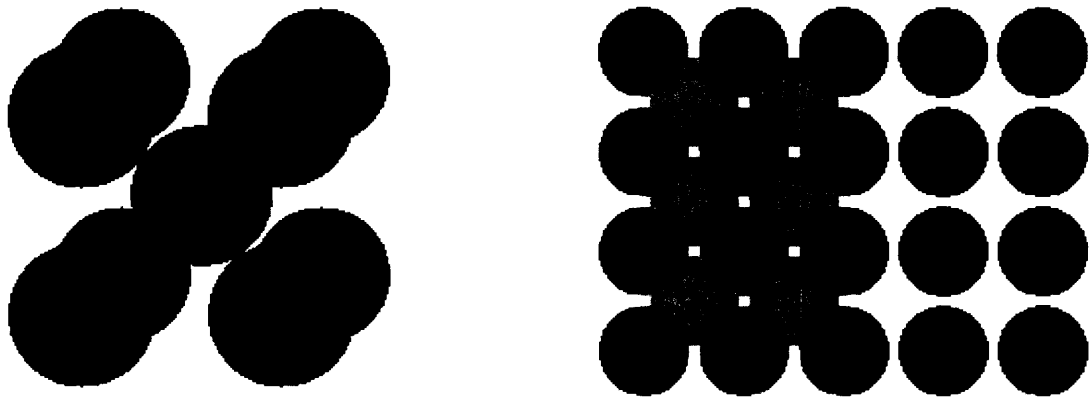

Figure A.4 Bcc(100) Unit Cell and Surface Plane

Binding strength is a flag variable referring to the strength of binding and the variable is 1, 2 or 3 for weak, intermediate or strong binding. Table A.3 lists the binding strengths of common molecules.

Table A.3 Binding Strength of the Adsorbate Molecules

Adsorbate Molecules	Examples	Binding Strength
Molecular radicals with delocalized radical electrons	O_2 NO	Weak binding
Closed shell molecules	H_2O, NH_3 and CH_3OH	Weak binding

Monovalent molecular radicals with tetra-valent central atoms	CH_3	Intermediate Binding
Molecular radicals with localized unpaired electrons	OH, SCH_3 and CH_3O	Strong binding

Coordination structure is a flag variable whose value is 1, 2 or 3 if the structure is symmetric, asymmetric or chelating, respectively. In symmetric coordination, the structure is symmetric about the contact atoms bound to the surface of the catalyst. Molecules such as acetylene HC $\equiv$CH, ethylene C_2H_4 and hydrogen peroxide HO--OH have symmetric coordinations, since the coordination structure is symmetric about the 2 C atoms in acetylene and ethylene and 2 O atoms in hydrogen peroxide. When there are dissimilar atom groups on either side of the contact atoms and the 2 contact atoms are directly bound to each other, the coordination structure is asymmetric. An example of asymmetric dicoordination is the binding of OCH_2 on a catalyst, where the O and C atom are bound to the catalyst surface. When the 2 contact atoms are not directly bound to each other, the coordination structure is chelating. An example of chelating coordination is the adsorption of HCOOH when the contact atoms are C atom and O atom of the hydroxyl part.

A.2.2 Monocoordinated Atomic Chemisorption Heats

The name of surface species is indicated by "(S)" in the string input, and this is used as an identifier for surface species. Monocoordinated atomic chemisorption heats correspond to the atomic heat of chemisorption of all the contact atoms bound to the catalyst in a hypothetical monocoordination mode. Please note that the monocoordinated chemisorption heats of atoms may be different from the experimental chemisorption heats of the same atoms when the true

coordination number of binding is greater than 1. The monocoordinated heats of chemisorption Q_{0A} is typically backed out from the experimental chemisorption heat $Q_A(n)$ and the coordination number n based on the UBI-QEP approach: $Q_{0A} = \frac{Q_A(n)}{2 - \frac{1}{n}}$. Here, n might be 3, 4 or 5 depending on whether the experimental heat of adsorption, $Q_A(n)$ corresponds to a three-fold fcc(111) or hcp(001) hollow, four-fold fcc(100) hollow or a five-fold bcc(100) hollow adsorption. The monocoordinated atomic chemisorption heats of common atoms on common transition metal catalysts are given in Table A.4 and the corresponding references for experimental atomic binding energies are given in Table A.5. The tables and the corresponding references are available in [1], the table is provided in this documentation for ready reference to look up numbers as inputs for the calculations.

Table A.4 Monocoordinated Atomic Heats of Chemisorption (kcal/mol.)

Catalyst / Atoms	Cu	Ag	Au	Ni	Pd	Pt
H	33.6	31.2	27.6	37.8	37.2	36.6
O	61.8	48.0	45.0	69.0	52.3	51.0
N	69.0	60.0	58.2	81.0	78.0	69.6
C	72.0	87.0	84.0	102.6	96.0	90.0
S	52.6	46.8	48.0	67.2	57.0	55.2

Table A.5 References for Atomic Heats of Chemisorption

Catalyst / Atoms	Cu	Ag	Au	Ni	Pd	Pt
H	[2,3]	[4]	est, [5]	[2,3]	[2]	[6]
O	[7]	[2,5]	[5]	[8,9]	[10]	[10]
N	Est	est	est	[2]	[2]	[10]
C	Est	est	est	[11]	[3]	[3]
S	[12]	[12]	est	[12]	est	[12]

A.2.3 Bond Dissociation Energies of Gas Phase Molecules

The dissociation energies of bonds in gas phase molecules correspond to the dissociation energies of all the bonds between the contact atom and rest of the molecule. In the example when ethylene is adsorbed to silver catalyst, the double bond between the 2 carbon atoms and 2 single bonds between C and H atoms are the bonds of interest. The energies needed to break the double bond and the 2 single bonds are 174.1 and 221.4 kcal/mol, respectively. Table A.6 lists the dissociation energies of common bonds.

Table A.6 Bond Dissociation Energies for Di- and Polyatomic Gas Phase Molecules

Molecule	Bond	Dissociation Energy (kcal/mol)
H_2	H-H	103
O_2	O-O	119
N_2	N-N	226
CO	C-O	256
NO	N-O	151
SO	S-O	125
OH	O-H	102
CH	C-H	81
NH	N-H	75
SH	S-H	82
CO_2	OC-O	127
NO_2	ON-O	73
SO_2	OS-O	132
SO_3	O_2S-O	83
CH_2	C-H_2	182
CH_3	C-H_3	293
CH_4	C-H_4	398
C_2H_5	C-C	99
	C-H	36
H_2O	HO-H	119
H_2O_2	HOO-H	88

	HO-OH	51
NH_2	N-H_2	169
NH_3	N-H_3	279
CH_3OH	CH_3O-H	104
	CH_3-OH	92
CH_3SH	CH_3S-H	87
	CH_3-SH	74
C_2H_4	H_2C-CH_2	175
C_2H_2	HC-CH	231
HCOOH	HCOO-H	106

Bond dissociation energies of many gas phase molecules and the standard state thermodynamic properties of gas phase molecules are available in literature and kinetics databases such as [13] and NIST kinetics database.

Figures A.5 through A.8 show how the input variables used in the calculation of thermodynamic parameters are entered in the worksheet. The user inputs the information in different pre-specified cells in the "Surface_Species_Information" worksheet. MATLAB code reads this information column-wise and writes into different vectors for reactants and products.

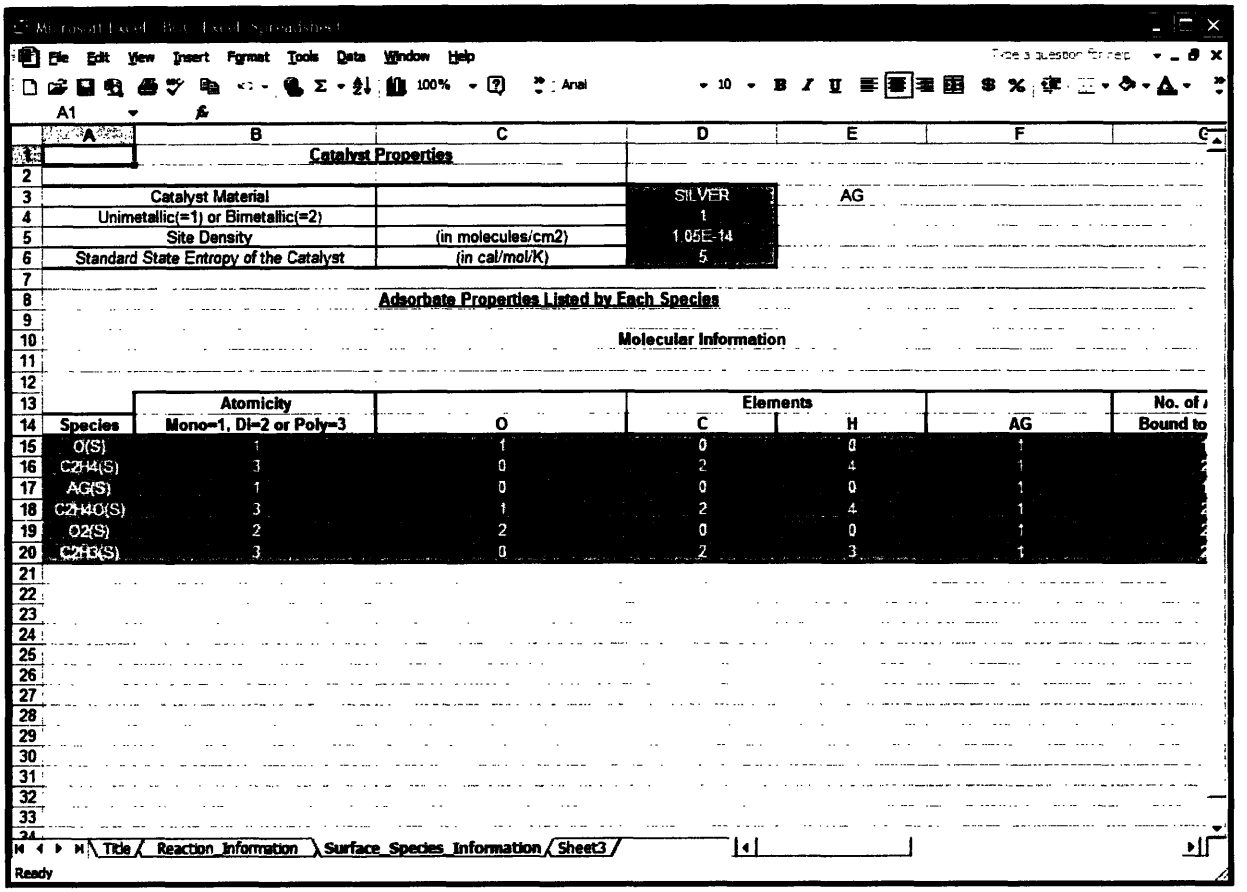

Catalyst Properties

Catalyst Material		SILVER	AG
Unimetallic(=1) or Bimetallic(=2)		1	
Site Density	(in molecules/cm2)	1.05E-14	
Standard State Entropy of the Catalyst	(in cal/mol/K)	5	

Adsorbate Properties Listed by Each Species

Molecular Information

	Atomicity	Elements				
Species	Mono=1, Di=2 or Poly=3	O	C	H	AG	No. of Bound to
O(S)	1	1	0	0	1	1
C2H4(S)	3	0	2	4	1	2
AG(S)	1	0	0	0	1	1
C2H4O(S)	3	1	2	4	1	2
O2(S)	2	2	0	0	1	2
C2H3(S)	3	0	2	3	1	2

Title / Reaction_Information / Surface_Species_Information / Sheet3

Ready

Figure A.5 Worksheet for Input Variables to Calculate Thermodynamic Parameters -Part 1

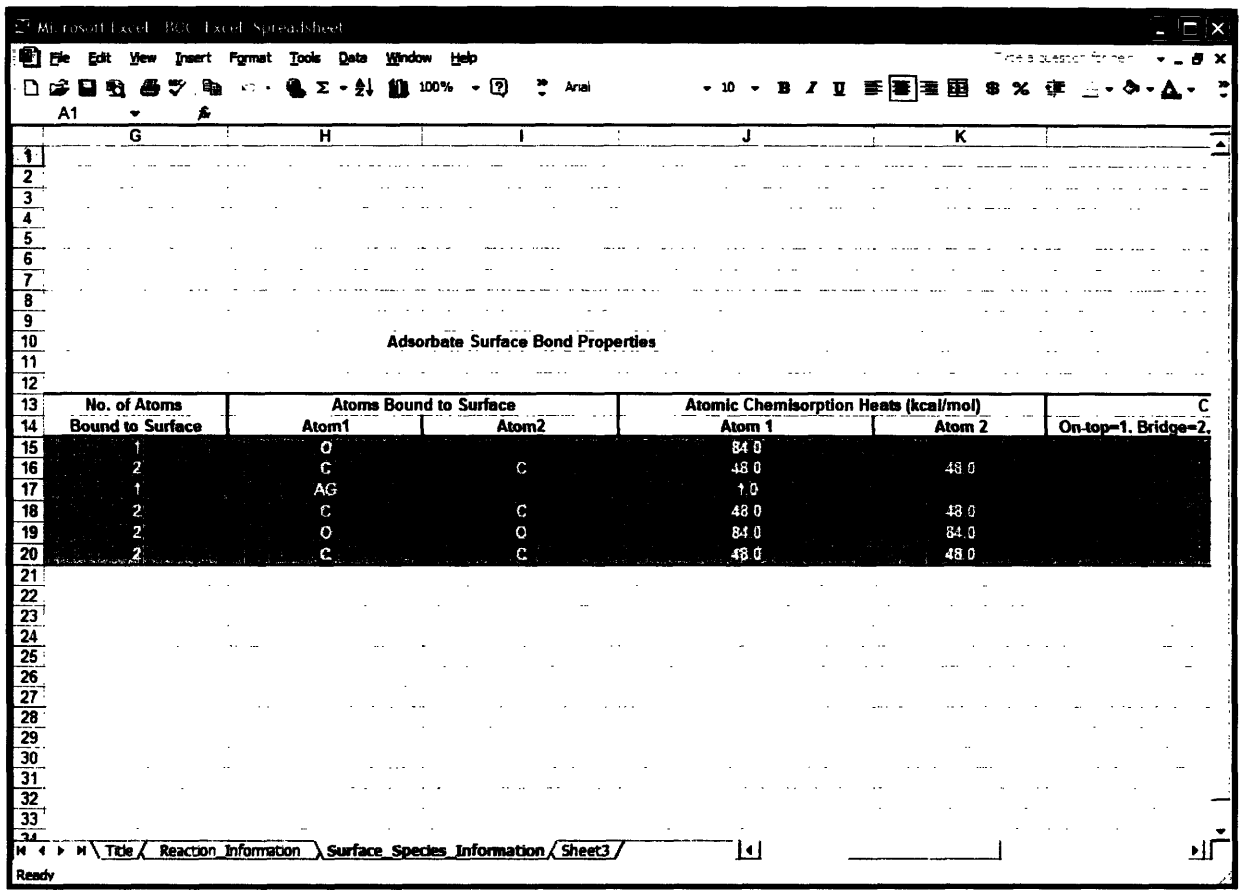

Adsorbate Surface Bond Properties

No. of Atoms Bound to Surface	Atoms Bound to Surface		Atomic Chemisorption Heats (kcal/mol)		C
	Atom1	Atom2	Atom 1	Atom 2	On-top=1. Bridge=2.
1	O		84.0		
2	C	C	48.0	48.0	
1	AG		1.0		
2	C	C	48.0	48.0	
2	O	O	84.0	84.0	
2	C	C	48.0	48.0	

Figure A.6 Worksheet for Input Variables to Calculate Thermodynamic Parameters -Part 2

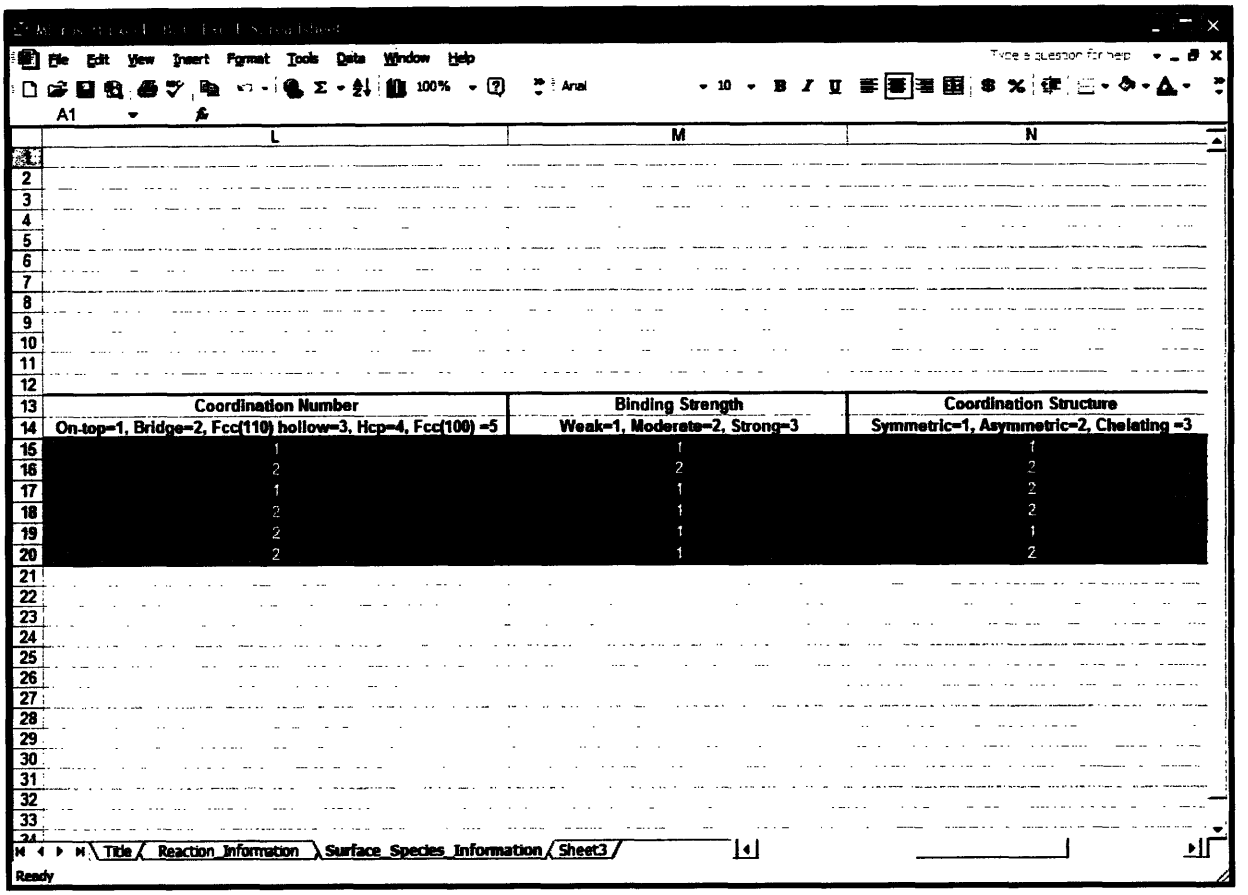

	L	M	N
13	Coordination Number	Binding Strength	Coordination Structure
14	On-top=1, Bridge=2, Fcc(110) hollow=3, Hcp=4, Fcc(100) =5	Weak=1, Moderate=2, Strong=3	Symmetric=1, Asymmetric=2, Chelating =3
15	1	1	1
16	2	2	2
17	1	1	2
18	2	1	2
19	2	1	1
20	2	1	2

Figure A.7 Worksheet for Input Variables to Calculate Thermodynamic Parameters -Part 3

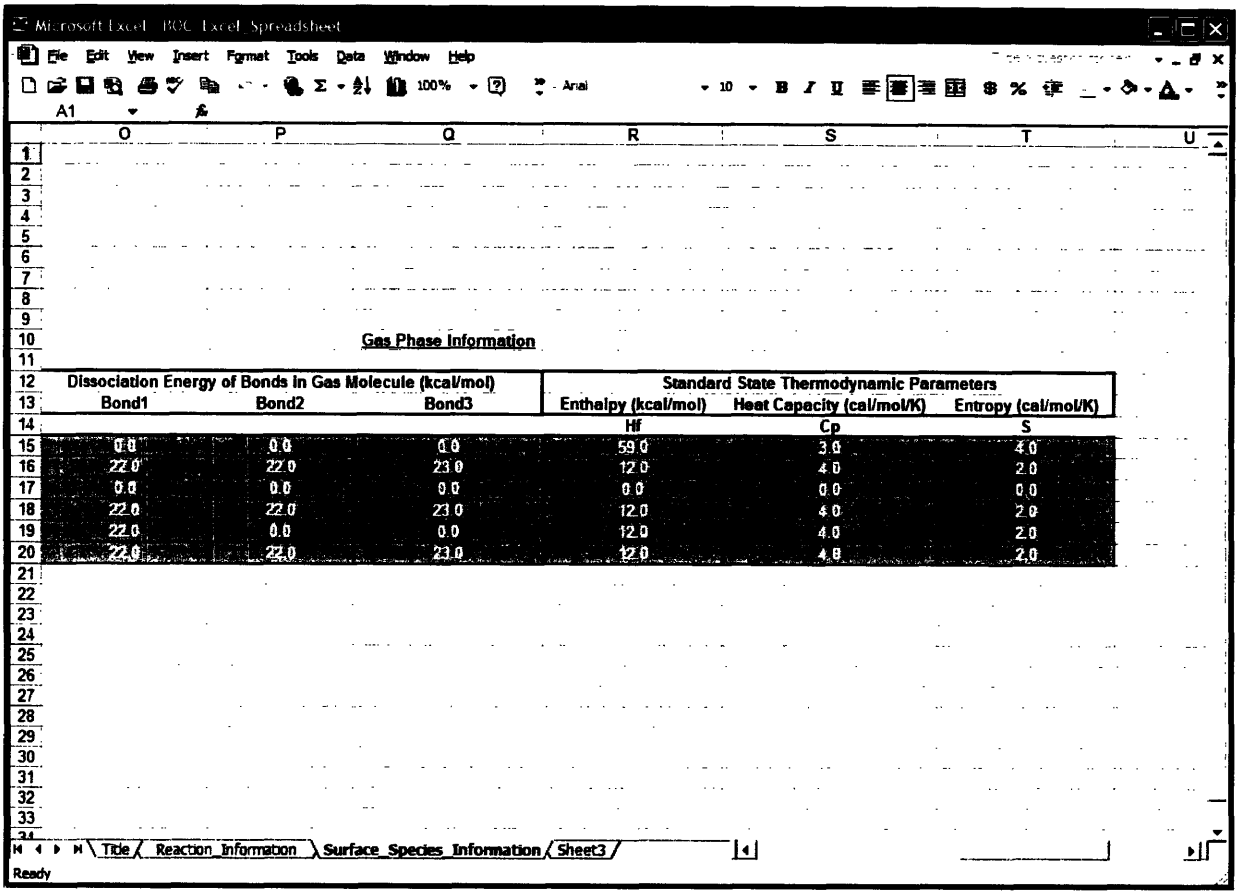

Gas Phase Information

Dissociation Energy of Bonds in Gas Molecule (kcal/mol)			Standard State Thermodynamic Parameters		
Bond1	Bond2	Bond3	Enthalpy (kcal/mol)	Heat Capacity (cal/mol/K)	Entropy (cal/mol/K)
			Hf	Cp	S
0.0	0.0	0.0	59.0	3.0	4.0
22.0	22.0	23.0	12.0	4.0	2.0
0.0	0.0	0.0	0.0	0.0	0.0
22.0	22.0	23.0	12.0	4.0	2.0
22.0	0.0	0.0	12.0	4.0	2.0
22.0	22.0	23.0	12.0	4.0	2.0

Figure A.8 Worksheet for Input Variables to Calculate Thermodynamic Parameters -Part 4

A.3 Calculation of Rate Parameters

Table A.7 lists the input variables for the calculation of rate parameters. For each variable, the definition, variable type and an example are given in the table. For illustration, the dissociative adsorption of oxygen on silver is chosen.

$$O_2 + 2\,AG(S) \Leftrightarrow 2\,O(S)$$

Table A.7 Input Variables for the Calculation of Rate Parameters

Variable	Definition	Variable Type	Units	Example
Reaction Number	Serial number of the reaction in a mechanism	Integer	N/A	1
Stoichiometry Reactant 1	Stoichiometric coefficient of first reactant	Floating point	N/A	1
Reactant 1	Name of the first reactant	String	N/A	O_2
Stoichiometry Reactant 2	Stoichiometric coefficient of second reactant (if it exists)	Floating point	N/A	2
Reactant 2	Name of the second reactant (if it exists)	String	N/A	AG(S)
Stoichiometry Product 1	Stoichiometric coefficient of first product	Floating point	N/A	2
Product 1	Name of the first product	String	N/A	O(S)
Stoichiometry Product 2	Stoichiometric coefficient of second product (if it exists)	Floating point	N/A	
Product 2	Name of the second product (if it exists)	String	N/A	
	Dissociation Energy of Bonds in Gas Molecules			
Reactant	Dissociation energy of bond broken in the reactant	Floating point	kcal/mol.	119.0
Product	Dissociation energy of bond formed in the product	Floating point	kcal/mol.	0.0
	Chemisorption Enthalpy of the Adsorbate-surface Bond			
Reactant	Enthalpy of the bond broken in the reactant	Floating point	kcal/mol.	0.0
Reactant	Enthalpy of the bond broken in the reactant	Floating point	kcal/mol.	0.0
Product	Enthalpy of the bond formed in the product	Floating point	kcal/mol.	84.0

Product	Enthalpy of the bond formed in the product	Floating point	kcal/mol.	84.0

In the above table, the string inputs for the surface species are indicated by "(S)" at the end of the string names. Species corresponding to a vacancy is indicated by the chemical formula of the catalyst material followed by the "(S)." For example, in the dissociative adsorption of oxygen on silver, the vacant sites participating in the reaction are indicated by AG(S). The "(S)" identifier for surface species and vacancy are quite important, since this identifier is used by the MATLAB code to recognize the number of gas phase species, surface species and vacant sites taking part in the reaction.

The dissociation energies of bonds in gas molecules are the bonds broken in the gas phase reactants and bonds formed in the gas phase products. The dissociation energies of bonds broken in gas phase reactants and bonds formed in gas phase products are specified as inputs for any general catalytic reaction, whether bonds are broken in the reactants and bonds are formed in the products in the particular reaction of interest. For those cases, where such bonds are not relevant, the input value for the corresponding bond dissociation energy is 0.0 kcal/mol. In the dissociative adsorption of oxygen, the double bond in diatomic oxygen is broken in the reactant, and no bond is formed as a gas phase product. Hence, the gas phase dissociation energy of the double bond broken in the reactant is 119 kcal/mol. and the gas phase dissociation energy of bond formed in the product is 0 kcal/mol. The bond dissociation energies of bonds in common gas phase molecules are available in Table A.6 and kinetics databases in literature such as [13] and NIST kinetics database.

Chemisorption enthalpy of the adsorbate-surface bond correspond to the atomic or molecular heats of chemisorption of reactants and products. The heats of chemisorption needs to

be input for all the surface reactants and products where the adsorbate-surface bonds are broken in the reactants and the adsorbate-surface bonds are formed in the product. The dissociation energies of adsorbate-surface bonds broken in reactants and bonds formed in products are specified as general inputs for any general catalytic reaction, whether bonds are broken in the reactants and bonds are formed in the products. For those cases, where such bonds are not relevant, the input value for the corresponding dissociation energy is 0.0 kcal/mol. In the dissociative adsorption of oxygen, no bond between the adsorbate and surface is broken in the reactant, and a bond between each atomic oxygen and silver catalyst is formed as a surface product. Hence, the chemisorption enthalpies of adsorbate-surface bonds broken in the reactants are each 0 and the chemisorption enthalpies of adsorbate-surface bonds formed in the product are each 84 kcal/mol, respectively.

The atomic and molecular chemisorption enthalpies for surface species calculated from the first module are used as inputs. The user has to specify all the surface species taking part in the reaction in the first module to calculate the thermodynamic parameters of all surface species taking part in the reaction.

Figures A.9 and A.10 illustrate how the input variables used in the calculation of rate parameters are entered in the worksheet. The user inputs the information in different pre-specified cells in the "Reaction_Information" worksheet. MATLAB code reads this information column-wise and collects different vectors pertaining to the reactants and products.

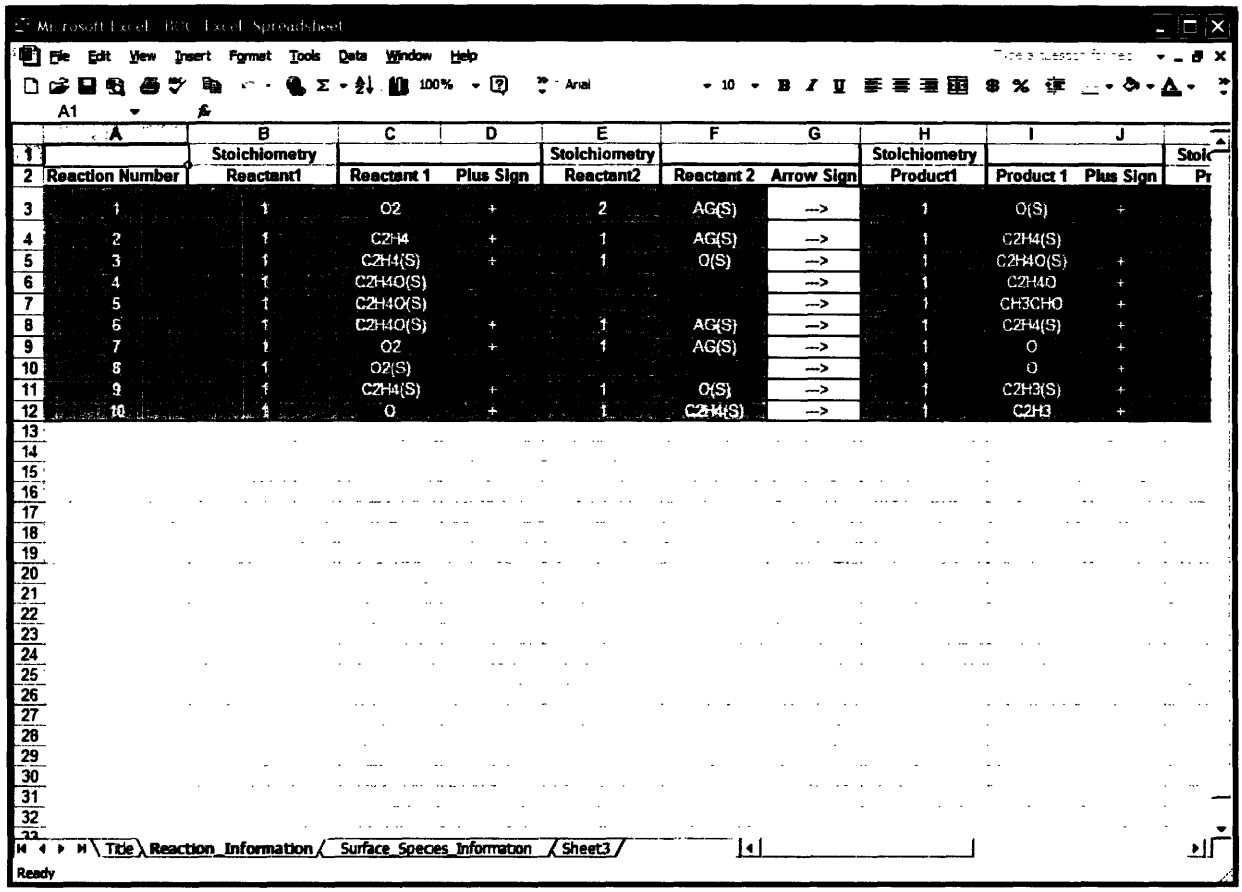

	A	B	C	D	E	F	G	H	I	J
1		Stoichiometry			Stoichiometry			Stoichiometry		
2	Reaction Number	Reactant1	Reactant 1	Plus Sign	Reactant2	Reactant 2	Arrow Sign	Product1	Product 1	Plus Sign
3	1	1	O2	+	2	AG(S)	-->	1	O(S)	+
4	2	1	C2H4	+	1	AG(S)	-->	1	C2H4(S)	
5	3	1	C2H4(S)	+	1	O(S)	-->	1	C2H4O(S)	+
6	4	1	C2H4O(S)				-->	1	C2H4O	+
7	5	1	C2H4O(S)				-->	1	CH3CHO	+
8	6	1	C2H4O(S)	+	1	AG(S)	-->	1	C2H4(S)	+
9	7	1	O2	+	1	AG(S)	-->	1	O	+
10	8	1	O2(S)				-->	1	O	+
11	9	1	C2H4(S)	+	1	O(S)	-->	1	C2H3(S)	+
12	10	1	O	+	1	C2H4(S)	-->	1	C2H3	+

Figure A.9 Worksheet for Input Variables to Calculate Rate Parameters -Part 1

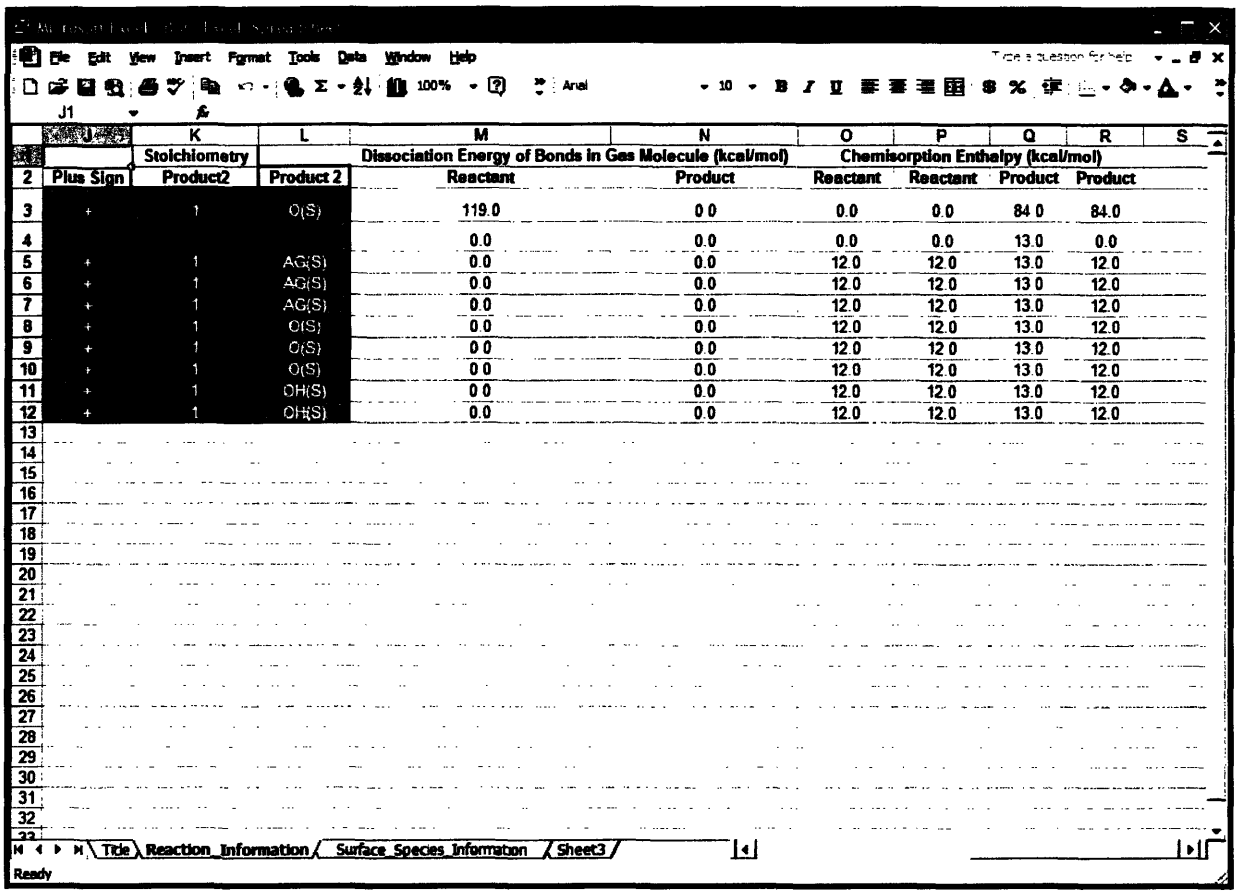

	J	K	L	M	N	O	P	Q	R	S
		Stoichiometry		Dissociation Energy of Bonds in Gas Molecule (kcal/mol)		Chemisorption Enthalpy (kcal/mol)				
2	Plus Sign	Product2	Product 2	Reactant	Product	Reactant	Reactant	Product	Product	
3	+	1	O(S)	119.0	0.0	0.0	0.0	84.0	84.0	
4				0.0	0.0	0.0	0.0	13.0	0.0	
5	+	1	AG(S)	0.0	0.0	12.0	12.0	13.0	12.0	
6	+	1	AG(S)	0.0	0.0	12.0	12.0	13.0	12.0	
7	+	1	AG(S)	0.0	0.0	12.0	12.0	13.0	12.0	
8	+	1	O(S)	0.0	0.0	12.0	12.0	13.0	12.0	
9	+	1	O(S)	0.0	0.0	12.0	12.0	13.0	12.0	
10	+	1	O(S)	0.0	0.0	12.0	12.0	13.0	12.0	
11	+	1	OH(S)	0.0	0.0	12.0	12.0	13.0	12.0	
12	+	1	OH(S)	0.0	0.0	12.0	12.0	13.0	12.0	

Figure A.10 Worksheet for Input Variables to Calculate Rate Parameters -Part 2

A.3.1 Look-up Tables and Databases

For ready reference by the user, the look-up tables and databases for the different input variables used in the calculation of thermodynamic and rate parameters are summarized below.

Table A.8 Look-up Tables and Databases for Different Input Variables

Input Variable	Tables and Databases
Coordination number and nature of binding site	Table A.2
Binding strength of the adsorbate molecules	Table A.3
Monocoordinated atomic heats of chemisorption (kcal/mol.)	Table A.4
Bond dissociation energies for diatomic and polyatomic molecules	Table A.6 [13]
Standard state thermodynamic properties	[14]
Atomic/Molecular chemisorption enthalpies	Output of Module 1

The code prompts the user to input the different atomic chemisorption enthalpies and the gas phase bond energies of different species in the worksheets. One of the future considerations is to link the code and spreadsheet to a database containing the atomic chemisorption enthalpies of standard adsorbates on common catalyst surfaces, and the dissociation energies of common bonds broken when different gas phase species are adsorbed on the surface of the catalyst. No prior knowledge of the bond dissociation energies or the chemisorption enthalpies would be required from the user and these values would be extracted and read from the database. If the database is included, the user will be allowed to choose between 2 options: 1. read the chemisorption enthalpies and bond dissociation energies from a database and 2. manually enter

more accurate values (if the values are available either through high level quantum calculations or sophisticated surface science studies).

A.3.2 Key Identifiers in the Input Variables of the Worksheet

Listed below are the key identifiers for specific input variables in the worksheet. These identifiers need to be input in the appropriate format so that the MATLAB code can recognize the inputs for calculating the thermodynamic and rate parameters.

Table A.9 Identifiers in Input Variables

Input variables	Identifiers	Function
Reactant 1 (2) Product 1 (2)	(S)	To identify surface species
	<Catalyst chemical formula>(S)	To identify vacant site
Plus sign	+	To separate reactants or products
Double arrow sign	$\rightleftharpoons$	To separate reactants from products

A.3.3 Chemkin® Formatted Output as Surface Chemkin Input File

The calculated thermodynamic and rate parameters form the the thermodynamic and reaction data in a Chemkin® formatted surface input file which could be linked to the set of core utilities and application programs of the SURFACE KINETICS software package. Figure A.11 shows a sample output. The output is a text file which can be saved as an appropriate input file (with file extension .inp) for SURFACE KINETICS calculation in surface Chemkin.

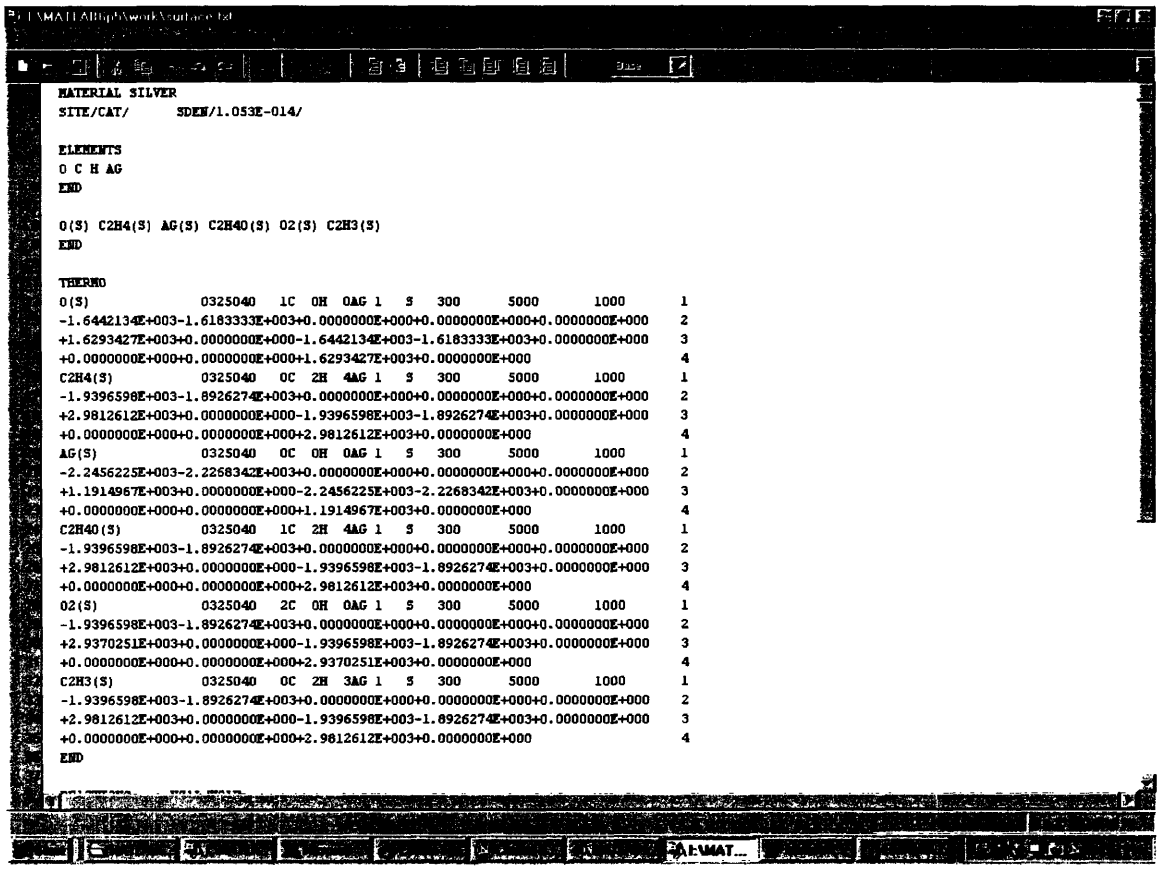

```
MATERIAL SILVER
SITE/CAT/      SDEN/1.053E-014/

ELEMENTS
O C H AG
END

O(S) C2H4(S) AG(S) C2H4O(S) O2(S) C2H3(S)
END

THERMO
O(S)              0325040   1C  0H  0AG 1   S   300      5000       1000       1
-1.6442134E+003-1.6183333E+003+0.0000000E+000+0.0000000E+000+0.0000000E+000    2
+1.6293427E+003+0.0000000E+000-1.6442134E+003-1.6183333E+003+0.0000000E+000    3
+0.0000000E+000+0.0000000E+000+1.6293427E+003+0.0000000E+000                   4
C2H4(S)           0325040   0C  2H  4AG 1   S   300      5000       1000       1
-1.9396598E+003-1.8926274E+003+0.0000000E+000+0.0000000E+000+0.0000000E+000    2
+2.9812612E+003+0.0000000E+000-1.9396598E+003-1.8926274E+003+0.0000000E+000    3
+0.0000000E+000+0.0000000E+000+2.9812612E+003+0.0000000E+000                   4
AG(S)             0325040   0C  0H  0AG 1   S   300      5000       1000       1
-2.2456225E+003-2.2268342E+003+0.0000000E+000+0.0000000E+000+0.0000000E+000    2
+1.1914967E+003+0.0000000E+000-2.2456225E+003-2.2268342E+003+0.0000000E+000    3
+0.0000000E+000+0.0000000E+000+1.1914967E+003+0.0000000E+000                   4
C2H4O(S)          0325040   1C  2H  4AG 1   S   300      5000       1000       1
-1.9396598E+003-1.8926274E+003+0.0000000E+000+0.0000000E+000+0.0000000E+000    2
+2.9812612E+003+0.0000000E+000-1.9396598E+003-1.8926274E+003+0.0000000E+000    3
+0.0000000E+000+0.0000000E+000+2.9812612E+003+0.0000000E+000                   4
O2(S)             0325040   2C  0H  0AG 1   S   300      5000       1000       1
-1.9396598E+003-1.8926274E+003+0.0000000E+000+0.0000000E+000+0.0000000E+000    2
+2.9370251E+003+0.0000000E+000-1.9396598E+003-1.8926274E+003+0.0000000E+000    3
+0.0000000E+000+0.0000000E+000+2.9370251E+003+0.0000000E+000                   4
C2H3(S)           0325040   0C  2H  3AG 1   S   300      5000       1000       1
-1.9396598E+003-1.8926274E+003+0.0000000E+000+0.0000000E+000+0.0000000E+000    2
+2.9812612E+003+0.0000000E+000-1.9396598E+003-1.8926274E+003+0.0000000E+000    3
+0.0000000E+000+0.0000000E+000+2.9812612E+003+0.0000000E+000                   4
END
```

Figure A.11 Output Text File as SURFACE CHEMKIN Input File

References

1. E. Shustorovich and H. Sellers (1998). The UBI-QEP method: A practical theoretical approach to understanding chemistry on transition metal surfaces. *Surface Science Reports*, 31, 1-119.
2. G. Ertl (1979). In T. N. Rhodin & G. Ertl (Eds.). Amsterdam: North-Holland.
3. W. Tsai, J. J. Vajo, and W. H. Weinberg (1985). Inhibition by hydrogen of the heterogeneous decomposition of ammonia on platinum. *Journal of Physical Chemistry*, 89, 4926-4932.
4. X. L. Zhou, J. M. White and B. E. Koel (1989). Chemisorption of atomic hydrogen on clean and chlorine-covered silver(111). *Surface Science*, 218, 201-210.
5. A. G. Sault, R. J. Madix and C. T. Campbell (1986). Adsorption of oxygen and hydrogen on gold(110)-(1*2). *Surface Science*, 169, 347-356.
6. G. E. Gdowski, J. A. Fair, and R. J. Madix (1983). Reactive scattering of small molecules from platinum crystal surfaces: formaldehyde-d2, methanol, formic acid, and the nonanomalous kinetics of hydrogen atom recombination. *Surface Science*, 127, 541-554.
7. E. Giamello, B. Fubini, P. Lauro and A. Bossi (1984). A microcalorimetric method for the evaluation of copper surface area in copper-zinc oxide catalyst. *Journal of Catalysis*, 87, 443-451.
8. D. Brennan, D. O. Hayward and B. M. W. Trapnell (1960). *Calorimetric determination of the heats of adsorption of oxygen on evaporated films*, A256, 81-105.
9. W. F. Egelhoff, Jr. (1987). Core-level binding-energy shifts at surfaces and in solids. *Surface Science Reports, Volume Date 1986,* 6, 253-415.
10. H. L. Sellers (1994). In H. L. Sellers and J. T. Golab (Eds.). New York: Plenum Press.
11. L. C. Isett, and J. M. Blakely (1975). Binding energies of carbon to nickel (100) from equilibrium segregation studies. *Surface Science*, 47, 645-649.
12. C. H. Bartholomew, P. K. Agrawal and J. R. Katzer (1982). Sulfur poisoning of metals. *Advances in Catalysis*, 31, 135-242.
13. S. W. Benson (1976). *Thermochemical kinetics : methods for the estimation of thermochemical data and rate parameters*. New York: Wiley.
14. P. J. Linstrom and W. G. Mallard (2003). NIST Chemistry WebBook, *NIST Chemistry WebBook*. Gaithersburg.

Appendix B: MATLAB Codes

```
%-------------------------------------------------------------------------
% SURF_THERM_KIN                                                          %
% A Software Code for the Estimation of Thermodynamic and Rate Parameters  %
% of Surface Reactions                                                    %
% Author: Bharthwaj Anantharaman, Massachusetts Institute of Technology   %
% Contact information: anb@mit.edu (Bharthwaj Anantharaman)               %
%                      whgreen@mit.edu (William H. Green Jr.)             %
%                      mcrae@mit.edu (Gregory J. McRae)                   %
% Date: March 18, 2004                                                    %
%-------------------------------------------------------------------------
% Application of the Code:
% a. Calculation of
%    1. Thermodynamic parameters
%    2. Rate parameters
%    of surface species and surface reactions on transition metal catalysts
% b. Integration with the SURFACE KINETICS package of CHEMKIN software
% Computed thermodynamic parameters of surface species:
% a. Molecular chemisorption enthalpies
% b. NASA polynomial coefficients
% Computed rate parameters of surface reactions:
% a. Preexponential factors
% b. Activation energies
% The computed thermodynamic and rate parameters form the thermodynamic and rate data of the
% SURFACE Chemkin input file
% This file could be integrated with the core utilities of the SURFACE KINETICS package of
```

% Chemkin software

% Two calculation modules in the Code:

% Module 1: Calculation of thermodynamic parameters

% Module 2: Calculation of rate parameters

% The variables are defined here

% NUMBER_REACTIONS Number of surface reactions in the mechanism

% N_G_R Number of gas phase reactants for which the bonds are broken

% N_G_P Number of gas phase prodcuts for which the bonds are formed

% N_S_R Number of surface reactants for which the bonds are broken

% N_S_P Number of surface species for which the bonds are formed

% REACTANT1_STOICHIOMETRY_VECTOR Number vector of stoich. coefficients of reactant 1

% REACTANT1_VECTOR String vector of reactant 1

% REACTANT2_STOICHIOMETRY_VECTOR Number vector of stoich. coefficients of reactant 2

% REACTANT2_VECTOR String vector of reactant 2

% VACANCY

% NUM_GAS_REACTANTS Number of gas phase species as reactants

% NUM_VACANCY_REACTANTS Number of vacant sites as reactants

% NUM_SURFACE_REACTANTS Number of surface species as reactants

% PRODUCT1_STOICHIOMETRY_VECTOR Number vector of stoich. coefficients of product 1

% PRODUCT1_VECTOR String vector of product 1

% PRODUCT2_STOICHIOMETRY_VECTOR Number vector of stoich. coefficients of product 2

% PRODUCT2_VECTOR String vector of product 2

% NUM_GAS_PRODUCTS Number of gas phase species as products

% NUM_VACANCY_PRODUCTS Number of vacant sites as products

% NUM_SURFACE_PRODUCTS Number of surface species as products

% NUMBER_SURFACE_SPECIES Number of surface species in the mechanism

% A_FORWARD A-factor of forward reaction for each reaction type

% A_REVERSE A-factor of reverse reaction for each reaction type

% A_forward_reaction	A-factor of forward reaction
% A_reverse_reaction	A-factor of reverse reaction
% E_forward	Activation energy of forward reaction for each reaction type
% E_reverse	Activation energy of reverse reaction for each reaction type
% E_forward_reaction	Activation energy of the forward reaction
% E_reverse_reaction	Activation energy of the reverse reaction
% R	Universal gas constant (=1.987 cal/mol/K)
% T_Standard	Standard Temperature (=298K)
% Size_B	Size of the data array B from Spreadsheet
% Size_D	Size of the data array D from Spreadsheet
% SDEN	Site density (in molecules/cm2)
% MATERIAL	Material name of the catalyst
% S_metal	Standard state entropy of the catalyst
% ELEMENTS	Elements in the surface species
% binding_atoms	Number of atoms bound to the catalyst
% species	Chemical formula of the surface species
% Hf_gas(j)	Enthalpy of formation of gas phase species
% Cp_gas(j)	Heat capacity of gas phase species
% S_gas(j)	Entropy of gas phase species
% Q_species_uni	Uni-coordinated atomic heat of chemisorption
% Q_species	Molecular chemisorption enthalpy
% Q_species_unia	Uni-coordinated heat of chemisorption of atom A
% Q_species_unib	Uni-coordinated heat of chemisorption of atom B
% D_AB	Gas phase dissociation energy between atom or group A and B
% Q_species_total	Molecular chemisorption enthalpy for intermediate binding
% D_a_group	Gas phase dissocn. energy between atom a and rest of group
% Q_species_unigroup	Molecular chemisorption enthalpy of group
% D_groupa_groupa	Gas phase dissocn. energy between group a and group a

% D_a_groupa Gas phase dissocn. energy between a and group a

% D_b_groupb Gas phase dissocn. energy between b and group b

% Q_species_unigroupa Molecular chemisorption enthalpy of group a

% Q_species_unigroupb Molecular chemisorption enthalpy of group b

% D_ax Gas phase dissocn. energy between atom a and group X

% D_bx Gas phase dissocn. energy between atom b and group X

% Q_species_unia_x Molecular chemisorption enthalpy of group aX

% Q_species_unib_x Molecular chemisorption enthalpy of group bX

% heat_capacity_contribution Contribn. to heat capapcity from the adsorbate-surface bond

% Hf_species(j) Enthalpy of formation of surface species

% Cp_species(j) Heat capacity of surface species

% S_species(j) Entropy of surface species

% Thermodynamic_Vector Vector of thermo: heat of formation, heat capacity and entropy

% NASA_Vector Vector of NASA polynomial coefficients

% reaction_type Type of each reaction

% reaction_reverse_flag Identification Flag for reversing the reaction

% REACTION_TYPE Type of each reaction

% d_reactant_sum Sum of gas phase dissocn. energies of all broken bonds in the reactant

% d_reactant Gas phase dissociation energy of broken bond in the reactant

% d_product_sum Sum of gas phase dissociation energies of all formed bonds in the product

% d_product Gas phase dissociation energy of formed bond in the product

% d_tot Difference in the total bond dissociation energies of reactants and products

% Q_reactant_sum Sum of the chemisorption enthalpies of all the reactants

% Q_reactant(j) Chemisorption enthalpy of reactant

% Q_product_sum Sum of the chemisorption enthalpies of all the products

% Q_product(j) Chemisorption enthalpy of product

% q_tot Difference in the total chemisorption enthalpies of reactants and products

```
% Following are the index variables used to represent the catalyst and
% adsorbate properties
% Atomicity                 Atomicity of the adsorbate species  (monoatomic=1, diatomic=2, and polyatomic=3)
% Metallicity          Metallicity of the catalyst
%                 (unimetallic=1, bimetallic=2)
% coordination_number          Coordination number of the adsorbate bound to catalyst (On-top=1,
%                 bridge=2, Fcc(110) hollow=3, Hcp=4,
%                 Fcc(100)=5)
% binding_strength                  Strength of binding (weak=1, moderate=2, strong=3)
% coordination_structure   Structure of the coordination of adsorbate on surface (symmetric=1,
%                 asymmetric=2, chelating=3)
clear
disp ('Surface_Therm_Kin_Version 1.0');
day_time = clock;
disp(sprintf('The Current Date is %d-%d-%d',day_time(2),day_time(3),day_time(1)));
disp(sprintf('The Current Time is %d:%d',day_time(4),day_time(5)));
% Reading reactions information from the worksheet
[A,B] = xlsread('Surface_Therm_Kin','Reaction_Information');
Size_B = size(B);
row_index_B = 2;
% Reading surface species information from the worksheet
[C,D] = xlsread('Surface_Therm_Kin','Surface_Species_Information');
Size_D = size(D);
row_index_C = 11;
row_index_D = 14;
% Standard temperature (in K)
T_standard = 298;
% Standard pressure (in atm)
```

```
P_standard = 1;
% Reaction temperature and pressure
T = C(1,7);
P = C(2,7);
% Define the number of reactions in the surface mechanism
NUMBER_REACTIONS = Size_B(1) - row_index_B;
NUMBER_REACTION_TYPES = 7;
global A_factor_forward_Reaction_Type
A_factor_forward_Reaction_Type = linspace(1,1,NUMBER_REACTION_TYPES);
% Function to calculate prexponential factors of surface reactions at
% required temperature and pressure
Calc_A_factor(T,P,T_standard,P_standard,NUMBER_REACTION_TYPES);
for i = 1:7
   A_FORWARD(i)=A_factor_forward_Reaction_Type(i);
   %A_REVERSE(i)=A_factor_Reaction_Type(2*i);
end
% Define the number of surface species in the surface mechanism
NUMBER_SURFACE_SPECIES = Size_D(1) - row_index_D;
echo on
% Universal gas constant (in cal/mol./K)
R = 1.987;
% delta S (in cal/mol./K) for desorption reaction given by Trouton's rule
deltaS_Trouton = 20;
T_matrix = [1 T_standard 0; 0 1 T_standard; 0 log(T_standard) T_standard];
SDEN = C(2,3);
MATERIAL = D{3,4};
ELEMENTS = [D{row_index_D,3} D{row_index_D,4} D{row_index_D,5} D{row_index_D,6}]';
s_m = C(1,3);
```

```
S_metal = C(3,3);
file = fopen('surface.txt','w');
file1 = fopen('enthalpy.txt','w');
fprintf(file1,'Species\t\t\tChemisorption Enthalpy\t\t\tEntropy\n');
fprintf(file,'MATERIAL %s\n',MATERIAL);
fprintf(file,'SITE/CAT/     SDEN/%4.3E/\n\n',SDEN);
fprintf(file,'ELEMENTS\n%s %s % s %s\nEND\n\n',D{14,3},D{14,4},D{14,5},D{14,6});
for k =  1:Size_D(1)-row_index_D-1
fprintf(file,'%s ',D{k+row_index_D,1});
end
k = Size_D(1)-row_index_D;
fprintf(file,'%s',D{k+row_index_D,1});
fprintf(file,'\nEND\n\n');
fprintf(file,'THERMO\n');
for j = 1:Size_D(1)-row_index_D
   Atomicity = C(row_index_C+j,1);
   binding_atoms = C(row_index_C+j,6);
   species = D{row_index_D+j,1};
   coordination_number = C(row_index_C+j,11);
   binding_strength = C(row_index_C+j,12);
   coordination_structure = C(row_index_C+j,13);
   Hf_gas(j) = C(row_index_C+j,17);
   Cp_gas(j) = C(row_index_C+j,18);
   S_gas(j) = C(row_index_C+j,19);
  if Atomicity == 1
    Q_species_uni = C(row_index_C+j,9);
    Q_species(j) = Q_species_uni*(2-1/coordination_number);
  elseif Atomicity == 2
```

```
disp('AB is the Diatomic Adsorbate');
if binding_strength == 1
  if coordination_number == 1
    disp('On-top Coordination of A and B With the A End Down.  M-A-B');
    Q_species_uni = C(row_index_C+j,9);
    D_AB = C(row_index_C+j,14);
    Q_species(j) = Q_species_uni^2/(Q_species_uni+D_AB);
  elseif coordination_number == 2
    Q_species_unia = C(row_index_C+j,9);
    Q_species_unib = C(row_index_C+j,10);
    D_AB = C(row_index_C+j,14);
    if coordination_number == 1
      disp('Bridge Coordination via A and B, with the Contact Atoms in an Ontop Site');
      a = (Q_species_unia^2)*(Q_species_unia+2*Q_species_unib)/((Q_species_unia+Q_species_unib)^2);
      b = (Q_species_unib^2)*(Q_species_unib+2*Q_species_unia)/((Q_species_unia+Q_species_unib)^2);
      Q_species(j) = (a*b*(a+b)+D_AB*((a-b)^2))/(a*b+D_AB*(a+b));
    else
      disp('Bridge Coordination with A and B, with the Contact Atoms Positioned Parallel to the Surface and
Across the M-M Bridge');
      a = 3*Q_species_unia/4;
      b = 3*Q_species_unib/4;
      Q_species(j) = 2*(a*b*(a+b)+2*D_AB*((a-b)^2))/(a*b+2*D_AB*(a+b));
    end
  else
    if binding_atoms  == 1
      disp('On-top Coordination of A and B with the A End Down on the Hollow Site.  Mn-A-B');
      Q_species_uni = C(row_index_C+j,9);
      D_AB = C(row_index_C+j,14);
```

```
            Q_species(j) = Q_species_uni^2/(Q_species_uni/coordination_number+D_AB);
          else
            disp('Hollow Coordination with A and B Bound to the Catalyst');
            Q_species_unia = C(row_index_C+j,9);
            Q_species_unib = C(row_index_C+j,10);
            D_AB = C(row_index_C+j,14);
            a = ((Q_species_unia*(coordination_number-1))^2)*(Q_species_unia*(coordination_number-
1)+2*Q_species_unib)/((Q_species_unia*(coordination_number-1)+Q_species_unib)^2);
            b = (Q_species_unib^2)*(Q_species_unib+2*Q_species_unia*(coordination_number-
1))/((Q_species_unib+Q_species_unia*(coordination_number-1))^2);
            Q_species(j) = (a*b*(a+b)+D_AB*((a-b)^2))/(a*b+D_AB*(a+b));
        end
        end
      elseif binding_strength == 2
        Q_species_total =  C(row_index_C+j,10);
        Q_species_unia = C(row_index_C+j,9);
        D_AB = C(row_index_C+j,14);
        Q_species(j) = 0.5*(Q_species_unia^2/(Q_species_unia/n+D_AB) +
(Q_species_total^2)/(Q_species_total+D_AB));

       else
        Q_species_total = C(row_index_C+j,10);
        D_AB = C(row_index_C+j,14);
        Q_species(j) = Q_species_total^2/(Q_species_total+D_AB);
      end
    else
      disp('Polyatomic Adsorbate');
      binding_atoms = C(j,2);
```

```
if binding_atoms == 1
  Q_species_uni = C(row_index_C+j,9);
  D_AB = C(row_index_C+j,14);
  if coordination_number == 1
    disp('Polyatomic Adsorbate and Coordianted via A Mono-coordinated M-A');
    Q_species(j) = Q_species_uni^2/(Q_species_uni(j)+D_AB);
  else
    Q_species(j) = Q_species_uni^2/(Q_species_uni/coordination_number+D_AB);
  end
else
  disp('More than One Atom Is Bound to the Catalyst');
  if coordination_number == 2
    if coordination_structure == 1
      disp('Symmetric Dicoordination');
      Q_species_unia = C(row_index_C+j,9);
      D_a_group = C(row_index_C+j,14);
      Q_species_unigroup = Q_species_unia^2/(Q_species_unia+D_a_group);
      D_groupa_groupa = C(row_index_C+j,15);
      Q_species(j) = 9*(Q_species_unigroup^2)/(6*Q_species_unigroup+16*D_groupa_groupa);
    elseif coordination_structure == 2
      disp('Asymmetric Dicoordination');
      Q_species_unia = C(row_index_C+j,9);
      Q_species_unib = C(row_index_C+j,10);
      D_a_groupa = C(row_index_C+j,14);
      D_b_groupb = C(row_index_C+j,15);
      D_AB = C(row_index_C+j,16);
      Q_species_unigroupa = Q_species_unia^2/(Q_species_unia+D_a_groupa);
      Q_species_unigroupb = Q_species_unib^2/(Q_species_unib+D_b_groupb);
```

```
        a =
(Q_species_unigroupa^2)*(Q_species_unigroupa+2*Q_species_unigroupb)/((Q_species_unigroupa+Q_species_uni
groupb)^2);
        b =
(Q_species_unigroupb^2)*(Q_species_unigroupb+2*Q_species_unigroupa)/((Q_species_unigroupb+Q_species_uni
groupa)^2);
        Q_species(j) = (a*b*(a+b)+D_AB*((a-b)^2))/(a*b+D_AB*(a+b));
      else
        disp('Bridge Coordination via A and B for the Chelate Structure with Atoms/Molecules X in Between');
        Q_species_unia = C(row_index_C+j,9);
        Q_species_unib = C(row_index_C+j,10);
        D_ax = C(row_index_C+j,14);
        D_bx = C(row_index_C+j,15);
        Q_species_unia_x = Q_species_unia^2/(Q_species_unia+D_ax);
        Q_species_unib_x = Q_species_unib^2/(Q_species_unib+D_bx);
        a =
(Q_species_unia_x^2)*(Q_species_unia_x+2*Q_species_unib_x)/((Q_species_unia_x+Q_species_unib_x)^2);
        b =
(Q_species_unib_x^2)*(Q_species_unib_x+2*Q_species_unia_x)/((Q_species_unia_x+Q_species_unib_x)^2);
        Q_species(j) = a+b;
      end
    else
      disp('Hollow Coordination with A and B Bound to the Catalyst');
      Q_species_unia = C(row_index_C+j,9);
      Q_species_unib = C(row_index_C+j,10);
      D_a_groupa = C(row_index_C+j,14);
      D_b_groupb = C(row_index_C+j,15);
      D_AB = C(row_index_C+j,16);
```

```
        Q_species_unigroupa = Q_species_unia^2/(Q_species_unia/(coordination_number-1)+D_a_groupa);
        Q_species_unigroupb = Q_species_unib^2/(Q_species_unib+D_b_groupb);
        a =
(Q_species_unigroupa^2)*(Q_species_unigroupa+2*Q_species_unigroupb)/((Q_species_unigroupa+Q_species_uni
groupb)^2);
        b =
(Q_species_unigroupb^2)*(Q_species_unigroupb+2*Q_species_unigroupa)/((Q_species_unigroupb+Q_species_uni
groupa)^2);
        Q_species(j) = (a*b*(a+b)+D_AB*((a-b)^2))/(a*b+D_AB*(a+b));
      end
    end
  end
  disp(sprintf('The Calculated Chemisorption Enthalpy of Species Molecule is = %15.2f',Q_species(j)));
  heat_capacity_contribution =
3/2*R*coordination_number+2*R*coordination_number+1*R/2*coordination_number;

  Hf_species(j) = Hf_gas(j)-Q_species(j);
  Cp_species(j) = Cp_gas(j)+heat_capacity_contribution;
  S_species(j) = S_gas(j)+S_metal-deltaS_Trouton;
  Thermodynamic_Vector = [Hf_species(j)/R Cp_species(j)/R S_species(j)/R]';
  NASA_Vector = T_matrix*Thermodynamic_Vector;
  if length(species) < 4
   fprintf(file,'%s\t\t\t\t  %02d%02d%02d%s\t%g%s\t%g%s\t%g%s\t%g\t%s\t%g\t\t %g\t\t%g\t
%g\n',species,day_time(2),day_time(3),day_time(1)-
2000,D{row_index_D,3},C(11+j,2),D{row_index_D,4},C(11+j,3),D{row_index_D,5},C(11+j,4),D{row_index_D,6
},C(11+j,5),'S',300,5000,1000,1);
  elseif length(species) <= 7
```

```
  fprintf(file,'%s\t\t\t  %02d%02d%02d%s\t%g%s\t%g%s\t%g%s\t%g\t%s\t%g\t\t %g\t\t%g\t
%g\n',species,day_time(2),day_time(3),day_time(1)-
2000,D{row_index_D,3},C(11+j,2),D{row_index_D,4},C(11+j,3),D{row_index_D,5},C(11+j,4),D{row_index_D,6
},C(11+j,5),'S',300,5000,1000,1);
  else
  fprintf(file,'%s\t\t  %02d%02d%02d%s\t%g%s\t%g%s\t%g%s\t%g\t%s\t%g\t\t %g\t\t%g\t
%g\n',species,day_time(2),day_time(3),day_time(1)-
2000,D{row_index_D,3},C(11+j,2),D{row_index_D,4},C(11+j,3),D{row_index_D,5},C(11+j,4),D{row_index_D,6
},C(11+j,5),'S',300,5000,1000,1);
  end
  fprintf(file,'%+15.7E%+15.7E%+15.7E%+15.7E%+15.7E   %g\n',NASA_Vector(2),NASA_Vector(3),0,0,0,2);
  fprintf(file,'%+15.7E%+15.7E%+15.7E%+15.7E%+15.7E
%g\n',NASA_Vector(1),0,NASA_Vector(2),NASA_Vector(3),0,3);
  fprintf(file,'%+15.7E%+15.7E%+15.7E%+15.7E\t\t\t\t  %g\n',0,0,NASA_Vector(1),0,4);
  fprintf(file1,'%10s\t\t\t%2.2f\t\t\t%2.2f\n',species,Q_species(j),S_species(j));
end
end
fprintf(file,'END\n\n');
fclose(file1);
fprintf(file,'REACTIONS    KCAL/MOLE\n');
REACTANT_STOICHIOMETRY_INDEX = [3 6];
PRODUCT_STOICHIOMETRY_INDEX = [9 12];
REACTANT_PRODUCT_STOICHIOMETRY_INDEX = [REACTANT_STOICHIOMETRY_INDEX;
PRODUCT_STOICHIOMETRY_INDEX];
for i = 1:NUMBER_REACTIONS
  REACTANT1_STOICHIOMETRY_VECTOR(i) = A(i,2);
  if length(B{row_index_B+i,3}) > 0
  REACTANT1_VECTOR(i,1:length(B{row_index_B+i,3})) = B{row_index_B+i,3};
```

```
end
REACTANT2_STOICHIOMETRY_VECTOR(i) = A(i,5);
if length(B{row_index_B+i,6}) > 0
REACTANT2_VECTOR(i,1:length(B{row_index_B+i,6})) =  B{row_index_B+i,6};
else
REACTANT2_VECTOR(i,1:length(B{row_index_B+i,3})) =  repmat(' ',1,length(B{row_index_B+i,3}));
end
VACANCY = [D{3,5} '(S)'];
NUM_GAS_REACTANTS(i) = 0;
NUM_VACANCY_REACTANTS(i) = 0;
NUM_SURFACE_REACTANTS(i) = 0;
for j = 1:length(REACTANT_STOICHIOMETRY_INDEX)
if length(B{row_index_B+i,REACTANT_STOICHIOMETRY_INDEX(j)}) > 0
   if length(findstr(B{row_index_B+i,REACTANT_STOICHIOMETRY_INDEX(j)},'(S)')) == 0
   NUM_GAS_REACTANTS(i) = NUM_GAS_REACTANTS(i) + 1;
   else
   if findstr(B{row_index_B+i,REACTANT_STOICHIOMETRY_INDEX(j)},VACANCY) == 1
   NUM_VACANCY_REACTANTS(i) = NUM_VACANCY_REACTANTS(i) + 1;
   else
   NUM_SURFACE_REACTANTS(i) = NUM_SURFACE_REACTANTS(i) + 1;
   end
   end
end
end
PRODUCT1_STOICHIOMETRY_VECTOR(i) = A(i,8);
if length(B{row_index_B+i,9}) > 0
PRODUCT1_VECTOR(i,1:length(B{row_index_B+i,9})) = B{row_index_B+i,9};
end
```

```
PRODUCT2_STOICHIOMETRY_VECTOR(i) = A(i,11);
if length(B{row_index_B+i,12}) > 0
PRODUCT2_VECTOR(i,1:length(B{row_index_B+i,12})) = B{row_index_B+i,12};
else
PRODUCT2_VECTOR(i,1:length(B{row_index_B+i,9})) = repmat(' ',1,length(B{row_index_B+i,9}));
end
NUM_GAS_PRODUCTS(i) = 0;
NUM_VACANCY_PRODUCTS(i) = 0;
NUM_SURFACE_PRODUCTS(i) = 0;
for j = 1:length(PRODUCT_STOICHIOMETRY_INDEX)
if length(B{row_index_B+i,PRODUCT_STOICHIOMETRY_INDEX(j)}) > 0
  if length(findstr(B{row_index_B+i,PRODUCT_STOICHIOMETRY_INDEX(j)},'(S)')) == 0
  NUM_GAS_PRODUCTS(i) = NUM_GAS_PRODUCTS(i) + 1;
  else
  if findstr(B{row_index_B+i,PRODUCT_STOICHIOMETRY_INDEX(j)},VACANCY) == 1
  NUM_VACANCY_PRODUCTS(i) = NUM_VACANCY_PRODUCTS(i) + 1;
  else
  NUM_SURFACE_PRODUCTS(i) = NUM_SURFACE_PRODUCTS(i) + 1;
  end
  end
end
end
reaction_type = 0;
reaction_reverse_flag = 0;
% Identifying the Type of Each Reaction
if NUM_SURFACE_REACTANTS(i) == 0
  if NUM_SURFACE_PRODUCTS(i) == 1
    if NUM_GAS_PRODUCTS(i) == 0
```

```
        reaction_type = 1;
      else
        reaction_type = 4;
      end
    else
      reaction_type = 2;
    end
  elseif NUM_SURFACE_REACTANTS(i) == 1
    if NUM_SURFACE_PRODUCTS(i) == 1
      if NUM_GAS_REACTANTS(i) == 0
        reaction_type = 5;
      else
        reaction_type = 7;
      end
    else
      reaction_type = 3;
    end
  else
    if NUM_SURFACE_REACTANTS(i) == 2 & NUM_SURFACE_PRODUCTS(i) == 2
      reaction_type = 6;
    end
  end
  if reaction_type == 0
    reaction_reverse_flag = 1;
    if NUM_SURFACE_PRODUCTS(i) == 0
    if NUM_SURFACE_REACTANTS(i) == 1
      if NUM_GAS_REACTANTS(i) == 0
        reaction_type = 1;
```

```
        else
          reaction_type = 4;
        end
      else
        reaction_type = 2;
      end
      elseif NUM_SURFACE_PRODUCTS(i) == 1
        if NUM_SURFACE_REACTANTS(i) == 1
          if NUM_GAS_PRODUCTS(i) == 0
            reaction_type = 5;
          end
        else
          reaction_type = 3;
        end
      end
    end
REACTION_TYPE(i) = reaction_type;
echo off
d_reactant_sum = 0;
d_product_sum = 0;
  d_reactant = A(i,13);
  d_product = A(i,14);
  if reaction_reverse_flag == 1
    d_reactant = A(i,14);
    d_product = A(i,13);
  end
  d_reactant_sum = d_reactant_sum + d_reactant;
  d_product_sum = d_product_sum + d_product;
```

```
disp(sprintf('The Total Dissociation Energies of all the Broken Bonds in Gas Phase Reactants =
%15.2f',d_reactant_sum));
disp(sprintf('The Total Dissociation Energies of all the Formed Bonds in Gas Phase Products =
%15.2f',d_product_sum));
echo on
% Calculate d_tot
d_tot = d_reactant_sum - d_product_sum;
disp(sprintf('Difference in Total Bond Dissociation Energies of Reactants and Products = %15.2f',d_tot));
Q_reactant_sum = 0;
Q_product_sum = 0;
S_reactant_sum = 0;
S_product_sum = 0;
for j = 1:2
   Q_reactant(j) = A(i,14+j);
   Q_product(j) = A(i,16+j);
   S_reactant(j) = A(i,18+j);
   S_product(j) = A(i,20+j);
   if reaction_reverse_flag == 1
      Q_reactant(j) = A(i,16+j);
      Q_product(j) = A(i,14+j);
      S_reactant(j) = A(i,20+j);
      S_product(j) = A(i,18+j);
   end
   Q_reactant_sum = Q_reactant_sum +  Q_reactant(j);
   Q_product_sum = Q_product_sum +  Q_product(j);
   S_reactant_sum = S_reactant_sum +  S_reactant(j);
   S_product_sum = S_product_sum +  S_product(j);
end
```

```
delta_S = S_product_sum - S_reactant_sum;
global E_forward
global E_reverse
% Initializing E_forward anmd E_reverse
E_forward = 0;
E_reverse = 0;
% Function to calculate activation energies of surface reactions
Calc_E(reaction_type,reaction_reverse_flag,Q_reactant_sum,Q_product_sum,d_tot,Q_reactant,Q_product);
echo on
% Output Modules
  E_forward_reaction(i) = E_forward;
  E_reverse_reaction(i) = E_reverse;


  A_forward_reaction(i) = A_FORWARD(reaction_type);
  %A_reverse_reaction(i) = A_REVERSE(reaction_type);
  A_reverse_reaction(i) = A_forward_reaction(i)*exp(-delta_S/R);
  if reaction_reverse_flag == 1
     E_forward_reaction(i) = E_reverse;
     E_reverse_reaction(i) = E_forward;
     A_reverse_reaction(i) = A_FORWARD(reaction_type);
     A_forward_reaction(i) = A_reverse_reaction(i)*exp(delta_S/R);
  end
 if length(B{row_index_B+i,6}) ~= 0
   if length(B{row_index_B+i,12}) ~= 0
   fprintf(file,'%g%-10s + %g%-10s => %g%-10s + %g%-10s %7.3E  %3.1f
%4.1f\n',REACTANT1_STOICHIOMETRY_VECTOR(i),REACTANT1_VECTOR(i,:),REACTANT2_STOICHI
OMETRY_VECTOR(i),REACTANT2_VECTOR(i,:),PRODUCT1_STOICHIOMETRY_VECTOR(i),PRODUCT1
```

```
_VECTOR(i,:),PRODUCT2_STOICHIOMETRY_VECTOR(i),PRODUCT2_VECTOR(i,:),A_forward_reaction(i),
0.0,E_forward_reaction(i));
   fprintf(file,'%g%-10s + %g%-10s => %g%-10s + %g%-10s %7.3E  %3.1f
%4.1f\n',PRODUCT1_STOICHIOMETRY_VECTOR(i),PRODUCT1_VECTOR(i,:),PRODUCT2_STOICHIOME
TRY_VECTOR(i),PRODUCT2_VECTOR(i,:),REACTANT1_STOICHIOMETRY_VECTOR(i),REACTANT1_V
ECTOR(i,:),REACTANT2_STOICHIOMETRY_VECTOR(i),REACTANT2_VECTOR(i,:),A_reverse_reaction(i),0
.0,E_reverse_reaction(i));
   else
   fprintf(file,'%g%-10s + %g%-10s => %g%-24s %7.3E  %3.1f
%4.1f\n',REACTANT1_STOICHIOMETRY_VECTOR(i),REACTANT1_VECTOR(i,:),REACTANT2_STOICHI
OMETRY_VECTOR(i),REACTANT2_VECTOR(i,:),PRODUCT1_STOICHIOMETRY_VECTOR(i),PRODUCT1
_VECTOR(i,:),A_forward_reaction(i),0.0,E_forward_reaction(i));
   fprintf(file,'%g%-24s => %g%-10s + %g%-10s %7.3E  %3.1f
%4.1f\n',PRODUCT1_STOICHIOMETRY_VECTOR(i),PRODUCT1_VECTOR(i,:),REACTANT1_STOICHIOM
ETRY_VECTOR(i),REACTANT1_VECTOR(i,:),REACTANT2_STOICHIOMETRY_VECTOR(i),REACTANT2
_VECTOR(i,:),A_reverse_reaction(i),0.0,E_reverse_reaction(i));
   end
 else
   if length(B{row_index_B+i,12}) ~= 0
   fprintf(file,'%g%-24s => %g%-10s + %g%-10s %7.3E  %3.1f
%4.1f\n',REACTANT1_STOICHIOMETRY_VECTOR(i),REACTANT1_VECTOR(i,:),PRODUCT1_STOICHIO
METRY_VECTOR(i),PRODUCT1_VECTOR(i,:),PRODUCT2_STOICHIOMETRY_VECTOR(i),PRODUCT2_V
ECTOR(i,:),A_forward_reaction(i),0.0,E_forward_reaction(i));
   fprintf(file,'%g%-10s + %g%-10s => %g%-24s %7.3E  %3.1f
%4.1f\n',PRODUCT1_STOICHIOMETRY_VECTOR(i),PRODUCT1_VECTOR(i,:),PRODUCT2_STOICHIOME
TRY_VECTOR(i),PRODUCT2_VECTOR(i,:),REACTANT1_STOICHIOMETRY_VECTOR(i),REACTANT1_V
ECTOR(i.:),A_reverse_reaction(i),0.0,E_reverse_reaction(i));
   else
```

```
   fprintf(file,'%g%-24s => %g%-24s %7.3E  %3.1f
%4.1f\n',REACTANT1_STOICHIOMETRY_VECTOR(i),REACTANT1_VECTOR(i,:),PRODUCT1_STOICHIO
METRY_VECTOR(i),PRODUCT1_VECTOR(i,:),A_forward_reaction(i),0.0,E_forward_reaction(i));
   fprintf(file,'%g%-24s => %g%-24s %7.3E  %3.1f
%4.1f\n',PRODUCT1_STOICHIOMETRY_VECTOR(i),PRODUCT1_VECTOR(i,:),REACTANT1_STOICHIOM
ETRY_VECTOR(i),REACTANT1_VECTOR(i,:),A_reverse_reaction(i),0.0,E_reverse_reaction(i));
  end
 end
end
fprintf(file,'END');
fclose(file);
%--------------------------------------------------------------------------
% Calc_A_factor                                                           %
% A Subroutine for the Calculation of Preexponential Factors at required    %
% Temperature and Pressure                                                %
% Author: Bharthwaj Anantharaman, Massachusetts Institute of Technology     %
% Contact information: anb@mit.edu (Bharthwaj Anantharaman)               %
%                      whgreen@mit.edu (William H. Green Jr.)             %
%                      mcrae@mit.edu (Gregory J. McRae)                   %
% Date: March 18, 2004                                                    %
%--------------------------------------------------------------------------
function A_factor_Reaction_Type = Calc_A_factor(T,P,T_standard,P_standard,NUMBER_REACTION_TYPES);
global A_factor_Reaction_Type
% The variables are intialized
A_factor_Reaction_Type = linspace(1,1,NUMBER_REACTION_TYPES);
A_FORWARD_UPPER_BASE = linspace(1,1,NUMBER_REACTION_TYPES)';
A_FORWARD_LOWER_BASE = linspace(1,1,NUMBER_REACTION_TYPES)';
A_FORWARD_UPPER_CORRECTION = linspace(1,1,NUMBER_REACTION_TYPES)';
A_FORWARD_LOWER_CORRECTION = linspace(1,1,NUMBER_REACTION_TYPES)';
% Upper and lower bounds based on collision theory, transition state theory
% and surface diffusion are set for the preexpeontial factors at base
% conditions: Standard temperature of 298K and standard pressure of 1 atm
   A_FORWARD_UPPER_BASE(1)= 1E+13; A_FORWARD_UPPER_BASE(2)= 1E+22;
A_FORWARD_UPPER_BASE(3)= 1E+18; A_FORWARD_UPPER_BASE(4)= 1E+13;
A_FORWARD_UPPER_BASE(5)= 1E+13;
   A_FORWARD_UPPER_BASE(6)= 1E+18; A_FORWARD_UPPER_BASE(7)= 1E+13;
   A_FORWARD_LOWER_BASE(1)= 1E+12; A_FORWARD_LOWER_BASE(2)= 1E+20;
A_FORWARD_LOWER_BASE(3)= 1E+17; A_FORWARD_LOWER_BASE(4)= 1E+12;
A_FORWARD_LOWER_BASE(5)= 1E+13;
   A_FORWARD_LOWER_BASE(6)= 1E+17; A_FORWARD_LOWER_BASE(7)= 1E+7;
```

```
% Temperature and pressure corrections for each reaction type

   A_FORWARD_UPPER_CORRECTION(1)=sqrt(T/T_standard);
A_FORWARD_UPPER_CORRECTION(2)=sqrt(T/T_standard); A_FORWARD_UPPER_CORRECTION(3)=1/1;
A_FORWARD_UPPER_CORRECTION(4)=sqrt(T/T_standard);
A_FORWARD_UPPER_CORRECTION(5)=(T/T_standard); A_FORWARD_UPPER_CORRECTION(6)=1/1;
   A_FORWARD_UPPER_CORRECTION(7)=sqrt(T/T_standard);
   A_FORWARD_LOWER_CORRECTION(1)=1/1; A_FORWARD_LOWER_CORRECTION(2)=1/1;
A_FORWARD_LOWER_CORRECTION(3)=(T_standard/T); A_FORWARD_LOWER_CORRECTION(4)=1/1;
A_FORWARD_LOWER_CORRECTION(5)=(T/T_standard);
A_FORWARD_LOWER_CORRECTION(6)=(T_standard/T);
   A_FORWARD_LOWER_CORRECTION(7)=(T_standard/T)^2;

% Calculation of preexponential factors at given temperature and pressure
   for i = 1:7
   A_FORWARD_UPPER(i)= A_FORWARD_UPPER_BASE(i)*A_FORWARD_UPPER_CORRECTION(i);
   A_FORWARD_LOWER(i)= A_FORWARD_LOWER_BASE(i)*A_FORWARD_LOWER_CORRECTION(i);
   % Geometric mean of the upper and lower bounds is set as the nominal
   % preexponential factor
   A_factor_Reaction_Type(i)=sqrt(A_FORWARD_UPPER(i)*A_FORWARD_LOWER(i));
   end

   return;
```

```
%-------------------------------------------------------------------------
% Calc_E                                                                  %
% A Subroutine for the Calculation of Activation Energies                 %
%                                                                         %
% Author: Bharthwaj Anantharaman, Massachusetts Institute of Technology   %
% Contact information: anb@mit.edu (Bharthwaj Anantharaman)               %
%                      whgreen@mit.edu (William H. Green Jr.)             %
%                      mcrae@mit.edu (Gregory J. McRae)                   %
% Date: March 18, 2004                                                    %
%-------------------------------------------------------------------------
function E =
Calc_E(reaction_type,reaction_reverse_flag,Q_reactant_sum,Q_product_sum,d_tot,Q_reactant,Q_product);

global E_forward;
global E_reverse;

q_tot = Q_reactant_sum - Q_product_sum;
E_expression1 = d_tot + Q_product(1) * Q_product(2)/ (Q_product(1)+ Q_product(2));
E_expression2 = E_expression1-(Q_product(1) + Q_product(2));
E_expression3 = E_expression2 + Q_reactant(1);
E_reverse_forward_difference = -(d_tot + q_tot);

% Formulas to calculate the activation energies
if reaction_type == 1
  E_forward = 0;
  E_reverse = Q_product(1);
   elseif reaction_type == 2
     E_forward = 0.5*(E_expression2);
     elseif reaction_type == 3
       E_forward = 0.5*(E_expression3);
       elseif reaction_type == 4
          E_forward = 0.5*(E_expression2);
          elseif reaction_type == 5
            E_forward = 0.5*(E_expression3);
end

E_reverse = E_forward + E_reverse_forward_difference;

if reaction_reverse_flag == 1
   temp = E_forward;
   E_forward = E_reverse;
   E_reverse = temp;
end

if reaction_type == 6
  E_forward = 0.5*(E_expression2 + Q_reactant(1) + Q_reactant(2));
elseif reaction_type == 7
  E_forward = 0.5*(E_expression2 - Q_reactant(1) + Q_reactant(2));
end

if (reaction_type == 6 | reaction_type == 7)
   if E_forward >= 0
      E_reverse = E_forward + E_reverse_forward_difference;
      if E_forward < 0
         if reaction_type == 6
```

```
            E_reverse = 0.5*(-d_tot + Q_reactant(1) * Q_reactant(2) / (Q_reactant(1) + Q_reactant(2)) +
Q_product(1) + Q_product(2) - (Q_reactant(1) + Q_reactant(2)));
            E_forward = E_reverse - E_reverse_forward_difference;
          else
            E_reverse = 0.5*(-d_tot + Q_reactant(1) * Q_reactant(2) / (Q_reactant(1) + Q_reactant(2)) - Q_product(1)
+ Q_product(2) - Q_reactant(1) - Q_reactant(2));
            E_forward = E_reverse - E_reverse_forward_difference;
          end
        end
    end
end

if E_forward <= 0
  E_forward = 0;
  E_reverse = -(d_tot + q_tot);
end

if E_reverse <= 0
  E_reverse = 0;
  E_forward = d_tot + q_tot;
end

return;
```

Appendix C: Glossary

C.1 Nomenclature

β_f	Vector of N_r temperature coefficients for forward reactions
β_r	Vector of N_r temperature coefficients for reverse reactions
μ	Coverage-dependent exponent in the expression for rate constant
ν_r	$N_r \times N_s$ matrix of stoichiometric coefficients of reactants
ν_p	$N_r \times N_s$ matrix of stoichiometric coefficients of products
η_r	Matrix of coverage-dependent coefficients in preexponential factors of forward reactions
η_p	Matrix of coverage-dependent coefficients in preexponential factors of forward and reverse reactions
μ	Matrix of coverage-dependent coefficients in surface coverages
θ	Vector of coverages of all surface species
ρ	Mass density, gm/cm^3
σ	Symmetry number
Γ	Surface site density, mol/cm^2
a_1 to a_5	NASA polynomial coefficients in the expansion for heat capacity. a_1: Dimensionless; a_2: K^{-1}; a_3: K^{-2}; a_4: K^{-3}; a_5: K^{-4}
c	$N_r \times N_s$ matrix of coverage-dependent coefficients in heats of formation of surface species

k_{ads}	Adsorption coefficient, $atm^{-1}s^{-1}$
k_f	Forward preexponential factor, mol-cm-s units
k_r	Reverse preexponential factor, mol-cm-s units
k_B	Boltzmann's constant, $JK^{-1}molecule^{-1}$
m_A	Mass of Species A
n	Coordination number
q	Rate of progress, mol/cm^2
s_k	Species concentrations, and they have different forms depending on whether the species are in gas phase (mol/cm^3) or surface (mol/cm^2)
x_A	Bond index of the bond between gas phase atom A and the catalyst
x_B	Bond index of the bond between gas phase atom B and the catalyst
x_{AB}	Bond index of the bond between atoms A and B in the gas phase
x_{AM}	Bond index of the bond between atom A and metal M
x_{BM}	Bond index of the bond between atom A and metal M
Δn_g	Change in number of moles of the gas phase species
Δn_s	Change in number of moles of the surface species
ΔH	Enthalpy of reaction, kcal/mol
ΔS	Entropy of reaction, cal/mol/K
A_f	Preexponential factor of forward reaction, mol-cm-s units
A_r	Preexponential factor of reverse reaction, mol-cm-s units
$A_f(\underline{\theta} = 0)$	Preexponential factor of forward reaction at zero coverage, mol-cm-s units
$A_r(\underline{\theta} = 0)$	Preexponential factor of reverse reaction at zero coverage, mol-cm-s units

BE	Bond energy of the chemical bond between adsorbate A and the metal atom, kcal/mol
C_P	Heat capacity of species, cal/mol/K
D	Surface diffusivity, m^2/sec
D_0	Surface diffusivity when the diffusion barrier is 0, m^2/sec
D_{AB}	Dissociation energy of the bond between atoms A and B in a gas phase molecule, kcal/mol
$D_{A\text{-}GroupA}$	Dissociation energy of the bond between atom A and group A in a gas phase molecule, kcal/mol
$D_{B\text{-}GroupB}$	Dissociation energy of the bond between atom B and group B in a gas phase molecule, kcal/mol
D_{tot}	Difference in sum of the bond dissociation energies of reactants and products, kcal/mol
$D_{group\text{-}group}$	Dissociation energy between the 2 atoms separating 2 groups in a gas phase molecule, kcal/mol
E_{diff}	Energy barrier for diffusion, kcal/mol.
E_f	Activation energy of forward reaction, kcal/mol
E_r	Activation energy of reverse reaction, kcal/mol
E_{total}	Total energy of interaction of all the bonds in an adsorbate species, kcal/mol
$E_f(\underline{\theta} = 0)$	Activation energy of forward reaction at zero coverage, kcal/mol
$E_r(\underline{\theta} = 0)$	Activation energy of reverse reaction at zero coverage, kcal/mol
H_f	Heat of formation, kcal/mol
H_{298}	Enthalpy of species at TK, kcal/mol

H_T	Enthalpy of species at TK, kcal/mol
$H(\underline{\theta} = 0)$	Heat of formation at zero coverage, kcal/mol
I	Moment of inertia, g/cm^2
K_p	$N_r \times N_s$ matrix of coverage-dependent coefficients of activation energies of reverse reactions
K_r	$N_r \times N_s$ matrix of coverage-dependent coefficients of activation energies of forward reactions
N_r	Number of reversible reactions
N_s	Number of species
Q_{0A}	Mono-coordinated heat of chemisorption of atom A, kcal/mol
Q_{0B}	Mono-coordinated heat of chemisorption of atom B, kcal/mol
Q_A	Molecular chemisorption enthalpy of species A, kcal/mol
Q_B	Molecular chemisorption enthalpy of species B, kcal/mol
Q_{AB}	Molecular heat of chemisorption of AB, kcal/mol
Q_{tot}	Difference in sum of the chemisorption heats of reactants and products, kcal/mol
Q_{group}	Molecular chemisorption enthalpy of the group of atoms or radicals, kcal/mol
Q_{0AX}	Molecular chemisorption enthalpy of the group of atoms AX, kcal/mol
Q_{0BX}	Molecular chemisorption enthalpy of the group of atoms BX, kcal/mol
$Q_{0GroupA}$	Molecular chemisorption enthalpy of Group A, kcal/mol
$Q_{0GroupB}$	Molecular chemisorption enthalpy of Group B, kcal/mol
Z_{TS}	Total partition function of transition state
Z_A	Total partition function of gas Species A
Z_{B*}	Total partition function of surface Species B^*

Z_{At}	Translational partition function of Species A
Z_{Ar}	Rotational partition function of Species A
Z_{Av}	Vibrational partition function of Species A
Z_{Bt}	Translational partition function of Species B
Z_{Br}	Rotational partition function of Species B
Z_{Bv}	Vibrational partition function of Species B
R	Universal gas constant, cal/K/mol
S	Entropy of formation, cal/mol/K
S	Vector of N_s gas and surface species
S_{298}	Entropy of species at TK
S_T	Entropy of species at TK
T	Temperature,K
W_k	Molecular weights of the gas phase species, gm/mol
Y_k	Mass fractions

C.2 Abbreviations

DFT	Density Functional Theory
EELS	Electron Energy Loss Spectroscopy
ESDIAD	Electron Stimulated Desorption Ion Angular Distribution
HF	Hartree Fock
LEED	Low Energy Electron Diffraction
LIF	Laser Induced Fluorescence Technique

MMBRS	Modulated Molecular Beam Relaxation Spectroscopy
RECP	Relativistic Effective Core Potentials
SHG	Second Harmonic Generation
TDS	Thermal Desorption Spectroscopy
TPD	Temperature Programmed Desorption
TPRS	Temperature Programmed Reaction Spectroscopy
UPS	Ultraviolet Photoemission Spectroscopy

Appendix D: Supporting Information

Bond Additivity Corrections for G3B3 and G3MP2B3 Quantum Chemistry Methods

Heats of formation for the reference set of molecules used for obtaining the BAC parameters are listed in Table D.1. The experimental heats of formation used are those recommended by IUPAC-subcommittee [1]. Unless otherwise noted, most of the recommended experimental values have been taken from evaluations or reviews. For comparison, the experimental values used in the previous BAC-G2 test set are provided [2].

Table D.1 Experimental Heats of Formation for the Reference Set of Molecules

Molecules	Heat of formation (kcal/mol)	
	Current work [1]	**Previous work** [2]
C	171.29	171.29
CCl_4	-22.90 ± 0.14	-22.90
CF_4	-223.21	-223.00
$CH_2\ ^1A_1$	102.46 ± 0.95	102.80
$CH_2\ ^3B_1$	93.40 ± 0.95	93.80
CH_2Cl_2	-22.80 ± 0.19	-22.80
CH_2F_2	-108.30 ± 1.90	-108.30
H_2CNH	21.58	21.58
CH_2NH_2	35.70	35.70
CH_2O	-25.96	-25.96
CH_2OH	-4.26 ± 0.31	-2.10
$CH_2(OH)_2$	-93.50	-93.50
CH_3	35.02 ± 0.10	34.89
CH_3Cl	-19.60 ± 0.16	-19.60
CH_3F	-55.60	-55.60
CH_3NH	42.40	42.40
CH_3NH_2	-5.50	-5.50
CH_3NHNH_2	22.60	22.60
CH_3NO_2	-17.86	-17.86
CH_3O	4.20 ± 0.90	4.20
CH_3ONO	-15.60	-15.60

CH_3ONO_2	-28.60	-28.60
$CH_3OO\ ^2A''$	2.50	2.50
CH_3OOH	-31.31	-31.31
CH_3SH	-5.50 ± 0.14	-5.50
CH_3SiH_3	-6.93	-6.93
CH_4	-17.88	-17.88
$CHCl_3$	-24.70 ± 0.31	-24.70
CHF_3	-166.89	-166.70
CO	-26.41 ± 0.04	-26.41
CO_2	-94.05 ± 0.03	-94.05
CS	66.63 ± 0.90	65.00
CS_2	28.01	28.01
HCN	32.27 ± 1.90	32.27
HCO	10.31	10.00
HCOOH	-90.54 ± 0.12	-90.54
HNCS	30.00	30.00
OCS	-33.99	-33.94
$CH\ ^4\Sigma^-$	157.41	157.41
CH_3PH_2	-4.36	-4.36
CCl_2F_2	-117.90	-117.90
$C\ ^5S$	267.70	267.70
CH_3OH	-48.18 ± 0.05	-48.18
$-CH_2CH_2O-$	-12.58	-12.58
$-CH_2CH_2S-$	19.69	19.69
$C_2H\ ^2\Sigma^+$	135.00 ± 0.69	135.00
HCCH	54.50 ± 0.24	54.50
HC(O)CHO	-50.66	-50.66
H_2CCH_2	12.53	12.53
C_2H_5	28.92 ± 0.38	29.00
CH_2CO	-11.40 ± 0.38	-11.40
$CH_3CH_2NH_2$	-11.35	-11.35
CH_3CH_2OH	-56.10	-56.10
CH_3CH_2ONO	-24.80	-24.80
CH_3CH_2SH	-11.00	-11.00
CH_3CHO	-39.63 ± 0.10	-39.63
CH_3CO	-2.44 ± 0.29	-2.44
CH_3NHCH_3	-4.43	-4.43
CH_3OCH_3	-43.99	-43.99
CH_3OOCH_3	-30.00 ± 0.31	-30.00
CH_3SCH_3	-8.89	-8.89
$OS(CH_3)_2$	-36.09	-36.09
$SiH_2(CH_3)_2$	-22.70	-22.70
CH_3COOH	-103.26	-103.26
CH_3CH_3	-20.10	-20.10
$-CH_2CH_2CH_2-$	12.73	12.73
$-CH_2OCH_2OCH_2O-$	-113.20	-113.20

CH_2CCH_2	45.63	45.63
CH_2CHCH_2	40.84	39.10
CH_3CCH	44.39	44.39
$CH_3CH_2CH_3$	-24.98 ± 0.07	-24.98
CH_3CH_2CHO	-44.79	-44.79
CH_3CHCH_2	4.83	4.83
CH_3COCH_3	-51.91 ± 0.10	-51.91
$CH_3CH_2CH_2CH_3$	-30.07	-30.36
$CH_2CHCHCH_2$	26.11	26.11
CH_3CCCH_3	34.71	
$CH_3CH(CH_3)_2$	-32.41	-32.41
C_6H_{12}	-29.50	
C_6H_6	19.81	19.81
OH	8.90 ± 0.09	9.39
H	52.10	52.10
HCl	-22.06 ± 0.02	-22.06
HF	-65.32 ± 0.17	-65.32
HN_3	70.30	70.30
HNO	27.02 ± 0.06	23.80
HO_2 $^2A''$	3.50	3.50
$HONO_2$	-32.28	-32.28
HONO CIS	-18.34	-18.34
HONO TRANS	-18.84	-18.84
NH $^3\Sigma$ -	84.10 ± 2.38	84.10
HOCl	-18.67	-18.64
HNO $^3A''$	45.50 ± 0.06	45.50
H_2	0.01	0.01
H_2NF	-5.00	-5.00
H_2O	-57.80 ± 0.01	-57.80
HOOH	-32.54	-32.54
NH_2	45.14 ± 0.31	44.30
NH_3	-10.98 ± 0.08	-10.98
H_2NNH_2	22.75	22.75
ClO	24.30 ± 0.02	24.30
FOF	5.90	5.90
ClNO	12.36	12.36
NO $^2\Pi$	21.57	21.57
N_2O	19.61	19.61
O	59.55 ± 0.02	59.55
OClO	22.80 ± 0.31	22.80
$ClNO_2$	3.00	3.00
NO_2	7.93	7.93
O_2 $^3\Sigma$ -	0.01	0.01
$FONO_2$	2.39	2.39
NO_3 $^2B_2$	17.60 ± 0.33	17.60
$ONNO_2$	19.80	19.80

$O_3\ ^1A_1$	34.10	34.10
O_2NNO_2	2.17 ± 0.40	2.17
NF_2	8.50	8.50
N	112.97 ± 0.10	112.97
FNNF Cis	17.90	17.90
N_2	0.01	0.01
F	18.97 ± 0.07	18.97
F_2	0.01	0.01
Cl	28.99	28.99
Cl_2	0.01	0.01
Si	107.55	107.55
$SiCl_4$	-158.20	-158.20
$SiH_2\ ^3B_1$	84.60	84.60
SiH_3	46.40	46.40
SiO	-24.60	-24.60
SiO_2	-66.60	-66.60
SiS	27.60	27.60
PH_2	32.80	32.80
P	75.61	75.61
$PH\ ^3\Sigma$ -	56.80	56.80
P_2	34.20	34.20
PN	42.80	42.80
H_2S	-4.92 ± 0.12	-4.92
S	66.24 ± 0.04	66.24
SH	34.20 ± 0.68	34.20
$SO\ ^3\Sigma$ -	1.20 ± 0.31	1.20
SO_2	-70.94 ± 0.05	-70.94
SO_3	-94.57	-94.57
SiF_4	-386.00[a]	
P_4	14.10[a]	
PH_3	1.70	1.70
$SiCl_2$	-40.30[a]	
SF_6	-291.70[a]	
ClSSCl	-4.00[a]	
$(CH_3)_2SO_2$	-89.20[a]	
$(CH_3)_3CSH$	-26.20[a]	
C_4H_8S	-8.20[a]	
-CHCHSC(CH$_3$)CH-	20.00[a]	
$C_5H_{10}S$	-15.20[a]	
$-CH_2SCH_2-$	19.60[a]	
Cl_2SO_2	-84.80[a]	
$C_{10}H_8$	36.08	

[a] - Heats of formation same as the ones used in Curtiss et al. [3,4]

Since the experimental heats of formation recommended by IUPAC-subcommittee are the most recent, we use these heats of formation for comparisons in our current work. Heats of formation for the molecules in the extended test set are given in Table D.2. Unless otherwise indicated in Table D.2, the heats of formation of molecules are those used in Curtiss et al. [3,4]. Heats of formation of Al and B compounds, along with their uncertainties, are taken from different literature sources.

Table D.2 Compounds Added into Test set of Molecules

Molecules	$H_{f,298K}$ (kcal/mol)
C_2Cl_6	-32.1
C_2Cl_4	-3.0
C_2F_4	-157.9
$-CH_2CH_2NH-$	28.3
NCCN	73.8
$-CH=CHCH_2-$	66.2
-CH2CHCHCH2-	34.7
$-CH_2C(=CH_2)CH_2-$	47.9
$CH_3CH_2NO_2$	-24.4
CH_3CN	17.7
CN	105.6
$CO\ ^3\Pi$	114.3
FNO	-15.7
HNCO	-24.9
HNNH Trans	50.9
HOF	-23.5
$HOSO_2$	-92.0
$O=C(NH_2)_2$	-58.7
O_3 Cyclic	70.0
$OHCH_2CH_2OH$	-93.9
SiH_3SiH_3	19.1
$SiH_2\ ^1A_1$	64.8
SiH_4	8.2
ClOO	23.3
C_2H_3	71.8
CH_2S	24.3
$CH\ ^2\Pi$	142.5
CH_2CHCCH	70.40 [5]
HCCCCH	111.00 [6]

CH_3S ($^2A'$)	29.8
SCl_2	-4.2
S_2	30.7
C_2H_5Cl	-26.8
PF_3	-229.1
PCl_3	-69.0
PCl_5	-86.1
PF_5	-381.1
PO	-9.0 [7]
PO_2 ($^2A_1$)	-69.6 [7]
HOPO Cis	-112.4 [8]
$HOPO_2$	-171.4 [8]
$(HO)_2P$	-90.1 [7]
$(HO)_2PO$	-158.8 [7]
$(HO)_3P$	-188.8 [7]
$CClF_3$	-169.2 [9]
C_2F_6	-321.3 [3]
$POCl_3$	-134.0 [3]
CF_3CN	-118.4 [4]
ClF_3	-38.0 [4]
AlH_3	30.8 ± 4.8 [10]
AlF_3	-139.7 ± 1.2 [10]
$AlCl_3$	-289.0 ± 0.7 [10]
BH_3	21 ± 2.4 [10]
BF_3	-271.5 ± 0.2 [11]
BCl_3	-96.68 ± 0.31 [10]
AlH	59.6 ± 0.8 [10]
AlF	-63.1 ± 0.7 [10]
AlCl	-12.2 ± 0.7 [10]
BH	106.6 ± 1.7 [10]
BF	-27.701 [12]
BCl	41.2 ± 6.0 [10]

Table D.3 lists the compounds for which the BAC-G2 had deviations higher than 1 kcal/mol. The table includes compounds not only from original reference set used for BAC-G2, but also those in the extended test set.

Table D.3 Errors in BAC Predicted Heats of Formation at 298K for Compounds with Highest Errors for BAC-G2 or BAC-G3B3

Molecule	**Error in heat of formation at 298K (kcal/mol)**

	BAC-G3B3	Raw-G3B3	BAC-G3MP2B3	Raw-G3MP2B3	BAC-G2	Raw-G2
Organic compounds						
CH_2Cl_2	0.8	1.0	0.6	0.0	1.1	-0.7
CS_2	-1.0	-3.0	-1.1	-5.3	-1.1	-2.2
C	-0.2	-0.1	0.2	-0.1	-1.2	-0.1
H_2CNH	-0.3	-0.6	-0.4	-0.8	-1.2	-1.0
$CHCl_3$	0.8	1.1	0.6	-0.4	1.3	-1.1
CS	0.4	-0.7	-0.6	-3.0	1.4	-0.7
$C\ ^5S$	-0.3	0.1	0.2	0.3	-1.5	0.4
CH_2OH	0.2	0.1	0.4	0.3	-1.6	0.4
HCN	-1.3	-1.7	-1.0	-1.8	-1.6	-1.2
CH_2CHCH_2	-0.6	-0.9	-0.1	-1.0	1.4	0.9
$CH_2\ ^1A_1$	-0.4	-0.8	-0.4	-1.0	-1.7	-1.2
CH_3O	0.3	0.1	0.3	0.3	1.8	0.5
$CH\ ^4\Sigma$ -	-0.1	0.1	-0.5	-0.7	2.3	3.9
$C_2H\ ^2\Sigma$ +	-0.2	-0.4	-0.2	-1.1	2.7	3.6
$-CH_2CH_2NH-$	2.1	2.5	2.1	2.6	1.4	2.0
$-CH=CHCH_2-$	2.2	1.9	2.1	1.2	1.3	2.7
C_2Cl_4	-2.2	-2.2	-2.3	-4.8	-1.8	-4.6
$OHCH_2CH_2OH$	2.7	2.5	3.0	3.0	2.3	1.2
$O=C(NH_2)_2$	3.1	3.0	3.9	4.3	2.8	1.8
C_2F_4	-3.4	-3.9	-3.1	-4.1	-1.3	-7.8
HNCO	-3.7	-4.3	-3.1	-3.9	-3.9	-4.7
CO ($^3\Pi$)	-3.7	-3.9	-4.3	-4.8	-2.0	-2.3
CH_2S	4.1	3.1	4.1	2.0	4.0	3.4
$-CH_2CHCHCH_2-$	4.6	4.3	4.5	3.5	3.6	5.3
C_2Cl_6	-7.3	-6.8	-6.4	-8.8	-7.7	-11.4
Inorganic compounds						
H_2NNH_2	1.0	1.3	0.6	1.7	1.1	0.8
HN_3	-0.1	-0.3	0.4	0.1	-1.2	-0.5
$ONNO_2$	0.6	-0.3	-0.1	0.5	1.2	-1.4
H_2	-0.3	-0.5	-0.9	-1.1	-1.4	-1.4
HNO	-1.1	-1.6	-1.6	-1.7	1.5	-2.5
N	-0.3	0.0	-0.1	0.0	-1.5	0.0
$O_2\ ^3\Sigma$ -	-1.0	-0.1	-1.1	0.4	1.6	2.4
$O_3\ ^1A_1$	-0.8	0.2	-1.0	1.3	-1.6	-1.1
F	-0.1	-0.1	0.0	-0.1	1.9	-0.1
SiO	0.5	0.2	0.5	-1.0	2	1.7
$SiH_2(CH_3)_2$	0.4	1.4	0.3	1.5	2.2	0.9
$NO_3\ ^2B_2$	0.8	0.0	1.8	2.3	3.9	1.5
PF_3	2.1	5.8	2.3	5.5	-4.4	5.3
HNNH trans	-2.4	-2.6	-2.7	-2.8	-3.5	-3.1
HOF	2.5	3.0	2.6	3.4	2.3	2.1
Si_2H_6	-3.4	-1.7	-3.3	-1.6	-1.1	-3

$HOSO_2$	3.9	7.3	3.8	7.8	1.6	8.1
O_3 cyclic	-4.2	-3.6	-5.6	-3.3	-4.3	-4.5
ClOO	4.2	5.2	4.5	5.7	5.2	6.4
FNO	-5.0	-5.5	-5.3	-5.3	-5.2	-7.7
PCl_5	-7.2	1.1	-7.8	-2.2	-7.7	0.4

From the table, we observe that the BAC-G3B3 procedure has addressed many of the errors for those species for which BAC-G2 is not accurate within 2 kcal/mol. In particular, highly oxidative species or species involving dative bonds (e.g. NO_3, HN_3 etc.) have improved significantly. Other molecules in the table show consistent predicted values across the row, independent of the quantum chemistry method or whether BAC corrections are applied. This suggests that perhaps the experimental values may be in error. Further investigation of both the experimental and theoretical values to ascertain their accuracy is recommended. The recent changes in the recommended values of experimental heats of formation (see Table D.4) are, for the most part, supported by the findings of the BAC-G3B3 method.

Specifically, the NIST Computational Chemistry Comparison and Benchmark Database has suggested alternative experimental heats of formation for some molecules whose heats of formation vary significantly from the experimental values used in this work. For example, the following compounds have significant changes in experimental heats of formation (Table D.4). Using the alternative heats of formation for those compounds would reduce the errors in the BAC-G3B3 predicted heats of formation. Those compounds would no longer be outliers (errors < 2 kcal/mol).

Table D.4 Heats of Formation (kcal/mol.) at 298K Suggested by NIST Computational Chemistry Comparison and Benchmark Database

Compound	**Alternative $\Delta H_f^0{}_{298}$**	**This work $\Delta H_f^0{}_{298}$**
$-CH_2CH_2NH-$	30.1	28.3

$OHCH_2CH_2OH$	-92.6	-93.9
$O=C(NH_2)_2$	-56.6	-58.7
CH_2S	27.4	24.3
$-CH_2CHCHCH_2-$	37.5	34.7

Table D.5 shows the differences in experimental heats of formation of molecules reported in various literature sources.

Table D.5 Different Experimental Heats of Formation Reported in Literature

Molecules	**Previous work** [2]	**Chase et al. and Binkley et al.** [13,14]	**IUPAC-subcommittee**	
	$H_{f,298K}$	$H_{f,298K}$	$H_{f,298K}$	**Reference**
OH	9.30	9.40	8.90	[15]
NH_2	44.30	45.10	45.14	[16]
HNO	23.80		27.02	[17]
CH_2 ($^3B_1$)	93.80	93.70	93.40	[16]
CH_2 ($^1A_1$)	102.80	102.80	102.46	[16]
CH_3	34.85	35.00	35.02	[16]
CN	103.97	104.90	105.60	[16]
HCO	10.00	10.0	10.31	[18,19]
CH_2OH	-2.10		-4.26	[20]
C_2H_3	72.40	71.6	71.77	[16]
C_2H_5	29.00	28.9	28.92	[16]
CH_3CN	15.37	18.0	17.70	[21]
$CH_2CH=CH_2$	39.10		40.84	[16]
n-C_4H_{10}	-30.36	-30.0	-30.07	[22]
HOF	-23.42		-23.52	[12]
CHF_3	-166.70	-166.6	-166.89	[16]
CF_4	-223.00	-223.0	-223.21	[23]
CS	65.00		66.63	[16]
OCS	-33.94		-33.99	[24]
HOCl	-18.64	-17.8	-18.67	[24,25]

Experimental heats of formation from Chase et al. [13] and Binkley et al. [14] have been used for comparison against G3 and G3X predicted heats of formation presented in Curtiss et al. [26].

References

1. http://www.iupac-kinetic.ch.cam.ac.uk/Thermo2003.pdf, 2004.
2. C. F. Melius and M. D. Allendorf (2000). Bond additivity corrections for quantum chemistry methods. *Journal of Physical Chemistry A*, 104, 2168-2177.
3. L. A. Curtiss, K. Raghavachari, P. C. Redfern and J. A. Pople (2000). Assessment of Gaussian-3 and density functional theories for a larger experimental test set. *Journal of Chemical Physics*, 112, 7374-7383.
4. L. A. Curtiss, K. Raghavachari, P. C. Redfern, V. Rassolov and J. A. Pople (1998). Gaussian-3 (G3) theory for molecules containing first and second-row atoms. *Journal of Chemical Physics*, 109, 7764-7776.
5. W. R. Roth, O. Adamczak, R. Breuckmann, H. W. Lennartz and R. Boese (1991). Resonance energy calculation; the MM2ERW force field. *Chemische Berischte*, 124, 2499-2521.
6. J. H. Kiefer, S. S. Sidhu, R. D. Kern, K. Xie, H. Chen and L. B. Harding (1992). The homogeneous pyrolysis of acetylene II: the high temperature radical chain mechanism. *Combustion Science and Technology*, 82, 101-130.
7. J. C. Mackie, G. B. Bacskay and N. L. Haworth (2002). Reactions of phosphorus-containing species of importance in the catalytic recombination of H + OH: quantum chemical and kinetic studies. *Journal of Physical Chemistry A*, 106, 10825-10830.
8. D. L. Hildenbrand and K. H. Lau (1994). Thermochemical properties of gaseous POBr and some H–P–O species. *Journal of Chemical Physics*, 100, 8373-8376.
9. L. V. Gurvich, I. V. Veyts and C. B. Alcock (1989). *Thermodynamic Properties of Individual Substances*, Fouth Edition ed.; Hemisphere Pub. Co.: New York.
10. L. V. Gurvich, I. V. Veyts and C. B. Alcock (1994). *Thermodynamic Properties of Individual Substances*; CRC Press: Boca Raton, FL, Vol. 3.
11. J. D. Cox, D. D. Wagman and V. A. Medvedev (1984). *CODATA Key Values for Thermodynamics*; Hemisphere Publishing Corp.: New York, Vol. 1.
12. M. W. Chase (1998). *Fourth Edition, Journal of Physical and Chemical Reference Data*, Monograph 9, 1.
13. M. W. Chase, C. A. Davies, J. Downey, D. J. Frurip, R. A. McDonald and A. N. Syverud (1985). JANAF Thermochemical Tables. Third Edition. Part II, chromium-zirconium. *Journal of Physical and Chemical Reference Data*, 14, 927-1856.
14. J. S. Binkley, J. A. Pople and W. J. Hehre (1980). Self-consistent molecular orbital methods. 21. Small split-valence basis sets for first-row elements. *Journal of American Chemical Society*, 102, 939-947.
15. B.Ruscic, D. Feller, D. A. Dixon, K. A. Peterson, L. B. Harding, R. L. Asher and A. F. Wagner (2001). Evidence for a lower enthalpy of formation of hydroxyl radical and a lower gas-phase bond dissociation energy of water. *Journal of Physical Chemistry A*, 105, 1-4.
16. J. A. Kerr and D. W. Stocker (2000). *Strengths of Chemical Bonds*, 81 ed.; CRC Press: Boca Raton, FL.
17. R. N. Dixon (1996). The heats of formation of HNO and of DNO. *Journal of Chemical Physics*, 104, 6905-6906.
18. R. Becerra, I. W. Carpenter and R. Walsh (1997). Time-resolved studies of the kinetics of the reactions of CHO with HI and HBr: thermochemistry of the CHO radical and the C-H bond strengths in CH_2O and CHO. *Journal of Physical Chemistry A*, 101, 4185-4190.

19. M. C. Chuang, M. F. Foltz and C. B. Moore (1987). T_1 barrier height, S_1–T_1 intersystem crossing rate, and S_0 radical dissociation threshold for H_2CO, D_2CO, and HDCO. *Journal of Chemical Physics*, 87, 3855-3864.
20. R. D. Johnson and J. W. Hudgens (1996). Structural and thermochemical properties of hydroxymethyl (ch_2oh) radicals and cations derived from observations of $B^2a'(3p) <-- X^2a''$ electronic spectra and from ab initio calculations. *Journal of Physical Chemistry*, 100, 19874-19890.
21. D. R. Lide (2000). *CRC Handbook of Chemistry and Physics*, 81 ed.; CRC Press: Boca Raton, FL, Vol. 5-4.
22. J. D. Cox and G. Pilcher (1970). *Thermochemistry of Organic and Organometallic Compounds*; Academic Press: London.
23. A. S. Rodgers, J. Chao, R. C. Wilhoit and B. J. Zwolinski (1974). Ideal gas thermodynamic properties of eight chloro- and fluoromethanes. *Journal of Physical and Chemical Reference Data*, 3, 117-140.
24. E. S. Domalski, D. Garvin and D. D. Wagman (1978). *National Bureau of Standards (U.S.)*, Special Publication 513, Appendix 1 in R. F. Hampson and D. Garvin.
25. L. T. Molina and M. J. Molina (1978). Ultraviolet spectrum of hypochlorous acid. *Journal of Physical Chemistry*, 82, 2410-2414.
26. L. A. Curtiss, P. C. Redfern, K. Raghavachari and J. A. Pople (2001). Gaussian-3X (G3X) theory: Use of improved geometries, zero-point energies, and Hartree–Fock basis sets. *Journal of Chemical Physics*, 114, 108-117.

Appendix E: Frequencies of Oxametallacycle and Transition State

Tables E.1 and E.2 list the vibrational frequencies and normal modes for oxametallacycle and transition state of the oxametallacycle reaction to acetaldehyde. Oxametallacycle frequencies are taken from Linic and Barteau [1], while transition state frequencies are computed in this work as explained in Section 7.2.9.

Table E.1 Frequencies of Oxametallacycle

Normal Modes	HREELS Frequencies (cm^{-1})	DFT-predicted Frequencies (cm^{-1})
Ring deform (C-C-O)	450	408
Ring deform (C-O)		790
CH_2 rock	860	840
CH_2 rock		881
Ring Deform (C-C)	1090	1020
CH_2 wag		1090
CH_2 wag (parallel to surface)		1220
CH_2 scissor	1475	1432
CH_2 scissor		1484
CH_2 stretch	2850-2950	2900-3000

Table E.2 Freqeuncies of Transition State leading to Acetaldehyde

Normal Modes	DFT-predicted Frequencies (cm^{-1})
Ring deform (C-C-O)	585
Ring deform (C-O)	795
CH_2 rock	852
CH_2 rock	899
Ring deform (C-C)	1149
CH_2 wag	1191
CH_2 wag (parallel to surface)	1257
CH_2 scissor	1326
CH_2 scissor	1504
CH_2 twist	1561
CH_2 stretch	3022
CH_2 stretch	3078

CH_2 stretch	3170
CH_2 stretch	3287

References

1. S. Linic and M. A. Barteau (2002). Formation of a stable surface oxametallacycle that produces ethylene oxide. *Journal of American Chemical Society,* 124, 310-317.

Appendix F: Oxidative Coupling of Methane

F.1 Introduction

Oil is widely used as an energy source and raw material for variety of products in the petrochemical industry. However the energy crisis in the world due to fast depleting oil-based sources and the need to slow global climate change have triggered an aggressive search for alternatives. Natural gas is abundantly available on earth and currently underutilized. Catalytic partial oxidation of lower hydrocarbons (C_1 and C_2) to higher molecular weight products (C_n) is a potential route to meet not only the growing energy requirements but also the needs of petrochemical industry. Catalytic partial oxidation of methane to ethane is thermodynamically more favorable than other methane conversion routes like dimerization of methane [1]. Oxidative coupling of methane (OCM) is a partial oxidation process built on natural gas capable of large volume production with low capital costs. OCM is a catalytic process where methane upon reacting with a limited amount of oxygen adsorbed on a catalyst, is converted to C_2 hydrocarbons: ethane and ethylene.

Since the pioneering article by Keller and Bhasin on synthesis of ethylene via oxidative coupling of methane, many catalysts have been synthesized for OCM [2]. However, yield and selectivity of the process are below the economic feasibility limits of 28% and 95%. Yield is defined as the product of conversion and selectivity. Conversion is the percentage of methane reacted in the reactor, while selectivity is the percentage of converted methane that forms C_2 products. The yield and selectivity figures, mentioned above, are based on OCM economic analysis by Gradassi and Green [3]. The analysis focused on profitability of OCM process by

considering two important economic figures: required capital investment and cash margin. Revenues and costs of OCM process were compared with those of existing methanol technology. From the analysis, it was recommended that OCM research be focused on identifying catalysts and reaction conditions that would improve yield.

F.2 Review of Chemistry

OCM process is thought to occur through a mechanism in which catalytic surface reactions interact with gas phase chain reactions. Reactions occur through a bimodal scheme in which free radicals are generated in the surface, and coupling of these radicals occurs in the gas phase. Gas phase reactions are relatively well understood compared to surface reactions. The surface reactions hypothesized by experimentalists are primarily based on observing free radicals in the gas phase and products at the reactor outlet. These observations are made through experiments like radical trapping, transient analysis of products, isotope-switching mass spectrometry studies, and magnetic resonance measurements.

Some surface reactions proposed by earlier experimentalists have been confirmed by others using different experimental techniques. There are still some surface reactions which are debatable. What follows is a literature review of the key surface and gas phase reactions occurring in OCM.

F.2.1 Primary Reactions

Oxygen Adsorption: Initiation of Surface Reactions

First step in OCM kinetics is the adsorption of oxygen onto catalytic surface. To understand the nature of this adsorption, Amorebieta and Colussi conducted dynamic mass spectrometry kinetic studies on methane oxidation over Li/MgO catalyst at low pressures (1-100 mTorr) and 800-1100K [1]. Methane consumption was nearly first order in CH_4 and half-order in O_2 at low concentrations of the reactants. But at high concentrations, the rate leveled off. Rate expression for methane consumption and the observed kinetic behavior led to a significant conclusion that oxygen underwent reversible dissociative chemisorption on the catalytic sites. This reaction is:

$$O_2 + 2V^* \Leftrightarrow O^* + O^* \qquad (S1)$$

Similar kinetic behavior was also observed on a different catalyst samarium sesquioxide through mass spectrometric studies on low pressure (0.20-20 Torr) oxidation of methane [4]. Besides, methane consumption rates were observed at different concentrations of CH_4 for a fixed O_2 concentrations and vice-versa. The observations were accounted by a Langmuir-type dissocative chemisorption of oxygen followed by an Eley-Rideal mechanism for methane oxidation over catalytic sites. This was confirmed by Nibbelke et al. who conducted isotope transient kinetic analysis on OCM over MgO-based catalysts [5].

Competitive adsorption of methane is:

$$CH_4 + V^* \Leftrightarrow CH_4^* \qquad (S2')$$

However, Amorebieta and Colussi, through equilibrium constant calculations for the 2 Steps: S1 and S2', found that Step S1 dominated over Step S2' at high temperatures (1100K) [1]. This indicates that adsorption of methane on the catalyst may be weaker than that of oxygen. Weak adsorption of methane on catalysts: MgO and Sm_2O_3 were experimentally observed by Buyveskaya et al. in the temperature range 373-1035K [6]. This was confirmed by other

experimentalists for different catalysts. As a result, Reaction S2' has not been included in many modeling efforts on OCM.

Methyl Radical Formation: Abstraction of Hydrogen from Methane

The key surface reaction following adsorption of oxygen is the abstraction of hydrogen from methane. Methyl radical is formed through abstraction of hydrogen from methane by adsorbed oxygen. Heterogeneous production of these gas phase methyl radicals followed by gas phase coupling initiates the formation of higher hydrocarbons: C_2H_4 and C_2H_6. The abstraction reaction is:

$$CH_4 + O^* \Leftrightarrow CH_3 + OH^* \qquad (S2)$$

Ito et al. and Driscoll et al. had detected methyl radicals above MgO and Li/MgO in OCM reactions using EPR spectroscopy [7,8]. Methyl radicals were also detected in Li/MgO catalyst bed through matrix isolated para-magnetic resonance measurements by Lunsford and coworkers [8-11]. The presence of methyl radicals was confirmed by many researchers through mass spectrometry studies of products [1,4], and isotope exchange experiments on Li/MgO [12].

Methyl radical formation mechanism had been a topic of debate in the literature. The main issue was whether methane competitively adsorbs on the catalyst surface before hydrogen is abstracted from methane or if gaseous methane collides directly with surface oxygen species producing methyl radicals by an Eley-Rideal mechanism. Many researchers found that methane interacts weakly with catalyst surface disfavoring adsorption of methane. Instead, methane is expected to collide directly with adsorbed oxygen resulting in the rapid release of methyl radicals in gas phase. Figure F.1 shows the schematic of the Eley-Rideal mechanism for H abstraction from methane on a catalytic surface.

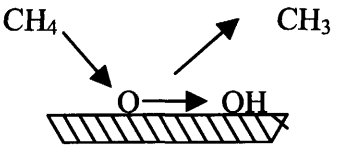

Figure F.1 Eley-Rideal Mechanism for H Abstraction

The released methyl radicals couple with each other to form ethane rapidly. Rapid formation of ethane molecules was proven by Buyevskaya et al. who carried out temporal analysis of OCM products, and observed that ethane exited the reactor at the same time as the inert tracer gas [6]. Since Eley-Rideal mechanism considers direct collision of gas molecules with adsorbed species, products are produced spontaneously.

Temperature is an important process variable affecting the production of methyl radicals. CH_3 yield was observed to pass through a maximum with increasing temperature (700-1100K) accompanied by decreasing selectivity [6]. The increase in yield is attributed to higher surface activity for H abstraction from methane at higher temperatures while the decrease in selectivity can be explained by an increasing activity of surface oxygen for radical oxidation. However, the activation energy of radical oxidation is expected to be lower than that of H abstraction from methane. The effects of temperature, though different on yield and selectivity, are important to understand and analyze in the radical formation reaction.

The role of catalyst is crucial in generation of methyl radicals. Several experimentalists detected surface-generated gas phase CH_3 over metal oxide catalysts by passing methane and oxygen over many oxides, including SiO_2, Al_2O_3 and MgO. MgO which was found as a superior catalyst contains defect centers or impurities conducive for production of methyl radicals [11]. Driscoll et al. found that addition of lithium to MgO enhanced methyl radical forming capability of the oxide [8]. This was thought to result from the presence of active sites, which are lattice

oxide ion defects that generate methyl radicals via hydrogen abstraction [1]. Many modifications to the catalyst have been tried in literature; but lithium-doped tin-promoted magnesia (Li/Sn/MgO), which was first reported by Ito et al., is one of the best catalysts available [7]. This catalyst was recommended by Korf et al., Lunsford and Wolf et al. [11,13,14].

Kinetic experiments have shown that hydrogen abstraction is most likely the rate-limiting step in the conversion of methane to ethane. The activation energy for hydrogen abstraction on Li/MgO catalyst was reported in the range 20 to 28 kcal/mol (87-115 kJ/mol) for various reaction conditions [1,9]. Reaction conditions in the former work were 0.001-0.1 Torr total pressure, 800-1100K temperature and the catalyst was 7% lithium-promoted magnesium oxide. Reaction conditions in the latter were: 0.2-20 Torr total pressure, 859-1100K, and the catalyst was Sm_2O_3.

Main Gas Phase Reactions following Methyl Radical Generation

It is demonstrated earlier that CH_3 is formed in gas phase. These methyl radicals react further through several gas phase reaction pathways to form different products. The main reaction pathways are depicted in Figure F.2.

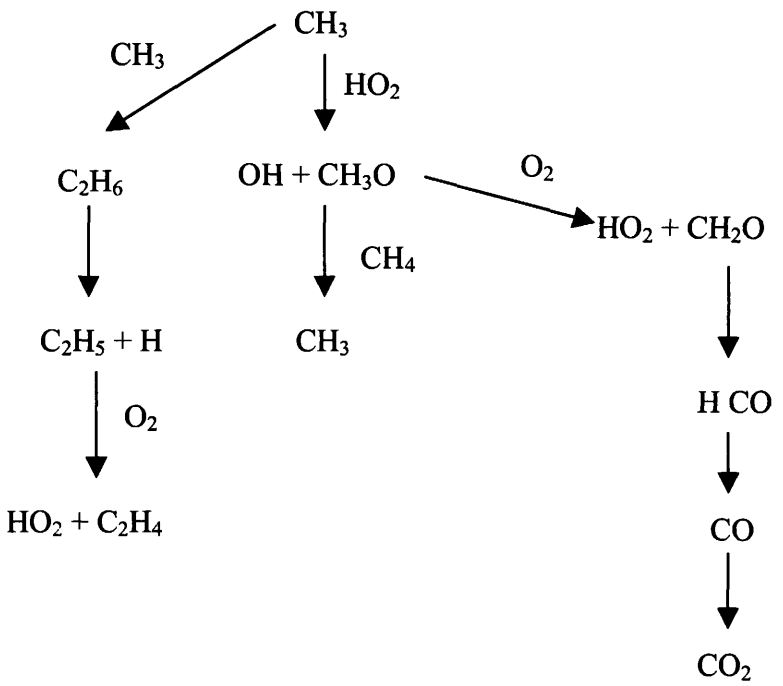

Figure F.2 Gas Phase Reaction Pathways for Methyl Radicals

The important features are:

1. Branching and competition between pathways: For example, CH_3 reacts with CH_3 or with HO_2. The first channel leads to C_2; while the second goes to CO
2. Generation/Destruction of chain-carrying radical intermediates: These radicals are usually in balance due to steady state. For example, CH_3. is formed primarily by surface reaction of CH_4 with O^* and reaction with OH in the gas phase. CH_3. is destroyed by the reaction with CH_3. and reaction with HO_2..

One of the pathways corresponding to the gas phase coupling of methyl radicals leads to the formation of ethane. Lunsford confirmed that the coupling reaction occurs in gas phase but not in surface [11]. He found that a metal oxide such as MgO does not promote the surface coupling of methyl radicals. He also conducted a separate study on the amount of methyl

radicals generated and managed to account for the entire ethane yield from gas phase methyl radicals. The coupling reaction is:

$$CH_3 + CH_3 \Leftrightarrow C_2H_6 \qquad (G1)$$

The presence of a third body is required for coupling due to energetic requirements. Hence, the coupling reaction is pressure-dependent and is favored when gas collisions are enhanced [15].

Ito et al. reported that CH_4 conversion and selectivity to C_2 increased with temperature, for temperatures below 973K [7]. Higher temperatures favoring production of more methyl radicals led to higher C_2 formation. However, above 973K, further oxidation of C_2 to CO and CO_2 became appreciable, decreasing C_2 selectivity.

Kinetic parameters for the coupling reaction are reported in Mims reaction library which includes almost 450 reversible elementary gas phase reactions with 115 species, exclusive of the catalyst [12]. Rate constants of the reactions were of the form:

$$k(T) = AT^n e^{\left(\frac{-E_a}{RT}\right)} \text{ at a fixed pressure}$$

and the kinetic parameters: log(A), n, and E_a were compiled in the library.

Water Formation and Regeneration of Active Sites

Water is formed by the combination of two surface hydroxyl species. The reaction is:

$$OH^* + OH^* \Leftrightarrow H_2O + O^* + V^* \qquad (S3)$$

The forward reaction is endothermic. Activation energies of the forward reaction on metal oxide catalysts: CaO/CeO_2 and Sn/Li/MgO are reported as 0 and 152.7 kJ/mol in Wolf et al. and Hoebink et al. [14,16]. The surface dehydroxylation reaction is favored at high temperature,

allowing regeneration of catalytic sites for oxygen activation. Hence, this reaction is a key source of regeneration of active sites crucial to the production of methyl radicals via Step S2.

Water formation is also expected to occur in the gas phase due to the reaction:

$$OH + CH_4 \Leftrightarrow CH_3 + H_2O$$

Primary Reaction Cycle: Production of Ethane

The three elementary surface reactions Steps S1 through S3 can be combined to give the overall primary reaction for catalytic production of methyl radicals:

$$4\ CH_4 + O_2 \Leftrightarrow 4\ CH_3 + 2\ H_2O \qquad (S1\text{-}S3)$$

This reaction and the gas phase methyl radical coupling reaction Step G1 can be combined to give the overall reaction for production of ethane:

$$4\ CH_4 + O_2 \Leftrightarrow 2\ C_2H_6 + 2\ H_2O \qquad (P)$$

Role of Oxygen in the Overall Reaction

O_2 plays three major roles:

1. Controls the redox state of catalyst surface, which is related to the number of surface vacancies and active catalytic sites.
2. Reacts with alkyl radicals in the gas phase leading to CO_x.
3. Replenishes surface oxygen.

The properties of surface oxygen which are closely tied to the properties of the catalyst are expected to be important in determining OCM selectivity. Buyveskaya et al. found that a high surface concentration of oxygen on Sm_2O_3 favors total oxidation of methane, while a low concentration leads to high selectivity towards C_2 products [6].

Surface oxygen is expected to trigger two types of reactions: 1. hydrogen abstraction from methane leading to methyl radicals which are desirable, and 2. surface oxidation of methyl radicals, which are undesirable. The latter reaction alters the C_2 selectivity through formation of surface methoxy complexes, which can oxidize rapidly with another surface oxygen to form formaldehyde [17]. There have been arguments that surface oxygen species capable of abstracting hydrogen from methane might as well react with methyl radicals. This argument is plausible, since the radical species which is more reactive and short-lived than methane molecules will increase the chance of second reaction.

Ethyl Radical Formation: Abstraction of Hydrogen from Ethane

Key secondary catalytic reactions in OCM are the production of ethyl and vinyl radicals. Since C-H bond energy in ethane is less than that in methane, hydrogen abstraction from ethane is at least as likely as hydrogen abstraction from methane (Step S2). The former reaction leads to the production of ethyl radicals:

$$C_2H_6 + O^* \Leftrightarrow C_2H_5 + OH^* \qquad (S4)$$

Ethyl radicals have been detected using matrix isolation electron spin resonance by Morales et al., in their study on oxidative dehydrogenation of ethane over Li/MgO catalysts at 893K and 798K [18]. Besides, they detected C_4 hydrocarbons which were expected to occur from the dimerization of C_2 radicals.

Ethylene Formation

Formation of ethylene, from ethane, has been reported to appear in the gas phase [19]. Ethylene is mainly formed from the reactions:

$$C_2H_5. \Leftrightarrow C_2H_4 + H \qquad (G2)$$

$$C_2H_5. + O_2 \Leftrightarrow C_2H_4 + HO_2. \qquad (G3)$$

These are the branched chain reactions reported in Chen et al. [20]. The first reaction is reported to dominate over the second reaction at 1 atm. However, when the pressure is increased to 4 atm, the second reaction dominates. This can be explained by the bimolecular nature of the second reaction which is strongly affected by the increase in pressure.

In addition to the above 2 reactions, other gas phase reactions also contribute to the production of ethylene, though in small quantities. One of the reactions is:

$$CH_3 + CH_3 \Leftrightarrow C_2H_4 + H_2 \qquad (G4)$$

F.2.2 Side Reactions: Reduction in Selectivity to C_2 Products

In addition to the main reaction cycle, there are side reactions occurring in surface and gas phase which reduce the selectivity of converted methane to form C_2 products. The challenge clearly involves finding a kinetically feasible process for OCM without loss of C_2 products to CO and CO_2.

Vinyl Radical Formation: Abstraction of Hydrogen from Ethylene

Hydrogen abstraction from ethylene is possible, since the C-H bond energy in ethylene is only 5 kJ/mol higher than that in methane (temperatures between 923 and 1023K). The abstraction reaction leads to undesirable formation of vinyl radical:

$$C_2H_4 + O^* \Leftrightarrow C_2H_3 + OH^* \qquad (S5)$$

Vinyl radical is an important source of CO.

Intermediate Formaldehyde Formation and Reaction

Surface Oxidation of Methyl Radicals:

McCarty considered a 2-step mechanism leading to formation of the intermediate formaldehyde from surface methoxy species which are presumably formed by the surface oxidation of methyl radicals [17]. This 2-step mechanism is:

$$CH_3^{\cdot} + O^* \Leftrightarrow CH_3O^* \qquad (S6)$$

$$CH_3O^* + O^* \Leftrightarrow OH^* + CH_2O + V^* \qquad (S7')$$

However, there is debate in literature, as to whether the second reaction is elementary or if it occurs in 2 rapid steps:

$$CH_3O^* + O^* \Leftrightarrow OH^* + CH_2O^* \qquad (S7)$$

$$CH_2O^* \Leftrightarrow CH_2O + V^* \qquad (S8)$$

In either case, the formaldehyde produced acts as an intermediate for formation of CO through gas phase chain reactions [20].

Reaction of Formaldeyde

Formaldehyde is known to undergo fast gas phase chain reactions leading to CO. Chen et al. proposed a gas phase reactions sequence leading to formation of CO from formaldehyde via formyl radicals [20]. CO is detected in mass spectra experiments by Colussi and Amorebieta [1].

Reaction of CO and Formation of CO_2

There had been debate in the literature as to whether most of the CO formed reacts further to CO_2 or stays as a product in OCM. Chen et al., considering CO as a stable species, have argued

that CO does not react catalytically to form CO_2 [20]. If CO were a reactive intermediate, then the following surface reaction is possible:

$$CO + O^* \rightarrow CO_2 + V^* \qquad (S9)$$

However the rate constant for this reaction over Sn/Li/MgO calculated by Chen et al. was negligible, ruling out the possibility of the reaction [20]. Besides, they observed the selectivity of methane to CO to be 15% which is too high to consider CO as a reactive intermediate.

However, earlier Van der Wiele et al. concluded that most of CO undergoes catalytic oxidation to CO_2 [21]. They conducted 2 separate experiments on ethane oxidation by feeding an equimolar mixture of ethane and oxygen. From the first experiment which was run using Li/MgO catalyst, it was observed that CO_2 and hardly any CO were produced. From the second experiment which was run in the absence of a catalyst, it was observed that CO and a small amount of CO_2 were produced. This led to a significant conclusion that most of CO is oxidized to CO_2, in the presence of catalyst. Peil et al. had done similar experiments on Li/MgO catalyst to prove catalytic oxidation of CO to CO_2 [22]. Hence, Reaction S9 may be important and needs to be included in surface chemistry.

Both CO and CO_2 are also expected to be produced through gas phase oxidation of methyl radicals and C_2 products. This view is plausible and many researchers have included these gas phase reactions in analysis of OCM. The kinetic parameters for these gas phase reactions are known with good degree of accuracy, either through quantum calculations or experimental measurements. For example, these reactions and the corresponding kinetic parameters are included in the gas phase reactions library [12].

As mentioned earlier, one of the routes for CO_2 formation is the catalytic oxidation of CO. Another route is the gas phase oxidation of alkanes and alkyl radicals. Tong and Lunsford

observed that at temperatures less than 973K, the non-selective products CO and CO_2 are formed by the gas phase oxidation of methane [23]. The gas phase oxidation of methane and alkyl radicals (methyl and ethyl radicls) have been included in gas phase mechanism by many researchers.

Radical Quenching

An important feature of the catalytic oxidative coupling of methane is the radical quenching reactions favored by catalyst. Sanches-Marcano et al. and Tulenin et al. found that catalyst not only produces but also quenches radicals [24,25]. An example of radical quenching is the surface reaction of peroxy radicals formed in OCM.

Hydroperoxyl radicals are expected to undergo fast hydrogen abstraction on catalytic surface [12,26]:

$$HOO + O^* \Leftrightarrow O_2 + OH^* \qquad (S10)$$

Since peroxide bond is weak, the adsorption of peroxide onto catalyst was also considered:

$$HOO + V^* \Leftrightarrow HO + O^* \qquad (S11)$$

They also considered the adsorption of methyl peroxy radicals:

$$CH_3OO + 2V^* \Leftrightarrow CH_3O^* + O^* \qquad (S12)$$

F.3 Review of Transport Mechanism

OCM is a reacting flow system with strong interplay between kinetic and transport mechanisms in gas and solid phase. There are 2 kinds of transport: mass and heat transport and several

species: reactants, products and radical intermediates involved in transport mechanism. The transport mechanism depends on the type of reactor and flow contacting used.

In literature, several OCM experiments have been carried out in packed bed reactors, with the catalyst beds diluted by inerts. By doing so, the temperature gradients in both radial and axial directions of the bed were negligible. Hence, modeling efforts on OCM have neglected temperature variations in the reactor. Earlier, Maers had devised mathematical criterions for including or neglecting heat transfer limitations and temperature gradients in intra- and inter-particle phase of fixed bed reactor systems [27]. The criterions were based on comparing heats of reaction with heat fluxes associated with convection and diffusion, for inter- and intra-particle phase respectively. These criteria should be used to model heat transfer both inside the catalyst pellets and interstitial phase.

Couwenberg conducted experiments on OCM in Sn/Li/MgO packed bed reactor such that there was no intra-particle mass transfer limitation for reactants or products [28]. When Couwenberg et al. modeled the above reactor, they identified irreducible mass transfer limitations on reactive intermediates: methyl, hydrogen peroxy, and hydrogen radicals [29]. These limitations were attributed to the high reactivity of radical intermediates, resulting in reaction rate much higher than intra-particle diffusion rate. Irreducible mass transfer limitations are expected to influence OCM yield and selectivity to C_2 products. For example, irreducible mass transfer limitation on methyl radicals will reduce the amount of methyl radicals coupling with each other in gas phase to form ethane. The mass transfer limitations can be reduced by decreasing the catalyst pellet size, but at the cost of increasing pressure drop. Thus, catalyst size is an important variable affecting the process yield.

Effect of pellet radius on C_2 selectivity has been observed by several experimentalists and modelers. Reyes observed a decreasing selectivity for increasing pellet sizes at low inlet methane-to-oxygen ratio of 2.0 [30]. This was connected to the possible transport limitations of C_2 products resulting in secondary reactions of C_2 to form CO_x products. Decreasing selectivity with increasing pellet diameter was also seen in the calculations by Couwenberg et al. [29,31].

In literature, OCM reactor models combining the effects of kinetics and transport have evolved from simple to complex schemes. Reyes et al. used three models: 1. homogeneous models, 2. homogeneous-heterogeneous models with no intra-particle concentration gradients, and 3. homogeneous-heterogeneous models with intra-particle concentration gradients [32]. As expected, yield and selectivity predicted by the first model were low (yield and selectivity less than 10% and 80%, at 1073K, 46.7 kPa CH_4 and 23.3 kPa O_2). This was attributed to the dominant gas phase combustion of methane and C_2 compounds, favored by absence of catalyst. The second model predicted higher yields (20-45%, at 1073K, 67 kPa CH_4 and 33 kPa O_2) due to the presence of catalytic sites which favor heterogeneous production of methyl radicals coupling further to give C_2. The third model predicted low yields (less than 10% at 1073K, 67 kPa CH_4 and 33 kPa O_2). Besides, it was concluded that intra-particle concentration gradients can be neglected for small pellet radius (less than 0.1 mm). Yield was affected for pellet radius higher than 0.1 mm.

References

1. V. T. Amorebieta and A. J. Colussi (1988). Kinetics and mechanism of the catalytic oxidation of methane over lithium-promoted magnesium oxide. *Journal of Physical Chemistry,* 92, 4576-4578.
2. G. E. Keller and M. M. Bhasin (1982). Synthesis of ethylene via oxidative coupling of methane. *Journal of Catalysis*, 73, 9-19.
3. M. J. Gradassi and N. W. Green (1995). Economics of natural gas conversion processes. *Fuel Processing Technology*, 42, 65-83.
4. V. T. Amorebieta and A. J. Colussi (1989). Mass spectrometric studies of the low-pressure oxidation of methane on samarium sesquioxide. *Journal of Physical Chemistry,* 93, 5155-5158.
5. R. H. Nibbelke, J. Scheerova, M. H. J. M. de Croon, and G. B. Marin (1995). The oxidative coupling of methane over mgo-based catalysts: a steady-state isotope transient kinetic analysis. *Journal of Catalysis*, 156, 106-119.
6. O. V. Buyevskaya, M. Rothaemel, H. W. Zanthoff and M. Baerns (1994). Transient studies on reaction steps in the oxidative coupling of methane over catalytic surfaces of MgO and Sm_2O_3. *Journal of Catalysis*, 146, 346-357.
7. T. Ito, T., Wang, J., Lin, C. and J. H. Lunsford (1985). Oxidative dimerization of methane over a lithium-promoted magnesium oxide catalyst. *Journal of American Chemical Society,* 107, 5062-5068.
8. D. J. Driscoll, W. Matrix, J. X. Wang and J. H. Lunsford (1985). Formation of gas-phase methyl radicals over MgO. *Journal of American Chemical Society*, 107, 58-63.
9. K. D. Campbell, E. Morales and J.H. Lunsford (1987). Gas phase coupling of methyl radicals during the catalytic partial oxidation of methane. *Journal of American Chemical Society*, 109, 7900-7901.L. V. Gurvich, I. V. Veyts and C. B. Alcock (1989). *Thermodynamic Properties of Individual Substances*, Fouth Edition ed.; Hemisphere Pub. Co.: New York.
10. K. D. Campbell and J. H. Lunsford (1988). Contribution of gas-phase radical coupling in the catalytic oxidation of methane. *Journal of Physical Chemistry*, 92, 5792-5796.
11. J. H. Lunsford (1992). Formation and reaction of methyl radicals over metal oxide catalysts. in *Methane Conversion by Oxidative Processes*, E. E. Wolf, Ed., Van Nostrand Reinhold, New York, 3-19.
12. C. A. Mims, R. Mauti, A. M. Dean and K. D. Rose (1994). Radical chemistry in methane oxidative coupling: tracing of ethylene secondary reactions with computer models and isotopes. *Journal of Physical Chemistry,* 98, 13357-13372.
13. S. J. Korf, J. A. Roos, L. J. Veltman, J. G. Van Ommen and J. R. H. Roos (1989). Effect of Additives on Lithium doped Magnesium Oxide Catalysts Used in the Oxidative Coupling of Methane. *Applied Catalysis*, 56, 119-135.
14. D. Wolf, M. Slinko and E. Kurkina Baerns (1998). Kinetic simulations of surface processes of the oxidative coupling of methane over a basic oxide catalyst. *Applied Catalysis A,* 166, 47-54.
15. G. A. Martin and C. Mirodatos (1995). Surface chemistry in the oxidative coupling of methane. *Fuel Processing Technology*, 42, 179-215.
16. J. H. B. J. Hoebink, P. M. Couwenberg and G. B. Marin (1994). Fixed bed reactor design for gas phase chain reaction catalyzed by solids: the oxidative coupling of methane. *Chemical Engineering Science*, 49, 5453-5463.

17. J. G. McCarty (1992). Mechanism of cooxidative methane dimerization catalysis: kinetic and thermodynamic aspects. in *Methane Conversion by Oxidative Processes*, E. E. Wolf, Ed., Van Nostrand Reinhold, New York, 320-348.
18. E. Morales and J. H. Lunsford (1989). Oxidative dehydrogenation of ethane over a lithium-promoted magnesium oxide catalyst. *Journal of Catalysis*, 118, 255-265.
19. Zhang et al.
20. Q. Chen, P. M. Couwenberg and G. B. Marin (1994). Effect of pressure on the oxidative coupling of methane in the absence of catalyst. *AIChE Journal*, 40, 521-535.
21. K. van Der Wiele, J. W. M. H. Geerts and J. M. N. van Kasteren (1992). Elementary reactions and kinetic modeling of the oxidative coupling of methane. in *Methane Conversion by Oxidative Processes*, E. E. Wolf, Ed., Van Nostrand Reinhold, New York, 259-319.
22. K. P. Peil, G. Marcelin and J. G. Goodwin Jr. (1992). The role of lattice oxygen in the oxidative coupling of methane. in *Methane Conversion by Oxidative Processes*, E. E. Wolf, Ed., Van Nostrand Reinhold, New York, 138-167.
23. Y. Tong and J. H. Lunsford (1991). Mechanistic and kinetic studies of the reactions of gas-phase methyl radicals with metal oxides. *Journal of American Chemical Society*, 113, 4741-4746.
24. J. Sanches-Marcano, C. Mirodatos, E. E. Wolf and G. A. Martin (1992). Inhibition of gas-phase oxidation of ethylene by various solids and influence of additives on the catalytic properties of lanthanum oxide towards the oxidative coupling of methane. *Catalysis Today*, 13, 227-235.
25. Y. Tulenin, A. Kadushin, V. Seleznev, A. Shestakov, and V. Korchak (1992). Effect of pressure on the process of methane oxidative dimerization: 1. The mechanism of heterogeneous inhibition of gas-phase reactions." *Catalysis Today*, 13, 329-337.
26. Y. S. Su, J. Y. Ying and W. H. Green Jr. An upper bound for the oxidative coupling of methane. *Journal of Physical Chemistry*.
27. D. E. Mears (1971). Diagnostic criteria for heat transport limitations in fixed bed reactors. *Journal of Catalysis*, 20, 127-131.
28. P. M. Couwenberg (1995). Gas phase chain reactions catalyzed by solids: the oxidative coupling of methane. Ph.D Thesis, Eindhoven Institute of Technology, Eindhoven, The Netherlands.
29. P. M. Couwenberg, Q. Chen and G. B. Marin (1996a). Irreducible mass transfer limitations during a heterogeneous catalyzed gas-phase chain reactions: oxidative coupling of methane. *Industrial Engineering and Chemistry Research*, 35, 415-421.
30. S. C. Reyes, E. Iglesia and C. P. Kelkar (1993b). Kinetic-transport models of bimodal reaction sequences-1. Homogeneous and heterogeneous pathways in oxidative coupling of methane. *Chemical Engineering Science*, 48, 2643-2661.
31. P. M. Couwenberg, Q. Chen, and G. B. Marin (1996b). Kinetics of a gas-phase chain reaction catalyzed by a solid: oxidative coupling of methane over Li/MgO-based catalysts. *Industrial Engineering and Chemistry Research*, 35, 3999-4011.
32. S. C. Reyes, C. P. Kelkar and E. Iglesia (1993a). Kinetic-transport models for the design of catalyst and reactors for the oxidative coupling of methane. *Catalysis Letters,* 19, 167-180.